LBL-36383
UC-401

Center for Advanced Materials

CAM

Carbon Monoxide Oxidation Over Three Different States of Copper: Development of a Model Metal Oxide Catalyst

G.G. Jernigan
(Ph.D. Thesis)

October 1994

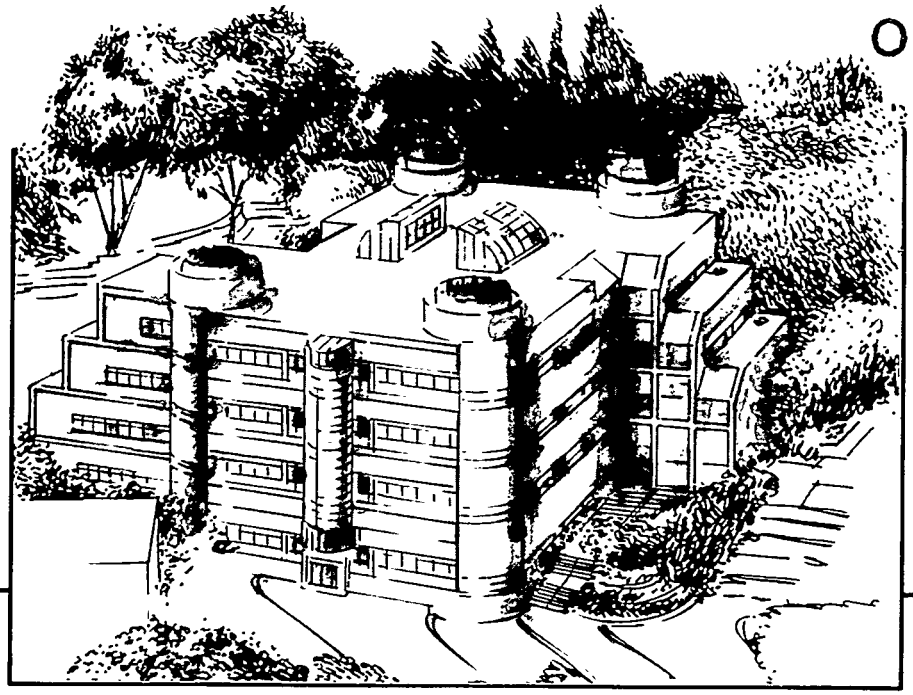

Materials and Chemical Sciences Division

Lawrence Berkeley Laboratory • University of California

ONE CYCLOTRON ROAD, BERKELEY, CA 94720 • (415) 486-4755

Prepared for the U.S. Department of Energy under Contract DE-AC03-76SF00098

LBL-36383
UC-401

CARBON MONOXIDE OXIDATION OVER THREE DIFFERENT STATES OF COPPER: DEVELOPMENT OF A MODEL METAL OXIDE CATALYST

GLENN GEOFFREY JERNIGAN
Ph.D. Thesis

DEPARTMENT OF CHEMISTRY
University of California

and

MATERIALS SCIENCES DIVISION
Lawrence Berkeley Laboratory
University of California
Berkeley, CA 94720

OCTOBER 1994

This work was supported by the Director, Office of Energy Research, Office of Basic Energy Sciences, Materials Sciences Division, of the U.S. Department of Energy under Contract No. DE-AC03-76SF00098

Abstract

Carbon Monoxide Oxidation over Three Different Oxidation States of Copper:
Development of a Model Metal Oxide Catalyst

by

Glenn Geoffrey Jernigan

Doctor of Philosophy in Chemistry

University of California at Berkeley

Professor Gabor A. Somorjai, Chair

Carbon monoxide oxidation was performed over the three different oxidation states of copper— metallic (Cu), copper (I) oxide (Cu_2O), and copper (II) oxide (CuO) as a test case for developing a model metal oxide catalyst amenable to study by the methods of modern surface science and catalysis. Copper was deposited and oxidized on oxidized supports of aluminum, silicon, molybdenum, tantalum, stainless steel, and iron as well as on graphite. The oxides of copper showed initial activity on the oxidized supports but became deactivated due to compound formation. Auger electron spectroscopy (AES) and x-ray photoelectron spectroscopy (XPS) were used to characterize the oxidation states of the supported copper. Graphite-supported copper was used to determine the kinetics of CO oxidation over Cu, Cu_2O, and CuO. Cu forms three dimensional islands on graphite which, upon oxidation, were found to wet the graphite surface. Copper was observed to oxidize slowly to CuO in a 66/33 Torr CO/O_2 gas mixture at 275°C during a catalytic reaction. Hence, kinetic measurements were made over Cu, Cu_2O, and CuO under 97/3, 90/10, and 66/33 Torr CO/O_2 gas mixtures, respectively, in order to maintain the catalyst

oxidation state during the reaction. The catalytic activity was found to decrease with increasing oxidation state (Cu > Cu_2O > CuO) and the activation energy increased with increasing oxidation state (Cu 9 kcal/mol < Cu_2O 14 kcal/mol < CuO 17 kcal/mol). Reaction mechanisms were determined for the different oxidation states. CO_2 was found to inhibit CO oxidation over Cu by dissociating on the catalyst surface, and over Cu_2O and CuO by blocking CO adsorption. The reduction of CuO in ultra high vacuum (UHV = absence of O_2) and in CO, and the oxidation of Cu in CO_2 and O_2 were studied by XPS to determine the interaction of each component in the carbon monoxide oxidation reaction with the catalyst surface. The activation energy for reduction of CuO to Cu_2O in UHV and in CO was found to be 26 and 9 kcal/mol respectively. A UHV environment was unable to further reduce Cu_2O to Cu. CO was able to completely reduce CuO to Cu with the rate of reduction from CuO to Cu_2O being faster than the rate from Cu_2O to Cu. The oxidation of Cu by O_2 and CO_2 was found to be an activated process. Exposure of Cu to O_2 at 25°C resulted in adsorbed and subsurface oxygen, while at 100°C Cu_2O was formed. CO_2 at 200°C was able to oxidize Cu to Cu_2O but was unable to further oxidize Cu_2O to CuO. Lastly, NO reduction by CO was studied. A Cu and CuO catalyst were exposed to an equal mixture of CO and NO at 300-350°C to observe the production of N_2 and CO_2. At the end of each reaction, the catalyst was found to be Cu_2O. There is a need to study the kinetics of this reaction over the different oxidation states of copper.

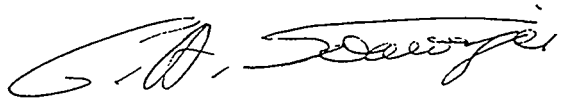

Table of Contents

List of Figures

List of Tables

Acknowledgments

As I approach the end of my graduate studies, I would like to thank those people whose influence and guidance has helped me achieve my goal of obtaining a Ph.D. in chemistry from Cal, the top program in the nation. Paramount to my success was my research advisor Professor Gabor Somorjai. He accepted me into his research group and provided me with the scientific questions that drove my research. He allowed me to purse those questions at my discretion and to interpret the results I obtained. This allowed me to mature as a scientific researcher and gave me the confidence to purse other scientific questions.

I would like to thank Professor John (Jack) Porter for his willingness to discuss both scientific and non-scientific matters. I give his critique of my first paper credit for its acceptance, without revisions, in the Journal of Catalysis. He also was kind enough to read and comment on this thesis. I would like to thank Tom Giannotti for his technical assistance with electrical problems and for his friendship. When either research or life had gotten me down, Tom was always there to pick me up. I enjoyed our lunches at the Bear's Lair and our afternoons on the golf course.

My initial instruction into the world of surface science came from Istvan Böszörméni and Dave Jentz. Istvan taught me the unique combination of surface science and catalysis that made this group famous, and he taught me how to be an accurate scientist. To Dave, I was a sidekick with whom, at anytime or place, it was fun to discuss anything scientific. I miss our discussions after the Physical Chemistry seminar and at Triple Rock. Neither of us knew the answers to the questions we posed, but we'd argue it out until we did.

Of the current Somorjai students, I would like to thank Craig Gerken and Nick Materer for allowing me to share what I have learned with them. Craig's "I call bull pucky!" always challenged what I knew. Additionally, his critique of this thesis was very

much appreciated. Nick and his wife L.J. are always good company as I could discuss science with Nick or literature/life with L.J. To the rest of the group, I truly enjoyed learning about the science that each of you pursued, and I wish all of you success in science. Outside the group, I would like to thank Jeff Emerson. His friendship on the racquetball court, at Cal football games, and in Europe gave me a life away from my UHV chamber. I would also like to thank Professor Somorjai's assistants, Bob Kerr and Brigid Tung. Their always friendly help guided me through the paper work of the university's bureaucracy.

Lastly, I would like to thank my mom. With relatives in the area, she did not burden me with local family commitments, and she did not complain about the hours and the life that I kept while attending school. She supported me in all that I did. Because of that, I never feared failing in anything of my pursuits.

This work was supported by the Director, Office of Energy Research, Office of Basic Energy Sciences, Materials Science Division of the U.S. Department of Energy under Contract No. DE-AC03-76SF00098.

Chapter 1

Introduction

Catalysis is a chemical field which has a great impact on society. According to a survey by the Department of Commerce in 1991, catalysis was responsible for 60% of the products made in the US [1]. This is understandable when one considers that most consumer goods consist of compounds which result from a chemical reaction on a natural raw material. Excellent examples are plastics which start as crude oil and become computer keyboards, coffee machines, drinking cups, etc. Catalysis achieves this by facilitating chemical reactions.

Chemical reactions often have energy barriers that slow the conversion of reactants into products. Catalysis facilitates the such reactions by lowering the energy barriers between the reactants and the products. A lower energy barrier makes it possible to convert more reactants into products in less time and using less energy. Catalysis makes chemical reactions more economical.

The question underlying catalysis is how and why does a catalyst facilitate a chemical reaction? Our initial understanding comes from kinetic studies where the conditions of the reaction are varied, and observations are made as to how to maximize the rate of the chemical reaction. An excellent example of this is the synthesis of ammonia from nitrogen and hydrogen over an Fe catalyst. Ammonia is used in the production of fertilizers and explosives [2] and is one of the top ten chemicals produced each year [3]. It was discovered that the rate of the reaction was enhanced by increasing the nitrogen

pressure and that the rate of reaction was decreased by an increase in the hydrogen pressure [4]. Figure 1.1 shows a possible series of elementary reaction steps in the synthesis of ammonia and three rate expressions derived from the assumption of a rate limiting step which could account for the observed changes in the rate with changes in the reactant's gas pressure [5]. The rate expressions are very similar and are hard to distinguish by kinetic measurements alone. If we assume that the first expression is correct, then the rate limiting step is the dissociation of nitrogen. It was also discovered that the rate of reaction could be enhanced if the Fe was deposited as small particles on alumina and doped with potassium [2]. How does this affect the observed kinetics and proposed mechanisms? The kinetics in themselves imply how a catalyst facilitates a reaction, but can not explain why. An understanding of the physical nature of the catalyst is needed to understand why the catalyst facilitates a chemical reaction.

Surface science provides a means to physically characterize a catalyst surface. The measured properties of the surface can then be correlated with the observed kinetic results to explain how and why catalysts facilitate chemical reactions. To continue the ammonia example, surface science studied different crystal faces of Fe and discovered that a surface with an Fe atom with 7 nearest neighbors was needed for the dissociation of nitrogen [6]. By placing the Fe on an alumina support, a greater number of Fe with 7 neighbors sites were created [7]. The doping of the catalyst with potassium affected the electronic properties of the Fe [8]. This weakened the bonding of ammonia to the surface and thus effectively allowed for the removal of product.

For the past 25 years surface science has successfully investigated the properties of metal catalyst surfaces for a variety of reactions [9], but this is only half of the reactions which are heterogeneously catalyzed. The other half consist of reactions over metal oxides. Very few surface science investigations on such reactions has been done. The reason surface science has had difficulty in studying metal oxide catalysts is because metal oxides are typically thermal and electrical insulators which limit the use of surface science

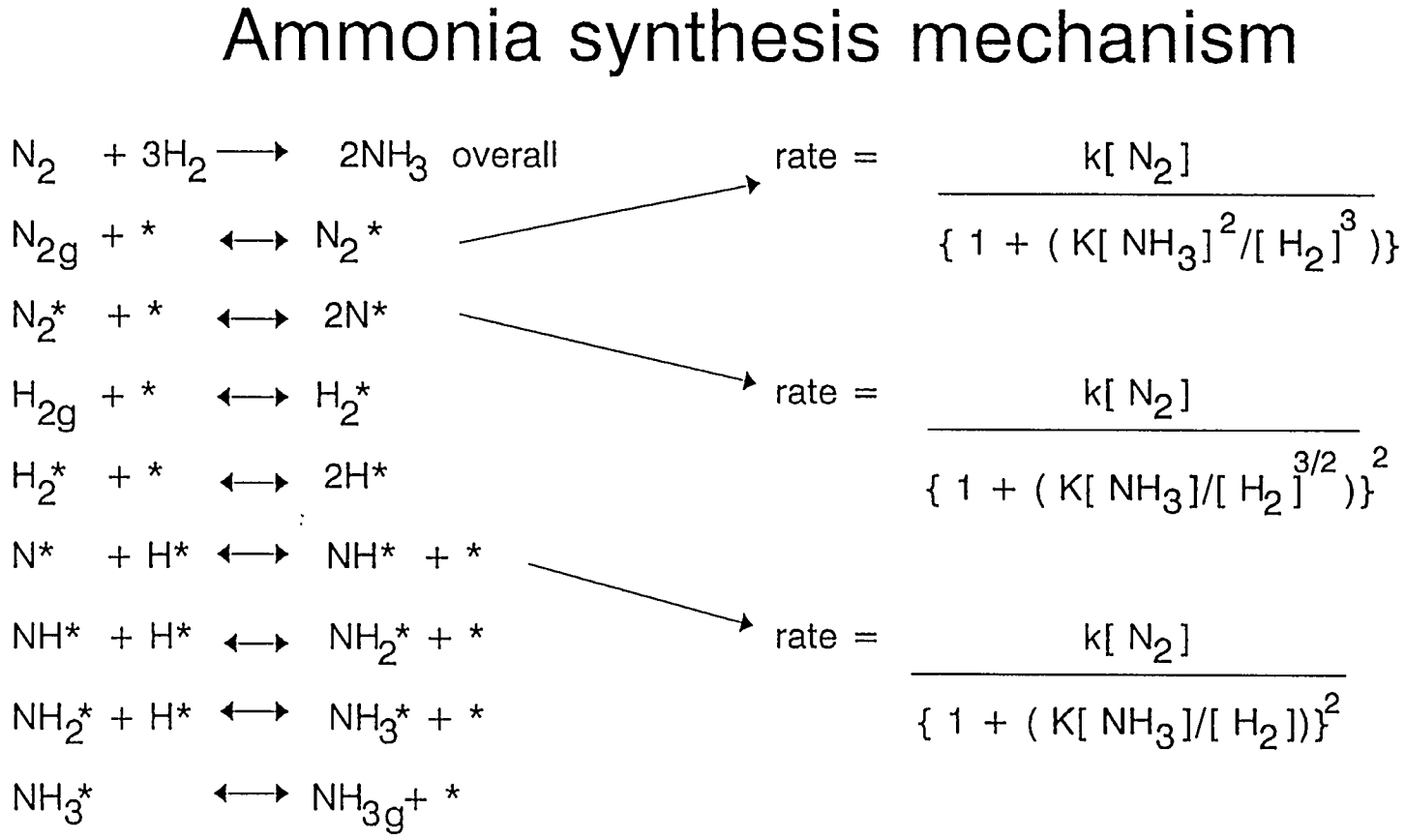

Figure 1.1. Potential reaction steps in the synthesis of ammonia and the rate expressions derived from assuming three different rate limiting steps [5].

spectroscopies [10]. When studies have been performed, the complex nature of the metal oxide has made the results hard to interpret. Metal oxides are also hard to study because they have lower turnovers than metals; this makes kinetic measurements over the small samples used in surface science very difficult. This thesis is an inroad into the study of metal oxide catalysis using the techniques of surface science.

1.1. Thesis Statement

The primary purpose of this research is to develop a method to study metal oxide catalysts using surface science techniques. Previous studies have observed the promotional effects of metal oxides on transition metal catalysts [11,12] , but none have observed any catalysis on the oxide itself. A secondary goal is then to actually measure catalytic turnovers on a model metal oxide catalyst under conditions of industrial relevance. The interaction of gases adsorbed on or desorbed from a metal oxide catalyst single crystal does not adequately describe the chemistry which occurs at higher pressures and temperatures in a catalytic reactor. So, a third motivation for this work is to develop an understanding of the mechanism of catalytic reactions over metal oxide catalysts.

Metal oxides are known to catalyze the partial oxidation of hydrocarbons [2]. Many mechanisms for this have been proposed [13-18]. The most popular mechanism is the Mars-van Krelven which suggests that metal oxides undergo a redox cycle. Only partial oxidation occurs because only enough energy to remove a lattice oxygen is needed in the reaction [16]. The lattice O reacts with a hydrocarbon to form the partial oxidation product. Later, the oxygen vacancy is regenerated by a gas phase oxygen molecule. This mechanism has not been conclusively proven for any partial oxidation reaction over any metal oxide. The three motivations given above are united in the study of the catalytic oxidation of carbon monoxide oxidation over copper oxide.

The catalytic oxidation of carbon monoxide to carbon dioxide over copper oxide was chosen for study for a number of reasons. First, it has potential use as an automotive exhaust catalyst. Second, there exists an uncertainty in the literature over the mechanism for the reaction as well as the rate of reaction and its activation energy. Third, copper oxide is one of the most active oxides for this reaction and is comparable to noble metal catalyst [19]. This means that a catalytic measurement on a small surface area sample is possible. Fourth, copper has two distinct oxides: +1 cuprous oxide and +2 cupric oxide. They are spectroscopically different from each other and from metallic copper allowing good catalyst characterization using the techniques of surface science. Lastly, carbon monoxide oxidation is an elementary step in many reactions catalyzed over copper catalysts.

1.2. Review of Copper Catalysis

It is important to explain the significance of CO oxidation as it pertains to the literature and to other related reactions before presenting any new results in this area. The following is a brief summary of the catalytic oxidation reactions which occur over copper and copper oxides. Although the main purpose of this thesis is to understand copper oxide chemistry, the potential redox effect on the catalysis makes it important to study the chemistry of copper metal as well. This is well founded in that there is a debate over the oxidation state of copper in all reactions that occur on its surface. The first reaction discussed is CO oxidation, as there is a discrepancy in the literature as to the results obtained by surface science measurements versus the results obtained by conventional catalytic reactor measurements. The second reaction discussed is the water gas shift reaction which is the conversion of CO and water to CO_2 and H_2. This reaction is very similar to CO oxidation except in the nature of the oxidant. Methanol synthesis is discussed third. This is probably where the greatest understanding of copper chemistry is

needed. With changing chemical and fuel needs, the synthesis of methanol is a very important field. Lastly, the oxidation of propylene to acrolein will be discussed as this is industrially relevant partial oxidation reaction.

1.2.1. Carbon Monoxide Oxidation

The oxidation of CO to CO_2 is an environmentally important process. Currently, this reaction is catalyzed over noble metal catalysts and is used to control pollution from mobile sources (automobiles). The cost of platinum does not make it economically feasible to be used for stationary sources (power plants) and is in limited supply for automotive sources [20]. This has lead to searches for other catalysts which are cheaper and more abundant. Copper oxide is an attractive alternative.

Surface science studies have shown that this reaction has a lower activation energy and greater rate over copper than platinum [21-26]. This is good news in that the current platinum catalyst requires high temperatures for the efficient conversion of CO and does a poor job when a car engine is cold at start-up. A copper catalyst should oxidize more CO upon a cold start-up of the engine as well as effect more complete conversion at higher temperatures. When copper was scaled up and deposited on a support, the catalytic results were not as favorable as the results obtained by surface science. The discrepancy was reported as being due to the pressure gap between low pressure UHV studies and high pressure reaction studies [26,27]. Chapter 4 will explain that the different results obtained by the high and low pressure studies are actually due to different catalysts and different reaction mechanisms. This was determined by obtaining results similar to both surface science and high pressure studies by running different oxidation states of copper under different CO to O_2 ratios. It is therefore important to know what results were obtained previously.

The low pressure reaction of CO oxidation over Cu single crystals is a relatively well understood phenomenon [21-25]. The mechanism is a Langmuir-Hinshelwood one with the rate limiting step being the reaction between adsorbed CO and adsorbed O. An Eley-Rideal mechanism could have been possible, as the reaction rate was found to be 0th order in O_2 and 1st order in CO. The Langmuir-Hinshelwood mechanism was conclusively proven by Campbell who observed that when CO gas was pre-heated prior to reaction with adsorbed O that no enhancement of the reaction rate occurred [21]. The activation energy measured for the reaction was found to be between 6-7.2 kcal/mol.

The oxidation reaction was found to depend on the species which predominated on the crystal surface [24,25]. In a UHV experiment, the surface is pre-covered with one reactant, which is subsequently removed by exposing it to the second reactant. Product formation can be measured by observing the loss of reactant from the surface or by measuring the concentration of gas phase product by mass spectroscopy. It was found that the reaction has a lower reaction probability if O was adsorbed on the surface and removed by CO [25]. Adsorbed O inhibits the adsorption of CO. If the exposure of O_2 to the surface is high initially, O is found to penetrate into the surface. As CO removes surface O, the vacancy is refilled by a subsurface O. Once all subsurface O had been removed, the rate of reaction increases as the adsorption of CO is no longer inhibited. When the reverse was performed, CO was not found to inhibit O adsorption. The reaction on the CO pre-covered surface was constant with exposure.

Unlike the low pressure studies, the high pressure studies are not well understood. Most likely this is due to an uncertainty as to the nature of the catalyst and the reaction mechanism. Table 1.1 lists a few high pressure studies along with the reported activation energy and believed active catalyst in each. In most cases, the catalysts are given a pretreatment before being tested catalytically in order to generate an active catalyst. A common feature of the pretreatments is the reduction of the catalyst, because metallic Cu is more active than oxidized Cu.

Table 1.1. Listing of literature values for the active catalyst for CO oxidation and the activation energy measured over each.

Low Pressure Studies	Catalyst	Activation Energy (kcal/mol)	Reference
Bootsma	Cu single crystal	6	25
Campbell	Cu single crystal	6.3-7.1	21
Goodman	Cu single crystal	6.5	26
van Pruissen	Cu single crystal	7.2	22
High Pressure Studies			
Blumenthal	CuO	19.1	28
Garner	Cu_2O	11.4	29
Halasz	$BaCuO_2$	15	30
Miro	Reduced Cu/zeolite	7.8	31
Miro	Oxidized Cu/zeolite	23	31
Prokowicz	CuO	14	32
Selwood	CuO	25	33
Sourirajan	CuO	12.8	34
Thomas	CuO	17	35
Vannice	Cu	17-22	27
Yu Yao	CuO	22	20

In all studies, the reaction rate has been found to be approximately 1st order in CO and 0th order in O_2 [20,27,28,31,36]. IR. studies have shown that the rate of reaction is proportional to CO adsorbed onto the catalyst surface [27,37]. This led many to propose a reaction mechanism similar to that observed in the low pressure studies. The different activation energies obtained were explained by the effect of the heat of adsorption of CO on the reaction. If the heat of adsorption of CO onto Cu is subtracted from the activation energy, the result is close to the values obtained at low pressures. This calculation was based on a similar explanation used to explain the difference between high and low pressure studies of CO oxidation over a platinum catalyst [38]. The fallacy in this argument is that the heat of CO adsorption is different on the different oxidation states of Cu, and this point is discussed in greater depth in chapter 4.

The catalysts used in the high pressure studies are characterized before being catalytically tested, but the characterization is not sensitive to what occurs to the surface

during the reaction. Those techniques which are used *in situ* (X-ray Diffraction—XRD, Electron Pair Resonance—EPR) are not sensitive to the surface. A bulk Cu particle may have a thin oxide layer covering the surface during reaction. XRD detects the Cu diffraction but not necessarily the oxide. Those techniques which are surface sensitive (adsorption / desorption studies) cannot be performed during a reaction. Titrations of the copper surface have led to incomplete oxidation or reduction of the surface and can not be well quantified. Attempts to characterized the nature of the Cu catalyst has led to the following proposals: (1) that the reaction is structure sensitive [33,39], (2) proceeds by an Eley-Rideal mechanism [32,36], and (3) has an strong metal support interaction (SMSI) effect on some supports [39].

The studies described in this thesis show how the observed kinetics at both high and low pressures are a function of the three oxidation states of Cu. The most important results being the kinetics and mechanism which occur over the Cu_2O and CuO surfaces. Many of the high pressure results can be explained by realizing that the catalyst is CuO and that the mechanism is different from the mechanism on Cu and Cu_2O. In chapter 4 it will be shown that the reaction has a higher activation energy over CuO than both Cu and Cu_2O, and it proceeds through a redox mechanism.

1.2.2. Water-Gas Shift Reaction

The water-gas shift (WGS) reaction is very similar to CO oxidation. CO is being oxidized by water as opposed to O_2 and hydrogen is produced as well as CO_2. This reaction has been well studied because it is currently utilized in industry [41-51]. The WGS reaction is used to produce H_2 for ammonia synthesis and hydrocarbon reactions and is also used in steam reforming and coal gasification [41,42]. The mechanism of the reaction, however, is not well understood [45].

The mechanism of the WGS reaction is related to either CO oxidation or methanol synthesis. Figure 1.2 shows two possible reaction paths for the WGS reaction. Path 1 shows a formate species forming on the surface. This species would be an intermediate in the production of methanol from CO and H_2. If water completely decomposes as in path 2, then the reaction would be similar to CO oxidation. The surface O would be removed by CO to regenerate the active site. This reaction has a higher activation energy, 16-18 kcal/mol, than does CO oxidation, so the rate limiting step is not CO_2 formation. Instead, the rate limiting step is the dissociation of H_2O on the surface [45,46]. The adsorption and dissociation of H_2O on copper is sensitive to the structure of the substrate, as is the reaction [42,44,45,52,53].

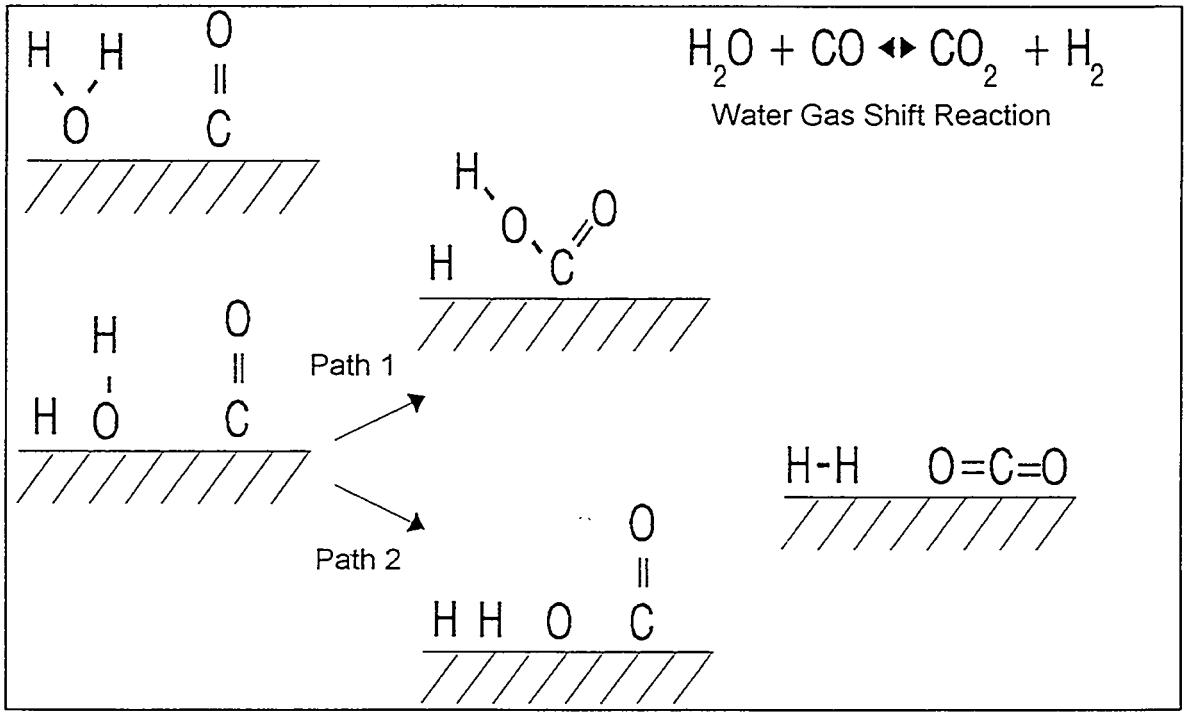

Figure 1.2. Schematic of the two possible reaction mechanisms for the water gas shift reaction.

The WGS reaction can be run in reverse, in which case CO_2 and H_2 react to produce CO and H_2O. This reaction is limited by the dissociation of CO_2 on the Cu surface [45,47]. It was proposed that for the forward and the reverse WGS reaction go

through a similar reaction intermediate [41,50,54]. The proposed reaction intermediate is formic acid [41]. In studies of formic acid decomposition, CO is not produced at the temperatures observed for the reverse WGS reaction [47]. This most likely disproves the formate intermediate but is not conclusive evidence.

If the WGS reaction occurs through a redox mechanism, adsorbed O has not been observed to build up on the surface. When exposed to WGS reaction conditions, a pre-oxidized copper surface will become metallic after a few minutes [42]. The formation of Cu (I) oxide has been seen in the reverse WGS reaction when the reactant gases are individually pulsed over the surface [46]. This is different from CO oxidation, where the oxidant has a greater affect on the surface than the reducing species. Although the nature of the reaction is similar between CO oxidation and the WGS reaction, it is important to note the properties of the reactants and their interaction with the Cu surface. The interaction of individual gases with the different oxidation states of Cu is discussed in chapter 6.

1.2.3. Methanol Synthesis

A great deal of interest in the catalytic chemistry of copper is due to its ability to catalyze the synthesis of methanol from a mixture of CO, CO_2 and H_2. Methanol is a valuable chemical as it can be catalytically converted into other basic, valuable organic chemicals like formaldehyde and acetic acid [55]. Methanol is also an octane enhancer for gasoline as an oxygenate additive and a potential alternative fuel source in its own right [55]. If methanol is to become a fuel source, increased production will be needed; this has led to a large number of studies attempting to determine the mechanism of methanol synthesis [55-65].

The mechanism of methanol synthesis over the industrial $Cu/ZnO/Al_2O_3$ catalyst is a hotly debated topic of scientific research, with two opposing theories. The first is that

methanol is formed from CO adsorbed on a Cu (I) site through a formyl intermediate [57,68]. The second is that methanol is formed from CO_2 adsorbed on a Cu (0) site through a formate intermediate [55,58,61,66,67]. Both mechanisms are shown schematically in figure 1.3, and each will be discussed. But first, a general overview of methanol synthesis will be presented.

The discovery by the Imperial Chemical Industries (ICI) that $Cu/ZnO/Al_2O_3$ catalyzed the synthesis of methanol from a mixture of $CO/O_2/H_2$ at low pressures (50 atm) and temperatures (500-570K) came in the mid 1960s [55] and replaced a ZnO/Cr_2O_3 catalyst which ran at higher pressures (100-250 atm) and temperatures (623-673) [2]. The formation of methanol from either CO or CO_2 is thermodynamically unfavorable with the free energies of formation being +4.5 and +10 kcal/mol, respectively. The high pressure of the reaction is needed to shift the equilibrium towards the formation of methanol. The industrial gas mixture is 10/10/80 $CO/CO_2/H_2$, and the production of methanol is dependent on all gases being present. As the synthesis from CO is more favorable thermodynamically, the question arose as to why CO_2 was needed in the reaction.

It was originally proposed that CO_2 was needed to create Cu (I) sites which were the active site for the reaction. CO_2 oxidizes Cu (0) to Cu (I) under the reaction conditions given above, and it is needed to prevent the gradual reduction of Cu (I) back into Cu (0). The heat of adsorption of CO on Cu (0) is between 12-16 kcal/mol [69-71] and on Cu (I) is 18 kcal/mol [72-74]. The increased bond strength between CO and Cu (I) is needed under reaction conditions if CO is to remain on the surface and become hydrogenated. The presence of ZnO is believed to stabilize the Cu (I) [75]. Cu (0) supported on SiO_2 does not produce methanol from a CO and H_2 mixture [76] , whereas Cu supported on ZnO will produce a small amount [77]. When CO_2 and H_2 were passed over a Cu/SiO_2 catalyst, methanol was produced in small quantities. It was believed that CO_2 oxidized the Cu (0) surface onto which the remaining CO adsorbed and

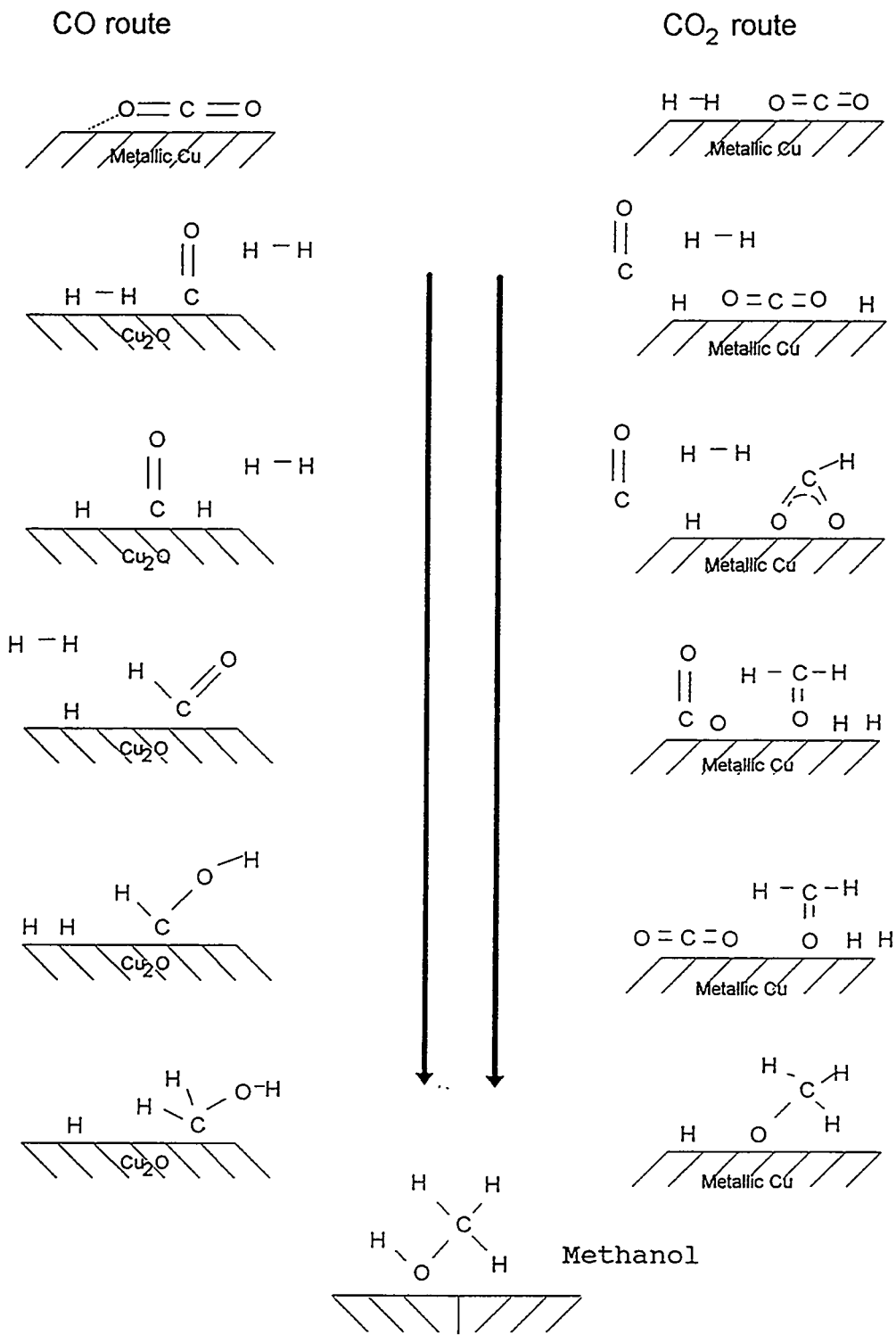

Figure 1.3. Schematic for the mechanism of methanol synthesis from either CO or CO_2.

hydrogenated. It was also discovered that alkali metal promote the reaction of CO and H_2, and again it was proposed that the alkali metal stabilized the Cu (I) sites [76]. Various techniques have been used to observe that Cu (I) is present under reaction conditions; however, a correlation between Cu (I) and methanol production has never been observed. A case in point is a study of Cu (I) supported on Cr_2O_3 where 2% of the sites were poisoned, resulting in a 30% decrease in activity [57]. It has also been shown that H_2O or O_2 [78] can be used in place of CO_2 to create Cu (I) sites and enhance the activity for methanol synthesis.

The strongest argument against the proposed Cu (I) active site is that CO_2 has been shown to be the major carbon source for methanol under industrial conditions [55]. In a radio-isotope labeling study, $^{14}CO_2$ and unlabeled CO were tested over an industrial catalyst. Mixtures with CO_2 to CO ratios between 0.02 and 1 were used and resulted in 70 to 100% labeled methanol as the product. It was then proposed that the CO is the extra species and not CO_2. In the production of methanol from CO_2, adsorbed O is a by-product. CO is needed in the reaction to maintain a metallic surface by removing the adsorbed O. CO oxidation occurs rapidly and produces CO_2 which can be reacted to produce additional methanol. The obtained results used to describe a mechanism over Cu (I) can also be used to explain a mechanism for CO_2 over Cu (0). The addition of H_2O or O_2 to the feed could increase the CO oxidation reaction and produce additional CO_2 for methanol . The alkali metal promotion can be explained by its enhancement of CO_2 adsorption [79]. Alkali metals and CO_2 from stable carbonate-like species on the surface of Cu (0). Finally, ZnO is needed to promote spillover of H_2 onto the Cu surface [58-63]. Under reaction conditions the Cu (0) surface is covered by CO and CO_2, hence H_2 cannot adsorb. Additionally even without a covered surface, the adsorption of H_2 on Cu (0) is small [80]. The complexity of the methanol synthesis stems from copper's ability to interchange CO - CO_2 and H_2O - H_2 by the removal or addition of an oxygen.

1.2.4. Propylene Oxidation

The oxidation of propylene to acrolein over Cu_2O was a commercial Shell process which has been replaced by newer mixed oxide catalysts [2,81,82]. The Cu_2O catalyst converted 20% of the propylene with an 85% selectivity to acrolein at 350°C and 200 kPa total pressure.

$$2CH_2CHCH_3 + O_2 \xrightarrow[Cu_2O]{} CH_2CHCHO$$

The mechanism of the reaction was never completely understood and only a few studies have been reported for the reaction over Cu_2O [81,83,84]. A series of recent publications by Cox and Schulz on the surface science of propylene adsorption on a Cu_2O single crystal have reopened the investigation of the mechanism [84-87].

The major question being asked is why Cu_2O partially oxidizes propylene as opposed to promoting complete combustion to CO and CO_2. The commonly held belief is that partial oxidation occurs when lattice oxygens can be incorporated into the product. If adsorbed O is present, then complete oxidation should occur. Correlations have been made which show that, with decreasing heat of dissociation of oxygen from an oxide, there is an increase in activity towards partial oxidation [2,88]. If lattice oxygen is incorporated into the product, a question arises regarding the nature of the surface intermediate.

When propylene adsorbs on Cu_2O, it forms a stable π-bonded allyl species on the surface by cleaving a C-H bond [89-90], shown in figure 1.4. The conversion of this intermediate into acrolein is debated as to when O inserts itself into the molecule and as to when the second H is abstracted. If O insertion happens before the second H abstraction, an allyloxy species forms [85,91], whereas if the second H abstraction occurs first, an aldehyde species will form [89,92]. The difference between the two mechanisms is shown in figure 1.4. The formation of an allyloxy species could be related to the methanol

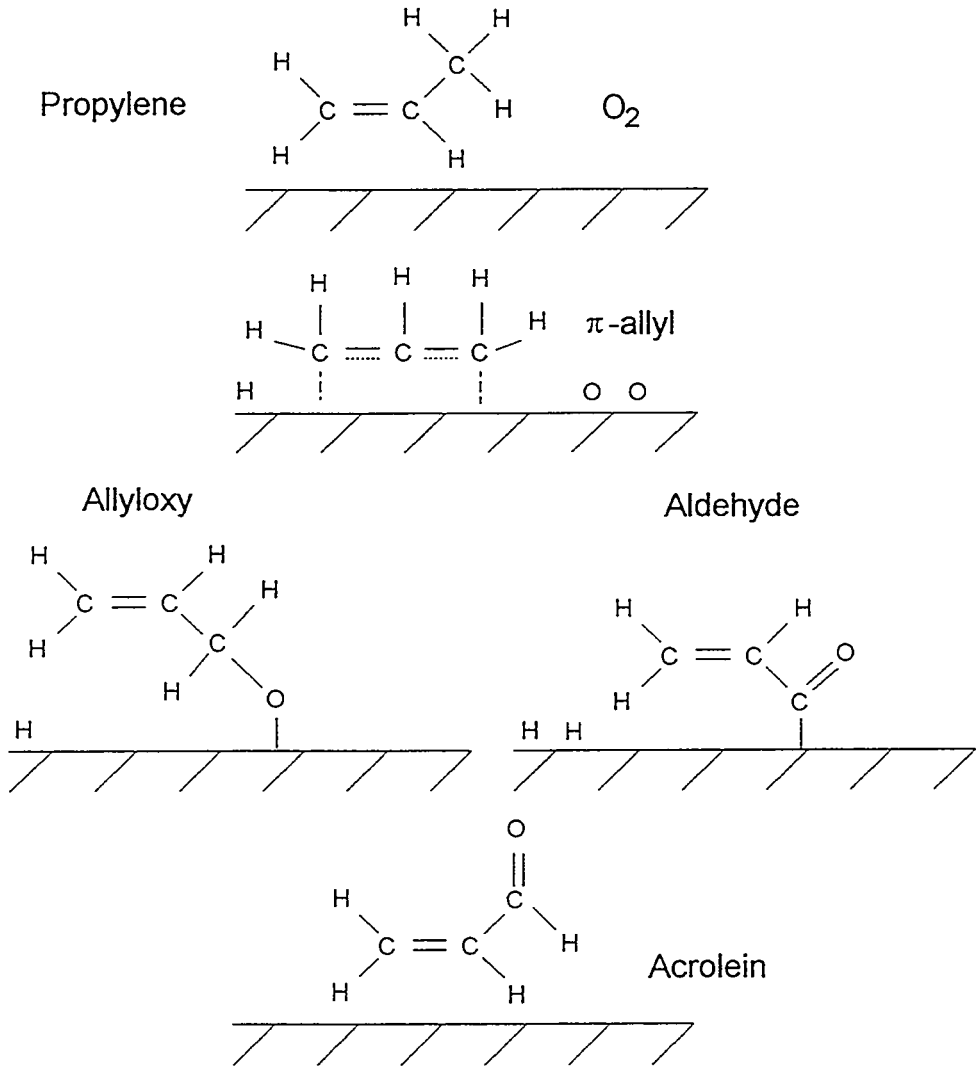

Figure 1.4. Schematic of propylene oxidation to acrolein showing the π-allyl intermediate which leads to either an allyloxy or aldehyde surface species.

synthesis mechanism, as it is seen in the studies of methanol decomposition on Cu [93-95]. The aldehyde species intermediate is similar to acetaldehyde and acetic acid which are by-products formed in the reaction. Currently the most popularly-accepted mechanism is the allyloxy species, which is believed to form in other similar systems.

1.3. Present Work

Described in the following chapters is work which will aid in the understanding of catalytic reactions over copper catalyst. Special interest is paid to the interaction of reactant and product gases with the catalyst surface. In order to observe how gases interact with the catalyst surface, the catalyst must be well characterized. Chapter 2 presents the four surface science techniques used in these studies (Auger Electron Spectroscopy, X-ray Photoelectron Spectroscopy, Ion Scattering Spectroscopy, and Thermal Desorption Spectroscopy) as well as the catalytic rate measurements used for characterizing the properties of a catalyst surface. Chapter 3 contains the characterization results for copper catalysts deposited on various substrates (Al_2O_3, SiO_2, Ta, Mo, Fe_3O_4, stainless steel, and graphite.) Copper was deposited on many supports in search of a substrate which would not interfere with the chemistry of copper oxide yet would provide providing good electrical and thermal conductivity. Thin films of copper oxide are used in order to observe uniformly any changes in oxidation state which may occur from the interaction of gases with the catalyst surface. The three oxidation states of copper were best characterized on the graphite substrate. Chapter 4 presents the results of CO oxidation over the three oxidation states of copper on graphite. The CO oxidation results were obtained by running different CO to O_2 ratios over Cu, Cu_2O, and CuO at 97/3, 90/10, and 66/33 Torr, respectively, to maintain the catalyst oxidation state during reaction. Rates and activation energies are obtained and the results are compared to a platinum foil run under similar conditions. Mechanisms are proposed for the reaction over each oxidation state. Chapter 5 reports the effect of CO_2 deactivation over Cu and Cu_2O surfaces. The different deactivation mechanisms are discussed and investigated by running additional catalytic reactions and performing XPS and TDS experiments. Chapter 6 addresses the ability to reduce the oxides of copper by annealing in UHV or CO and the ability to oxidize metallic copper by heating in O_2, CO_2, and NO. The energetics of

changes in the oxidation state of copper are viewed in light of the catalytic reactions which can occur on the catalyst surface. Chapter 7 concludes the work by illustrating the results obtained from a large amount of experimental work.

Chapter 2

Experimental

This chapter describes the equipment and techniques used in the study of copper and copper oxide surfaces and is divided into the tools of surface science and catalytic reaction measurements. These two areas are combined in a special ultra high vacuum (UHV) chamber which was designed for this purpose. Crucial to field of surface science is the need for UHV. This requirement stems from the contamination of a surface which can occur by gas adsorption. From the kinetic theory of gases, the number of gas molecules which adsorb onto a surface can be estimated. There will be an equilibrium concentration of gas molecules which adsorb from the gas phase and molecules which desorb from the surface, defined by

$$[n_a]_{gas} \underset{k'}{\overset{k}{\Leftrightarrow}} [n_a]_{surface}.$$

The rate of adsorption onto the surface is proportional to the flux of gas, F, colliding onto the surface,

$$F = k[n_a]_{gas}$$

where $[n_a]_{gas}$ is the concentration of gas in mol/m^3, k is the frequency of a gas molecule colliding with the surface in $m^{-2}s^{-1}$ and comes from the kinetic theory,

$$k = \alpha\left(\frac{RT}{2\pi M_a}\right)^{1/2}$$

where α is a sticking probability, R is the gas constant (8.314 J/mol K), T is the thermodynamic temperature in K, and M_a is the molecular weight of the gas in kg.

The concentration of molecules on the surface is then the flux of gas onto the surface times an equilibrium time, *t*, before desorption,

$$[n_a]_{surface} = F\,t.$$

The equilibrium time is an exponential function of the heat of adsorption of the gas, E_{ads}, onto the surface,

$$t = t_o \exp(E_{ads} / RT).$$

Substituting the equation for the flux of gas molecules onto the surface into the equation for concentration of molecules remaining on the surface and simplifying, one obtains a relationship between concentration of surface species and gas pressure, P_a

$$[n_a]_{surface} = \alpha\left(\frac{RT}{2\pi M_a}\right)^{1/2}[n_a]_{gas}\,T_o \exp(E_{ads} / RT)$$

$$[n_a]_{surface} = \alpha\frac{RT[n_a]_{gas}}{(2\pi M_a RT)^{1/2}}T_o \exp(E_{ads} / RT)$$

$$[n_a]_{surface} = P_a\alpha\frac{N_a}{(2\pi M_a RT)^{1/2}}T_o \exp(E_{ads} / RT)$$

where N_a is Avagadro's number (6.023×10^{23}) and $P_aN_a = RT[n_a]_{gas}$.

Using realistic numbers to calculate the concentration of CO adsorbed on a copper surface with $P_a = 10^2$ Pa, $\alpha = 0.1$, $T_o = 10^{-12}$, $E_{ads} = 80$ kJ/mol, and T = 300 K, the surface concentration of CO would be 3.8×10^{20} molecules/cm^2. A typical metal surface has only 10^{15} sites in 1 cm^2, so the surface would be covered by 100,000 layers deep! This result is misleading because the sticking probability of CO on top of a preexisting CO layer is much smaller than $\alpha = 0.1$. The result does, however, illustrate the need for UHV, because even with the use of better models, under atmospheric pressures every surface is covered with adsorbed gas. In UHV pressures of 10^{-10} Torr, surfaces stay free of adsorbed gases for many hours. The additional benefit of working in UHV is the long mean free path of particles in the chamber. Surface scientists use thermal, ion, and electron spectroscopies to study a surface where the emitting species must travel through the gas phase into a detector. The mean free path in 10^{-10} Torr is approximately 1 km, indicating that particles will collide with the walls of the chamber before interacting with any other species.

In contrast to surface science and UHV experiments, catalytic measurements are made under high pressures where frequent collisions between gases and the surface are desired. A catalytic reaction can be viewed as a series of events on a surface: adsorption, surface diffusion, rearrangement, reaction, and desorption. A common reaction mechanism is the Langmuir-Hinshelwood [96] which equates the rate of a reaction with the coverage of species on the surface,

$$r_R = K * \prod_{i=1}^{n} \Theta_i$$

where r_R is the rate of reaction, K is the rate constant, and Θ_i is the surface coverage of ith species. The surface coverage, Θ_i, is obtained from the rate of adsorption and desorption of the species from a surface. The rates are expressed as

$$r_a = k_a * P_i$$
$$r_d = k_d * \Theta_i$$

where r_a is rate of adsorption, r_d is the rate of desorption, k_a is the adsorption rate constant, k_d is the desorption rate constant, and P_i is the pressure of ith species. At equilibrium, the rate of adsorption will equal the rate of desorption making the coverage proportional to the pressure,

$$\Theta_i = k_i P_i \quad \text{where } k_i = {}^{k_a}\!/_{k_d}.$$

When more than one species is present, the coverage must be solved simultaneously for all species and placed into the rate equation. Any species which has a large k_a will be adsorbed on the surface during the reaction and affect the overall reaction rate.

2.1. Experimental Apparatus

2.1.1. UHV Chamber

All of the experiments presented in this thesis were performed in one stainless steel manufactured ultrahigh vacuum chamber by MDC. The chamber is depicted in Figure 2.1. The chamber is equipped with a double pass cylindrical mirror electron energy analyzer with an integral electron gun, a Perkin Elmer 04-458 dual anode x-ray source, a Varian 981-2043 sputter ion gun, a Varian 4-grid low energy electron diffraction optics, a UTI 100c quadrupole mass spectrometer, a copper deposition source, two variable leak valves, and an external atmospheric reaction cell. The chamber is pumped by a liquid nitrogen

cold trapped Varian VH-6 oil diffusion pump and a Varian titanium sublimation pump. Santovac 5, a polyphenyl ether, was used in the diffusion pump. The chamber has a base pressure of $2x10^{-10}$ Torr. All pressures reported in this thesis were made by a Granville Phillips nude ionization gauge and are uncorrected for individual gas sensitivity.

This chamber was originally designed by Ken Lewis for studies of vanadium oxide on gold [97]. It has been modified to be able to perform catalytic studies. The chamber differs from both the standard surface analysis chamber and the combined internal atmospheric reaction cell-UHV chamber in three ways: an external high pressure reactor, a transfer system designed for resistive heating of the sample, and a off-axis manipulator to allow the use of many surface science techniques in one UHV chamber

2.1.2. High Pressure Reaction Cell

First, by having the reaction cell external to the chamber, reaction gases are kept from degrading the vacuum in the chamber. An internal reaction cell exposes the chamber to any gases that have been adsorbed on the walls of the cell. Slowly over time, an equilibrium will be reached of adsorption-desorption from the walls. With many experiments, that equilibrium raises the chamber's base pressure requiring a "bake-out" (discussed in section 2.1.5) to re-establish ultrahigh vacuum. Because the reaction cell is external and separated from the chamber by a gate valve, there is no gradual desorption of gas into the chamber. Only during the transfer of the sample is the chamber exposed to gases from the reaction cell. The pressure in the chamber rapidly returns to its base pressure. There is a very long time period for degradation of the vacuum in the chamber by sample transfer.

The high pressure cell is a 6 way cross depicted in figure 2.1. The ports are occupied by 1) gate valve to the chamber, 2) rear viewport, 3) sample entrance gate valve, 4) front viewport, 5) sample manipulator, and 6) gate valve to roughing pump. The

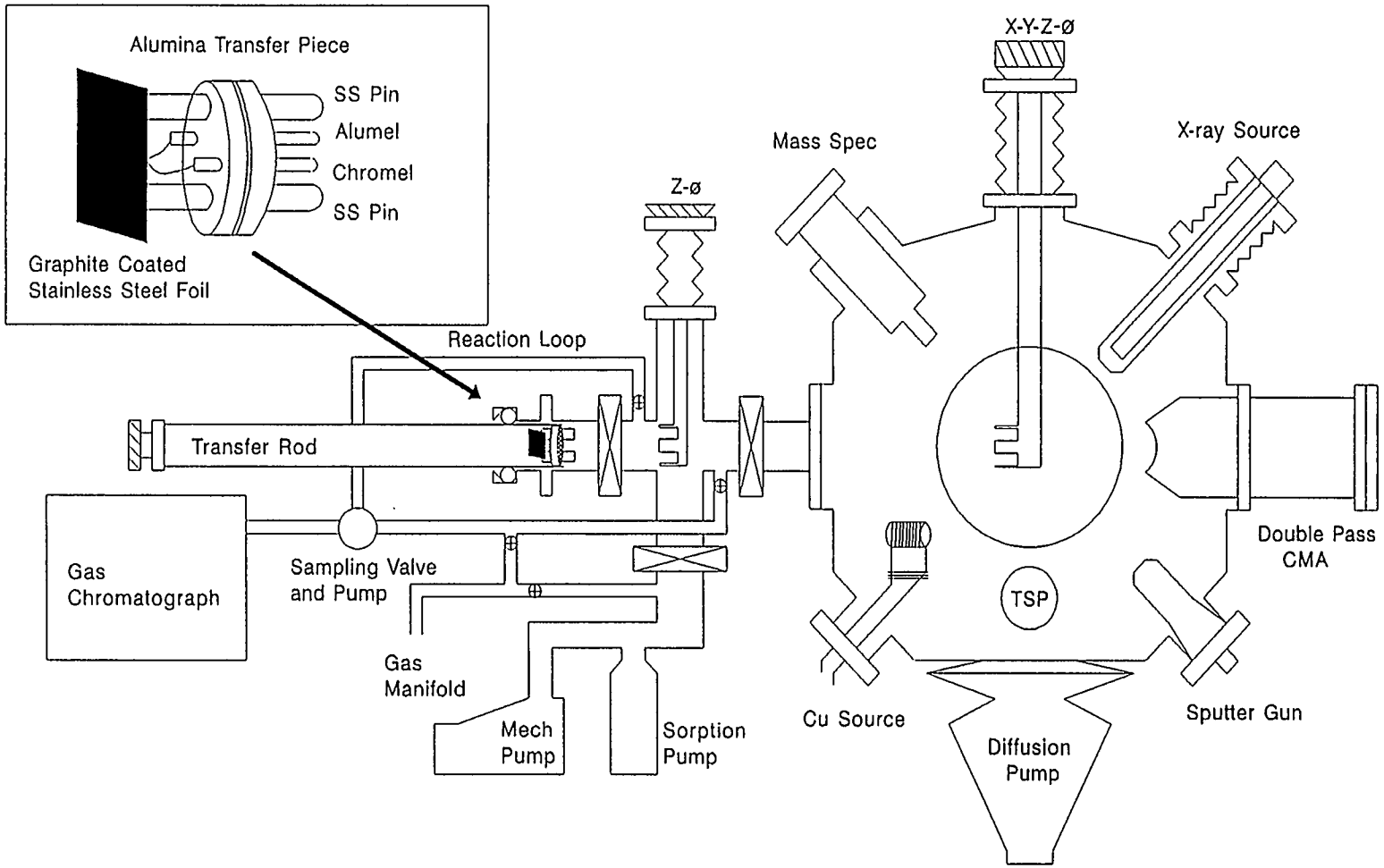

Figure 2.1. Drawing of the combined UHV chamber - high pressure cell apparatus used in these experiments. The inlet shows the sample transfer piece and how the sample is mounted.

volume is 680 ml and can withstand a pressure of 2 atm. The maximum pressure attainable is limited by the pressure the viewports can withstand. The viewports are necessary for placing the sample into the high pressure cell manipulator. The manipulator can be moved upward to allow the sample to be transferred into vacuum and has a set of mating pins in a ceramic block for insertion of the sample. Gas enters the cell from a spacer flange in front of the sample face. A thermocouple gauge is attached to the high pressure cell on the same flange to monitor the pumping down of the cell and the gas handling manifold. The gas exits through a pipe attached to a second spacer flange above the roughing pump gate valve. The direction of gas flow is over the face of the sample and is controlled a by recirculating pump. The rate of flow at 1 atm. can be controlled between 200 and 10 cm^3/s. An automatic sampling loop is in series with the recirculating pump. The limiting vacuum of the roughing pumps is 10 mTorr, and with the cell open to the chamber, the chamber's base pressure rises to $1x10^{-8}$ Torr. The limit to the chamber pressure, when the gate valve to the cell is open, is due to water from the high pressure cell as it is not baked out.

2.1.3. Transfer System

Secondly, the design of the transfer system is unique. The sample is shuttled on a transfer piece which consists of four pins in a cylindrical alumina holder shown in the inlet of figure 2.1. Two large pins are stainless steel across which the sample is mounted and resistively heated. The other two small pins are alumel and chromel making a type K thermocouple. 5 mil alumel and chromel wires extend from the pins and are joined on the backside of the sample. Part of each pin is threaded allowing for locking nuts to hold the pin in the alumina holder. The alumina holder has a stainless steel ring welded around its' circumference for gripping by the transfer rod. The transfer rod has an opening mouth which closes on to the transfer piece. The stainless steel ring fits into a groove inside the

transfer rod mouth in order to pull the sample from the manipulator. The transfer piece pins fit snugly into mating receptacles on the UHV manipulator and the reaction cell manipulator. Most commercially designed transfer systems are not designed for heating of a sample. In some cases, they can be modified for either electron beam heating or radiative heating in UHV but these can not be used in an atmosphere of gas.

2.1.4. Manipulator

Lastly, by not having an internal reaction cell, the manipulator can be of the off axis type. The manipulator depicted in figure 2.1 has the sample mounted at the end of the arm. This manipulator has five potential degrees of freedom: x, y, and z translation, Θ rotation, and *P* flip (not engaged.) An internal cell requires an on axis manipulator in order for the reaction cell to enclose the sample. An on axis manipulator has only one degree of freedom: Θ rotation. The value of having more degrees of freedom in a manipulator is the ability to position the sample at the optimal focal point of more than one surface science tool. For the on axis manipulator, the surface science tools must be on movable bellows to bring them to the focal point of the sample and must be in the same horizontal plane to prevent an oval projection of the sample.

2.1.5. UHV practice

Periodic maintenance of equipment inside the chamber requires the breaking of vacuum. This is done by backfilling the chamber with Ar. The gate valve between the high pressure cell and the chamber is opened in order to use the gas manifold manometer. The chamber is filled with slightly over one atmosphere of Ar prior to the removal of any equipment from the chamber. Ar is used instead of N_2 as it can be obtained dry (without water), is denser than air, and is easily pumped out. When a chamber is opened,

contamination from atmospheric pressure water and oxygen is to be avoided as they can damage electron multipliers inside the chamber. Additionally their adsorption on the walls of the chamber limits the lowest base pressure obtainable in the chamber.

Vacuum is broken to either repair a piece of equipment under vacuum or to add a piece of equipment. It is then important to assure that no contaminants or non-UHV compatible materials are placed in the chamber. A common example of a contaminant to be avoided is oil. Oil has a significant vapor pressure at room temperature. In UHV, oil will vaporize, and due to the long mean free path, will cover the internal surfaces of the chamber. It will dissociate on hot filaments forming carbon deposits through out the chamber. Carbon will in turn lead to charging problems as well as alter the properties of the surface under study. To avoid problems like these, everything to be placed in UHV must be thoroughly cleaned. Cleaning consists of many cycles of rinsing with acetone, washing with water, ultrasonic agitation in methanol, and heating with dry air. Methanol and drying should be the last steps to assure no impurities from the acetone or water are placed on the equipment.

During every breakage of vacuum, there will be some water and oxygen which enters the chamber. In order to regain UHV, the chamber must be placed under vacuum and "baked out". Baking out is the act of heating the walls of the chamber to remove any adsorbed gas. This chamber was heated to 170°C for 40 hours to desorb contaminants and then cooled to room temperature before use.

2.2. Surface Science Techniques

The purpose of this section is describe the techniques of surface science used in this research so that the reader will be able to understand the results which are obtained. A working view point as opposed to a theoretical one will be taken in describing how each

technique is of value. As an example both Auger electron spectroscopy and X-ray photoelectron spectroscopy can both be used to determine the elemental composition of a surface, but Auger spectra are easier to acquire, requiring less time, and the technique is more sensitive. Therefore, x-ray photoelectron spectroscopy will not be discussed as a means of elemental composition but rather for its ability to determine the oxidation state of an atom on a surface, which can not be done by Auger electron spectroscopy. In addition to these techniques, temperature desorption spectroscopy and ion scattering spectroscopy will also be discussed. Although not a technique of surface science, the deposition of copper in UHV will be discussed as it does occur in vacuum and is different from other methods for the deposition of metal. But before any technique can be described the method of data acquisition will be described.

2.2.1. Data Acquisition

Data acquisition was performed using an IBM AT personal computer and a Techmar Labmaster Interface. The Labmaster is a computer board which plugs into an expansion slot in the AT. It has 2 digital to analog (D/A) outputs, 16 analog to digital (A/D) inputs, 40 timer/pulse counting (TTL) connections, and 24 lines for 3 (x8) communication ports. The board operates at 60 kHz and has direct memory access for storage of large quantities of data. The connections between the board and the analytical instruments is made through an external interface box in which all lines have BNC connections. Each input line has a zener diode in series which will break down at greater than 10 volts to prevent damage to the Labmaster. The Labmaster is controlled using ASYST Data Acquisition Software. ASYST is a programming environment which contains pre-defined functions that allow the user to control the functions of the data acquisition board and to manipulate, display, retrieve, and store data. Programs for AES, XPS, and TDS already existed prior to this work and were modified and improved for this

experimental setup. A description of each program will be given with the description of the individual surface science techniques.

2.2.2. Auger Electron Spectroscopy

Auger Electron Spectroscopy (AES) is the most common surface science technique and is used to determine the elemental composition of a surface. AES is a three electron process, depicted in figure 2.2, where the first electron (a core electron) is removed by a high energy electron incident on the surface. The vacancy formed is filled by a second electron from a higher energy orbital. The energy released in filling the vacancy is transferred to a third electron, which can then escape into the vacuum. As the quantization of energy

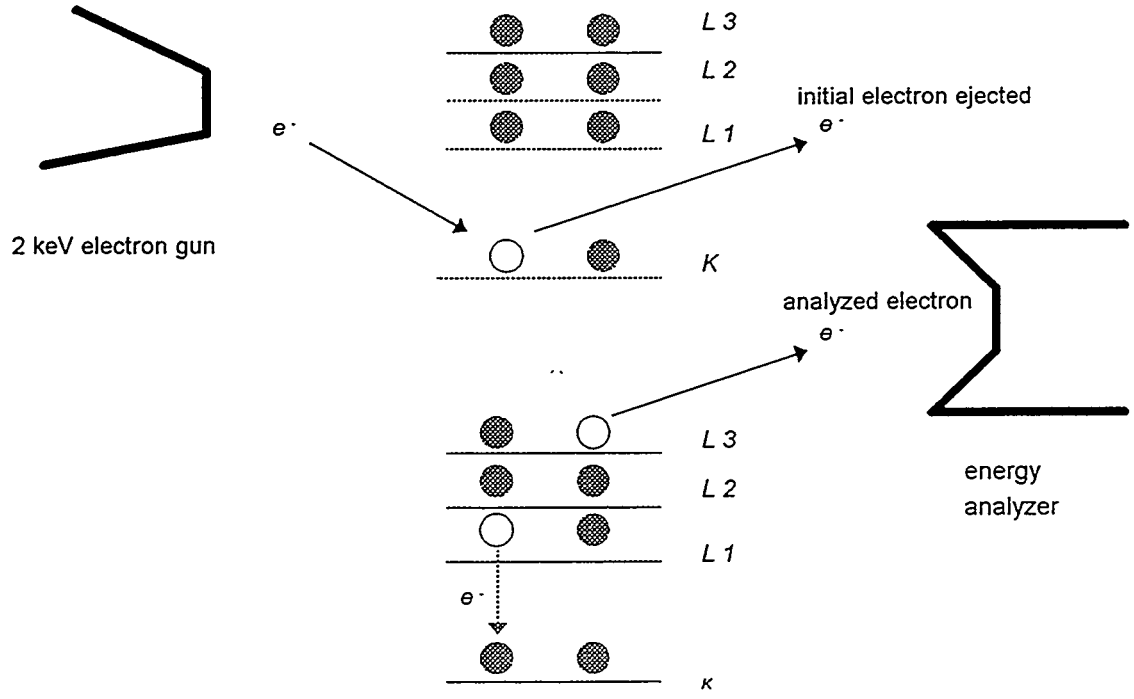

Figure 2.2. Schematic of the Auger process.

levels is characteristic to every atom in the periodic table, the kinetic energy of the ejected electron will be characteristic of the atom from which it came and can be expressed by the following equation

$$K.E. = (B.E._1 - B.E._2) - B.E._3 + \Phi,$$

where K.E. is the kinetic energy, B.E. is the binding energy of each level, and Φ is the work function of the spectrometer. Depending on the initial form of ionization and the experimentally determined cross sections for each atom, AES is sensitive to 1% of a monolayer (10^{13} atoms) and can quantitatively determine the composition of a surface [98]. Table 2.1 lists the kinetic energies of the elements found in this study for use as reference to the data presented later [99]. The values are approximate and will vary depending both on the system from which the spectrum is acquired and the energy of the peak. The resolution of AES is 0.7% of the kinetic energy, so at higher energies the absolute resolution becomes poorer [100].

Table 2.1. Alphabetical listing of elements found in the AES spectra and their most intense transitions [99].

Element	Kinetic Energy in eV
Al	68
Ar	215
Au	43/69, 141/150/160, 239/255
C	272
Cl	181
Cr	36, 489/529/571
Cu	61, 776/849/920
Fe	47, 598/651/703
K	252
Mo	28, 161/186/221
N	381
Ni	61, 716/783/848
O	510
Pt	43/64, 150/158/168,
S	217/237/251
Si	152
Ta	92
	26, 166/171/179

The experimental setup for AES using a CMA is shown in figure 2.3. It is important to note how a spectrum is acquired. In AES electrons are energy selected by ramping a negative potential on the outer cylinder while keeping the inner cylinder at ground potential. Only electrons within an energy window will travel through the CMA without colliding with the walls. The energy range is decided by the peak to peak voltage which rides on top of the outer cylinder voltage ramp and is oscillated at a fixed frequency set by the locking amplifier. The electrons are accelerated into an electron multiplier (in this case a Channeltron). The electron multiplier electrically floats and is referenced to the inner cylinder. The multiplication voltage is placed between the front of the multiplier (- sign) and the cascade (+ sign). Finally the formed electron cloud is accelerated into the collector which is slightly higher in potential than the cascade. The current generated goes through a DC filter, thereby removing the electron multiplier voltage, to a pre-amplifier which converts the current to a voltage for the lock-in amplifier. The lock-in then makes a measurement of the voltage in phase with the frequency of the peak to peak voltage. That measurement along with the energy of the ramp on the outer cylinder are the y and x axis of an AES.

The ASYST program is designed to operate the ramp on the outer cylinder and accept the output signal from the lock-in amplifier. The CMA analyzer control accepts a 0-10 V computer generated input which will equal a 0 to 4000 V output to the outer cylinder. The outer cylinder ramp is created by the program which inputs the starting and ending energies, the number of data points in between, and the time of data acquisition at each point. The computer accepts an input voltage from the lock-in amplifier at each data point. The voltages to the analyzer control and from the lock-in are converted to kinetic energy and counts for an XY spectra displayed in figure 2.4. Data was typically acquiredusing a 2 keV primary electron beam with a 1 mA emission current and

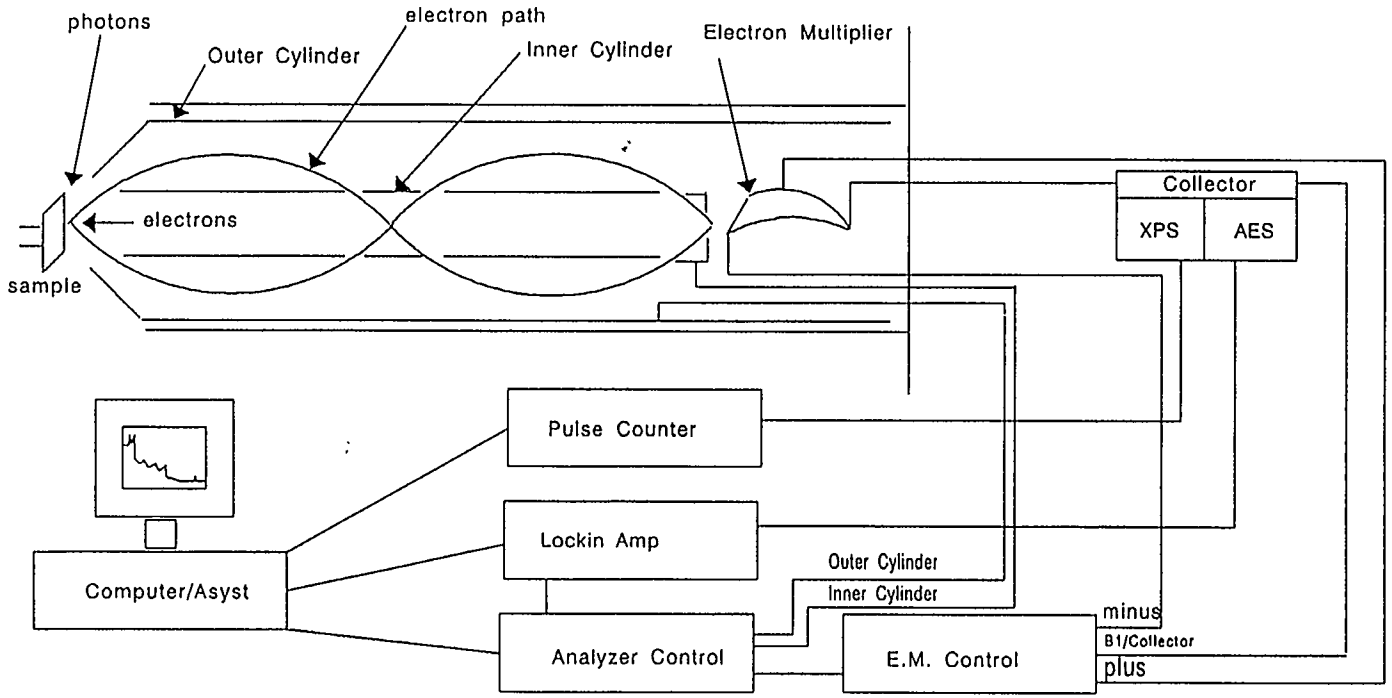

Figure 2.3. A schematic of the CMA and the equipment setup to operate the CMA.

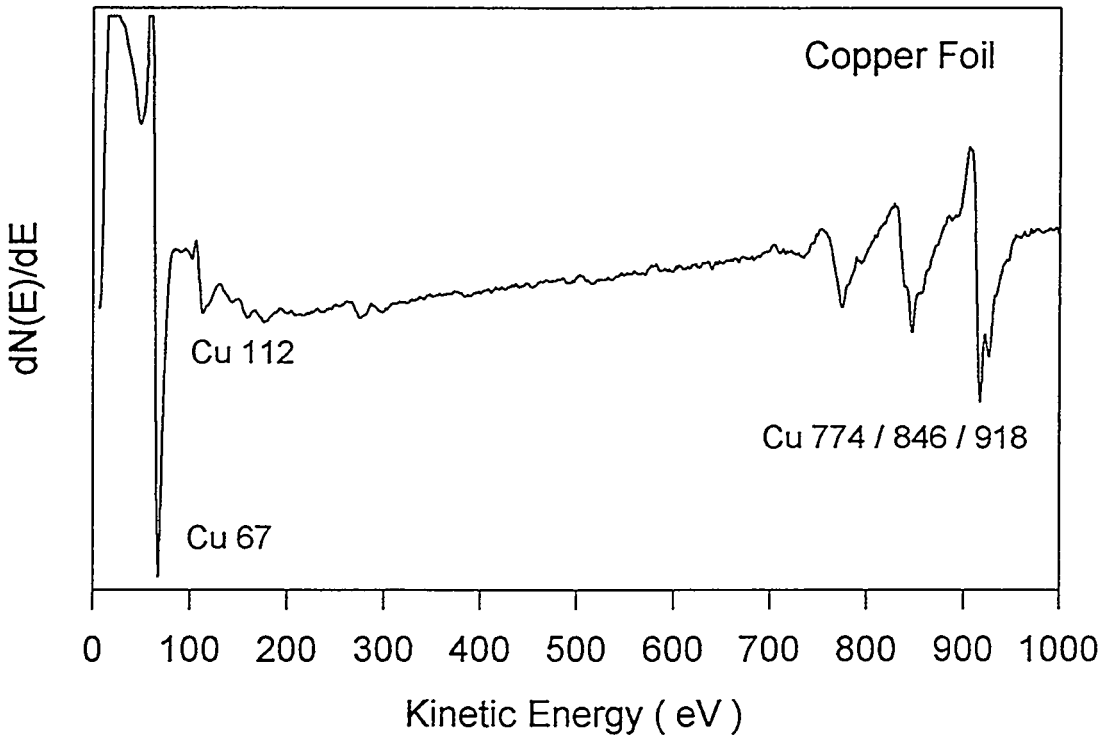

Figure 2.4. A representative AES of a copper foil. The most intense peaks are labeled.

approximately a 30 uA beam current. The analyzer had a 4 V peak to peak modulation at 3 kHz and was scanned at 100 ms per eV from 1 to 1000 eV. A sample spectrum of a clean copper foil is shown in figure 2.4.

2.2.3. X-ray Photoelectron Spectroscopy

X-ray Photoelectron Spectroscopy (XPS) is used to determine the oxidation state of atoms on a surface. In XPS, an x-ray is used to eject a core level electron and the binding energy of the electron is different for each oxidation state of an atom. This is schematically shown in figure 2.5. In reality we measure the kinetic energy of the ejected electron which can be related back to the binding energy by

$$E_b = h\nu - E_k - \Phi \pm R,$$

where E_b is the binding energy of the core level, *hv* is the energy of the x-ray photon, E_k is the kinetic energy of the ejected electron, Φ is the work function of the spectrometer, and R is a relaxation term. When the oxidation state of an atom changes, there is a shift in the binding energies of the remaining electrons to shield the nuclear charge. This will change the observable kinetic energy of the ejected electron.

It should be noted why AES is not sensitive to oxidation state changes while XPS is sensitive. First and most importantly, AES uses an electron to eject the core electron. Electron sources are not monochromatic making the error in calculating a binding energy larger than an observable shift due to a change in oxidation state. A typical width in energies from an electron gun at 1500 V is 5-10 eV as compared to an x-ray with a natural line width of a 0.4-1 ev [101]. Secondly even if a very monochromatic high energy electron can be used, AES uses the difference between levels which may be unchanged as

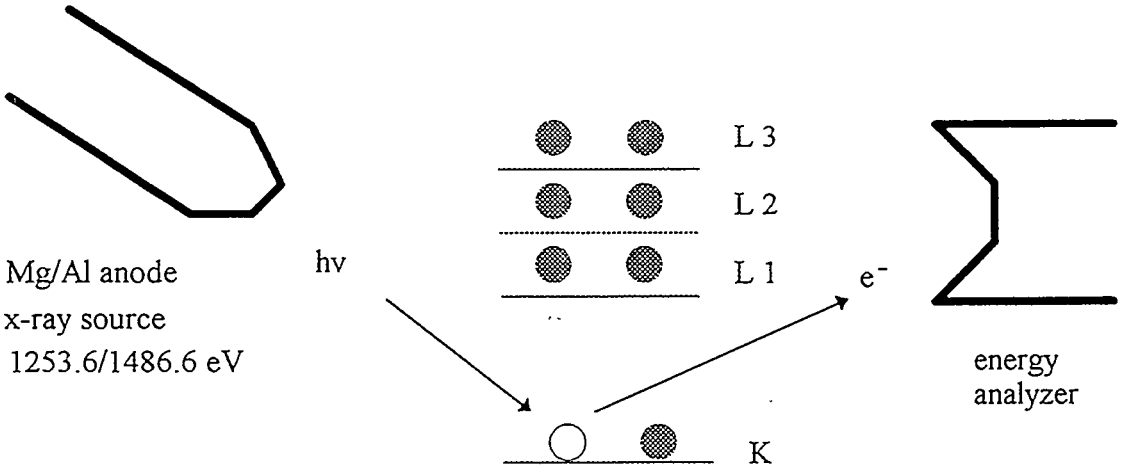

Figure 2.5. A schematic of the XPS process.

both levels may shift equally upon oxidation. If the level shift differently from a change in oxidation state the difference would be small making the measurement difficult.

The XPS experiment also uses the CMA as the energy selective detector but in a manner different from AES. The CMA is used in a retarding field mode where a voltage is placed on both the inner and outer cylinders. There is a potential difference between the inner and outer cylinders which is the pass energy. The resolution in XPS is determined by 0.7% times the pass energy [100]. The effect of the pass energy on the resolution and intensity of XPS can be seen in figure 2.6. Electrons are energy selected by ramping both cylinders with an increasing negative potential while maintaining the pass energy. The electron multiplier is operated in a manner similar to AES with two exceptions and both are due to the increased resolution of XPS resulting in lower signal intensity. The first being that the electron multiplier is run at a higher potential in XPS to increase the gain. This is still insufficient to make an analog measurement. The second exception being the signal is pulse counted. When sufficient current is built up, a TTL (true test logic) pulse is sent to the computer and the number of pulses within a scanning interval are summed. This manifests itself in higher counts at higher binding energies (lower kinetic energies) and can be seen in the XPS example spectrum in figure 2.7.

The ASYST program was designed to operate the ramp on the outer cylinder (and therefore the inner cylinder as well) and to pulse count at each energy. Again, similar to AES, a 0-10 V computer generated output is sent to the CMA analyzer control which converts this a 0-1800 eV energy range. The range of energies to be scanned is different in XPS than AES. The computer generated ramp is determined by inputting both the beginning and ending energies, the number of points to be acquired, and the length of time for data acquisition at each point. The number of scans to be acquired is also inputted as signal averaging is needed in XPS. The computer records the number of TTL pulses at each energy point and stores it until the end of the scan. At the end of each scan the program displays the sum of all scans up to that time. A plot of counts versus kinetic

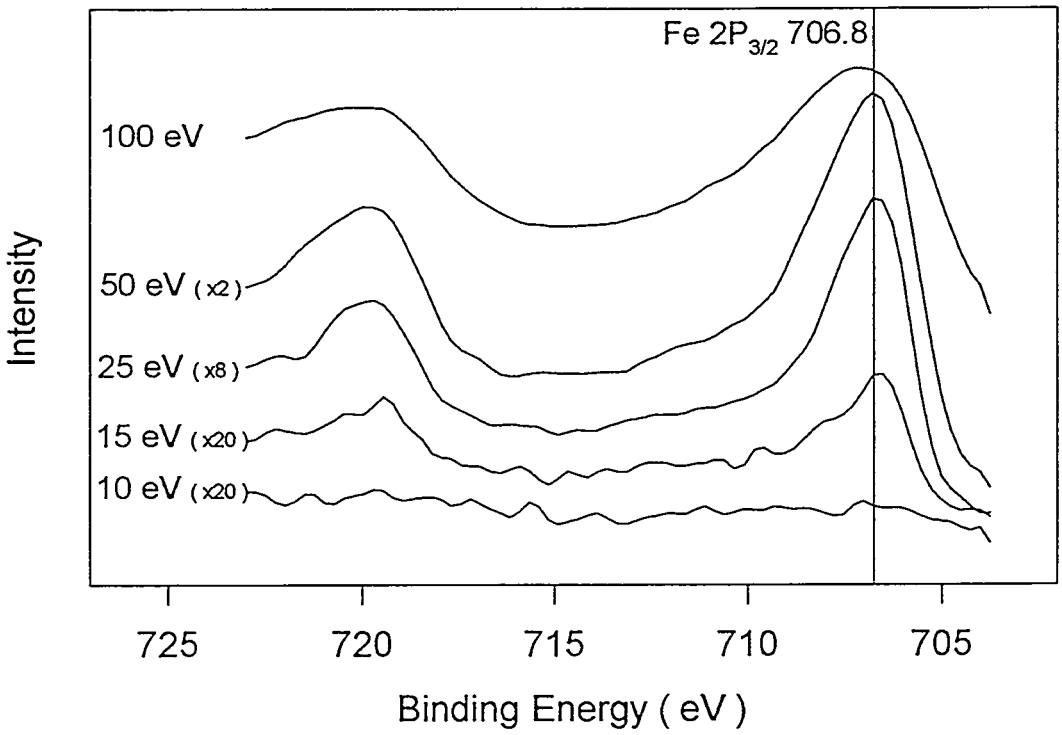

Figure 2.6. XPS of the Fe $2P_{3/2}$ peak at different CMA pass energies to determine the optimal combination of resolution and signal.

energy is displayed. Other software is used to convert the kinetic energy to a binding energy. The data can be stored either as an ASYST or an ASCII data file for later manipulation. The XPS program also has the ability to manipulate acquired data, load previous data, and to manipulate and store AES data.

There are two standard conditions for acquiring XPS data: a utility mode and a high resolution mode. In both modes, the x-ray source is run at 400 W of power using either the Mg anode ($h\nu$ = 1253.6 eV) or the Al anode ($h\nu$ = 1486.6 eV) and an electron multiplier potential of 3000 V. In the utility mode, the pass energy was 200 eV and data was taken over a 1000 eV range every 1 eV for 200 msec. In the high resolution mode, the pass energy was 25 eV and data was acquired over a 50-100 eV range every 0.25 eV. The energy ranges measured depended on the species to be observed. Table 2.2 list the common species observed and their energy range in both kinetic and binding energy [102].

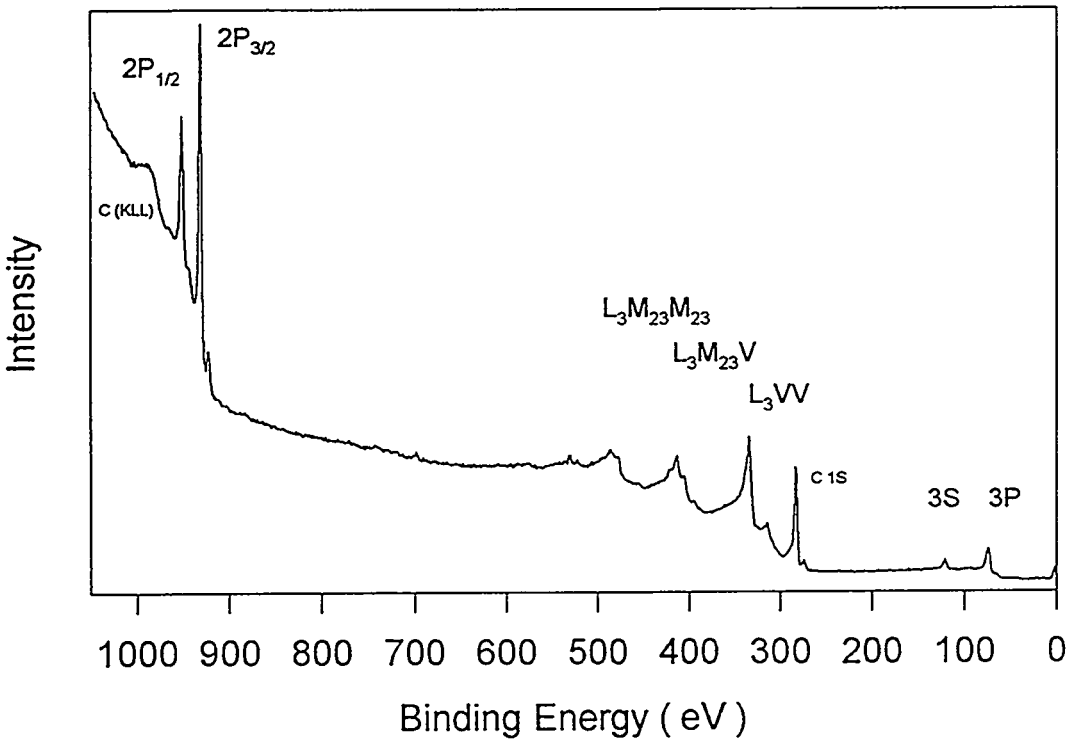

Figure 2.7. A representative XPS of copper deposited on graphite. The most intense peaks are labeled.

Table 2.2. Alphabetical listing of elements found in the XPS spectra, their binding energies (in eV) and the corresponding kinetic energy (in eV) range scanned by the CMA.

Element and orbital	Peak Binding Energies	Kinetic Energy range (with Mg anode)
Al 2P	73	1150-1200
Au 4F	87/84	1150-1200
C 1S	284	940-990
Cr 2P	583/574	650-700
Cu 2P	953/933	280-330
Cu LVV	335	890-940
Fe 2P	719/706	520-570
Mo 3D	231/228	1000-1050
O 1S	531	700-750
Pt 4F	74/71	1150-1200
Si 2P	99	1125-1175

XPS can readily distinguish between the different oxidation states of copper. Figure 2.8 shows both the Cu 2P region and the Cu LVV region. The Cu LVV peaks are Auger peaks where the incident x-ray ejects the core electron to begin the Auger process. Auger peaks induced by x-rays can be sensitive to changes in oxidation states if there is a significant difference between energy levels. The LVV peak shows a very large shift in kinetic energy when copper is oxidized from 0 to +1. The shift is 2 eV. The 2P region does not show a large shift when copper is oxidized from 0 to +1, but can be used to distinguish between Cu^{+1} and Cu^{+2}. Cu^{+2} has a very characteristic spectrum where the normal XPS peaks are accompanied by shake-up peaks. A shake-up peak occurs when a paramagnetic element losses an electron and the final state of the ion is not the ground state. In the expression to calculate the binding energy of an electron from the measured kinetic energy, there is a term for the relaxation of the atom. When Cu^{+2} losses an electron, it can excite (negative relaxation) a 3d to 4s transition [103] which requires 8.4 eV causing the appearance of a second peak at higher binding energies. This occurs for both the $2P_{3/2}$ and $2P_{1/2}$ peaks. The intensity ratio of the shake-up peak to the normal XPS peak is a constant value. The extent of oxidation between Cu^{+1} and Cu^{+2} can be determined by measuring the amount of the shake-up peaks relative to the intensity of the 2P peaks. The extent of oxidation between Cu^{0} and Cu^{+1} must be determined by measuring the amount of either the XPS or AES O signal.

2.2.4. Electron Mean Free Path in Solids

Common to both AES and XPS is the measurement of electrons which escape from the surface of the solid. The probability that an electron will be ejected into the vacuum is a function of the energy of that electron and the amount of surface through which it must pass. The relationship between electron energy and escape depth from the

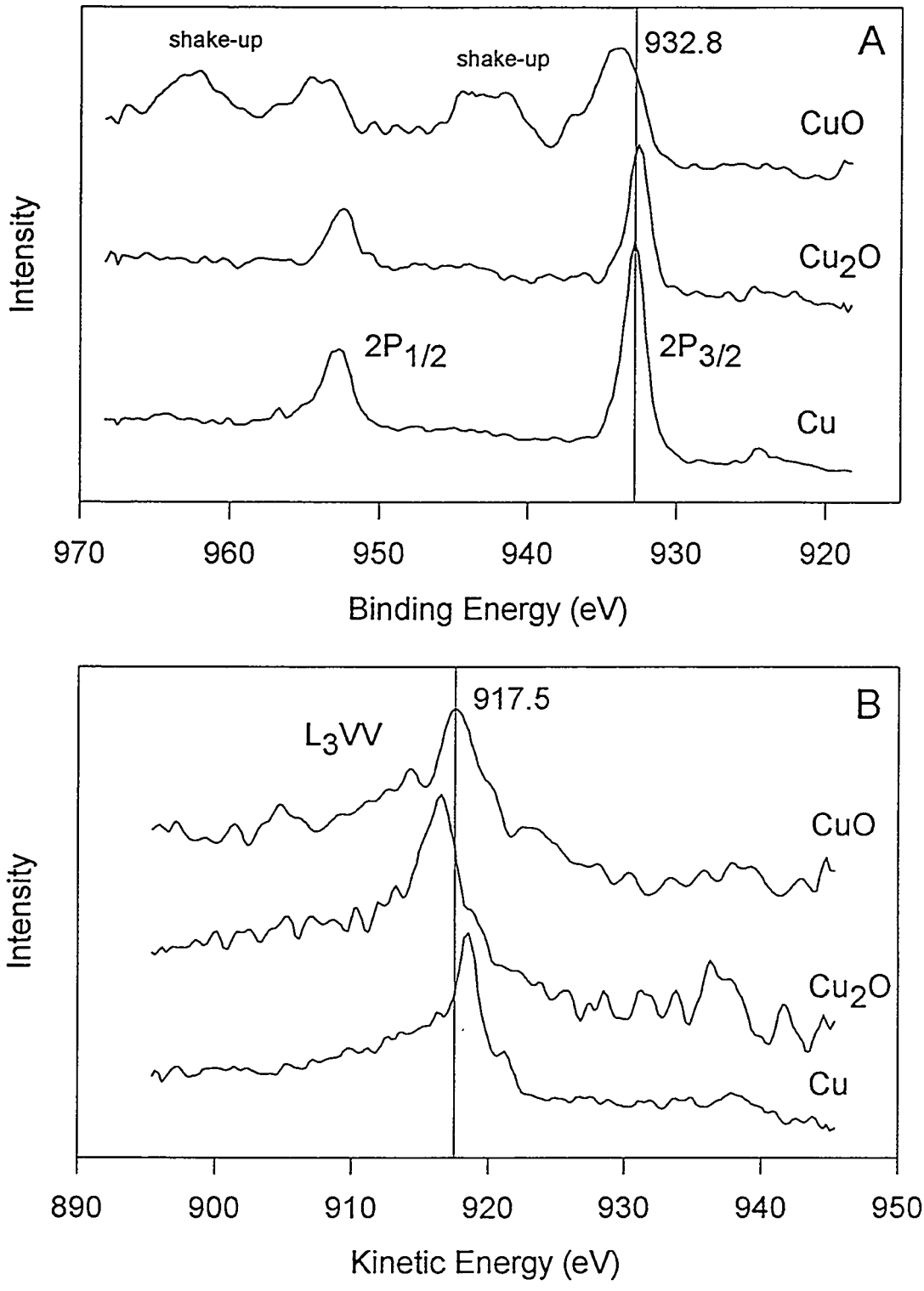

Figure 2.8. A) Cu 2P region and B) Cu LVV region for copper, copper(I) oxide, and copper (II) oxide. These spectra are used as reference.

surface is not linear, but curves. The shape of this curve, shown in figure 2.9, is independent of the solid from which the electron escapes, hence it is called the Universal Curve of electron escape depths. Seah and Dench [104] fitted the universal curve to an analytical expression for the inelastic mean free path of an electron in a solid as a function of its energy. The result was

$$\lambda_n = 143 \times E^{-2} + 0.054 \times E^{½}$$

where λ_n is the distance in nanometers and E is the energy in electron volts.

The importance of this equation is that it calculates the distance an electron can travel in the solid without undergoing a loss in energy. The loss in energy can occur by many processes making the energy loss difficult to use as a measure of the surface electronic properties. Another way to view the usefulness of the universal curve is that electrons far in the solid will not escape into the vacuum to be measured.

The electron energy range used in AES and XPS gives a penetration depth into the surface between 5 and 20 Å. This can be useful in determining if alloying of a deposited surface film occurs or if bulk impurities segregate to the surface. A comparison of the intensity of peaks at different energies can be used to distinguish where an atom is in the surface region. As an example Cu has AES peaks at 61 and 920 eV. The 61 eV peak has a path length of 5 Å and the 920 eV peak has a path length of 17 Å. If 10 Å of Fe is deposited onto a pure Cu surface, the 61 eV electron would not escape through the Fe layer whereas the 920 eV would escape. By watching the decrease in the Cu 61 eV peak signal, we can observe the growth of the Fe film. As the iron film continues to grow, the Cu 920 eV peak would also be attenuated until the Fe film thickness is greater than the Cu 920 escape depth when no signal would be observed. On the other hand if an Fe film does not cover the Cu surface but alloys instead, the Cu 61 eV peak would be observed

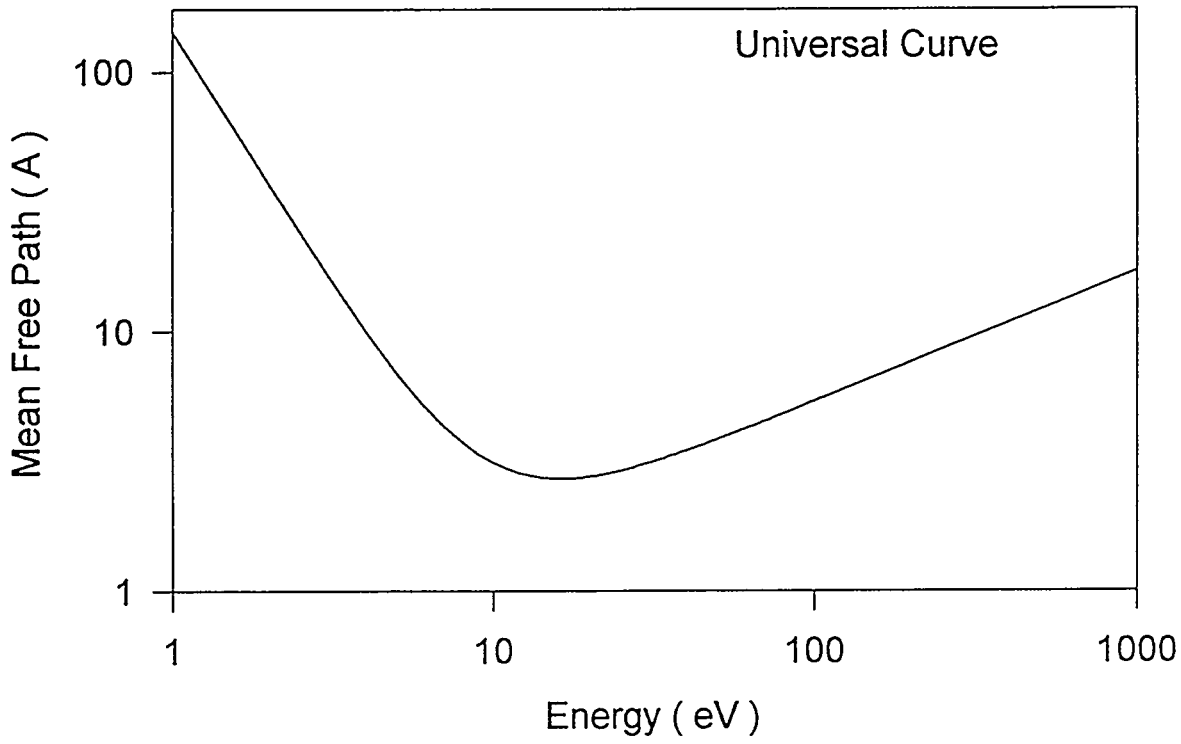

Figure 2.9. The Universal curve for the inelastic mean free path of an electron in a solid as a function of electron energy calculated from the equation of Seah and Dench [104].

throughout the growth process. Both Cu 61 eV and 920 eV peaks would decrease in intensity during Fe deposition due to a dilution effect.

The observations of how the emitted electrons from a solid are attenuated by film growth can provide structural information on the growing deposited film. This is commonly called an Auger uptake curve [105]. A plot of peak intensity for both the solid and the film as a function of film deposition can be used to determine if the film is growing layer-by-layer (Frank & van der Merwe), a monolayer followed by multilayer islands, (Stranski & Krastanov), or multilayer islands alone (Volmer & Weber). Figure 2.10 shows qualitatively what would be observed in the Auger uptake curves for each growth mode. The distinct breaks are indicators that a monolayer has been formed. It will be shown that Cu on Fe grows in a layer-by-layer manner, while on carbon it forms multilayer islands. An uptake curve of Cu on Al_2O_3 does not give conclusive evidence for

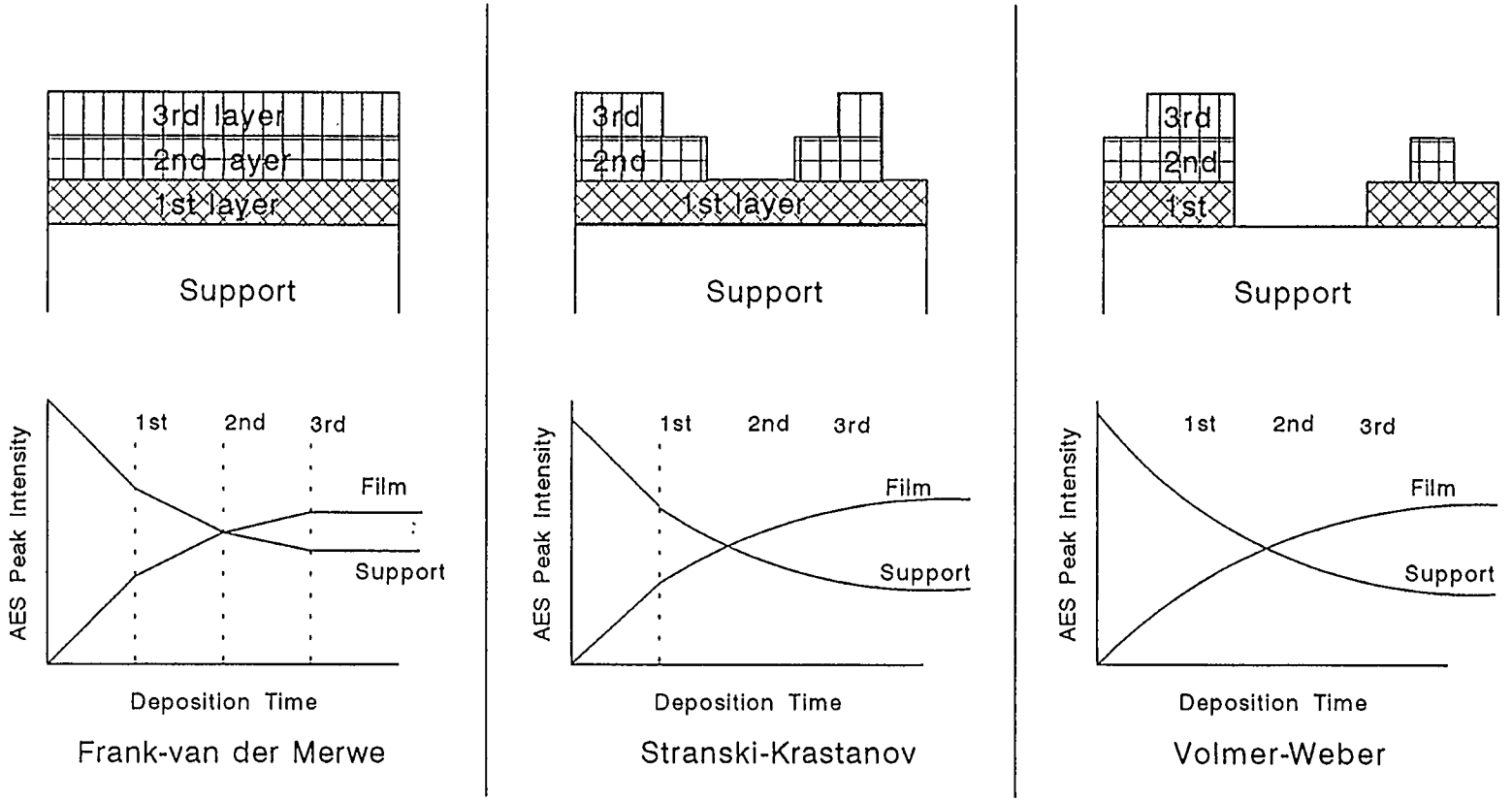

Figure 2.10. Growth models and the corresponding AES uptake curves.

monolayer followed by islands or islanding alone growth, so other techniques like low energy ion scattering spectroscopy are needed to compliment the uptake curves.

2.2.5. Low Energy Ion Scattering Spectroscopy

Low energy ion scattering spectroscopy (LEIS) is the most surface sensitive technique used to characterize a surface. Unlike AES and XPS which have sampling depths of a few angstroms, LEIS only probes the outermost layer. LEIS can be viewed as a classical energy and momentum transfer problem in physics. An ion of known mass and energy is collided with the surface. Assuming a short range large interaction between the ion and an atom in the surface, then the collision can be viewed as a two body collision. The ion will bounce off of the surface atom both elastically and inelastically. Energy and momentum will be transferred into the surface atom and the ion will recoil with less energy and new momentum. The loss in energy of the ion can be measured and used to calculate the mass of the surface atom from which it collided. The relationship between energy of the ion and the masses of the two bodies is

$$\frac{E}{E_o} = \frac{1}{\left(1 + {M_1}/{M_2}\right)^2}\left[\cos\theta \pm \left(\left({M_1}/{M_2}\right)^2 - \sin^2\theta\right)^{1/2}\right]^2$$

where E_o is the initial energy of the ion, E is the final energy, M_1 is the mass of the ion, M_2 is the mass of the surface atom, and θ is the scattering angle relative to the incident trajectory. This is schematically shown in figure 2.11. This equation simplifies when the

scattering angle is 90° to

$$\frac{E}{E_o} = \frac{M_1/M_2 - 1}{M_1/M_2 + 1}.$$

With an increasing mass of the surface atom, the collision becomes less inelastic and the ratio of E/E_0 goes to 1. At the other extreme, no mass less than the ion mass can be observed and the ratio of E/E_0 goes to 0.5. If the mass of the ion is greater than the surface atom or if the energy of the ion is too great, damage to the surface will occur. This damage can be used as a tool for the removal of material from the surface and is referred to as surface sputtering.

In practice a 500 V He ion is used to scatter off of the surface. He^+ is sensitive to all atoms with the exception of hydrogen and deuterium. Vurens gives a detailed description of how a CMA can be used to energy select positive ions [106]. Briefly, the CMA is converted to energy select positive ions by using 2 300 V batteries to create a 600 V bias on the outer and inner cylinders. The CMA is operated in the retarding field mode with a 200 eV pass energy similar to XPS. The cylinders are ramped with an increasing negative potential causing the retarding field to be less positive. Scanning goes from $E/E_0 = 1$ to $E/E_0 = 0.5$. The signal is pulse counted. A sample spectra is shown in figure 2.12. The scattering angle was not 90° thus explaining the discrepancy between the measured E/E_0 and the expected values. LEIS can be a very quantitative tool which can provide structural information as well as compositional information if the sample is a well ordered single crystal. Because in this research the surface will be amorphous, LEIS is only used as a qualitative tool to determine the composition of the outermost surface.

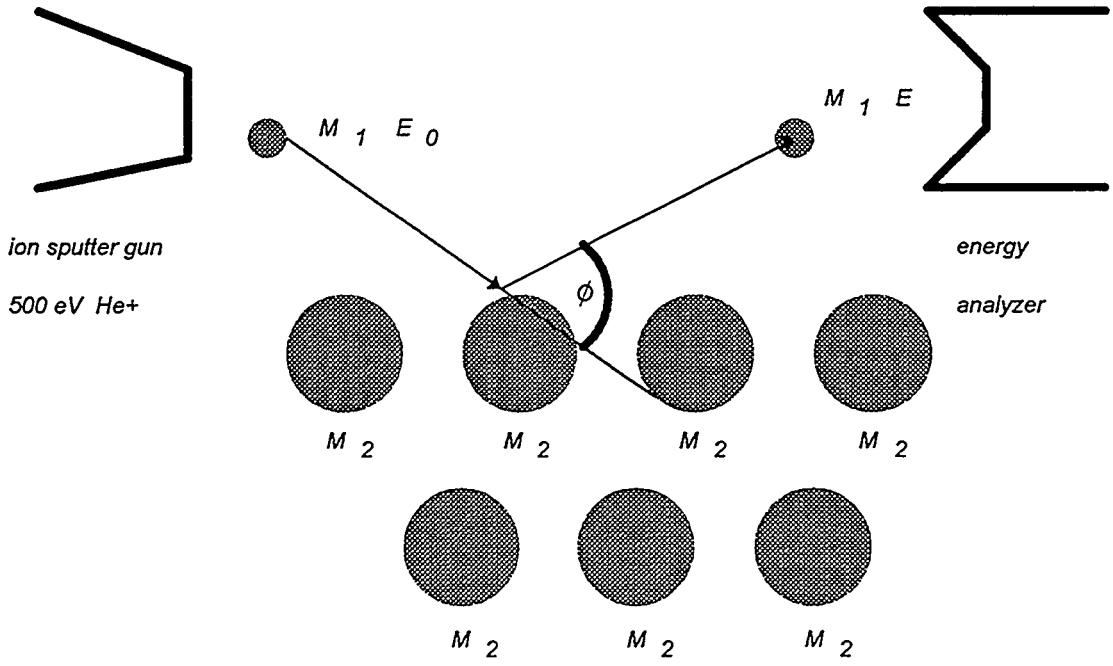

Figure 2.11. A schematic of the ISS process.

2.2.6. Temperature Desorption Spectroscopy

Temperature desorption spectroscopy (TDS) is used to study adsorbed species on a surface. It is sensitive to the number of species on a surface as well as the energetics of the surface adsorbate bond. It can be used to determine what has adsorbed on a surface during a reaction or as a means of measuring surface sites.

In the TDS experiment, the surface is heated to desorb any surface species which then are measured by mass spectrometry. The temperature at which the maximum number of species desorbed can be related to the heat of desorption through a Redhead analysis [96]. The Redhead analysis assumes a very fast pumping speed to remove desorbing gas and a linear heating rate. These assumptions are valid in a UHV experiment. Depending on the order of desorption, the heat of desorption is calculated by varying the linear heating rate and observing how the temperature of maximum desorption varies. This can

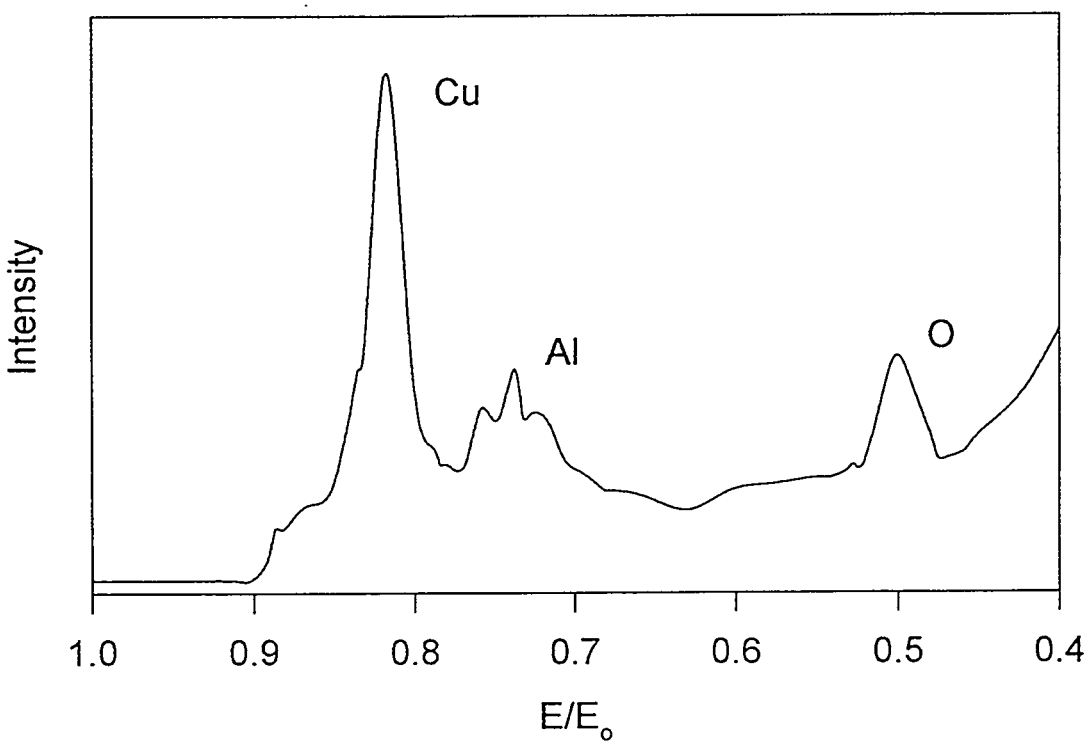

Figure 2.12. A representative ISS for Cu deposited on Al_2O_3.

be seen in the Redhead equation

$$\frac{E_d}{RT_p^2} = \frac{\nu n \sigma^{n-1}}{\beta} \exp\left(\frac{-E_d}{RT_p}\right)$$

or

$$Ln(\beta) = \frac{-E_d}{RT_p} + \left[Ln\left(\nu n \sigma^{n-1}\right) - Ln\left(\frac{E_d}{RT_p^2}\right)\right]$$

where E_d is the heat of desorption, T_p is the temperature of maximum desorption, R is the gas constant, ν is the frequency of desorption, n is the order of desorption, σ is the surface

coverage, and β is the heating rate. If instead one assumes a value for the frequency of desorption, typically 10^{13} s^{-1}, the heat of desorption can be calculated from one experiment.

The order of desorption is related to the process of desorption. If hydrogen gas dissociatively adsorbs on a metal surface, when it desorbs the H atoms must recombined prior to desorption. This is an example of a second order desorption because it requires two steps in the process. Carbon monoxide does not dissociate on most metal surfaces when it adsorbs, so when it desorbs from a surface it has a first order dependence. The order of desorption can be seen in the shape of the desorption peak as a function of coverage. A first order peak will be asymmetrically shaped and the T_p will not change with coverage. The asymmetry results from nearest neighbor interactions. A second order peak will be symmetrically shaped and will shift to lower temperatures with increasing coverage. The shifting to lower temperatures comes from the increased probability that each site will have a nearest neighbor with which to desorb.

Very often TDS is used as a measure of the number of exposed surface sites. Assuming that each adsorbing molecule covers a number of surface atoms, the concentration of desorbing molecules will be proportional to the number of surface atoms. In a supported catalyst the surface area of deposited metal particles is not known. By adsorbing a probe molecule onto the metal surface and then desorbing it, one can determine the surface area of the metal particles. This technique is better than a simple BET (Bruanaer, Emmit, Teller) isotherm, because the probe molecule may be specific to a particular surface. Carbon monoxide is a typical probe molecule because it can only adsorb onto metal sites. Hence it would not measure the surface area of the support. Additionally, the temperature at which CO desorbs will vary with the type of metal to which it has adsorbed, so it can be used to determine the area of two or more different metal sites. In this thesis acetonitrile (CH_3CN) was used to determine the surface area of

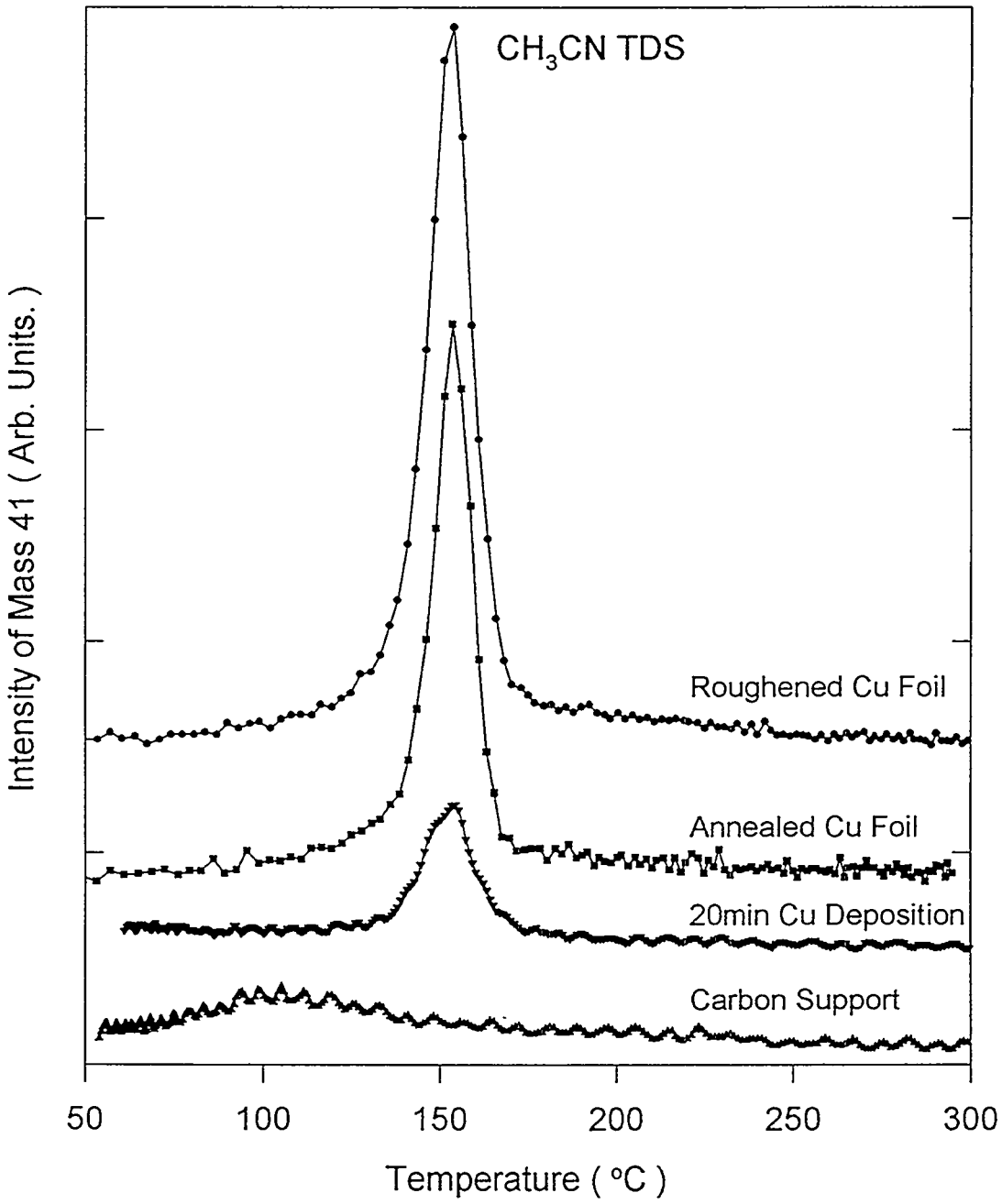

Figure 2.13. A representative TDS of CH_3CN desorption from copper.

deposited Cu atoms on graphite. Figure 2.13 shows the TDS of CH_3CN desorbing from graphite, a 20 minute deposition of Cu on graphite, an annealed 1 cm^2 Cu foil and a roughened 1 cm^2 Cu foil. The roughened foil has the greatest surface area and the peak is the most intense. Comparing the area under the annealed foil and the 20 minute deposition, the surface area of the 20 minute deposition can be estimated at 0.45 cm^2.

TDS can also be used to determine what, if any species have adsorbed on a surface during a reaction. After a catalytic run the sample would be transferred back into UHV and heated in front of the mass spectrometer to desorb any remaining surface species. It is known that CO_2 deactivates CO oxidation, but it is not known if the deactivation is due to CO_2 adsorption on the surface, $CuCO_3$ formation or CO_2 decomposition back into reactants. Chapter 5 addresses this question, so at the end of the reaction it is important to measure the amount of CO_2 which has adsorbed, if any.

2.2.7. Copper Deposition

Copper was deposited by evaporation from an alumina crucible. An alumina crucible was used because wrapping a hot tungsten filament with a copper wire would have lead to alloying of copper with tungsten. Alloying causes a eutectic in the melting point which lowers the temperature at which the wire will break. The lifetime of a tungsten filament source is limited by the rate of alloying and was too short for the amount of copper deposited in these experiments. The copper source, shown in figure 2.14, consists of the crucible, an alumina encasing, and a tantalum faceplate with a 0.75 cm^2 opening. The source is mounted on a bellows which lowers the crucible from behind a Ta shield down to the plane of the sample. The crucible was heated to 1500°C by passing current through tungsten wire wrapped around the outside. The alumina encasing is used to increase the heating of the crucible while preventing radiative heating of the chamber.

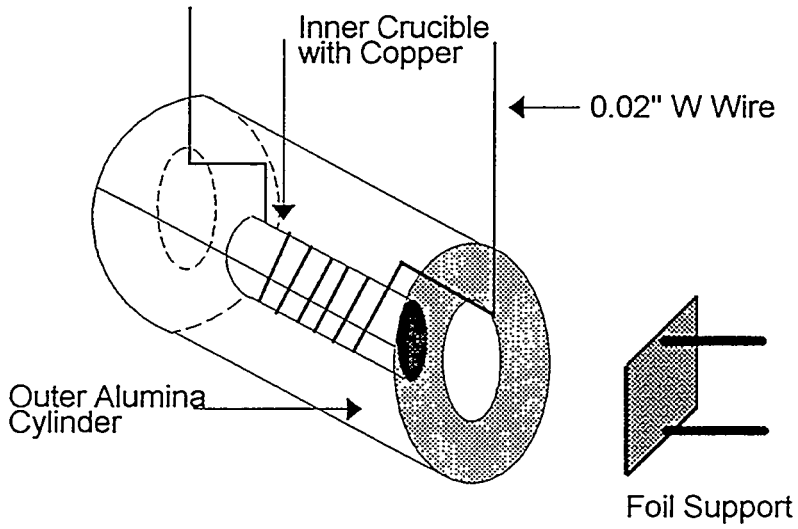

Figure 2.14. Drawing of the source used to deposit copper in these experiments.

The crucible was heated for 20 min. prior to deposition to assure a steady flux of copper atoms. The rate of flux can be controlled by changing the current through the tungsten wire An AES uptake curve of Cu deposited onto a pure Fe foil at 3 different filament currents is shown in figure 2.15. The distinct breaks can be seen at Cu/Fe ratios of 2.5, 0.7, and 0.3 in each curve and clearly demonstrates layer by layer growth. A 7.5 amp current was used in depositing copper resulting in a deposition rate of approximately 0.5 monolayers per minute . The deposition of 10 monolayers of metallic copper was the first stage in the preparation of all of the copper catalysts used in these experiments unless otherwise stated

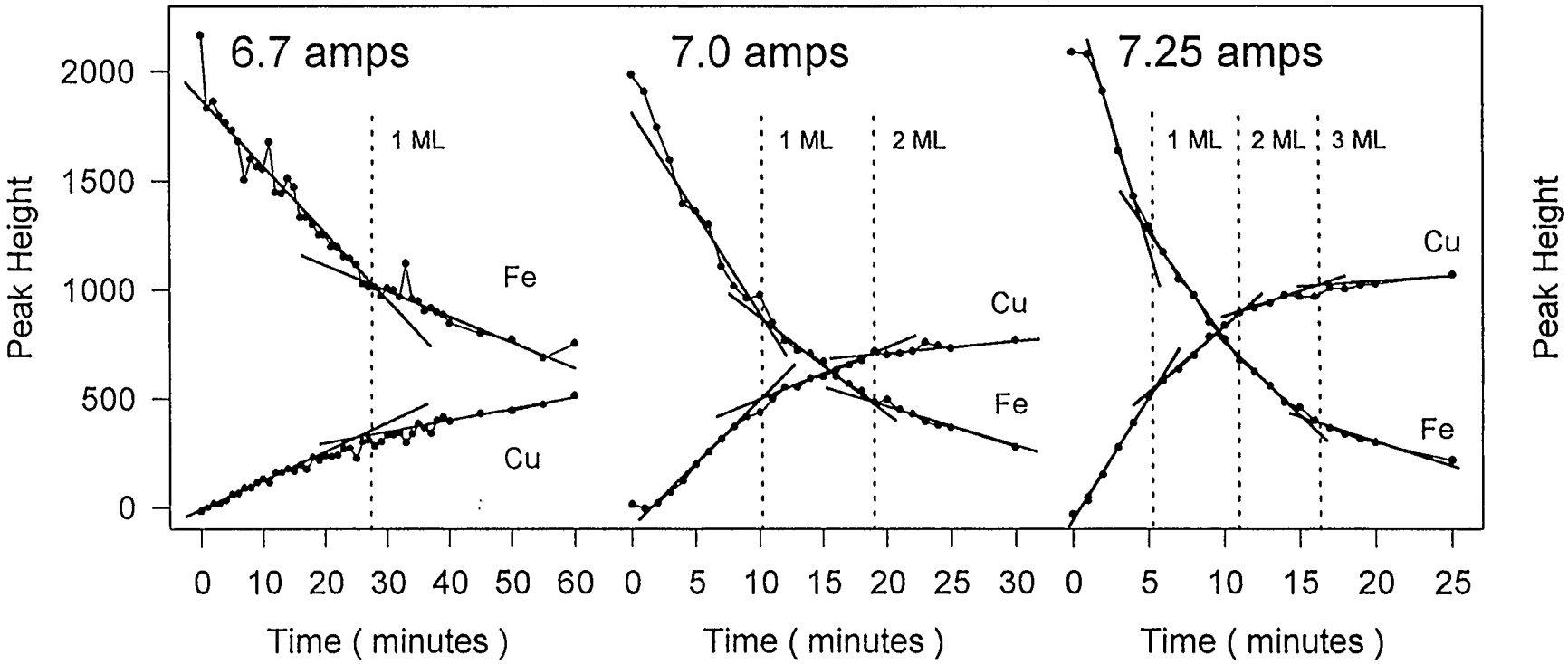

Figure 2.15. AES uptake curves to determine the flux of copper onto an iron foil from the copper source at different heating currents.

2.3. Catalytic Reactions

Crucial to the ability to characterize a surface is the ability to measure catalytic activity on the surface. Reactions are run over all surfaces prepared in this thesis to characterize a surface's ability to catalyze the oxidation of CO to CO_2. The conditions under which each catalyst is tested is described in chapters 3 and 4, and the reaction conditions range between 200-400°C, 100-760 Torr total pressure, and CO to O_2 ratios of 98/2 to 50/50. The results are presented as the percentage of CO converted to CO_2. Common to all reactions are control of sample temperature and measurement of the gas composition by chromatography for kinetic rates and activation energy determination. These will be discussed shortly, but before that, gas purification and gas mixing will be discussed as special precautions were taken to avoid problems in these areas.

2.3.1. Gases

An impurity of 1 part in 1000 in 100 Torr of gas can deactivate a 1 cm^2 surface by irreversibly adsorbing on the surface. Therefore, before any gas can be used for a catalytic reaction, any impurities must be removed. This is especially a problem with the use of CO. CO (Airco grade 2.3) will form $Fe(CO)_5$ in the standard gas cylinder under the high pressures of the gas cylinder. $Fe(CO)_5$ will decompose at temperatures greater than 150 °C and deposit Fe atoms on a catalyst surface. To avoid this $Fe(CO)_5$ was trapped with a 5 Å molecular sieve trap in a liquid nitrogen bath. At 77K, $Fe(CO)_5$ will form an ice. At these temperature CO still has a sufficient vapor pressure to be useful for reactions. O_2 (Airco grade 2.6) was not purified as its main impurities were inert gases. In the oxidation and reduction studies in chapters 5 and 6, CO_2 and NO are used. CO_2 (Airco bone dry) is only 99.8% pure with the main impurities being N_2, O_2, and CH_4. The impurity of O_2

was found to be 0.1% using gas chromatography. Attempts to remove the O_2 impurity, as it might interfere with the oxidation measurements, were made by condensing the CO_2 at dry ice/acetone temperatures and pumping away the gas phase O_2. This was unsuccessful, so the CO_2 was used without any trapping. NO (Matheson C.P.) is only 99.0% pure with the main impurities being N_2 and other oxides of nitrogen. The NO was purified by condensing the gas in a 5 Å molecular sieve trap in a liquid nitrogen bath. The trap was allowed to warm to 130 K where NO melts while the other oxides of nitrogen are still solids. The vapor pressure of NO was used and the remaining N_2 impurity was ignored.

The purified gases were stored in a 1L stainless steel vessel before admittance into the high pressure cell. When catalytic reactions were performed CO and O_2 were premixed in the vessel. CO was placed in the vessel first because of the low pressure of CO due to the trapping process. O_2 was added to the CO in the correct partial pressure to obtain the desired reaction ratio. The pressure of each gas was measured by a Wallace and Tiernan differential pressure gauge with a range of 0-4 atm and a sensitivity of 5 Torr. The vessel could be pressurized to 2 atmospheres but was never greater than 1 atmosphere. CO and O_2 were premixed to prevent either gas from preferentially adsorbing on the catalyst surface. As was mentioned in the introduction, O_2 inhibits CO adsorption on a Cu surface. Once gas was admitted into the high pressure cell, the gases were recirculated at 100 cm^3/min using a metal bellows vacuum pump from Cole Palmer, and the sample was heated to reaction temperature.

2.3.2. Sample Heating

The sample was resistively heated using a Eurotherm temperature controller. The controller maintained the sample temperature to within 1°C over the 2 hour length of a reaction. The sample was brought to reaction temperature from room temperature within

4 minutes. The slow rise to reaction temperature was done to prevent the exothermic nature of the reaction from carrying the sample temperature above the desired temperature. Additionally, heating of the sample too quickly in the pressure of gas has on occasion blown the support. During the initial rise in temperature, the reaction is not monitored, but the gas phase composition is measured 30 seconds after the reaction temperature is reached and used as the initial gas composition.

2.3.3. Gas Chromatography

In order to make kinetic measurements, the progress of the reaction must be monitored as a function of time. This is done by analyzing the reaction gas composition at precise time intervals using gas chromatography. Gas chromatography is the separation of a gas mixture into individual components by passing the gas over a solid material. The solid material is placed in a quartz or metal tube and is referred to as a column. The column separates the gas mixture by a combination of physical and chemical properties. Parameters like gas flow rate and column temperature determine how well the gas mixture is separated and how fast the gases elute off of the column. The separated gases are then quantitatively measured after eluting from the column. The following describes the conditions of gas sampling from the reaction, the column conditions used to separate the gas, and the detection of gas.

2.3.4. Gas Sampling

Gas sampling was performed using a VICI Valco Instruments air actuated, 2 position, 6 port valve (A3C6UWP) and a digital valve interface (DVI.) The DVI was used to interface the control of the sampling valve with the gas chromatograph (GC) runs. The sampling valve removed a volume of 1 ml of gas from the reaction cell. A typical

experiment lasted 2 hours and sampling was performed every 11 or 15 minutes removing a total of 12 ml of gas out a total volume of 680 ml. The decrease of less than 2% of the total gas was considered negligible. When longer experiments were run, the sampling time was either doubled or quadrupled to prevent significant gas removal. The sampling volume when being charged with gas becomes part of the recirculating loop of the reactor allowing the gas to continue flowing over the catalyst surface. The time for filling the sampling volume is 1 minute before being sent to the GC and is controlled by the GC.

2.3.5. Chromatographic Conditions

The GC consists of two parts: an integrator and the GC. The integrator is used to begin the GC run and to report the detection of gas. The integrator is a complex strip chart recorder. It contains programs which control the start of a GC run, the delay between GC runs, and the reporting/analysis of gas detection. The display of gas detection comes as peaks as a function of time from the start of the run. The peaks are voltages from the detector as gas elutes off the column through the detector. The integrator determines the time of peak elution, area under each peak, and the width of each peak. The area of the peak is proportional to the concentration of gas through the detector. The detector used in these experiments is a thermal conductivity detector (TCD) and will be discussed shortly.

The GC is made from 4 parts: the electronic controls, the ovens, the column, and the detector. The electronic controls determine the time for sampling valve operations, the temperatures of the ovens, and the sensitivity of the detector. The sampling valve is operated at the start of the GC run to inject gas into the GC and again with 1 minute remaining in the run to charge the sampling valve for the next injection. There are 2 ovens inside the GC. One oven is used to heat the column. At increased column temperatures the gas will elute faster. Because we wish to balance good separation of gases and speed,

the column temperature is typically elevated and ramped as a function of time. In these experiments, the column oven was run at 120°C or at 105°C and not ramped. The second oven heats the detector. As gas elutes off the column it will enter the detector. If the detector is colder than the column, gas may condense. In the case of a TCD, the detector temperature is also important to the sensitivity. The TCD temperature is held constant at 225°C. The column used in these experiments is a Carboxen 1000 (Supelco). A He carrier gas is used to carry the gas mixture through the column. This column is specially designed to separate permanent gases and light hydrocarbons. The column is used to separate mixtures of O_2, N_2, NO, CO, and CO_2. The gases are flowed over the column at a pressure of 35 psig., a rate of 40 ml/min, and a temperature of 105 or 125°C depending on which gases are being separated. Under CO oxidation reactions the column is held at 125°C to elute CO_2 within 10 minutes, but under NO reduction reactions the column is held at 105°C to better separate the gases. Table 2.3 lists the peak elution times and width for the various gases.

Table 2.3. Gas elution times at two temperatures from a Carboxen 1000 GC column.

Gas	Elution time/Peak width (minutes) 105°C	125°C
O_2	2.8 / 0.096	2.3 / 0.082
N_2	3.0 / 0.079	
NO	3.4 / 0.139	
CO	3.6 / 0.209	2.8 / 0.117
CO_2	13.4 / 0.495	9.0 / 0.327

2.3.6. Thermal Conductivity Detector

There are many detectors available to measure the quantity of gas eluting from a chromatographic column. In these studies a thermal conductivity detector (TCD) was used. The TCD consists of 2 hot filaments over one flows the gas and the other is a

reference. As gas passes over the hot filament, heat is conducted away. The difference between the gas sample temperature and the reference temperature is recorded. The amount of heat removed varies with the gas eluting. Table 2.4 lists the thermal conductivity of the gases measured in this work. When calculating the catalytic conversion of CO to CO_2, a correction for the different thermal conductivity is needed. Multiplying the thermal conductivity by the different molecular weights and different peak widths, the heat conducted away by CO_2 will be 1.1 times larger than that for CO. For all reportings of catalytic conversions in this thesis, a corrected CO_2 signal will be used. No correction is needed for the other gases as their molecular weights, peak widths, and thermal conductivites are all similar.

Table 2.4. Thermal conductivity of gases used in this thesis

Gas	x 105 g·cal/(sec·cm^2)(°C/cm)
He	33.60
CO	5.43
CO_2	3.39
N_2	5.68
NO	5.55
O_2	5.70

Chapter 3

Characterization of Supported Catalysts

3.1. Preface

The true benefit surface science brings to catalysis is the ability to characterize the properties of the catalyst's surface, for it is on the catalyst surface where the chemical reaction occurs. By changing the catalyst and the associated properties of the surface, changes in catalytic activity can be observed. A great amount of research has gone into the study of metallic catalysts by surface science in a successful attempt to understand how these catalysts operate [9,108]. Only recently has surface science branched out to study more than simple metal systems. It has begun to study the effect of metal oxide supports and promoters on the metal catalysts [109,110,119]. But prior to this thesis, no model surface science studies have been done on the metal oxide as a catalyst itself. Work has been done on metal oxides as interfaces for electronics but on a limited scale [111].

Surface science studies have had little effect in the study of metal oxides for a number of reasons. First, most surface science techniques probe the electronic properties of the surface. The electronic properties of most metal oxides are poorly understood both theoretically and experimentally at this time [10]. Calculations of bulk band structure for a metal oxide is complicated by such factors as the degree of ionic and covalent bonding, overlap of metal orbitals with oxygen p orbitals, ligand field splittings, assignment of formal charge between mixed valence metal ions, crystal structure, and vacancies or interstitials in the lattice. These same problems exist at the surface and become much

worse due to the asymmetry of the chemical environment for atoms at the surface. A common difficulty in probing the electronic properties is the stability of an ion after the ejection of electron by AES or XPS [112]. The localization of charge changes the chemical environment and thereby affects future electron emission. This is typically seen as charging in the sample or as a relaxation term in the binding energy of the next electron. It is this localization of charge when electrons are being removed and the resistance to future electron removal that explain why most metal oxides are charge gap insulators .

Assuming that the metal oxide is sufficiently conducting such that electron spectroscopies can be done, there is a difficulty associated with the preparation of the metal oxide surface. Studies have shown that a metal oxide crystal cleaved and polished in air versus cleaved in vacuum are different [10]. Depending on the surface cleaved, a metal oxide must redistribute charge at the surface. If the surface is metal terminated, in air it may adsorb oxygen or in vacuum change oxidation states. Likewise, an oxygen terminated surface may desorb oxygen or change coordination at the surface. What is most commonly observed is that the surface has many defects which are a combination of changes in the metal's oxidation state and oxygen coordination [113]. This has led to the proposal that the chemistry of metal oxides may be associated with such defects.

An actual metal oxide catalyst is not a homogeneous single crystal but a structurally complex solid. These solids have large surface areas which will not be visible to electron surface science techniques but would be to adsorption studies. Using probe molecules to determine the properties of a metal oxide is probably the best means currently available to study the surface, but probe molecules are limited. The greatest limitation might be an inability to understand how the probe interacts with the surface. Temperature programmed reaction spectroscopy is a technique not requiring UHV and can be used on a high surface area sample. It works by adsorbing a molecule at a low temperature and slowly heating the catalyst to observe what products are evolved. The

results must be interpreted as to what precursors are present and why the products formed without knowledge of how the surface itself was affected.

The solution to the difficulties associated with metal oxides is to synthesize the metal oxide as part of the study. The following chapter discusses the search for a good support on which to grow copper oxide films. By preparing the metal oxide *in situ* as a thin film, problems associated with the bulk and charging are eliminated. The formation of a film makes possible a uniform distribution of the surface in which defects can be observed. Lastly, it becomes possible to observe only the surface on which a reaction can occur as there are no hidden internal surfaces.

3.2. Introduction

Thin films of metallic copper, copper (I) oxide and copper (II) oxide were prepared on various substrates in an attempt to find a support which would not interfere with either the catalytic or surface science measurements. The substrates tried were oxidized: aluminum, silicon, tantalum, molybdenum, stainless steel, and iron, as well as graphitic carbon. This chapter presents the knowledge gained by studying copper on these supports. In the end, all of the supports studied, with the exception of graphite, developed difficulties preventing their use for kinetic measurements on the different oxidation states of copper. But before discussing each support, it is valuable to mention why the copper oxide catalysts were prepared in this manner.

3.2.1. Unsupported Copper

Previous attempts have been made to grow copper oxides on metallic copper [114-116]. Problems were encountered when copper (II) oxide is formed on the metal. In a

test case, CO oxidation was run over a Cu foil under stoichiometric conditions in a glass test reactor. The orange foil turned black during the run. This is indicative of copper being oxidized to the +2 oxidation state [107]. As the sample was being removed from the reactor, the black copper (II) oxide flaked off of the foil revealing a orange color underneath. This demonstrated that copper (II) oxide does not adhere to metallic copper. Additionally, the thickness of the oxide layer was macroscopic. The growth of copper oxide follows a logarithmic function of time and the mechanism of growth is by copper cation diffusion through the forming oxide layer [117,118]. Attempts to study CO oxidation in which the surface is oxidized can lead to uncertainty in the extent of bulk oxidation. Reduction of a bulk copper oxide as a consequence of surface reactions would also be difficult to observe. As the surface reduces, the mechanism of oxidation does not reverse itself. Copper atoms do not diffuse through the underlying oxide as there is no chemical potential gradient into the oxide during reduction. With reduction, the surface becomes covered and passivated by metallic copper. Bulk reduction is possible through mechanisms which involve the formation of fractures in the solid thereby destroying the crystallinity in the process [115,117]. By having a thin film of copper, the sample can be oxidized and reduced without flaking off of the support, forming uncertain oxidation states, or passivating layers.

3.2.2. Redox Reactions

Many catalytic reactions over metal oxide catalysts are partial or complete oxidations where lattice oxygen is believed to be involved in the process. The mechanism proposed is a redox cycle where lattice oxygen is incorporated into the products and regenerated from the reactants. Attempts to prove that a redox mechanism exists have been ^{18}O labeling studies where either the gas phase reactant or the catalyst is labeled and the other is not [120]. Assuming the catalyst is labeled, a difficulty arises in determining

how the labeled product would be observed. If the reaction did involve a lattice oxygen then with the first turnover of the catalyst, the surface would be depleted of labeled oxygen. The depleted site could be filled either from the gas phase or bulk diffusion. If it is a gas phase regeneration, then the second and all subsequent turnovers would be unlabeled. Therefore one would be attempting to see, in the first fraction of a second, a labeled product in a high background of unlabeled product. This is difficult to do but it can be done in a pulsed system. If the depleted site is filled by bulk diffusion, the catalyst will be consumed in the reaction, and hence is not a catalyst. This can be detected by observing a reduced catalyst at the end of the reaction and by a change in activity with time.

The use of a thin film allows us to determine if there is a change in surface oxygen due to the reaction. Because there is no bulk phase (film thickness of 10 Å), all oxygen is observable by surface science techniques. If the surface is reduced or oxidized during the reaction this can be seen. A bulk sample would provide a reservoir of oxygen which could affect the surface science measurements by diffusing into or out of the surface, masking the overall change in oxidation. For any particular gas phase composition, there will be an equilibrium state between the gas phase oxygen and the surface. This will be demonstrated later in the exposure of metallic copper on graphite to a mixture of CO and O_2.

3.2.3. Electrical Conductivity

As mentioned earlier the electrical properties of most metal oxides make them insulators and prevent electron spectroscopies from being performed on them. The use of a thin catalyst film on a conductive support will minimize any charging problems. Copper oxide was grown on substrates with thin native oxides. The native oxide was grown on the metal support followed by copper deposition and subsequent copper oxidation. The

native oxide typically is partially conductive as there is an excess of metal due to the remaining unoxidized bulk. The electrical vacancies caused by the spectroscopies in copper oxide and the native oxide can be filled from the underlying metal substrate. Therefore although the bulk oxides are insulating, the thin films will not have charging problems because of electron donation from the bulk of the support.

3.2.4. Oxidized Supported Catalysts

The decision to support the catalysts is also beneficial as most catalysts are supported on some high surface area inert oxide. Copper and its oxides used industrially are typically supported on alumina or silica. Prior to copper deposition onto any of the supports, the supports were oxidized for two reasons, the first being a practical one and the second a necessity. The supports were oxidized because when the oxides of copper are to be formed the substrate will also become oxidized. By pre-oxidizing the surface, the surface becomes more resistant to additional oxidation. All of the substrate metals used here are covered with a native oxide which under atmospheric pressure and room temperature does not continue to grow. Extreme conditions are needed to completely oxidize these metals. The necessity of oxidizing the support prior to use was to prevent copper from alloying with the metal of the substrate. Both brass and bronze alloys form from Cu dissolved in Zn and Sn, respectively. An oxide layer on a metal substrate should impede or prevent Cu from diffusing into the solid. Cu could not be deposited on inert supports of Au and Ag as they are completely miscible with Cu and their oxides re not stable. The group VIII noble metals can not be used as supports for Cu as they are active for CO oxidation. This returns us to copper supported on non-transition metal oxides of Al and Si.

3.3. Copper on Al_2O_3/Al

3.3.1. Introduction

Copper on Al_2O_3 has been a well studied system as it has importance to the catalysis and microelectronics industries [111,121-135]. There remain questions about the interfaces of Cu, Cu_2O, and CuO on Al_2O_3 pertaining to their stability and reactivity in various chemical environments. One of the earliest studies, performed by Pierron [130], showed that the activity of a CuO/Al_2O_3 sample varied with catalyst pre-treatment. The *in situ* XRD showed that the highest activity for CO oxidation occurred on a sample where CuO had been reduced to Cu_2O or Cu. Unfortunately XRD is only sensitive to long range crystalline order and was not a good probe of the surface composition. The analysis of CuO on Al_2O_3 is complicated by the formation of a spinel, $CuAl_2O_4$. Friedman [128] observed that CuO/Al_2O_3 did form a spinel structure and that it was a function of Cu weight loading and calcination temperature. At temperatures less than 600°C, separate phases of CuO and Al_2O_3 are more stable than bulk $CuAl_2O_4$ [136], but if the weight loading of Cu was less than 4%, the spinel was stable. For high weight loadings, e.g. 20%, heating at temperatures greater than 900°C resulted in the formation of CuO on $CuAl_2O_4$. Diffuse reflectance spectroscopy was used by Hierl [129] and LoJacono [125] to show the formation of a surface spinel. Cu^{+2} in the spinel will occupy both octahedral and tetrahedral sites, whereas in CuO, Cu ions are only in a single site of distorted tetrahedral geometry. The signal from the octahedral ion was a probe for the extent of spinel formation. This indicated that most if not all CuO/Al_2O_4 industrial catalysts began as the spinel compound.

Prior to use, an industrial catalyst typically goes through a series of reducing and oxidizing pretreatment steps. The activity of the spinel was enhanced by reduction. Laine [121] proposed that reduction led to Cu ions on the Al_2O_3. Ertl [135] and Tikhov [133]

both observed that indeed Cu formed from the reduction of the spinel but that the spinel would reform at lower temperatures than were initial needed to form the bulk spinel. This indicated that Cu possibly remained associated with the Al_2O_3. It is believed that Cu remains attached to the surface through an oxygen bond and is different from a pure Cu sample [137-139]. Tikhov did an extensive IR study of the reduction process of $CuAl_2O_4$ to Cu on Al_2O_3 using CO as a probe molecule [133]. It was observed that a more active Cu was formed from the reduction of the spinel as compared to the reduction of a CuO/Al_2O_3 sample. Combining the fact that lower weight loadings more readily form the spinel with the fact that a reduced spinel has greater activity than CuO/Al_2O_3, one can explain why Huang [124] reported that CO oxidation over CuO/Al_2O_3 to be a structure sensitive reaction. He was observing spinel formation at low weight loadings which gave higher activity upon reduction. When the weight loading was high, the spinel did not form which resulted in less activity upon reduction.

Experiments continue today to understand the interaction of Cu with Al_2O_3 and the compounds which form between the two under reducing and oxidizing conditions. Recent work by Chen [134] has shown that Cu deposited on Al_2O_3 at 95K grows epitaxially for the first monolayer. During growth, EELS can observe the underlying Al-O stretching modes which should not be observable if Cu is interacting with the surface. Epitaxial growth only occurs on a dissimilar substrate when the overlayer forms a more stable bond with the surface than it does with itself. Annealing of the surface to temperatures greater than 500°C resulted in Cu diffusion into the Al_2O_3 without changing the Al-O modes. Guo [111] also observed this but believed that the deposited copper forms a Cu-O surface bond with Cu being in the +1 oxidation state. Guo performed a UPS study that showed the Fermi edge of Cu shifted with increased Cu deposition from 3.2 eV to 2.5 eV, the value of bulk Cu. Both Chen and Guo deposited Cu onto an oxidized Al (111) substrate which was reported by a number of researchers as being

Al_2O_3 [126,131,132]. This gave rise to the question if this is a good model for comparison to the CuO/Al_2O_3 catalysts.

The following sections describe our work to form the various oxidation states of Cu on Al_2O_3 and measure their catalytic ability. We hope to elucidate the chemical nature of Cu on Al_2O_3 under reducing and oxidizing conditions and compare the catalytic results to industrial catalysts. This is valuable because only the work of Pierron [130] was done *in situ* and all others were unable to make measurements of catalytic activity and characterization on the same sample without transfer through air. In the process, we hope to give support to using oxidized Al as a model for Al_2O_3. We studied Cu deposited on oxidized Al foils using AES, XPS, ISS, and catalytic reactions.

3.3.2. Experimental

A 99.999% pure 1 x 1 x 0.005 cm Al foil was oxidized to form the Al_2O_3 substrate. Prior to oxidation the foil was cleaned by sputtering the surface using $5x10^{-5}$ Torr of Ar at 1000 V followed by annealing of the surface at 300°C. The surface was oxidized in $1x10^{-6}$ Torr of O_2 at 300°C for 5 minutes and then annealed at 300°C for 5 minutes. This was reported to generate an alpha Al_2O_3 layer a few atomic spacings in thickness [126,131,132]. Copper was then deposited for 20 minutes (10 ML) onto this surface. The copper was oxidized in various ways to generate different oxidation states of Cu, and these treatments are reported with the results. The catalysts were tested for CO oxidation activity. The tests were performed under a 50/100 Torr CO/O_2 gas mixture at 300°C.

3.3.3. Results/Discussion

The AES of a clean and oxidized Al polycrystalline foil is shown in figure 3.1. Clean Al has a single peak at 72 eV. Upon oxidation two new Al peaks appear at 43 and 60 eV along with an O peak growing in at 510 eV. A small metal peak can still be seen. This indicates the oxide layer is thinner than the mean free path of a 72 eV electron which, from the universal curve, is 8 Å. A 3 minute deposition of copper onto the oxidized aluminum is also shown in figure 3.1. The intensity of the Cu 65 eV peak obscures the Al peaks. There is also an attenuation of the O peak associated with the Al. An AES uptake curve of Cu on oxidized Al plots the Cu 918 eV peak and O 510 peak versus time shown in figure 3.2. An uptake curve using the Al 43 or 60 eV peaks could not be made because they are overlapped by the Cu 65 eV peak. There is a large initial drop in intensity of the O peak followed by a gradual decline. The Cu signal slowly rises with increase deposition time. The curves may have an break at 1.5 minutes which would indicated a monolayer followed by multilayer growth. Because there were not sufficient number of points taken along the curve this can not be used to distinguish monolayer followed by multilayer growth from island formation where no breaks would be observed in the uptake curve.

ISS was performed to determine the growth mode of Cu on Al_2O_3. Figure 3.3 shows the ISS spectra of clean Al, oxidized Al, and a 3 minute deposition and subsequent oxidation of copper on Al_2O_3. Clean Al has only one peak at E/Eo at 0.76. The rising background with decreasing values of E/Eo is due to He^+ that has scattered from elsewhere in the chamber. Oxidized Al has two peaks; the Al peak seen in the clean ISS and a new peak due to O. The O peak is at a lower E/Eo of 0.60 as would be expected from its atomic mass. Upon deposition and oxidation of copper onto the substrate, a copper peak can be seen at E/Eo of 0.85. Intensity from the Al can still be seen. This point is beyond the possible break in the AES uptake curve indicating that a monolayer of copper is not formed over the Al_2O_3. With increasing Cu coverage, a small Al peak can

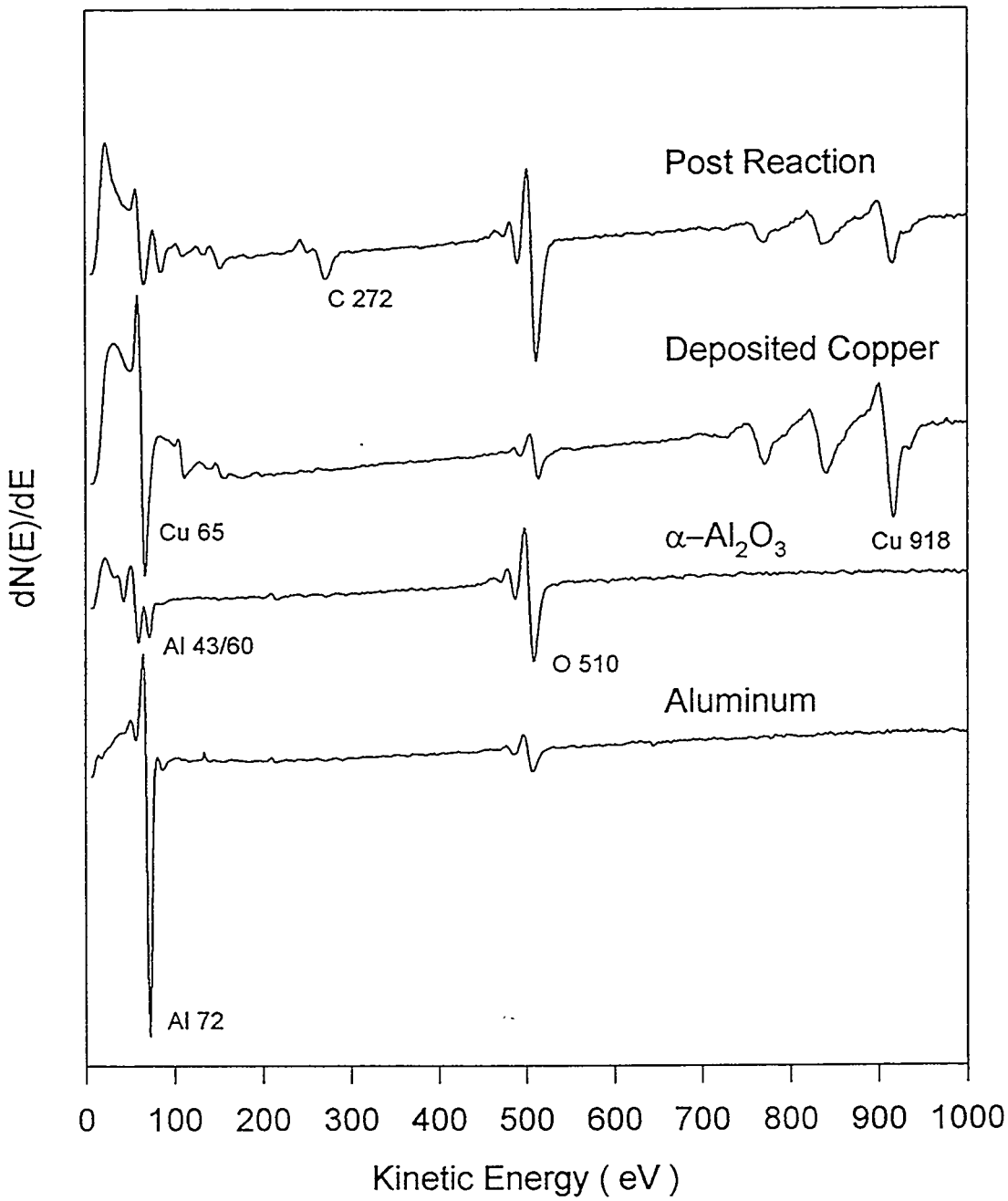

Figure 3.1. AES of the Cu/Al_2O_3 system. Shown are clean Al, Al_2O_3, a 20 minute Cu deposition, and a 20 minute Cu_2O sample after reaction in 50/100 Torr CO/O_2 at 300°C.

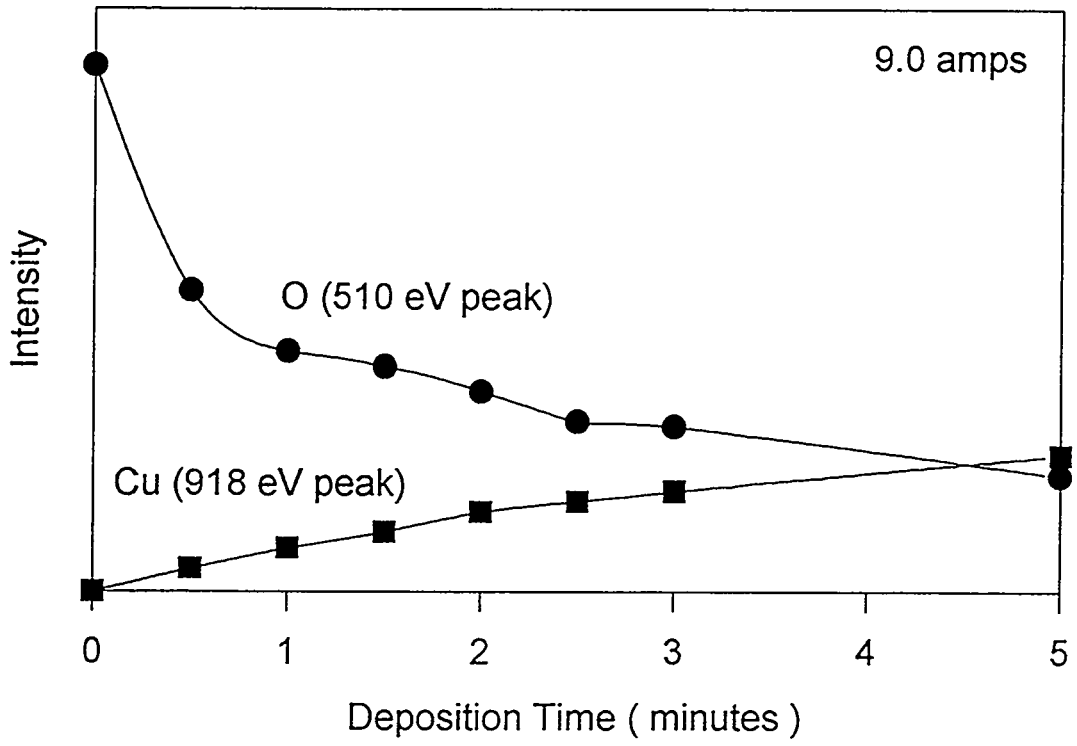

Figure 3.2. AES uptake curve for the deposition of Cu on Al_2O_3.

still be seen. This indicates that oxidized copper either forms islands on or alloys with Al_2O_3.

Experiments were performed using different oxidation treatments of copper to see if copper could be prepared in the +1 and +2 oxidation states. The first method tried was to oxidize the freshly deposited Cu in $1x10^{-6}$ Torr of O_2 at 300°C for 5 minutes. XPS indicates a shift in LVV kinetic energy from metallic copper. An increase in the O signal due to oxidation was seen in the AES. The second method tried was to oxidize the Cu through a series of O_2 dosages. Each dosage was $1x10^{-5}$ Torr for 100 seconds of O_2 followed by an anneal at 500°C. 9 consecutive doses were performed. Dosing the copper with O_2 did not result in an oxidation of the surface. The third method was to sputter the Cu with oxygen ions. The surface was sputtered with $1x10^{-6}$ Torr of O_2 at 500 V for 5 minutes. The result were no different than oxidizing the surface in a pressure of $1x10^{-6}$ at

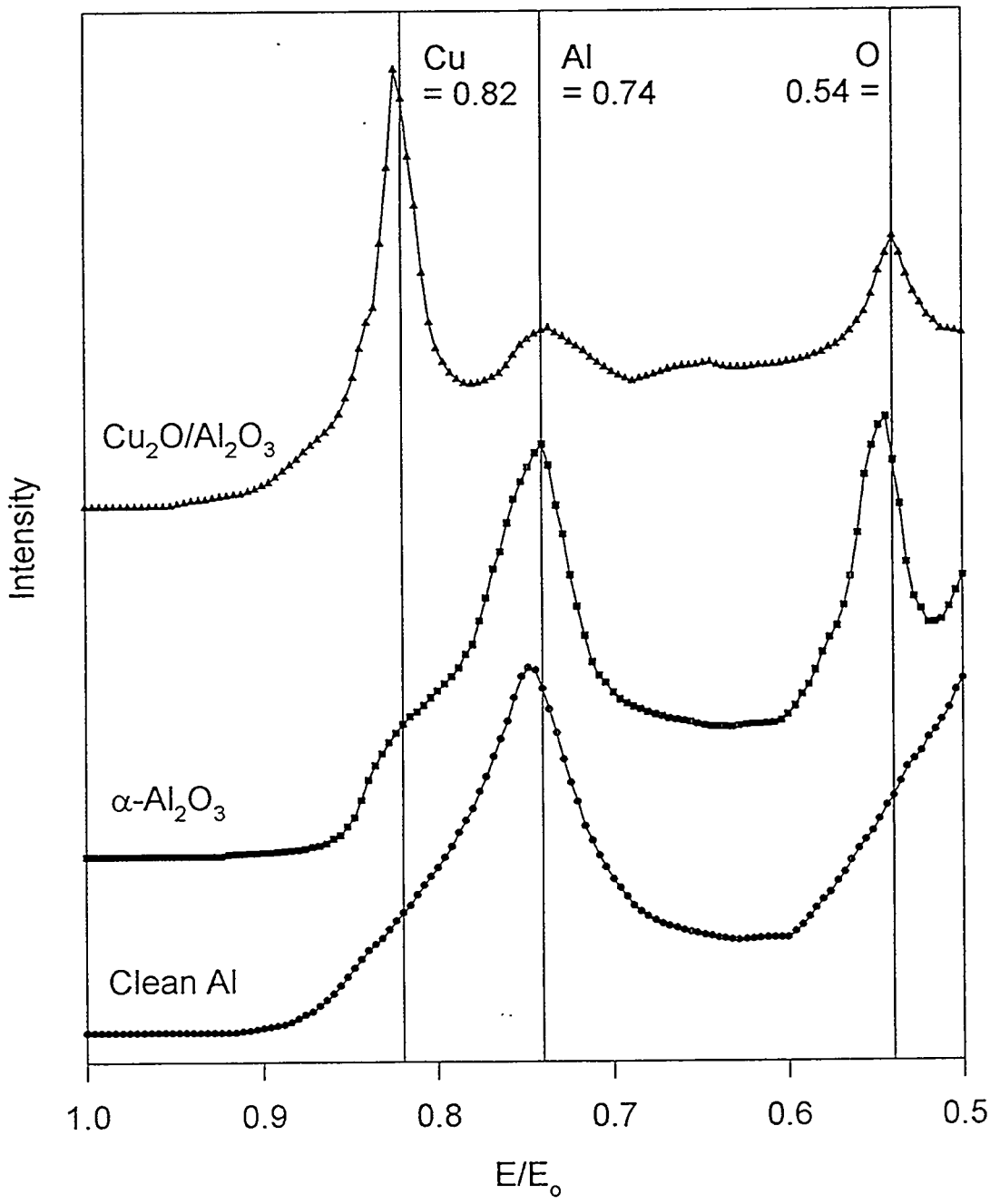

Figure 3.3. ISS of clean Al, Al_2O_3, and Cu_2O on Al_2O_3.

300°C. The last method attempted in UHV was to deposit the Cu in a partial pressure of O_2. A partial pressure of oxygen of $1x10^{-7}$ Torr was used. The XPS of the Cu had a similar shift in kinetic energy as oxidizing the Cu after deposition. In all attempts, the oxidation state of copper could not be accurately deduced from comparison to literature standards. Later it was decided to assign the Cu oxidized by heating in $1x10^{-6}$ Torr of O_2 or in $1x10^{-7}$ during deposition as being in the +1 oxidation state. No shake-up peaks were observed indicating that Cu^{+2} could not be formed in UHV. The +2 oxidation state could be readily formed by placing the Cu in the reaction cell and exposing it to 100 Torr of O_2 at 300°C for 20 minutes.

The catalytic activity for Cu on alumina catalysts is shown in figure 3.4. In all reactions the majority of product is made within the first 30 minutes. This is followed by a period of low activity. The activity of an unoxidized Cu catalyst is equivalent to a blank Al_2O_3 foil. In a post reaction AES spectrum, no Cu could be observed. The Cu went through the Al_2O_3 layer and into the bulk of Al. A 20 minute Cu deposition catalyst which was oxidized by being deposited in $5x10^{-7}$ Torr of O_2 produced 15% conversion in the first 20 minutes. The following 100 minutes produce 2% more conversion. The low activity again can not be distinguished from the background. AES after the reaction showed the Cu remained in the near surface region and is shown in figure 3.1. XPS showed that the oxidation state of Cu was +2. The top two curves in figure 3.4 are 40 and 60 minute Cu depositions, respectively, which were also deposited in a partial pressure of O_2. They produce more initial activity by 2 and 3 times the 20 minute deposition, hence, the initial activity is proportional to the amount of copper. The catalysts deactivate less rapidly than the 20 minute deposition. The activity does, however, drop to that of the background as in the 20 minute deposition. The reason proposed for deactivation is the formation of a spinel. CuO should have activity as it has been observed on other supports, but $CuAl_2O_4$ may not. Its reported activity has never been confirmed. Or even if it is active, the activity is indistinguishable from the

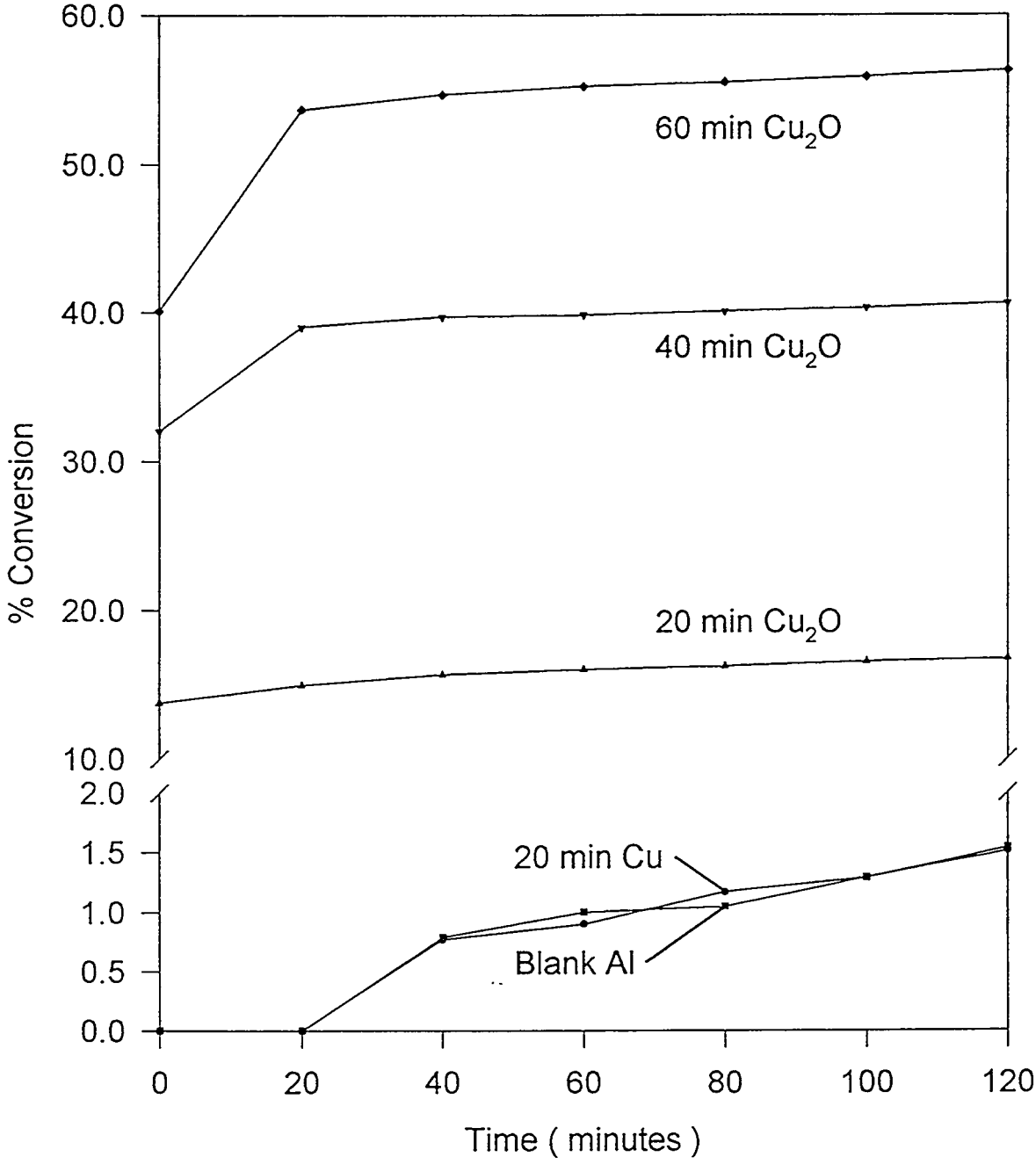

Figure 3.4. CO oxidation results for a blank Al foil and depositions of 20 min Cu, 20 min Cu_2O, 40 min Cu_2O, and 60 min Cu_2O run under a 50/100 Torr CO/O_2 gas mixture at 300°C.

background in this experiment. Later experiments showed that the background in these experiments is due to heating the Al foil.

3.4. Copper on SiO_2/Si

3.4.1. Introduction

Silica is the most common inert support used in the catalysis industry and as such it was evaluated after alumina as a support for copper in this study. Silica by itself could not be used as a support as it is non-conductive so an n-doped silicon wafer was used in a manner similar to aluminum. A native oxide of silica was gown on Si to mimic SiO_2. Literature studies of the Cu/silica system are predominantly IR studies of gases adsorbed to Cu [32,140-143]. SiO_2 is an excellent support for such studies as it is invisible to IR radiation in addition to being inert to the adsorption of most gases. The few studies of Cu on silica show that Cu does not stick well to SiO_2 [140.144]. In order for Cu to adhere it must break a siloxane bond, Si-O-Si, to form a Cu-O-Si bond. In studies where Cu is impregnated in a SiO_2 support, the catalyst is calcined at high temperatures to form Cu-O-Si bonds at the edge of the Cu particles [145].

The Cu-SiO_2 system has been looked at for CO oxidation as well as NO reduction by CO and the water gas shift reaction. Prokopowicz [32] reported kinetic results for CO oxidation in which he showed that the reaction was first order in CO pressure but his IR studies did not show CO adsorbed to the copper surface. From this he proposed that the reaction mechanism is an Eley-Rideal mechanism. The rate limiting step was the collision of gas phase CO with adsorbed O on the copper surface producing CO_2. The activation energy he calculated was 59 kJ/mol (14.1 kcal/mol) which was low compared to studies of Cu on Al_2O_3. In other work, CO adsorption has been used by many groups to determine

both the surface area and oxidation state of Cu on SiO_2[141-143]. The stretching frequency of CO differs on different crystal planes of copper as well as different oxidation states of Cu. Prokopowicz was probably observing a reaction on an oxide surface where the CO stretching mode would be at a different frequency. Hence, he would observe CO oxidation while not observing the IR signal of CO adsorption on the catalyst surface and conclude the reaction to have an Eley-Rideal mechanism.

The studies performed on the Cu/SiO_2 system in this thesis were limited to only a few UHV experiments. This was due to the difficulty of transferring and heating the Si wafer in the high pressure cell. The physical act of plugging the transfer piece into the reaction cell manipulator shattered a few samples. When the piece was successfully placed in the reactor, the uncertainty of heating the sample made running a reaction difficult. Attempts were made to heat the sample by conduction from a stainless steel support which was resistively heated. The thermocouple could not be directly attached to the Si wafer, hence the temperature could not be accurately known. The indirect nature of sample heating lead to fluctuations in the sample temperature. The large thermal mass of the Si wafer compared to the stainless steel support required heating the stainless steel to a temperature above the desired temperature for Si. This lead to an increase in background activity.

3.4.2. Experimental

A 1 x 1 cm n-type silicon (100) wafer was placed in a stainless steel support for mounting across the resistive heating pins of the transfer piece. The Si was heated by conduction from the stainless steel support. A thermocouple was attached to the sample between the Si wafer and the stainless steel support at a corner. The Si was cleaned by sputtering in $5x10^{-5}$ Torr of Ar, 1000 V, at 300°C followed by annealing at 600°C. The order of the surface was not checked by LEED. Si was oxidized by annealing the surface

at 300°C in $1x10^{-6}$ Torr of O_2 for 5 minutes followed by a brief anneal at 300°C. Copper was deposited on this surface and oxidized in $1x10^{-6}$ Torr of O_2 at 300°C.

3.4.3. Results/Discussion

AES was used to gain insight into the deposition of copper. Unlike the Al foil, the Si is an ordered single crystal making possible structural studies of Cu and its oxides. It was hoped that the initial AES experiments might lead to later LEED experiments. Unfortunately the inability to achieve catalytic results resulted in not continuing with Si as a support.

Clean Si has a single AES peak at 97 eV seen in figure 3.5. Oxidation of the Si results in a small O peak and a shift in the Si peak to higher kinetic energies. A 5 minute deposition of Cu and subsequent oxidation onto this surface produced a dramatic change in the spectrum, seen in figure 3.5, as compared to Si alone. The most obvious difference is the intensity of the O peak. Correcting for sensitivity factors, the ratio of the O peak to the Cu peak is that of Cu_2O. This was not observable in the Al case. The overall spectrum shows an increase both in noise and in the background. The change in the background can be seen both at low energies and with the gradual increase at higher energies. This may be due to an enhancement of secondary emission over that of Si. The deposition also shows that the surface becomes contaminated with both potassium and carbon with peaks at 250 and 272 eV, respectively. The percentage of contamination can be estimated from experimental cross-sections to be less than 5%.

Increasing the deposition time to 30 minutes of copper brings additional changes to the spectrum, also shown in figure 3.5. The most important result is that the Si peak can still be easily seen, while the intensity of all other peaks except the Cu 65 eV peak have decreased. All spectra were performed under identical conditions. The penetration depth of the Si 97 eV peak is only 6Å, therefore Si must be either on top of the surface or

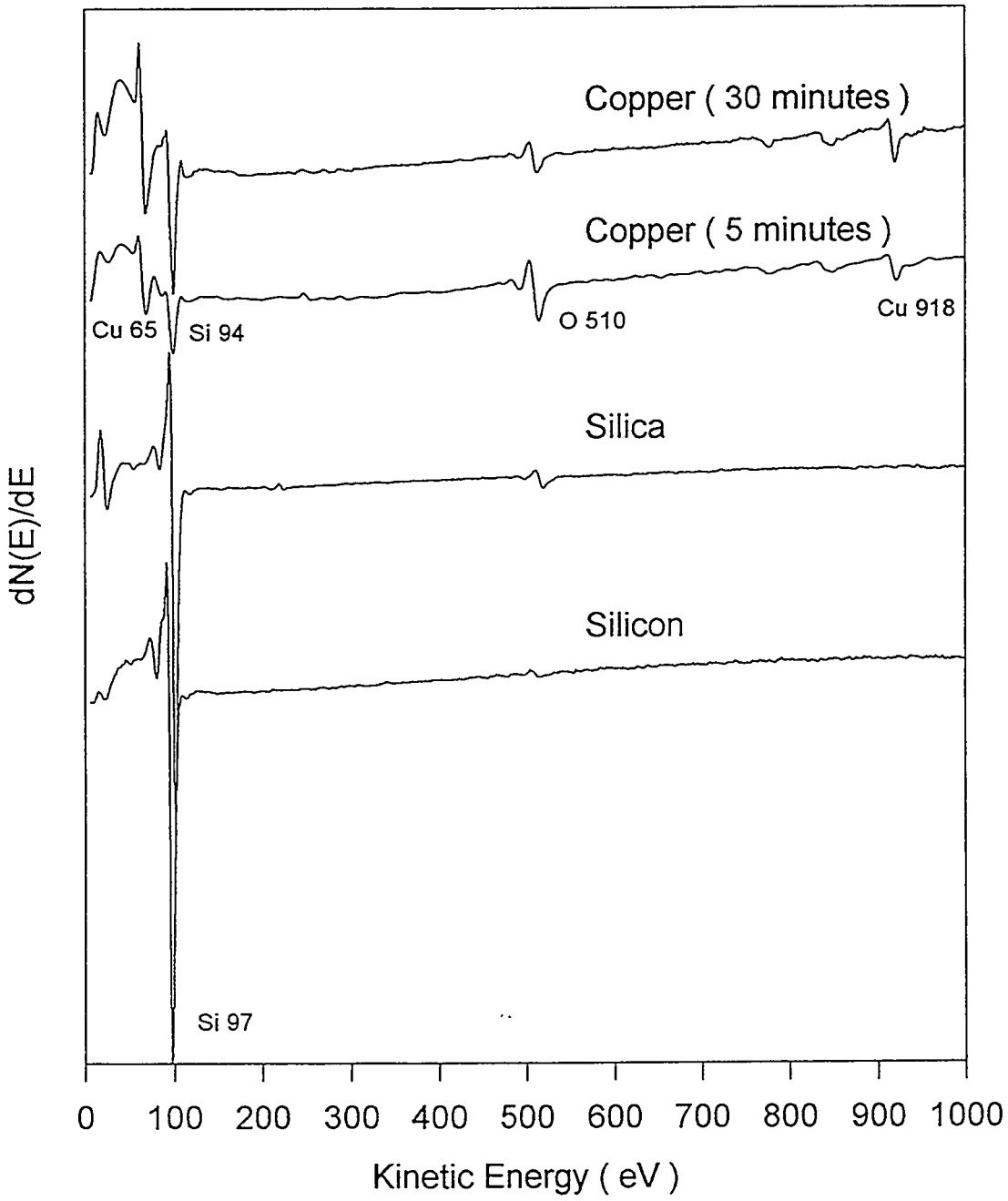

Figure 3.5. AES of the Cu/SiO_2 system. Shown is clean Si, oxidized Si, and oxidized Cu depositions of 5 and 30 minutes.

within the first 2 layers. Because signal remains for the Cu 65 eV peak, the Si has not covered the surface of the deposited Cu. We might expect Si to cover Cu as it has a lower surface free energy. What is probably occurring is either the Cu is forming tall islands or Si is diffusing into the Cu to form a copper silicide, Cu_4Si. In either case, we also see a decrease in the O and K peaks. The K is an impurity of the alumina crucible which is not always present. The K may be diffusing into the Si wafer. The Cu to O ratio may change as the surface changes, if Si is incorporating into Cu_2O. The background also flattens out with increased deposition which is unexplainable.

The results for Cu on SiO_2 are similar to that on Al. An oxide of Cu will keep Cu from diffusing into Si. At longer deposition times, a compound forms between the copper oxide and support oxide. The inability to bury the Si peak indicated that it incorporated itself into the growing Cu_2O film. This result is consistent with the work of Balkenade [143] and Goodman [140], both of which indicated that Cu on SiO_2 formed Cu-O-Si bonds at the surface.

3.5. Copper on TaO_2/Ta and MoO_3/Mo

Molybdenum and tantalum foils were tried in an attempt to find a support which was not active for CO oxidation while being interesting to the surface science community. Because both metals are refractory (require high temperatures to melt) they are used in many surface science applications. Their most common usage is as supports for single crystals in UHV manipulators. The heating of single crystals to anneal the surface or remove impurities from the bulk conventially occurs at temperatures near 2/3 of the melting temperature of the crystal. Therefore the support for the crystal must be of even higher melting temperature material. In addition, the support material must be machinable

and capable of being spot welded to the sample in order to provide resistive heating. For these reasons and others, Mo and Ta are frequently used in UHV.

Ta has not been reported to have catalytic activity for any reaction [147]. This may be due to it being a very poor catalyst or that it has not been tried. It may not have been tried for reactions in reducing environments because it embrittles when heated in H_2. Its activity for reactions in an O_2 environment also have not been mentioned. Because it is unknown how Ta would react in O_2, it was tested in this thesis. A Cu multilayer was deposited onto a 0.002" Ta foil and exposed to a 152/76 Torr CO/O_2 gas mixture at 300°C. The catalyst was tested for activity. Within one hour, the foil was unable to be resistively heated. The loss of conductivity was due to oxidation of the Ta foil. The oxide corroded the foil causing the foil to fall from the sample holder during transfer. Hence, Ta can not be used as a support in an oxidizing environment.

Mo is different from Ta in that it has catalytic activity in both a H_2 and an O_2 environment. Metallic Mo is a hydrodesulfurization catalyst and facilitates the removal of sulfur from hydrocarbons [148]. Mo when heated in O_2 forms MoO_3 which is active in the oxidation of hydrocarbons [149]. Combination of MoO_3 with other metal oxides leads to catalysts which are active and selective for partial oxidation [150]. A Bi_2O_3 and MoO_3 catalyst is very active for the oxidation of propylene to acrolein [151]. MoO_3 by itself, only produces complete combustion products and Bi_2O_3 by itself is inactive. A $CuMoO_4$ catalyst is active for the oxidation of butene to crotonaldehyde [152]. Yet, neither Mo or MoO_3 have been reported for CO oxidation. A Cu multilayer was deposited onto a 0.002" Mo foil and tested under the same conditions as Ta. Unfortunately, similar results to Ta occurred. The foil oxidized leading to an inability to resistively heat the foil. CO_2 was produced but this could have been due to the oxide that formed or the increased current need to heat the sample or many other possibilities.

The refractory metals were not good supports under high partial pressures of O_2. Their use in UHV is fine because the metals will not be exposed to large enough quantities

of O_2 completely oxidize. If an oxide overlayer were to form on either metal, the oxide can be remove by flashing the metal to high temperatures to vaporize the oxide. The difficulty of finding a substrate that is metallic but will not be consumed in the oxidizing environment lead to the use of stainless steel as a possible support.

3.6. Copper on Oxidized Stainless Steel

3.6.1. Introduction

Stainless steel (SS) is a common material used in the manufacture of catalytic reactors. As such, it has not been found to catalyze any reaction but is known to decompose methanol and other substituted hydrocarbons. SS was tried as a support because it does not form a bulk oxide and will not interfere in the CO oxidation reaction. There are a variety of AISI stainless steels which vary in hardness, strength, and chemical reactivity. A 304 SS was chosen because it contains the lowest content of C. A 316 SS might have been a better choice, per Boschi [153], as it would have fewer surface impurities after an acidic or basic cleaning. The SS foils were cleaned in UHV to remove O before use so any surface impurities would also be removed at that time.

3.6.2. Experimental

A 1 x 1' x 0.005 cm 304 stainless steel foil was used to support Cu. Prior to introduction to UHV, the foil was rinsed with acetone to remove any machine oil and then rinsed with methanol to remove any acetone residues. The sample was placed into the chamber and cleaned with alternating treatments of annealing and sputtering. The foil was annealed at 700°C to segregate any S or K impurities. The surface was sputtered

using a 1500 V beam of $5x10^{-5}$ Torr Ar at 300°C to remove any O and the impurities. Once clean, as determined by AES, the surface was oxidized to prevent possible future oxidation during Cu deposition or catalytic reactions. The surface was oxidized by sputtering the surface with a 500 V beam of $1x10^{-7}$ Torr O_2 and $1x10^{-5}$ Ar while heating to 300°C. Copper was deposited in $1x10^{-7}$ Torr of O_2. Catalytic reactions were performed at 300°C in 50/100 Torr mixture of CO/O_2.

3.6.3. Results/Discussion

The effect of cleaning the 304 SS foil can be seen in figure 3.6. All constituents are present, but their ratio is different from that of the bulk composition. Additional cleaning does not change the spectrum, hence with this surface composition there must be a complimentary subsurface layer in order to have a correct overall composition. If preferential sputtering was responsible for the differing composition, continued sputtering would have eventually resulted in a rough surface with the correct composition. It should also be noted in the clean spectrum that the carbon is carbidic. The shape of the C signal is quite different from the amorphous carbon which can be deposited by gas phase contaminates [154].

Oxidation of 304 SS would seem to be an impossibility as SS is supposed to be resistant to oxidation and the associated discoloration. This is a fallacy in that SS can be oxidized as is demonstrated in figure 3.6. The AES shows that upon oxidation C, Cr, and Ni all vanish as an Fe oxide layer forms on the top layer of the surface. This oxidation does not continue into the bulk. SS is resistant to bulk oxidation because it forms a Fe_2O_3 layer on top of a Cr_3O_4 layer [155]. The Cr_3O_4 layer limits the diffusion of ions across it, thereby stopping continued oxidation. Additional proof is given in figure 3.7 which shows the XPS spectrum of clean SS and an oxidized SS. Both Cr (with peaks at

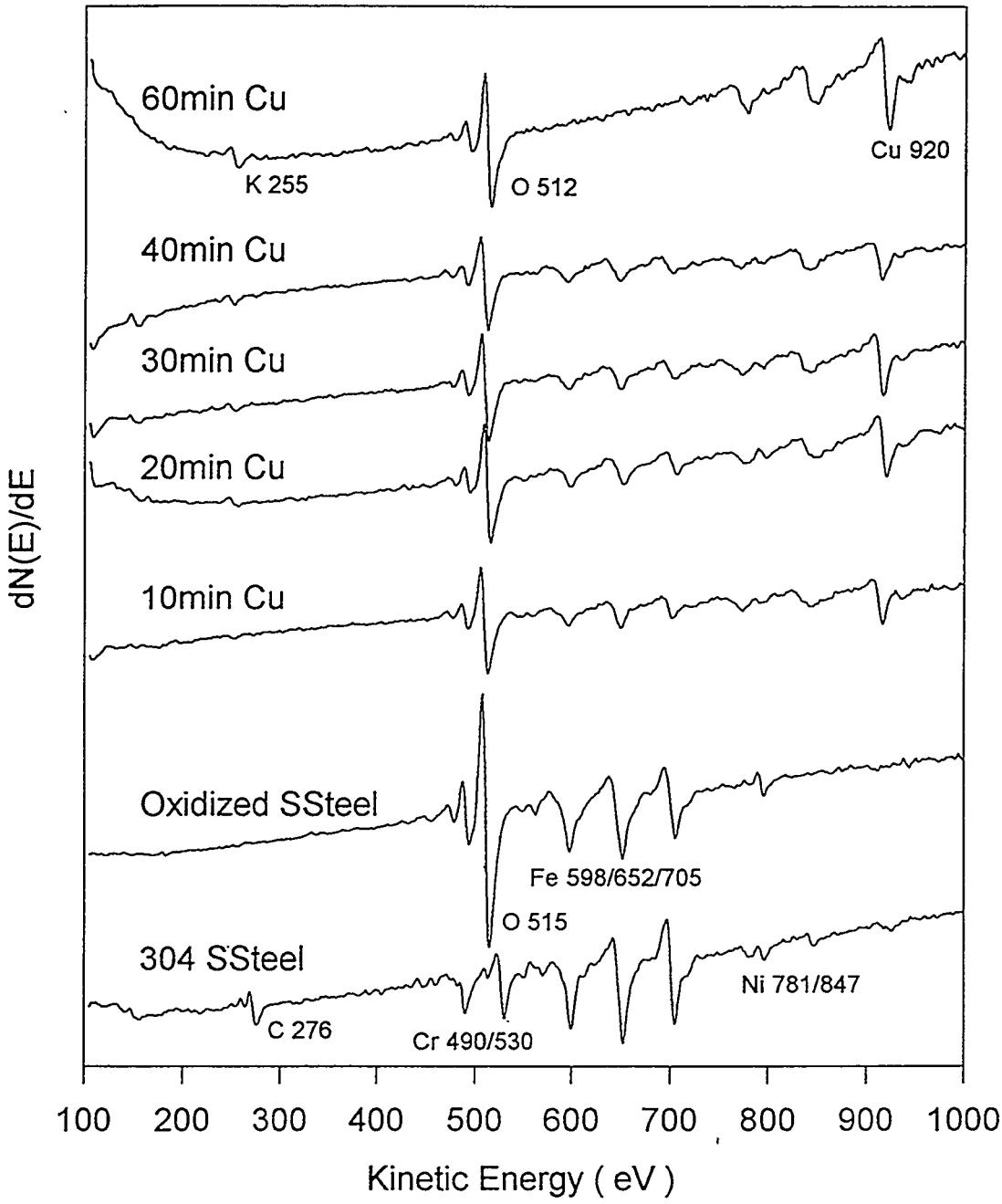

Figure 3.6. AES of the Cu/SSteel system. Shown are clean 304 SSteel, oxidized SSteel, and deposition of 10, 20, 30, 40, and 60 minutes of copper.

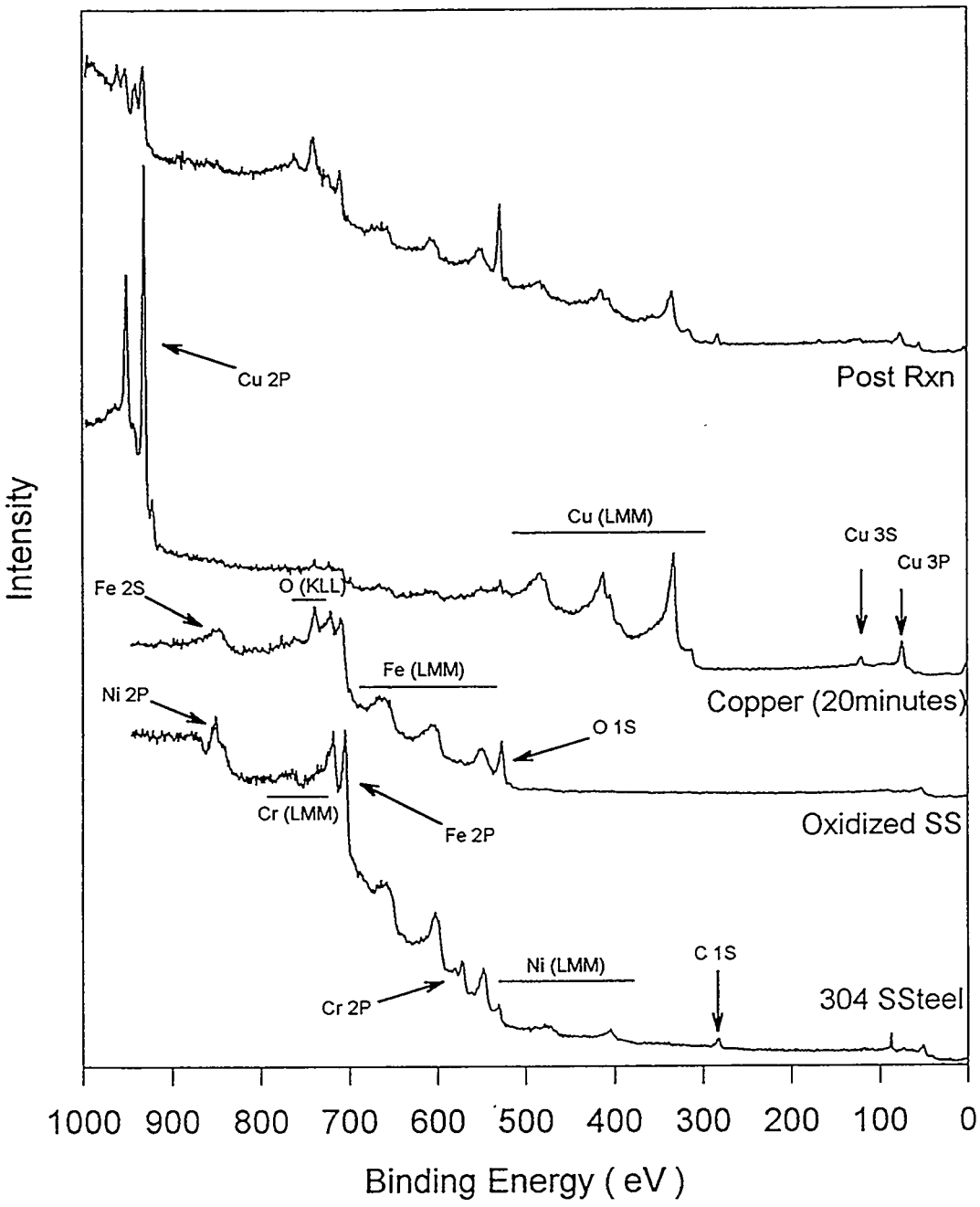

Figure 3.7. XPS of the Cu/SSteel system. Shown are clean SSteel, oxidized SSteel, and a 20 minute copper deposition before oxidation and after a catalytic reaction run under a 50/100 O/O_2 gas mixture at 300°C.

764 and 574 eV) and Ni (with peaks at 478 and 407 eV) disappear after oxidation leaving a spectrum characteristic of Fe_2O_3.

Deposition of varying amounts of copper on oxidized SS is shown in figure 3.6. The deposition does contaminate the surface with a small amount of C which is distinguishable from the carbide of SS. There is an increasing attenuation of the Fe signal with deposition time up to 60 minutes of deposition where Fe can no longer be observed. Each deposition was performed in the presence of O_2, so the O signal can not be deconvoluted between Fe_2O_3 and the copper oxide. An XPS spectrum of a 20 minute deposition of Cu without an O_2 partial pressure is shown in figure 3.7. Under these conditions, the Cu is almost sufficient to bury both the O and Fe signal. Therefore, the oxidation of Cu may be forming a $CuFe_2O_4$ compound. Only after significant deposition times does Cu_2O form on the Cu/Fe/O surface.

To understand the stability of Cu_2O on the Cu/Fe/O surface, an annealing experiment was performed. Figure 3.8 displays the AES spectra of a 60 minute Cu deposition anneal for 5 minutes at incremental temperatures. The sample was cooled to room temperature before each spectrum was taken. At 300°C, a temperature at which reactions are run, an Fe signal can now be seen. There also seems to be a slight increase in the Cu signal as well. The Cu/Fe/O surface is stable up to 600°C. At 600°C, the Cr peaks return and the Fe peaks vanish while Cu remains. There may be a decrease in the O intensity but this can not be distinguished from the Cr peaks. At 700°C we see a maximum in the S signal at 152 eV. There is no change in the Cr-O region but the Cu does decrease slightly. Possibly a $CuCr_2O_4$ compound replaces the $CuFe_2O_4$ compound. Cu-Cr compounds have been observed to be active for CO oxidation [36].

The catalytic activity for the Cu/Cr surface, Cu on the Cu/Cr surface, and Cu/Fe/O surface were measured. The results are shown in figure 3.9. The Cu/Cr surface has activity and produces 3% conversion in 120 minutes. When Cu is deposited onto this surface, there is a large increase in initial activity. Cu_2O on Cu/Cr produced 25% CO_2

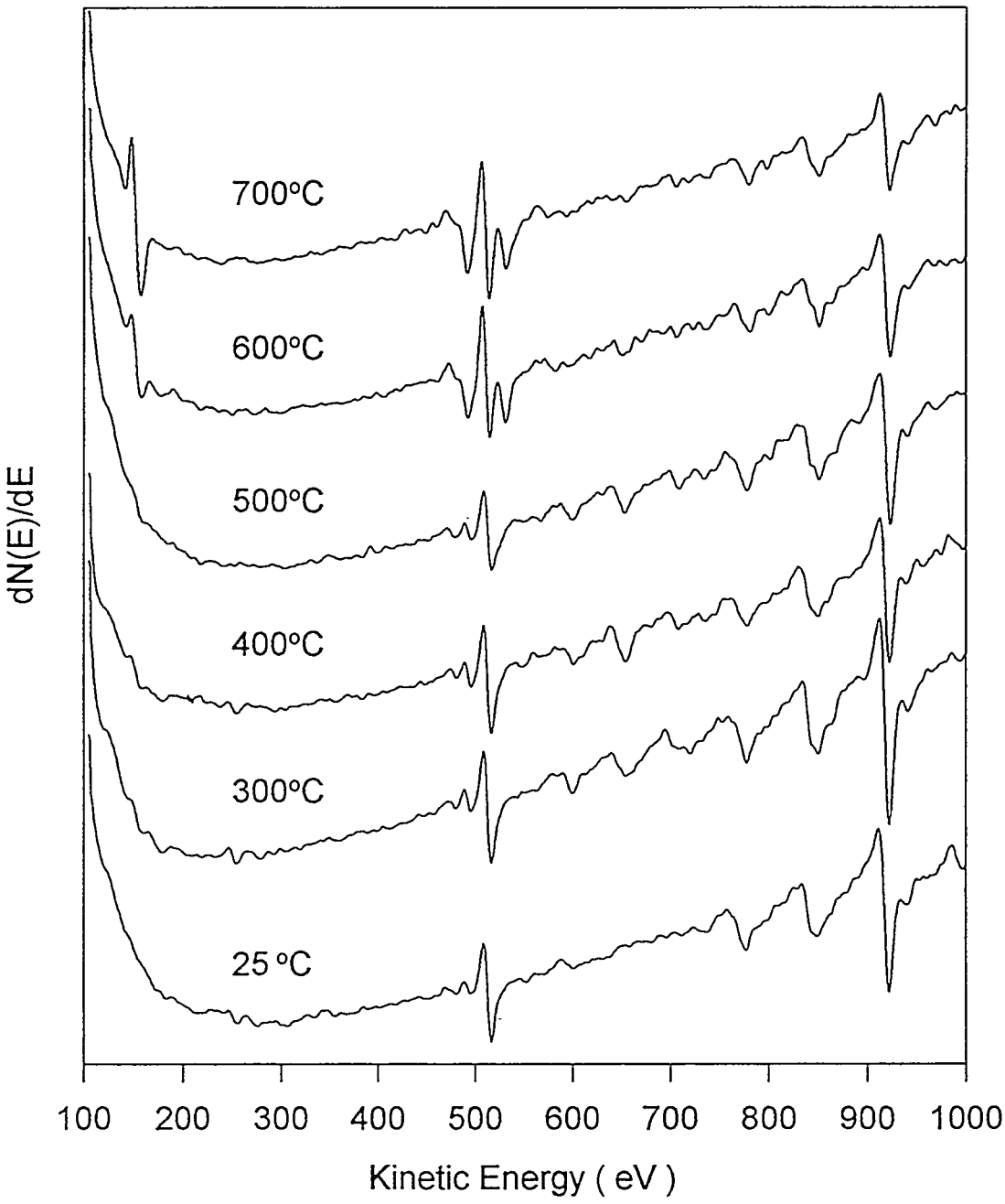

Figure 3.8. AES of a 60 minute copper deposition on SSteel annealed at 25, 300, 400, 500, 600, and 700°C for 5 minutes. Cr surface segregates at 600°C.

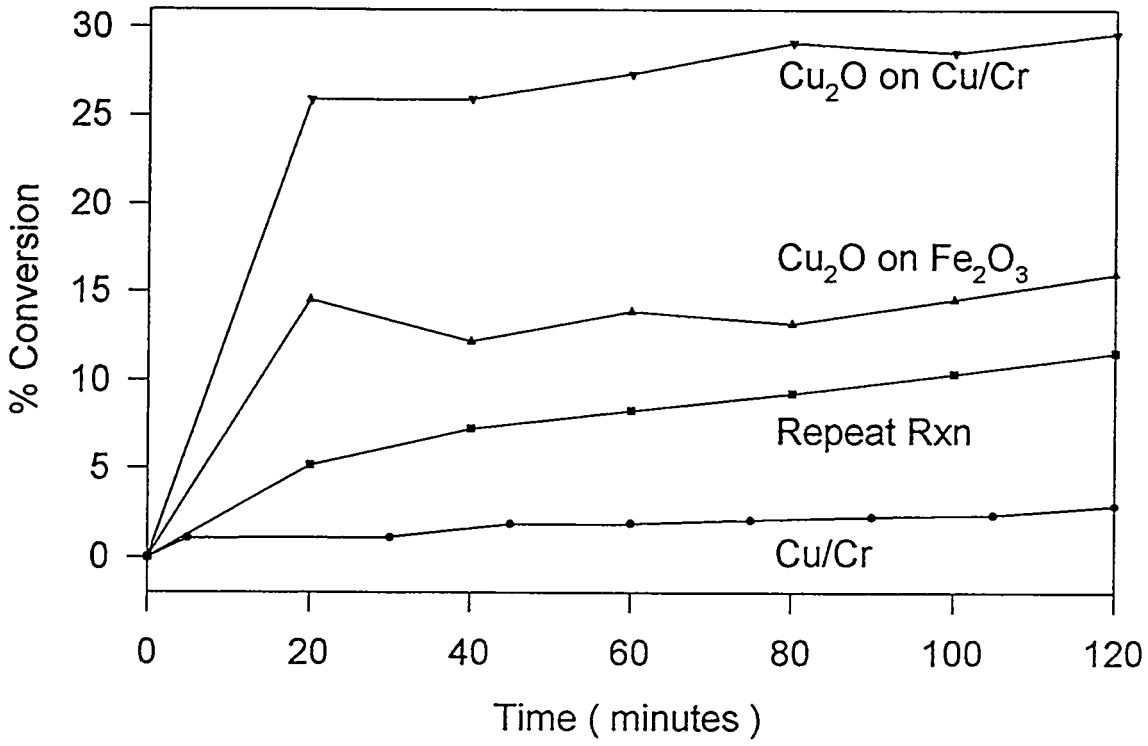

Figure 3.9. CO oxidation results for Cu_2O on Cu/Cr, a repeat reaction for Cu_2O on Cu/Cr, Cu_2O on Fe_2O_3, and a Cu/Cr alloy under a 50/100 Torr CO/O_2 gas mixture at 300°C.

within 20 minutes. The following 100 minutes produced only 4 % conversion. A repeat run was performed on this surface immediately afterwards. The old gases were removed and the sample was pumped to UHV. Fresh gases were admitted and the reaction was begun again. The result was still a period of high initial activity followed by a slow period. The production of CO_2 must affect the catalytic activity. At the beginning of the reaction when no CO_2 has been produced, the reaction proceeds rapidly. When CO_2 is present, the rate changes to about 4% in 100 minutes. A comparison of activity between Cu_2O on Cu/Cr and Cu/Cr alone shows that the greater activity of Cu_2O on Cu/Cr is not solely due to the presence of more Cu. The greater initial activity for the fresh Cu_2O on Cu/Cr surface must be due to copper which has not dissolved into the surface compound. A

Cu/Fe/O surface does not produce as much initial activity a did the Cu_2O on Cu/Cr surface. After the high initial activity, the surface seems to deactivate, although there is scatter in the data. The deactivation may be due to CO_2 having a greater influence on the Cu/Fe/O surface as compared to the Cu/Cr surface. In all reactions, the final oxidation state was +2. The shake-up peaks due to Cu^{+2} formation can be seen in the post reaction XPS in figure 3.7. The complexity of the surface compounds formed make it necessary to simplify the system. As Cr is toxic, the activity of Cu on Fe was pursued next.

3.7. Copper on Fe_3O_4/Fe

3.7.1. Introduction

Copper was deposited onto a pure Fe foil to observe a difference between the effect of Fe and Cr in the stainless steel on Cu activity. Surface science has studied the reverse system, Cu on Fe, from which we can glean some valuable information [156-163]. Fe on Cu is of interest as a model for growing thin magnetic films for magnetic storage applications [156]. Fe is a body centered cubic metal (bcc) which can under go a phase transition at 700°C to a face centered cubic structure (fcc). The lattice constant for the fcc structure of Fe is within 1% of that of the fcc structure of metallic Cu. This indicates that Fe may grow epitaxially on Cu. Unfortunately, thermodynamics works against this. The surface free energy of Fe is greater than that of Cu [146], so islanding is expected to occur. A mixture of those two facts is what controls growth. For growth less than 2 monolayers, Fe exchanged positions with lattice Cu in the near surface region [156,163]. The Fe maintained the lattice registry. Continued growth up to 10 monolayers resulted in an epitaxial film. After 10 monolayers, the Fe adopts a bcc lattice. With the growth of Cu on Fe, we might expect to obtain similar results. Because Cu has the lower surface free

energy, it should remain on top of the Fe surface. The interaction of Cu on Fe was strong enough to induce epitaxy in Fe, so we might expect Fe to induce epitaxy in the growing Cu film as well. This was observed in AES uptake curve shown in figure 2.15 of chapter 2. The growth is layer by layer for the first 3 monolayers.

O.P. Van Pruissen extensively studied Fe films deposited by chemical vapor deposition on Cu (111) and Cu (110) along with their interaction with O_2, CO, and H_2 [159-162]. The results are valuable to the understanding of what might be found in this study for both the oxidation of Cu and the catalytic activity for CO oxidation. When exposing Fe on Cu to O_2, the Fe was found to oxidize before Cu. Hence, in this study Cu can not be oxidized without oxidizing the Fe support as well. Reduction of the oxidized surface with CO would only occur on the Cu. The Fe oxide could not be reduced by CO. Therefore, the catalytic activity for CO oxidation on Fe will not proceed through a surface redox cycle. H_2 was needed to reduce the Fe oxide. CO exposure to the Fe on Cu lead to dissociation. This is not unexpected as Fe is a Fischer Tropsch catalyst and is known to decompose CO as a reaction step in the hydrogenation of CO to form higher hydrocarbons. An apparent activation energy for CO oxidation was obtained as a function of Fe coverage on Cu. At low coverages a value of 8 kcal/mole was calculated and is in agreement with pure Cu. At near monolayer coverages, the activation energy dropped to approximately 4 kcal/mol. The explanation given was that Fe has a much higher CO heat of adsorption. CO would adsorb on Fe and migrate to Cu where it would be oxidized. Their work leaves open the possibility of studying the activity of the Cu on Fe system to see if similar results are found at higher gas pressures and to study the activity of more oxidized surfaces.

3.7.2. Experimental

A 99.99% pure 1 x 1 x 0.005 cm Fe foil was used. It was cleaned by sputtering with a 1500 V beam in $5x10^{-5}$ Torr of Ar and annealed at 400°C for various times. The major contaminant was S which could not be completely removed from the bulk. The foil was used when the near surface region was depleted of S. Oxidation of the foil was done by annealing the surface in $1x10^{-6}$ Torr of O_2 at 300°C for 5 minutes. This was reported to form an Fe_3O_4 layer [164]. Cu was deposited on to this surface both in the presence of $1x10^{-7}$ Torr of O_2 and in the absence of O_2. Catalytic reactions were performed in a 50/100 Torr mixture of CO and O_2, respectively, at 300°C.

3.7.3. Results/Discussion

The AES results of surface preparation and post reaction analysis are shown in figure 3.10. Clean Fe has a distinctive triplet of peaks between 550 and 750 eV and a low energy peak at 52 eV. The clean surface is free S which has a peak at 154 eV but does have tiny C and O peaks due to background CO which has dissociated on the surface. Oxidation of Fe leads to a huge increase in the O signal, a vanishing of the C signal, and a change in the low energy Fe peak. The signature of the Fe 57 eV peak is that of Fe_3O_4 even though the AES peak ratio of O to Fe is only 3.0. The reported ratio for Fe_3O_4 is 3.7 [164]. A surface of FeO would have a ratio of 2.3. The difference between the oxidation of the Fe foil and a pure Fe_3O_4 sample may be due to the surface roughening by oxidation or the formation of a passivating oxide layer. In either case, the Fe signal would be enhanced. Deposition of 20 minutes of Cu in O_2 leads to a large decrease in O and Fe signal intensity. The Cu 67 eV peak obscures the low energy Fe peak. The Cu to O ratio can not be used to determine the oxidation state of Cu because of the FeO_x already on the

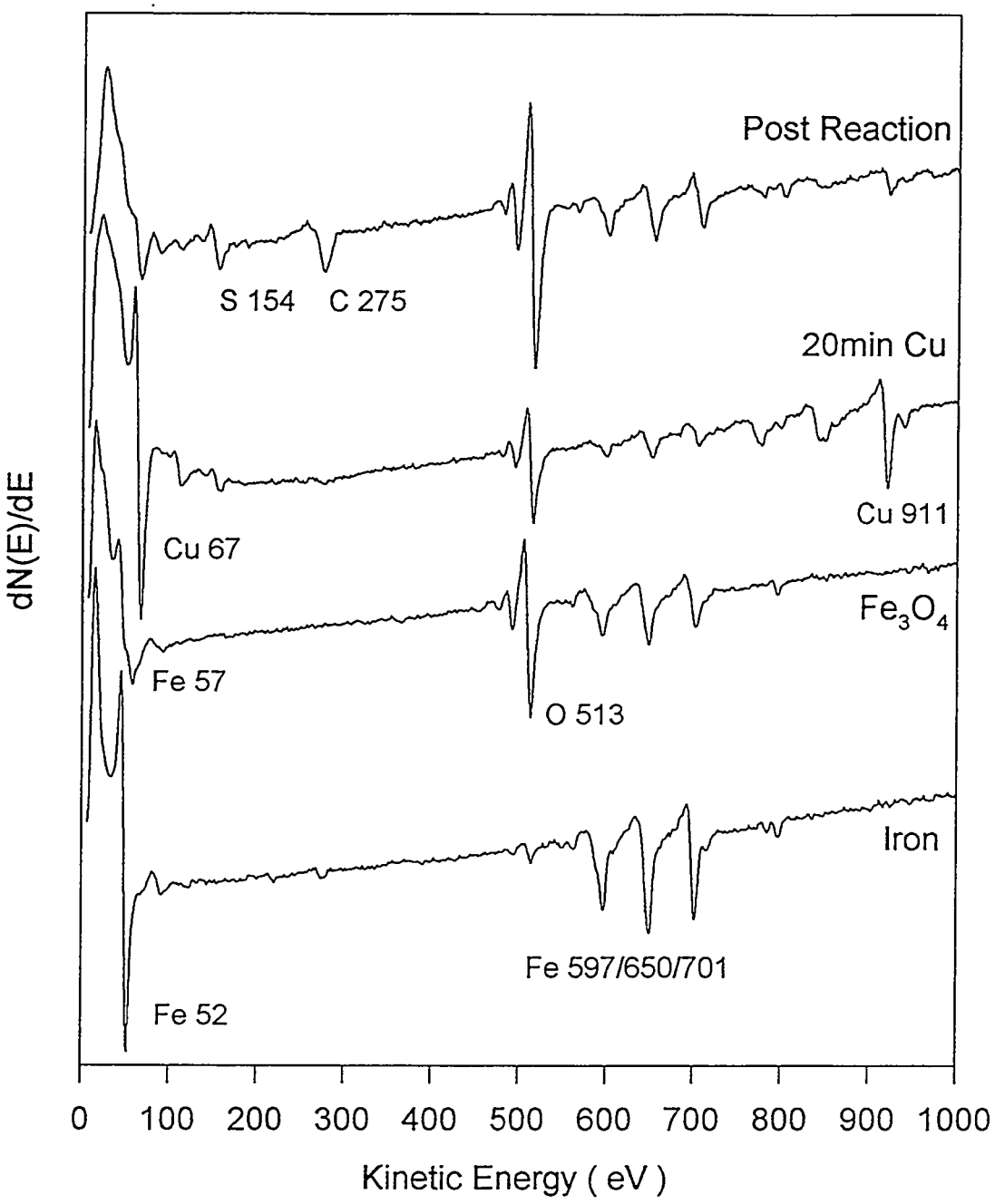

Figure 3.10. AES of the Cu/Fe_3O_4 system. Shown are clean Fe, oxidized Fe, a 20 minute Cu deposition, and a Cu on Fe surface after a catalytic reaction run under a 50/100 Torr CO/O_2 gas mixture at 300°C.

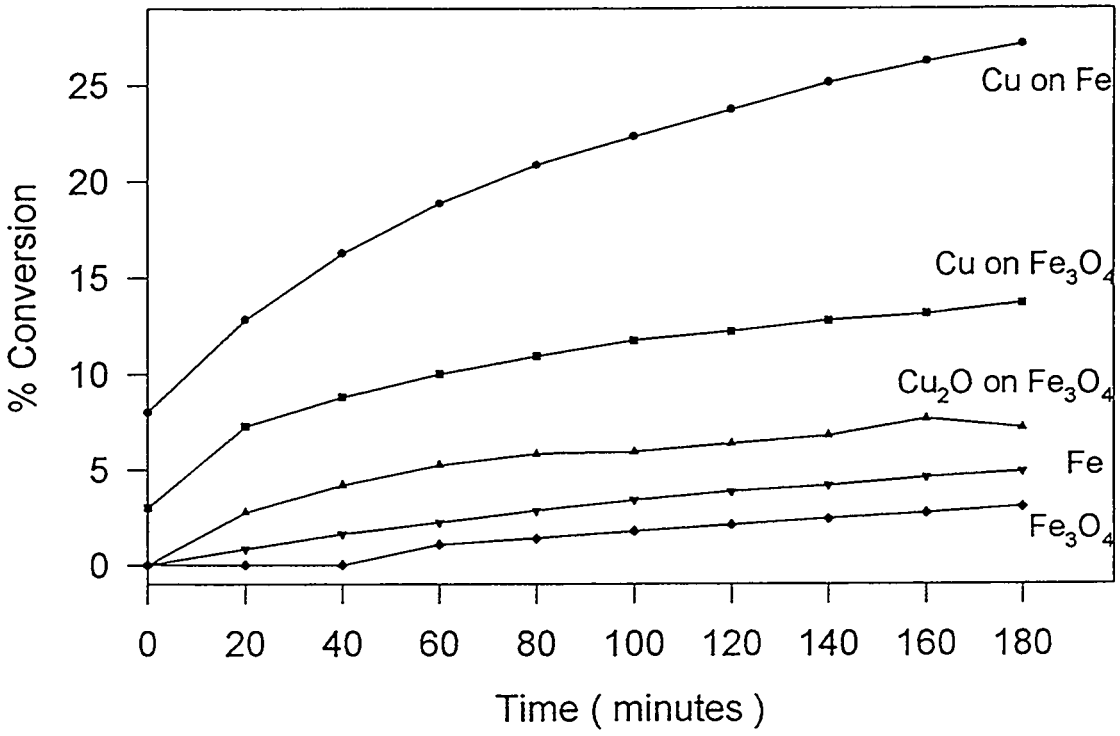

Figure 3.11. CO oxidation results for Cu on Fe, Cu on Fe_3O_4, Cu_2O on Fe_3O_4, Fe, and Fe_3O_4 run under a 50/100 Torr CO/O_2 gas mixture at 300°C.

surface. Cu and Fe can be easily seen in addition to O on the surface. A higher resolution scan of the Cu LVV peak indicated that Cu was in the +1 oxidation state.

Catalytic reactions were performed on five surfaces: metallic Cu on unoxidized Fe and Fe_3O_4, Cu_2O on Fe_3O_4, and blanks without Cu of Fe and Fe_3O_4. The results are shown in figure 3.11. It should be immediately noted that the Fe and Fe_3O_4 blanks possess catalytic activity. There is an induction period for Fe_3O_4 after which the activity is equivalent to Fe. The activity of the blanks need to be subtracted from any reaction on a Cu containing surface. The activity of Cu is markedly different if Cu is oxidized or not on the Fe_3O_4 surface. This is the first positive result demonstrating that different oxidation states of Cu might possess different catalytic activity. The metallic Cu was more active than the Cu_2O. When metallic Cu was deposited on Fe, the activity was even

greater than on Fe_3O_4. The oxidation of the support negatively affected catalytic activity. In comparison to the SS foil, Cu on Fe produces as much CO_2 as did Cu_2O on Cu/Cr/SS. The Fe system did not have as large of an initial activity but it also did not deactivate as rapidly. The Cu_2O on Fe_2O_3/SS is also more active than its counterpart, Cu_2O on Fe_3O_4. The use of an Fe foil shows that the Cr does enhance the activity of Cu but deactivates more quickly.

Post reaction AES, shown in figure 3.10, of Cu on Fe indicates that the surface is oxidized during the reaction and that S segregates to the surface. Post reaction analysis of Cu on Fe_3O_4 and Cu_2O on Fe_3O_4 show similar spectra. This indicates that the surface is going to change during the reaction making it difficult to assign activity under these reaction conditions. The presence of S is a problem in that S poisons the activity of Cu [20]. It has been shown that when chalcopyrite, a $CuFeS_2$ compound, is oxidized it results in a decomposition to Fe_3O_4 and CuS [165]. CuS is not active for CO oxidation [20]. It is feared that this is what may be forming on the surface during a catalytic reaction.

3.8. Copper on Graphite Coated Stainless Steel

3.8.1. Introduction

The decision to deposit copper on carbon was tried after encountering difficulties with the oxidized supports. The use of carbon as a support however posed new potential problems. Carbon has been used as a support in reactions where the carbon itself is not reactive [2]. It was unclear whether the carbon would combust during the CO oxidation reaction. The choice to use graphitic carbon as opposed to carbonaceous or activated carbon was important to the stability during reaction. Carbonaceous carbon comes from

many carbon sources, e.g. wood, coal, or petroleum, and may contain metal impurities and volatile organic compounds. The metal impurities may catalyze CO oxidation and the volatile organic compounds may oxidize during the reaction making carbonaceous carbon a bad choice for a support. Activated carbon is carbonaceous carbon which has been heated in vacuum to remove volatile organics and then exposed to steam to create oxygen species on the surface. In the process, a high surface area is obtained. Activated carbon is often used in chromatographic columns. Activated carbon was not used as it is typically not stable at elevated temperatures. The pores formed from activation may collapse and the oxygen species may desorb. Additionally the activated carbon may adsorb or react with the CO, O_2, or CO_2 in the reaction.

The use of graphitic carbon was not without problems. Graphite is an inert support on which studies of the effect of Cu particle size has been observed [166-169]. Because the copper does not adhere to graphite [167], it will be difficult to deposit copper from an evaporation source. Additionally, if the reaction does have structure sensitivity, the effect of particle size will be important but controlled in these types of studies. There is also the possibility that at higher temperatures copper may intercalate between the graphite sheets. Lastly, it is not known whether copper may catalyze the oxidation of graphite.

The graphite used in this work was Aerodag, a commercial product used in the electronics industry instead of a highly oriented pyrolytic graphite (HOPG) crystal. Aerodag provides good electrical conductivity while being inert. An atomic force microscope image showed that Aerodag consists of the micron-sized particles. The sticking probability of copper on Aerodag was estimated at 10 times greater than on HOPG by comparing the deposition times needed to obtain comparable Cu AES peak intensity. The reason for this is the particles have more low coordination sites for the adsorption of Cu. This aids the observation of catalytic ability by increasing the copper area while preventing sintering.

3.8.2. Experimental

The sample was a 1 x 1 x 0.005 cm graphite coated stainless steel foil onto which copper was deposited. The graphite coated stainless steel foil was prepared by cleaning a 304 stainless steel foil with methanol then spraying it with Aerodag (a registered trademark of Acheson) and allowing it to dry. Aerodag is a dry film lubricant of micron-sized graphite particles suspended in isopropyl alcohol, per the label. The thermal stability of Aerodag was tested by heating a sample in pure oxygen (100 Torr). No CO_2 was produced at temperatures less than 450°C and AES showed no delamination of the graphite, which would have been observed as signal from the underlying stainless steel. Prior to copper deposition, the foil was annealed at 600°C in UHV to remove any remaining alcohol and surface oxygen species. Initial catalytic reactions were performed in a 66/33 CO/O2 mixture at 275°C.

3.8.3. Results/Discussion

The AES of graphite coated stainless steel is depicted in figure 3.12. The sample was introduced to UHV and annealed at 600°C. The absence of an oxygen peak is due to removal of carboxyl and hydroxyl groups from the graphite surface [170] by annealing. The Auger peaks for Fe, Cr, and O of the stainless steel substrate are not seen. A post blank reaction of a graphite coated stainless steel foil exposed to 66/33 CO/O_2 ratio at 300°C for 2 hours is also shown in figure 3.12. It contains a small oxygen signal which disappears upon annealing at temperatures greater than 300°C. One reason for choosing graphite as a substrate was that it could be cleaned of oxygen and does not readily oxidize. Hence any oxygen signal appearing in the AES or XPS could be associated with oxygen bound to copper. Graphite is also highly conductive which allowed the electron

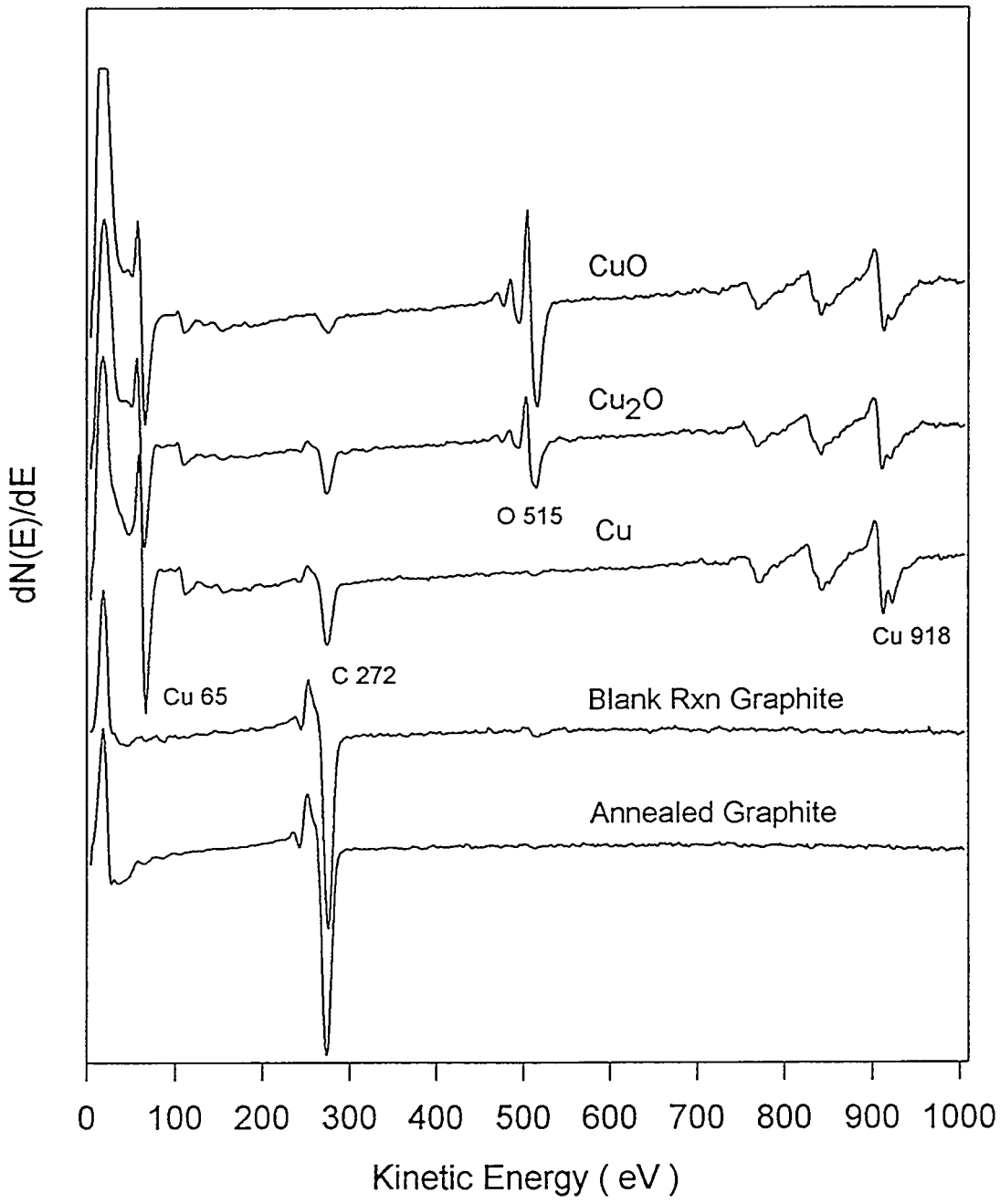

Figure 3.12. AES of the Cu/graphite system. Shown are a annealed graphite substrate, a substrate after reaction under a 66/33 Torr CO/O_2 gas mixture at 300°C for 2 hours, and catalyst films of Cu, Cu_2O, and CuO.

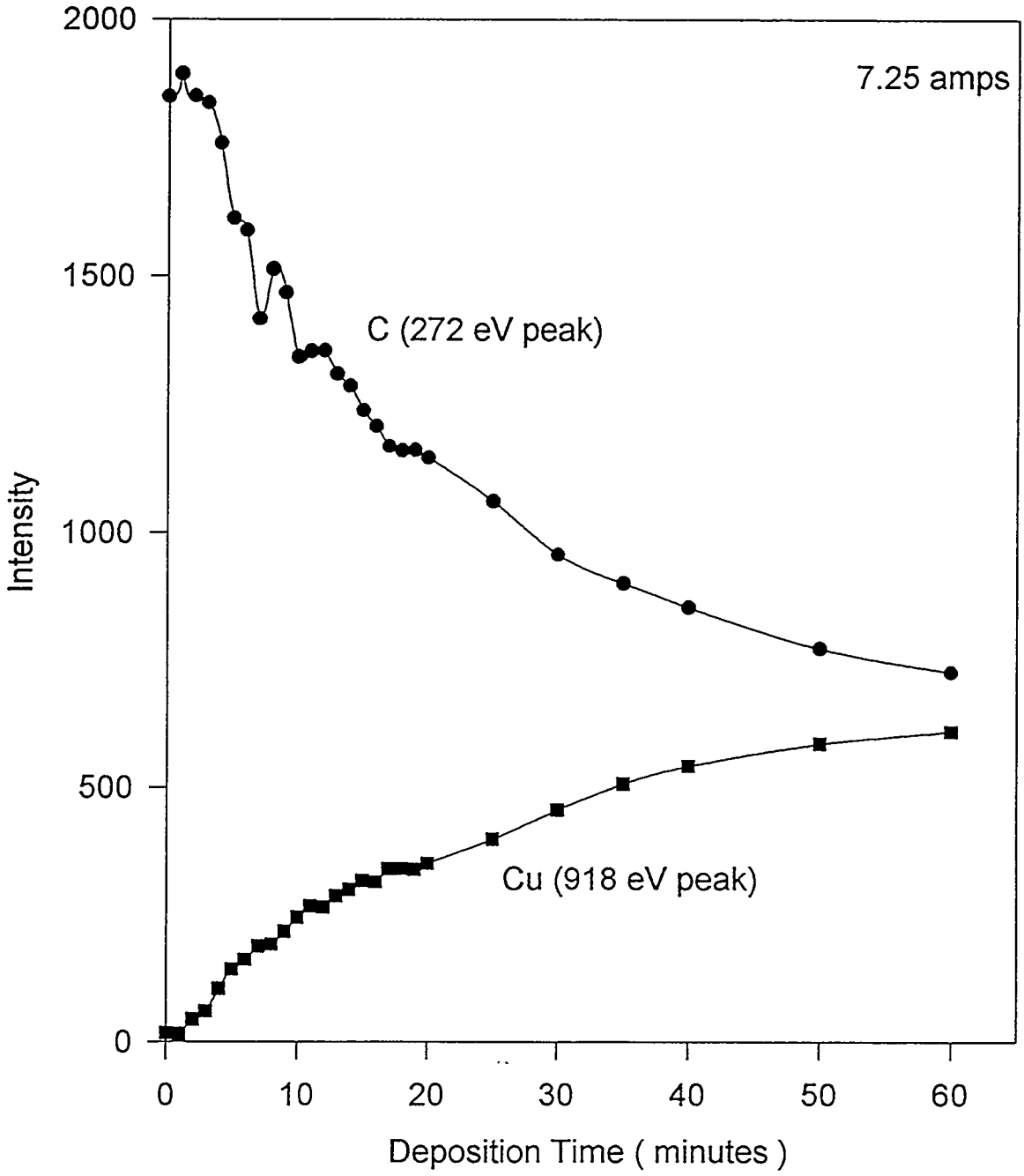

Figure 3.13. AES uptake curve for Cu on graphite at a crucible heating current of 7.25 amps. Multilayer island formation is observed.

spectroscopies to be performed without sample charging difficulties. A 20 minute copper deposition onto the graphite coated substrate resulted in an attenuation of the carbon peak, as seen in figure 3.12. This corresponds to approximately 10 monolayers. An AES uptake curve of Cu 918 eV and C 272 eV peak intensity versus deposition time did not show any distinct breaks, shown in figure 3.13, but followed a smooth curve indicative of a Volmer-Weber growth mode (island formation). With the oxidation of metallic copper to copper (I) oxide, the carbon 272 eV peak intensity decreases further while the copper 918 eV peak remained unchanged. We interpreted this to be due to the spreading of the copper (I) oxide islands on the graphite. Upon further oxidation to copper (II) oxide there was an additional decrease in the carbon peak without a change in the copper peak, indicative of further spreading of the oxide islands on the graphite. These observations are consistent with a progressive decrease in the surface tension of the islands as the copper is oxidized. As the surface tension decreases, the islands wet the graphite surface. This model is valid if the interfacial energy between the islands and graphite is small and that would be expected based on the chemical-inertness of graphite.

In figure 2.8 are the copper 2P and LVV XPS peaks for metallic copper, copper (I) oxide, and copper (II) oxide prepared on graphite for these experiments and used as reference. Spectroscopically, the different oxidation states of copper can be distinguished

Table 3.1. Reference values for metallic copper, copper (II) oxide, and copper (II) oxide on graphite.

	Auger Ratio O/Cu	Cu 2P3/2 Binding Energy	Cu LVV Kinetic Energy	Auger Parameter
Metallic copper	---	932.8	918.5	1851.3
Copper (I) oxide	1.1	932.6	916.5	1849.1
Copper (II) oxide	2.3	933.8 (942.5 S.U.)	917.6	1851.4

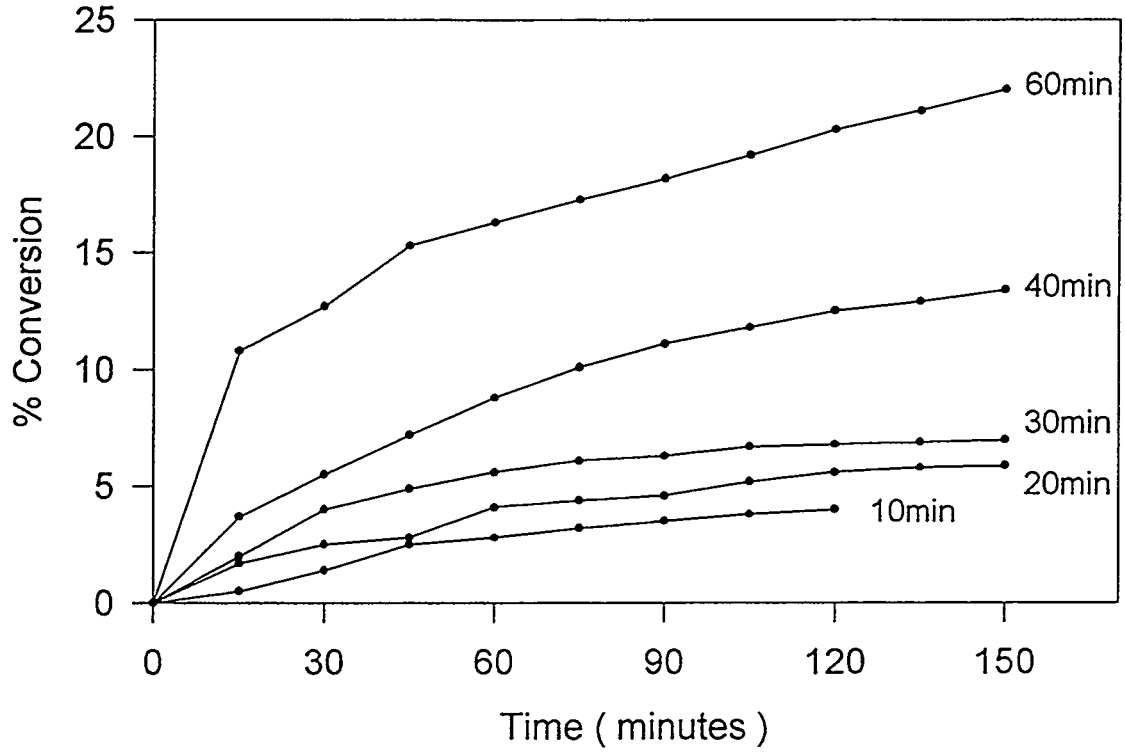

Figure 3.14. CO oxidation results for 10, 20, 30, 40, and 60 minute Cu depositions on graphite under a 66/33 Torr CO/O_2 gas mixture at 275°C.

by their Auger parameter (the sum of the $2P_{3/2}$ binding energy and the LVV kinetic energy) as well as by the presence of shake up peaks for copper (II) oxide [102,129,171-173]. Table 3.1 lists the Auger parameter data. AES relative peak intensities of the oxygen 515 eV peak to the copper 918 eV peak can also be used for quantitative analysis of stoichiometry. Auger copper to oxygen ratios are listed in Table 1 for copper (I) oxide and copper (II) oxide.

The catalytic ability of copper for different deposition times is shown in figure 3.14. The curves do not smoothly vary with time. All curves show a large initial rate followed by a slow rise in activity. A comparison between curves shows that the activity is not proportional to copper deposition time. The change in activity occurs between 30

and 45 minutes into the reaction. This may be due to deactivation or a change in the deposited copper. To determine what was causing the change in activity, an XPS experiment was performed. The sample was heated in the reaction gas mixture for a short time then transferred into UHV to observe any changes in the catalyst.

One can readily study the oxidation of metallic copper during a catalytic reaction. The results of exposing a metallic copper surface to a 66/33 Torr CO/O_2 gas mixture at 275°C is shown in figure 3.15. Time zero is the initially deposited metallic copper and each subsequent curve is an 11 minute exposure totaling 66 minutes for the experiment. For the first exposure, there was a significant shift to lower kinetic energies for the Cu LVV transition seen in figure 3.15A. The Cu $2P_{3/2}$ peaks shifts to slightly lower binding energies for the first exposure seen in figure 3.15B. The 11 through 66 minute exposures show a gradual shift back to higher kinetic energies for the Cu LVV peak. The Cu $2P_{3/2}$ peak shifts to higher binding energies between 11 and 66 minutes and the shake up peak increases in intensity with each exposure. The changes in the spectra are consistent with metallic copper being oxidized to copper (I) oxide for the first 11 minutes and copper (I) oxide being oxidized to copper (II) oxide for the remaining 55 minutes. This finding agrees well with other studies of the oxidation of copper [172,173]. All exposures produced CO_2. The amount of CO_2 produced decreased with increasing exposure showing that metallic copper, copper (I) oxide, the partial oxides between copper (I) and copper (II), and copper (II) oxide were all active for CO oxidation. The decreasing production of CO_2 explains the activity curves in figure 3.14. The lack of proportionality with copper deposition time may be due to the rate at which the catalyst oxidized while producing CO_2.

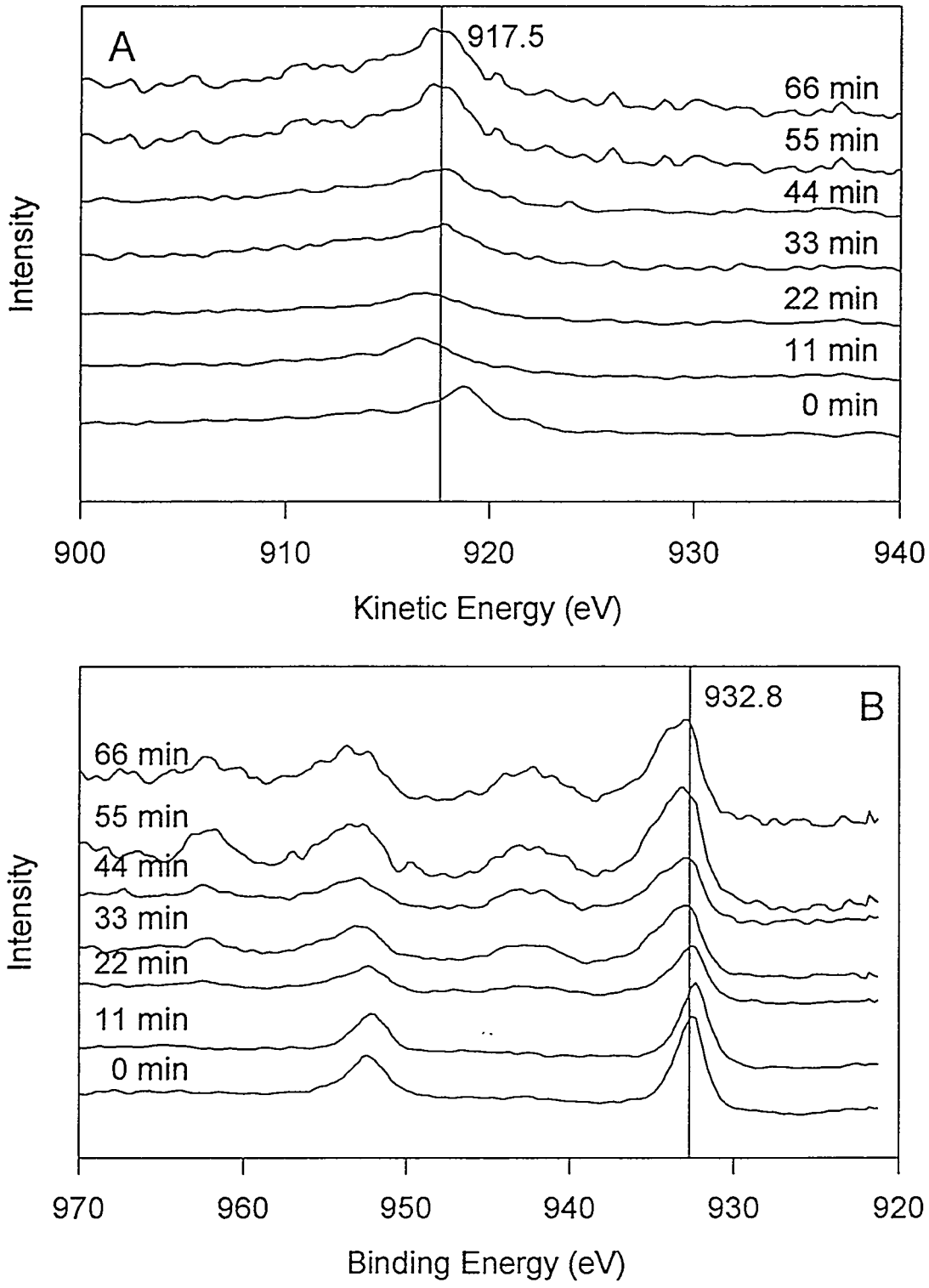

Figure 3.15. XPS of the A) Cu LVV and B) Cu 2P regions for a metallic catalyst exposed to a 66/33 Torr CO/O_2 gas mixture at 275°C for 11 minute intervals.

3.9. Summary

Copper was deposited on oxidized supports of aluminum, silicon, molybdenum, tantalum, stainless steel, and iron as well as graphite in an attempt to find a support which would not interfere in the catalytic chemistry of copper oxides. The oxides of copper needed to be supported on materials which would provide thermal and electrical conductivity to the copper films. The copper films needed to be thin to allow for complete characterization of the catalyst without difficulties associated with a bulk sample.
None of the oxidized supports were useful as supports as they formed compounds with the copper oxides or completely oxidized during a catalytic reaction. The compounds did have activities greater than or equal to the support without catalyst but were not good as models.

Copper deposited on graphite was found to be a good model system. The three oxidation states of copper could be prepared and characterized. The growth of copper on graphite showed 3 dimensional islands which wet the surface when oxidized. The graphite was found to be stable under more oxidizing conditions and at higher temperatures than to be used in studying CO oxidation over Cu. The activity of Cu on graphite was found to change during a catalytic reaction in 66/33 Torr CO/O_2 at 300°C. An XPS experiment showed that the catalyst could oxidize during the reaction. Hence in order to measure activity over a particular oxidation state of Cu, the CO/O_2 ratio must be fixed to prevent a change in the catalyst oxidation state. Chapter 4 discusses the activity of Cu, Cu_2O and CuO on graphite tested under different CO/O_2 ratios to obtain kinetic results specific to the oxidation state of copper.

Chapter 4

Carbon Monoxide Oxidation

4.1. Introduction

Oxidation of carbon monoxide over copper catalysts has significance in understanding methanol synthesis, the water-gas shift reaction, and automotive exhaust controls to mention a few major applications. Studies have shown that methanol synthesis is likely to occur by the hydrogenation of carbon dioxide and that carbon monoxide is needed to scavenge oxygen left on the surface [174,175]. In the water gas shift reaction, carbon monoxide removes surface hydroxyls or oxygen produced by the dissociation of water [42,46]. Copper has been explored as a possible substitute for palladium and platinum for the reduction of nitrogen oxides by carbon monoxide in automotive catalytic converters [176,177]. The reaction is believed to occur through the decomposition of NO_X forming nitrogen gas and adsorbed oxygen on the surface which then reacts with carbon monoxide. Even though the importance of the oxidation of carbon monoxide over copper has been recognized, the reaction remains poorly understood because of changes in the copper oxidation state as the reaction conditions are altered. It is usually assumed that copper is active in a particular oxidation state, or in the case of a redox reaction, that it cycles between two oxidation states. There has been no attempt to date to investigate how the rate of a reaction varies as a function of copper oxidation state.

We report here the first high pressure study of carbon monoxide oxidation on model low surface area copper and copper oxide surfaces.

$$CO + \frac{1}{2}O_2 \xrightarrow[Cu_2O]{Cu} CO_2$$
$$\xrightarrow[CuO]{}$$

We studied the catalytic oxidation of carbon monoxide over copper in such a way that by adjusting the CO/O_2 partial pressure ratio in the reactant mixture and the temperature we could fix the oxidizing power. Within certain ranges of CO/O_2 we could stabilize the copper catalyst in its zero, +1, or +2 oxidation state. The catalyst was a thin film of copper deposited onto a graphite support in ultra high vacuum (UHV). In this way the copper oxidation state throughout the film would be uniform as the sample could rapidly equilibrate to the oxidation state imposed by the CO/O_2 ratio and could be measured.

Studies of carbon monoxide oxidation on copper by others have been performed in high vacuum using single crystals [21-26] and also on supported copper catalysts [27-37]. The single crystal studies react carbon monoxide at pressures of less than or equal to $1x10^{-4}$ Torr with saturation coverages of oxygen pre-dosed on the copper surface. In these cases the reaction conditions are very reducing (CO/O_2 ratio greater than 100) to maintain a metallic surface. There is little information from these studies on how the reaction and surface change when higher pressures and more oxidizing conditions are used. Additionally, the reaction on the single crystal typically turnover only once. Therefore, the reaction is not catalytic. Carbon monoxide oxidation performed on supported copper catalysts were studied under total pressures between 10 and 760 Torr with an oxidizing gas mixture (CO/O_2 ratios less than the stoichiometric value of 2). The catalysts are formed first by calcining a copper salt to copper (II) oxide (CuO). The catalyst is either used in this state or pretreated. The pretreatments result in a reduction of the catalyst to metallic copper, copper (I) oxide (Cu_2O), or a mixed oxide typically

measured by bulk X-ray diffraction prior to the reaction. These studies do not determine the surface oxidation state of the copper.

This chapter bridges the gap between the low pressure single crystal studies and the studies of the supported catalysts that were carried out at high pressures. Copper and its oxides were investigated in this study using surface science techniques and a high pressure reactor under reaction conditions where the CO/O_2 ratios overlap the conditions utilized in both single crystal and supported catalyst studies. To do this we constructed in our laboratory a special high pressure reactor and transfer system which was capable of operating in oxidizing conditions and connected it to a UHV chamber. We carried out CO oxidation at 100 Torr total pressure and CO/O_2 ratios between 2 and 100 over the temperature range of 200-350°C. X-ray Photoelectron Spectroscopy (XPS) and Auger Electron Spectroscopy (AES) were used to characterize metallic copper, copper (I) oxide, and copper (II) oxide that were deposited onto a graphite support. Reactions were also performed using a platinum foil to provide a reference for the activity of the copper surfaces in their different oxidation states.

We find that the reaction rate of CO oxidation is fastest on metallic copper, and at 300°C the rate decreases with increasing copper oxidation state: $Cu^0 > Cu^{+1} > Cu^{+2}$. The apparent activation energies for the reaction increases in a similar order: 9 kcal/mol Cu^0 < 14 kcal/mol Cu^{+1} < 17 kcal/mol Cu^{+2}. The reaction rate on platinum at 300°C was approximately equal to the rate on metallic copper but was greater then the rates for the oxides of copper. The activation energy, 20 kcal/mol, for the reaction on platinum was greater than the three copper samples. The different activation energies obtained for the reaction on copper in different oxidation states indicates a changing mechanism that will be discussed. We hope that these studies will aid the development of a better understanding of the role played by copper in catalytic reactions in its various oxidation states.

4.2. Experimental

Copper was deposited by evaporation from an alumina crucible. The crucible was heated to 1500°C by passing current through a tungsten wire wrapped around the outside. The crucible was heated for 20 minutes prior to deposition to assure a steady flux of copper atoms. A deposition rate of approximately 0.5 monolayers per minute was measured by an AES uptake curve of Cu deposited onto a pure Fe foil. The deposition of 10 monolayers of metallic copper was the first stage in the preparation of all of the copper catalysts used in these experiments. The freshly deposited copper was used as is for the metallic copper measurements. Copper (II) oxide was produced by oxidizing the metallic copper in the reaction cell in 100 Torr of oxygen at 300°C for 20 minutes. Copper (I) oxide was obtained by annealing copper (II) oxide in UHV at 400°C for 10 minutes. The platinum foil was cleaned by repeated cycles of sputtering at 1500 V in $1x10^{-5}$ Torr of argon at 600°C, heating in oxygen at 600°C, and briefly annealing at 700°C.

Reactions were run between 200 and 350°C in a batch reactor with a volume of 0.68 liters. The sample was resistively heated during the reaction using a Eurotherm temperature controller which maintained the sample temperature to within 1°C over the course of the reaction. CO and O_2 were pre-mixed in a separate vessel in partial pressure ratios of 66/33, 90/10, and 97/3, CO to O_2 respectively, before admittance to the reactor. CO (Airco grade 2.3) was distilled with 5 Å molecular sieve trap in a liquid nitrogen bath to remove metal carbonyls prior to use, and O_2 (Airco grade 2.6) was used without purification. For each reaction a total of 100 Torr of mixed gas was used. The gases were recirculated in the reactor at 100 cm^3/min. The sample was brought to the reaction temperature in the presence of the gases in approximately 4 minutes. The production of CO_2 and the decrease of CO and O_2 was monitored by gas chromatography using a Supelco Carboxen 1000 column run isothermally at 125°C with a helium carrier flow of 30 ml/min and measured by a thermal conductivity detector. The sensitivity of the thermal

conductivity detector was calibrated using known partial pressures of the individual gases. A 1 ml aliquot gas sample was removed by an automatic sampling valve every 11 minutes and injected into the gas chromatograph. After the reaction, the cell was pumped to less than 50 mTorr then the sample was transferred into UHV. A 10 minute delay was necessary to allow the base pressure to return to less than $1x10^{-9}$ Torr before post reaction analysis was performed.

4.3. Results/Discussion

This work has been motivated by the lack of knowledge concerning how a catalyst's surface oxidation state affects its catalytic ability and if the changes in the surface oxidation are part of the catalytic mechanism. This is especially important in selective oxidation and combustion reactions over mixed metal oxide catalysts. For these reactions, it is commonly proposed that the reaction mechanism does occur through a redox cycle. The initial step in the reaction being the reduction of the surface by a gas phase reactant. The oxidized reactant can then undergo rearrangements prior to leaving the surface. The final step in the reaction is the reoxidation of the catalyst by gas phase oxygen. This mechanism has yet to be experimentally verified but there are some reports which strongly suggest [178] it is valid. The obstacle to experimentally determining this reaction mechanism has been the inability to monitor the surface oxidation state. This is difficult because there is a rapid reoxidation of the surface by the gas phase and by diffusion of bulk oxygen to the catalyst surface.

We circumvent these difficulties by using a thin (10 monolayers) copper catalyst. In this way the whole catalyst can be viewed as a surface without different bulk properties. The use of a bulk sample would have resulted in a reservoir for oxygen or metallic copper. A thick film would not be appropriate because the electron spectroscopies have a limited

penetration depth into the surface. This has importance to studying metallic copper where oxygen can go into the near surface region [22,179,180]. As will be demonstrated in the kinetic results of CO oxidation over metallic copper at 250°C, the presence of subsurface oxygen can affect the reaction rate.

The success of using a thin copper catalyst was also demonstrated in the timed exposure of a metallic copper catalyst to a 66/33 CO/O_2 ratio at 275°C seen in chapter 4. There is a competing reaction between the oxidation of the catalyst surface and the oxidation of CO. We are seeing the kinetics of surface oxidation on a time scale which is much greater than the kinetics of CO oxidation. Knowing that there can be a solid state reaction, and working to avoid it, allows us to better understand how the reaction is occurring over the different copper catalysts.

Catalytic reactions were performed with different CO to O_2 partial pressure ratios for metallic copper, copper (I) oxide, and copper (II) oxide using 97/3, 90/10, and 66/33 respectively, because the surface oxidation state can change as a function of the gas composition, temperature, and exposure time. These ratios were chosen because in each case the 300°C post reaction XPS indicated that the copper oxidation state had not changed from the oxidation state prior to the reaction. By performing CO oxidation under conditions where the oxidation state of the catalyst does not change, we were able to obtain activation energies for the 3 different oxidation states of copper. Platinum was tested under the same conditions used for the three different oxidation states of copper. The results are reported as the percentage of CO in the reactor that was converted to CO_2 versus time. Defined as

$$\%CO = \left(\frac{P_{CO_2}}{P_{CO} + P_{CO_2}} \right) \times 100$$

where P_{CO} and P_{CO_2} are the partial pressures of CO and CO_2 respectively. Rates obtained from the initial slopes of percentage of CO converted versus time were used to calculate the activation energy for CO oxidation.

Working with gas mixtures of CO and O_2 where the catalyst composition does not change on the time scale of the reaction, we are able to compare the activity and activation energies for the different oxidation states of copper. Different rate determining steps for each of the oxidation states of copper could be indicated from having obtained different activation energies. The rate determining step could be 1) adsorption of species onto different sites for each surface, 2) reactions between adsorbed species, 3) reactions between adsorbed species and the catalyst surface, 4) reactions between adsorbed species and the gas phase, and 5) reaction between the catalyst surface and the gas phase. Let us consider which of these steps might control the rate for a given copper oxidation state.

4.3.1. Metallic Copper

4.3.1.1. Activity 97/3 CO/O_2

Representative kinetic data for CO oxidation on a metallic copper catalyst are shown in figure 4.1A. A CO/O_2 ratio of 97/3 was used and could result in a maximum CO conversion of 6.2 % where O_2 is the limiting reagent. There was a rapid rise in conversion for curves a) 350, b) 300, and c) 275 °C resulting in the complete use of oxygen. At 200°C, the initial rate is not rapid but gradually rises. The 250°C data, shows a slow initial rate but at 89 minutes there is rapid rise in the percent conversion. A comparison of the XPS and Auger spectra before and after the change in activity for the 250°C reaction shows that the rapid rise is due to the copper becoming metallic. Hence, even under these very reducing conditions, the catalyst is slightly oxidized upon exposure to the reactant gas mixture. The reduction of the surface is very slow at temperatures

below 250°C. Using the reaction rate where the catalyst is known to be metallic at 350, 300, 275, and 250°C after the break, gave an activation energy of 8.8 ± 1.0 kcal/mol for CO oxidation on the metallic copper catalyst in figure 4.1B. This is in good agreement with UHV studies of CO oxidation on copper single crystal [21-25]. Using the reaction rate where the surface is oxidized at 200 and 250°C before the break gave a higher activation energy of 11.2 ± 1.0 kcal/mol . The error in the activation energies for the metallic copper catalysts are large because of the few points available in calculating the slope for the rapid rise of the high temperature reactions and in the very low conversion for the reactions at the lower temperatures.

4.3.1.2. Mechanism

We believe the mechanism of CO oxidation over the metallic copper catalyst to be of the Langmuir-Hinshelwood type and that the presence of oxygen affects the adsorption of CO. Our kinetic results showed that the reaction had different rates when there was surface oxygen present. The rate of CO oxidation was slower on an oxidized surface. Surface oxygen was found during reactions run at temperatures less than 275 °C. With time, the oxidized surfaces were gradually reduced. Upon returning to a metallic oxidation state, the rate of reaction increased over the metallic copper surface. For reactions run at temperatures greater than 275°C, the surface did not oxidize and had a faster rate for CO oxidation than the oxidized surface. This changing rate had been seen by O.P. van Pruissen [24] who attributed it to two different sites for oxygen, surface and subsurface. The reaction is limited by the adsorption of CO which was postulated to be inhibited by surface oxygen. At the start of the reaction, there is a low surface coverage of CO. The CO reacts with the surface oxygen which is replenished by subsurface oxygen. When the bulk is depleted of subsurface oxygen, the concentration of CO on the surface can increase. The reaction rate changes because adsorbed CO does not inhibit the

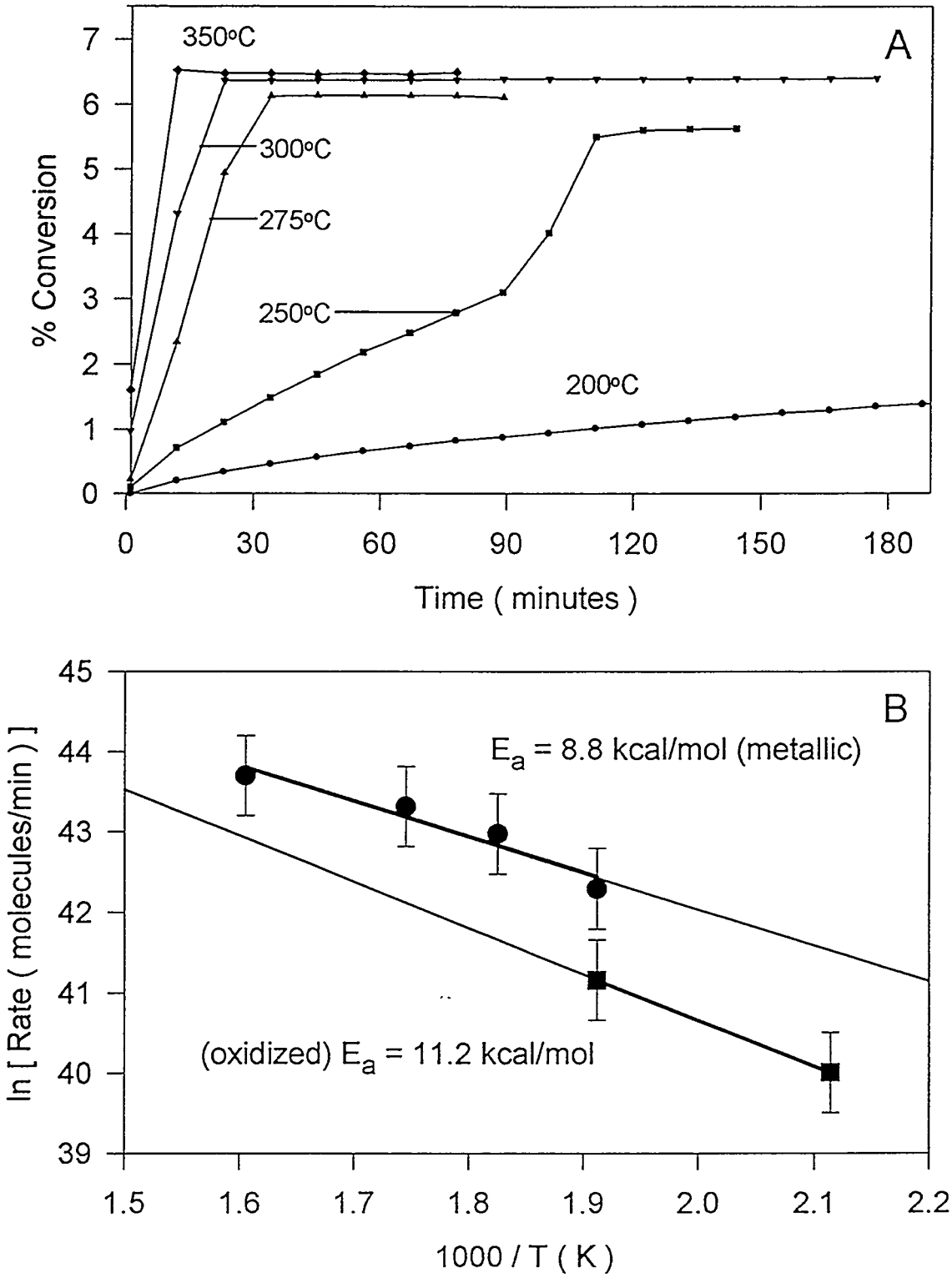

Figure 4.1. CO oxidation results for a metallic copper catalyst run under a 97/3 CO/O_2 ratio. **A)** shows the activity as a function of temperature and **B)** shows the Arrhenius plots for metallic and oxidized copper determined from the initial reaction rates.

adsorption of O_2. Hence gas phase O_2 upon adsorption can react rapidly with the CO present. We agree with that interpretation of the change in the reaction rate. XPS results did show that oxygen was present when the reaction rate was slow and absent when the reaction rate was fast. This fits well with other UHV studies in the literature which postulate that the reaction mechanism can be described with the Langmuir-Hinshelwood model [21]. For metallic copper the reaction rate is different over an oxygen saturated surface and a carbon monoxide saturated surface.

4.3.2. Copper (I) Oxide

4.3.2.1. Activity 90/10 CO/O_2

Representative kinetic data for CO oxidation on a copper (I) oxide catalyst are shown in figure 4.2A. A ratio of 90/10 was used and could result in a maximum CO conversion of 22.2% based on complete use of gas phase oxygen. The kinetic curves at 350, 300, 275, 250, and 200°C, are smoothly varying with time. This indicates that there is no change in the catalyst oxidation state as was seen in the metallic copper catalyst data. The 350°C run does approach complete use of the gas phase oxygen. XPS showed that for an extended run at 350°C the catalyst surface does not reduce until all of the gas phase oxygen had been consumed. Using the initial reaction rates an apparent activation energy of 13.9 ± 0.5 kcal/mol for CO oxidation on copper (I) oxide was calculated. The Arrhenius plot for copper (I) oxide is shown in figure 4.2B.

4.3.2.2. Mechanism

Studies of the mechanism of CO oxidation over copper (I) oxide is complicated by many subtleties. Copper (I) oxide is only stable under a small range of CO/O_2 ratios. A

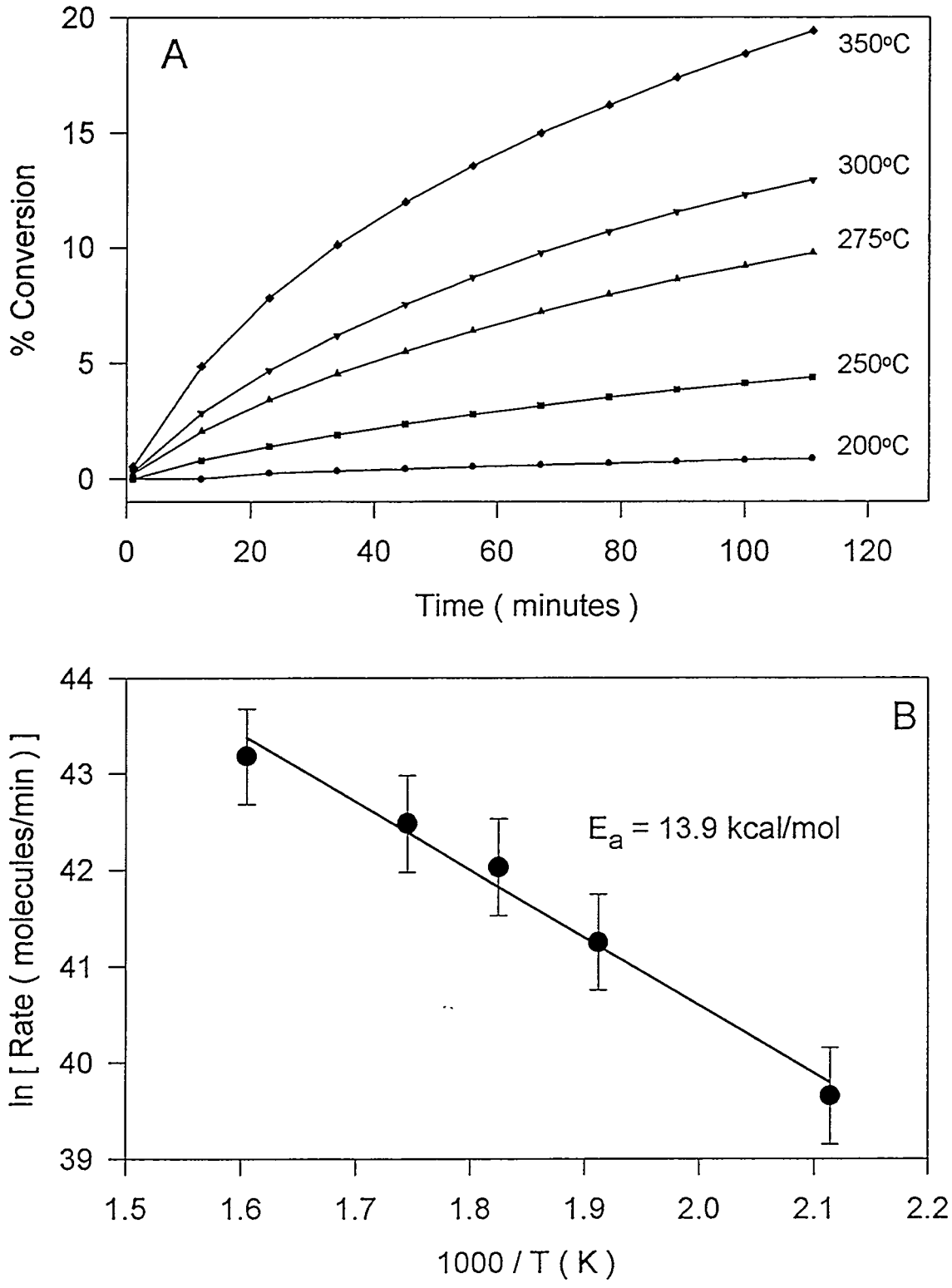

Figure 4.2. CO oxidation results for copper (I) oxide run under a 90/10 CO/O_2 gas mixture. **A)** shows the activity as a function of reaction temperature and **B)** shows the Arrenhius plot determined from the initial reaction rates.

smaller CO/O_2 ratio would result in the oxidation of the surface and a higher ratio would result in a reduction of the surface. During the course of a reaction, the CO/O_2 ratio will increase as the limiting reagent, oxygen, is depleted. The surface will most likely be reduced at a point in the reaction. A second difficulty arises from the possibility that the reaction might undergo a redox cycle involving the surface oxidation state. The mechanism could cycle between Cu_2O and CuO where the first step in the reaction is the oxidation of the surface, or the mechanism could cycle between Cu_2O and metallic copper and the first step in the reaction would be the reduction of the surface. The last concern is if the reaction does not involve a change in the oxidation state of the surface how does the reaction proceed?

From the kinetic curves obtained for the reaction of a 90/10 CO/O_2 ratio over copper (I) oxide some insight can be gained. First, the curves are smoothly varying with time. This most likely indicates that there is not a change in the reaction mechanism as was seen over a metallic copper catalyst. Second, it was discovered that the surface did not reduce until all gas phase oxygen had been reacted. This is also in contrast to what occurs over metallic copper. These two facts discount a redox cycle between metallic copper and copper (I) oxide. If the redox cycle was occurring, as oxygen was being removed from the gas phase, fewer sites would be reoxidized to copper (I) oxide. Therefore as the reaction proceeds the surface would gradually become reduced to metallic copper. This does not occur because we do not see any reduction in the surface during the reaction. Lastly, there is no apparent deactivation in the catalyst. The formation of CO_2 may not inhibit the reaction.

We propose the mechanism of CO oxidation over copper (I) oxide to be of the Langmuir-Hinshelwood type and is related to the metallic copper catalyst case where subsurface oxygen was present. The reaction rate for copper (I) oxide is similar to an oxidized metallic copper catalyst, and the activation energy for an oxidized metallic copper catalyst is between the values for an unoxidized metallic copper catalyst and

copper (I) oxide. The difference between the two catalysts is that the energy barrier for subsurface oxygen in metallic copper to diffuse to the surface and react is lower than the dissociation energy of copper (I) oxide into metallic copper and an oxygen atom. We do not see any change in the oxidation state of copper (I) oxide during the reaction and so believe that no dissociation occurs. The reaction on an oxidized metallic copper was explained by a model where adsorbed CO reacts with adsorbed oxygen and oxygen inhibits CO adsorption. This is what we believe happens on copper (I) oxide and that the higher activation energy could be due to the extra energy needed to dissociate O_2 on the copper (I) surface. There is one study which reports that the heat of adsorption of CO on copper (I) oxide is greater than on metallic copper [74]. The higher heat of adsorption of CO on copper (I) oxide as compared to metallic copper could be due to a lower surface coverage as heats of adsorption typically decrease with increasing coverage. The higher heat of adsorption does indicate that CO should be present on the surface during the reaction. The presence of oxygen on the copper (I) oxide surface can be implied from its ability to further oxidize to copper (II) oxide, because in order to further oxidize, the copper (I) oxide surface must be able to dissociate O_2.

4.3.3. Copper (II) Oxide

4.3.3.1. Activity 66/33 CO/O_2

Representative data for CO oxidation on a copper (II) oxide catalyst are shown in figure 4.3A. A CO/O_2 ratio of 66/33 was used and could result in a CO conversion of 100% based on complete use of gas phase oxygen. The kinetic curves at 350, 300, 275, 250, and 200°C have fast initial rates. For all the curves, at 22 minutes the rates begin to decrease. Extended catalyst runs beyond 2 hours resulted in complete deactivation of the catalyst. The catalyst does not completely use all of the gas phase oxygen present. This

deactivation is believed to be due to CO_2 adsorption onto the surface [35]. Post reaction XPS did not show the presence of a carbonate peak although this has also been proposed to be the cause of catalyst deactivation [26]. After deactivation, the reaction cell was evacuated and admittance of fresh gases returned the catalyst to its initial activity. Hence, we believe that CO_2 does not modify the catalyst surface but does block adsorption sites. Using the initial reaction rates an apparent activation energy of 16.7 ±0.5 kcal/mol for CO oxidation on the copper (II) oxide was determined. The Arrhenius plot is shown in figure 4.3B. This is in good agreement with supported catalyst measurements [27,28].

4.3.3.2. Mechanism

CO oxidation over a copper (II) oxide catalyst has been studied by many researchers [27-37], but there is no consensus as to the mechanism. There is an agreement that the reaction rate is enhanced by exposing the catalyst to a reducing pretreatment. This work has shown that with decreasing copper oxidation state the CO oxidation rate is faster and in agreement with the enhancement found by reducing the catalyst surface. The possibility that different pretreatments may result in the catalyst surface having an oxidation state between 0 and 2 can explain why a consensus on the reaction mechanism has not been reached. It should also be mentioned that the catalyst surface might change depending on the gas phase composition during the reaction, as was demonstrated in figure 3.15 where metallic copper under 66/33 CO/O_2 ratio at 275°C oxidized to copper (II) oxide. If a reaction was carried out where metallic copper was the starting catalyst and it was tested under stoichiometric reaction conditions, then the catalyst would change with time. If the reaction rate was measured at the start of the reaction or after some period, then different activation energies would be obtained from an Arrhenius plot. This fact complicates the interpretation of the current literature.

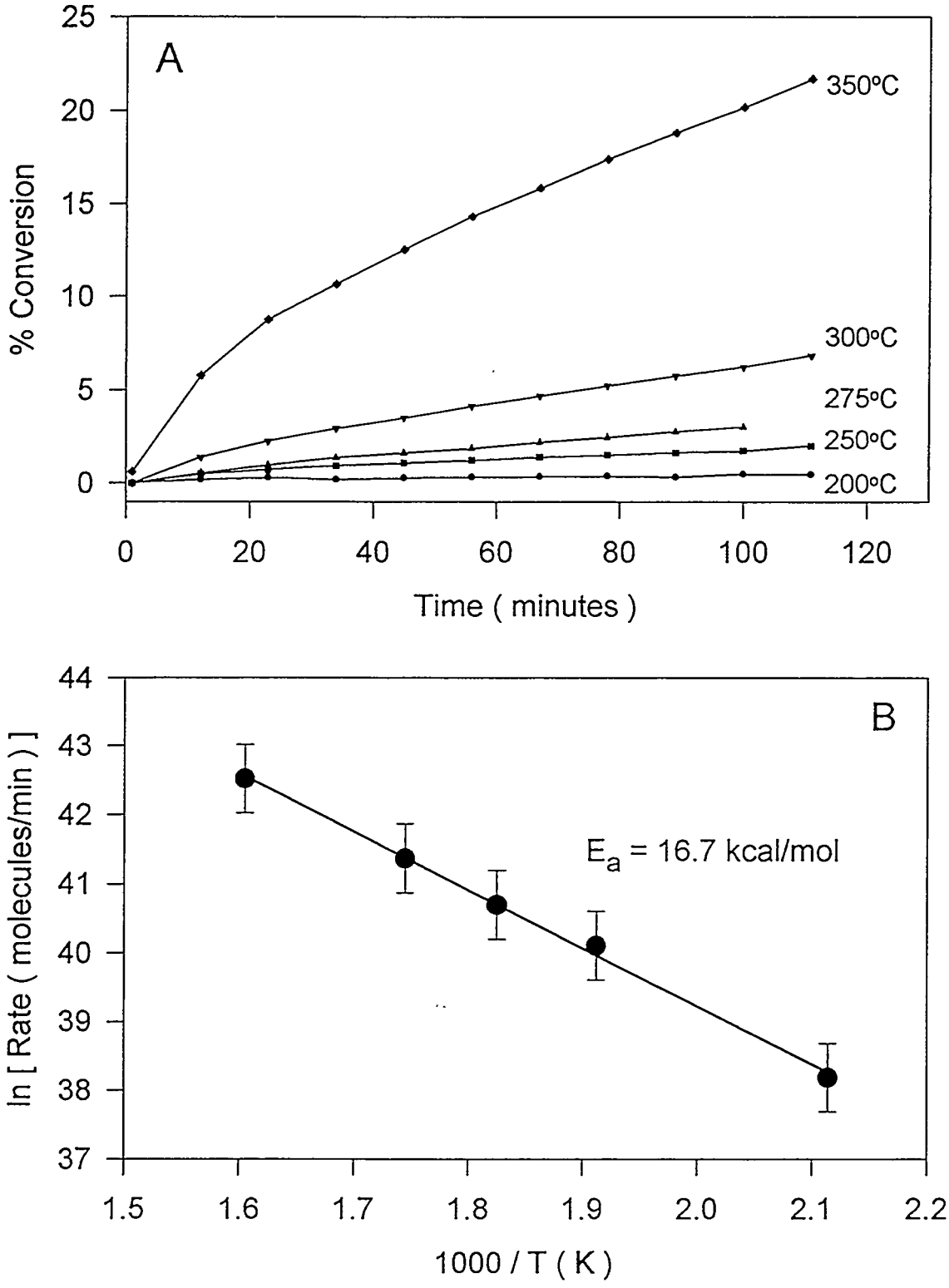

Figure 4.3. CO oxidation results for copper (II) oxide run under a 66/33 CO/O_2 gas mixture. **A)** shows the activity as a function of reaction temperature and **B)** shows the Arrenhius plot determined from the initial reaction rates.

Combining our results of the oxidation of copper and the kinetic results obtained for CO oxidation under a 66/33 CO/O_2 ratio, we propose a redox cycle mechanism between CuO and Cu_2O where the rate limiting step is the reduction of copper (II) oxide by CO. We know that the reaction rate has a first order dependence in CO and that the reaction only proceeds if there is adsorbed CO on the catalyst surface [27]. This indicates that the reaction is dependent on the surface coverage of CO. The adsorbed CO must react with either a gas phase oxygen or a surface oxygen. O_2 dissociation only occurs when electrons are donated from the surface to the O_2 molecule leading to a metal cation and oxygen anion pair [181]. Because copper (II) oxide is an insulator and can not donate electrons, oxygen will not dissociate. Hence for there to be CO_2 production, CO must reduce the catalyst surface. Under reaction conditions where the ratio of CO to O_2 is less than or equal to 2, the surface will be rapidly oxidized to copper (II) oxide. The oxidation of the catalyst surface is faster than the reaction rate, which equals the rate of surface reduction. The deactivation in our kinetic results is due to CO_2 adsorption on the copper (II) oxide surface [35]. CO_2 could be blocking CO adsorption sites on the surface or decomposing on a reduced surface site to adsorbed CO and oxygen. We believe the decomposition is unlikely because the high O_2 gas phase partial pressures would rapidly oxidize any reduced surface sites.

To test if a surface redox reaction is responsible for the catalytic activity, a test of activity as a function of copper oxidation was performed. The experiment consisted of depositing and oxidizing copper to +2 on a preexisting CuO layer. The results are shown in figure 4.4. A series of 5 minute depositions, all show similar activity. The activity is not proportional to the total copper amount as the initial 5 minute activity is equivalent to the 5 minute deposition onto 15 minutes of CuO. A 20 minute deposition however resulted in a 4 fold increase in activity over the 5 minute depositions. When an additional 20 minutes was added no increase over the initial 20 minutes is found. The last curve shows the activity of a fresh 60 minute deposition and oxidation. These results can be

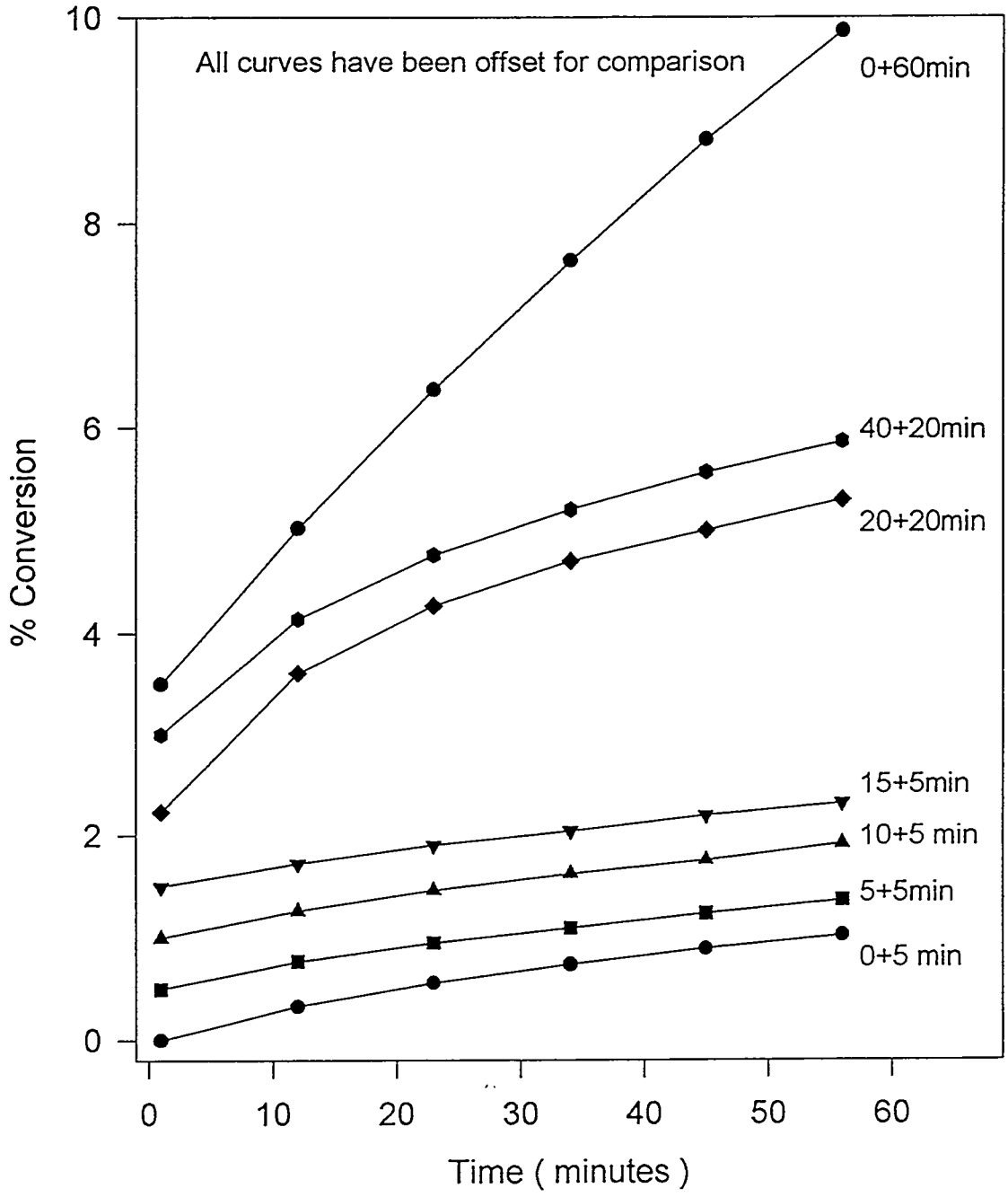

Figure 4.4. The effect of copper oxidation on CO oxidation over a copper (II) oxide. The copper amounts are shown as the initial oxide deposition time + the fresh oxide deposition time.

explained by assuming the activity is due to oxygen removal from the edges of CuO. When copper is deposited on graphite it adheres to the step edges. When additional copper is deposited, the new layer adheres to the copper oxide already present. By adding fresh copper oxide, it expands the oxide from the step edge. It could be viewed as a moving reaction front. The terrace formed by the copper oxide is not reactive as the oxygens in the terrace are well coordinated. When more copper is deposited the island size changes resulting in a new periphery and more activity. The 60 minute deposition is not 3 times greater than the 20 minute depositions indicating a limit to the 2 dimensional island size.

4.3.4. Platinum Foil

4.3.4.1. Activity under 66/33, 90/10 and 98/2 CO/O_2 mixtures

The kinetic data for CO oxidation over a platinum foil under similar conditions to the experiments performed over copper and copper oxides is shown in figures 4.5 and 4.6. The results of CO oxidation on a platinum foil under a 66/33 CO/O_2 ratio are shown in figure 4.5A. The reaction at 350°C has a very large initial rate and slowly decreases as the reaction approaches 100 % conversion. At lower temperatures, 300, 275, 250, and 200°C, are nearly linear with time with the initial rate being slightly greater. Extended runs at 300°C resulted in complete use of CO and O_2. The slow decrease at 350°C as the catalyst approached 100% conversion is the result of decreasing reactant concentration. Post reaction AES for all temperatures did not show any surface oxygen present. Using the initial reaction rates an apparent activation energy of 19.9 ± 0.5 kcal/mol for CO oxidation on was determined from an Arrenhius plot, shown in figure 4.6B.

Platinum tested in a 90/10 CO/O_2 mixture, shown in figure 4.5B, reaches complete use of the gas phase oxygen is less time than the 66/33 mixture, but the initial rates are

similar. The curves show a large initial activity which decreases as the reactants are consumed in the reaction. The activation energy calculated under these conditions was 19.9 ± 0.5 kcal/mol and is plotted in the bottom of figure 4.6B.

A 98/2 mixture of CO/O_2 completely uses the gas phase oxygen within 40 minutes at all temperatures except 200°C. The initial rate is hard to determine as the reactants are used very rapidly. An apparent activation energy calculated for these results gives a value of 17.1 ± 1.0 kcal/mol. This is outside the error for the 66/33 and 90/10 mixtures. The reason for this may be due to changes in adsorption of O_2 on platinum when the CO pressure is so much greater. At higher O_2 pressures, islands of O can form on platinum because O does not desorb from platinum until 500°C. At the low pressures of O_2 an island may not be able to form. The island would provide stability against reaction resulting in a higher activation energy. The presence of O islands on platinum have been observed and used to explain the oscillatory behavior found for CO oxidation on platinum [182-184]. The apparent activation energy for the 66/33 and 90/10 mixtures is in close approximation to the values reported for similar temperatures and gas pressures for CO oxidation in a flow reactor [185].

4.3.4.2. Mechanism

CO oxidation over platinum and the other noble metals has been a well studied reaction and is therefore a good reference to compare with metallic copper, copper (I) oxide, and copper (II) oxide. For an excellent review of CO oxidation over the noble metals the reader is referred to the work of Engel and Ertl [38]. The mechanism for CO oxidation over platinum is of the Langmuir-Hinshelwood type and has two regimes. The regimes are divided by the temperature of maximum CO desorption from the surface. At temperatures less than the desorption maximum, CO is adsorbed on the surface and the reaction rate law has a negative first order dependence on gas phase CO and a positive

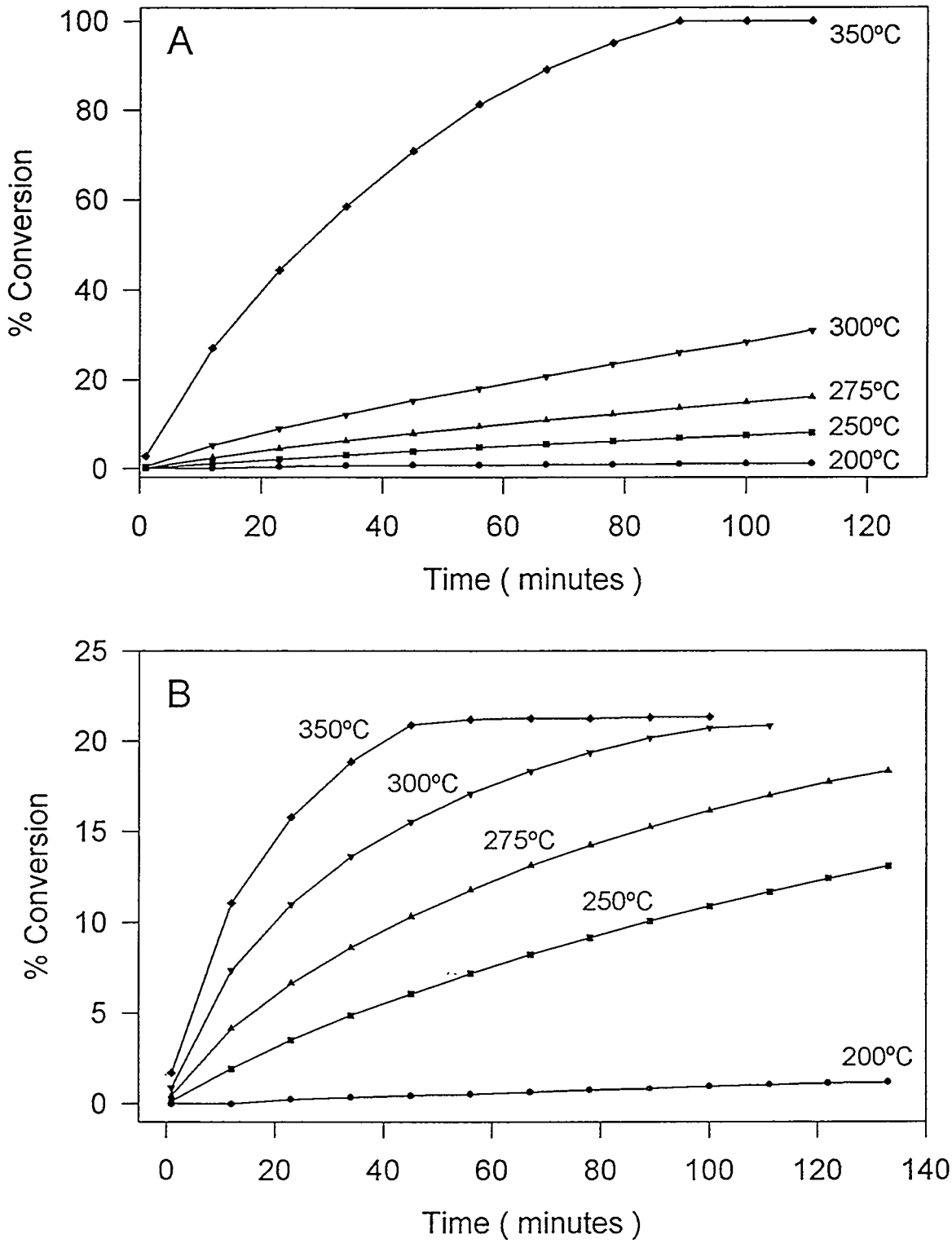

Figure 4.5. CO oxidation results for a platinum foil run under A) 66/33 and B) 90/10 Torr CO/O_2 gas mixture as a function of reaction temperature.

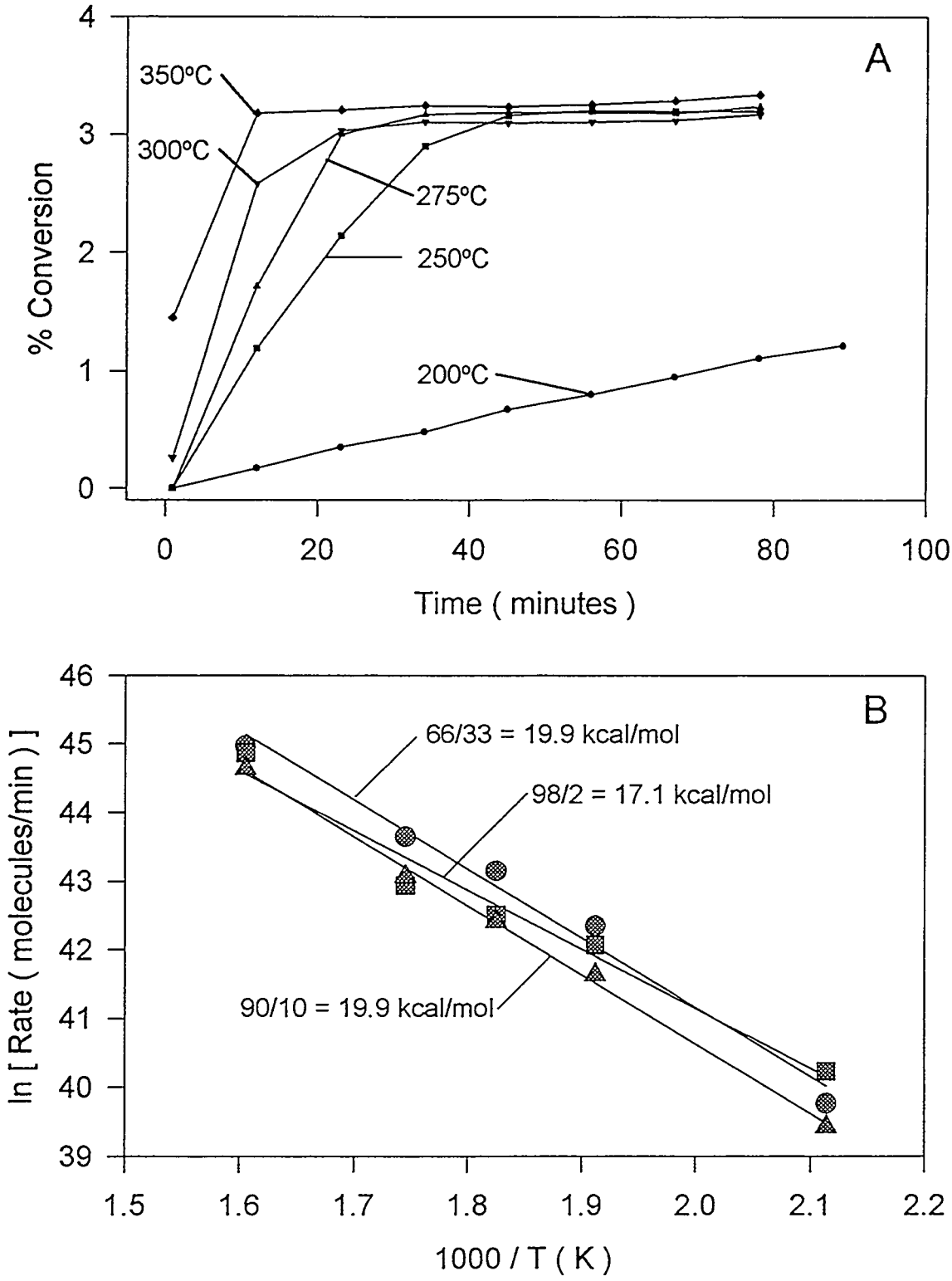

Figure 4.6. A) CO oxidation result for a platinum foil run under a 98/2 Torr CO/O_2 gas mixture as a function of reaction temperature. B) Arrenhius plots for platinum determined from the initial reaction rates for CO oxidation run under 66/33, 90/10, and 98/2 CO/O_2 gas mixtures.

first order dependence on gas phase oxygen. Adsorbed CO inhibits O_2 adsorption which explains the pressure dependences. At temperatures greater than the desorption maximum, CO is not adsorbed on the surface allowing oxygen to saturate the surface. The reaction has a first order dependence on CO. In this study, platinum was tested under conditions where the temperature of the reactions was lower than the temperature for CO desorption. Hence the surface is covered with adsorbed CO which inhibits O_2 adsorption giving the previously mentioned partial pressure dependences [185].

4.3.5. Comparison Between Copper and Platinum

The adsorption of CO and O_2 onto the copper catalyst surfaces is different from the platinum surface. For the reactions over the copper catalysts there is a positive dependence on the CO gas phase pressure. CO is weakly bound to the copper catalysts at these temperatures and pressures. Higher CO gas pressures will result in an increased surface coverage of adsorbed CO and a faster rate. We see no pressure dependence on O_2 for the reactions over the copper catalysts. There is an O_2 pressure dependence on the oxidation of the copper surface. The lack of a pressure dependence on O_2 for CO oxidation can be explained by the abundance of surface oxygen on the copper surface. Hence CO oxidation over the copper catalyst is similar to a platinum catalyst run at temperatures greater than the CO desorption maximum temperatures.

Although the copper catalysts have similar pressure dependences, the activation energies differ for CO oxidation over all of the catalysts. If one starts with the assumption that the mechanism for CO oxidation over the three different copper catalysts is Langmuir-Hinshelwood like platinum [27] , then the apparent activation energy, E_{App}, should equal the difference between the energy need for the Langmuir-Hinshelwood step, E_{LH} (reaction of adsorbed CO and adsorbed O), and the heat of adsorption of CO, E_{CO}.

$$E_{App} = E_{LH} - E_{CO}$$

We measured a decrease in E_{App} with increasing copper oxidation. If E_{LH} is constant for all three copper catalyst, then E_{CO} would have to decrease with increasing oxidation. It was reported [174] that the heat of adsorption of CO on copper (I) oxide was greater than that on metallic copper. This means that the assumption E_{LH} is constant is not valid. We might expect E_{LH} to differ on the different copper surfaces because of the changes in the bonding of oxygen to copper. This was demonstrated in the ability to reduce oxidized metallic copper but not copper (I) oxide during the reactions. Also, the three different copper catalysts were tested under different CO gas phase concentrations. This affects the amount of CO adsorption and therefore the CO heat of adsorption on the different copper surfaces. Lastly, a Langmuir-Hinshelwood reaction requires adsorbed oxygen on the surface, and in the case of copper (II) oxide we believe that the oxygen in the reaction comes from the catalyst. This implies that the different activation energies are due to different reaction mechanisms.

The reaction rates for CO oxidation over the copper catalysts also changed with surface oxidation. The reaction rate decreases with increasing surface oxidation. The kinetics of copper (II) oxide have been most often compared in the literature to a platinum catalyst as a potential substitute. Figure 4.7 shows how platinum compared with the three oxidation states of copper tested in this thesis. The activation energy of platinum was higher than all of the copper catalysts but had a greater rate at 350°C. A review by Kummer [19] showed copper (II) oxide being approximately 10 time less active but at 100°C lower in temperature. Under similar conditions to Kummer's, we measured copper (II) oxide being approximately 100 times less active. These results are not corrected for the different surface areas between the copper (II) oxide film and the platinum foil. This leads to the question of comparing surface areas or active sites between the three copper catalysts. Unfortunately a measurement of the surface area or number of active sites on

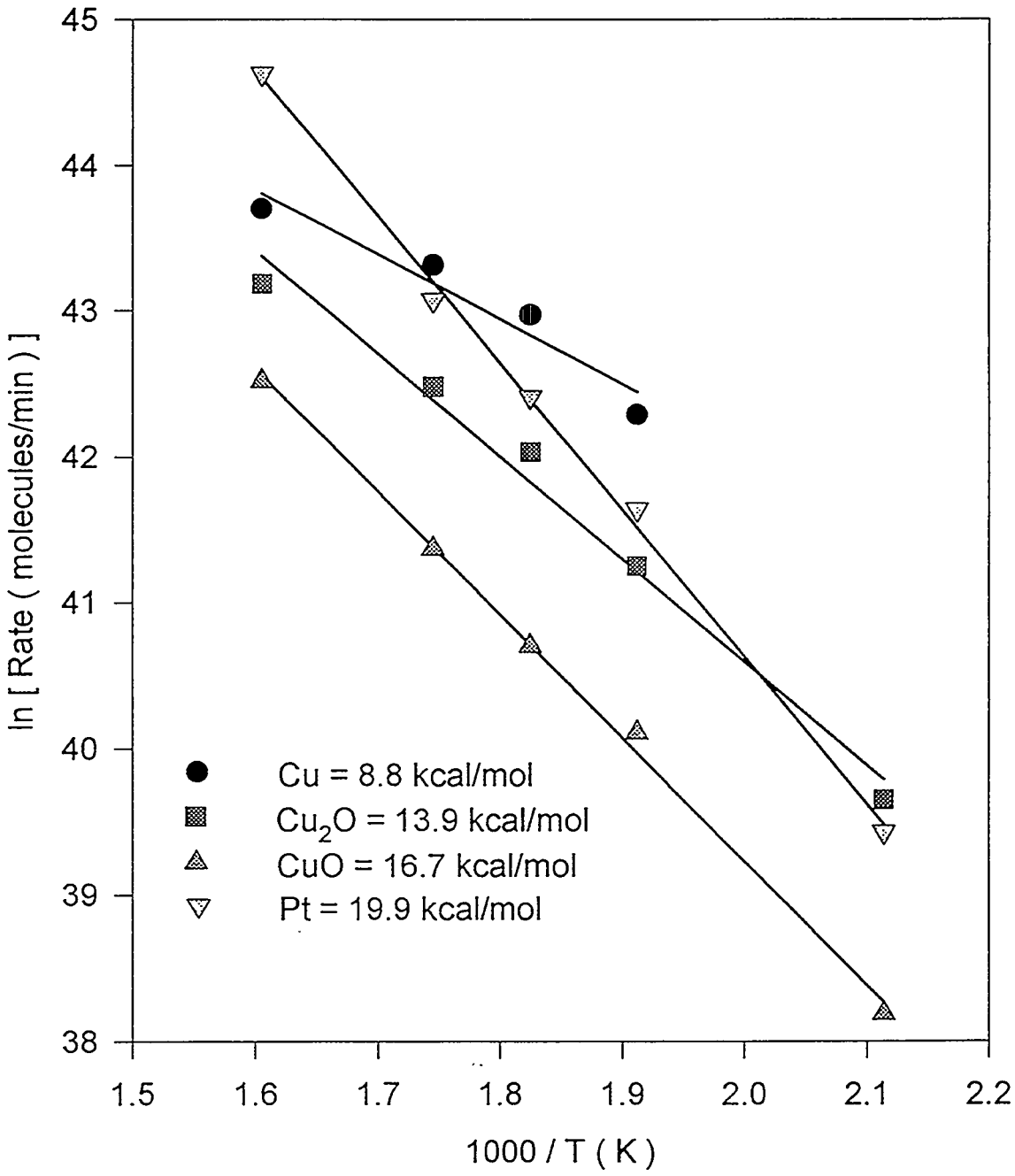

Figure 4.7. A comparison of Arrenhius plots for CO oxidation over metallic copper, copper (I) oxide, copper (II) oxide and platinum.

such a small amount of the oxidized copper catalysts is very difficult and could not be made. We believe that upon oxidizing the metallic copper catalyst to copper (I) and copper (II) oxide, there is a loss in active sites giving rise to the possibility that turnover frequencies may be similar between the copper catalysts.

4.4. Summary

The three oxidation states of copper were formed and tested for the catalytic ability to oxidize CO to CO_2 using O_2. Metallic copper was generated by depositing the metal in UHV onto a graphite coated stainless steel foil. XPS showed that copper (II) oxide was formed by oxidizing metallic copper in a 100 Torr of oxygen at 300°C for 20 minutes, and copper (I) oxide was formed by annealing copper (II) oxide at 400°C for 10 minutes in UHV. Under reaction conditions of 66/33 CO/O_2 partial pressure ratio at 275°C, metallic copper completely oxides to copper (II) oxide in approximately one hour. In order to prevent the oxidation state of the copper catalysts from changing during a catalytic test, the CO/O_2 ratio was fixed at 97/3, 90/10, and 66/33 Torr for metallic copper, copper (I) oxide, and copper (II) oxide, respectively. Metallic copper was found to be the most active and that with increasing copper oxidation the activity decreased. The activation energy showed a reverse trend and increased with increasing oxidation. Metallic copper compared favorably to a platinum sample having a faster rate for temperatures less than 350°C and a lower activation energy. Copper (I) and copper (II) oxide were less active than the platinum sample but had lower activation energies. The mechanism for CO oxidation over the three copper catalysts was affected by subsurface oxygen and oxide formation.

Chapter 5

Carbon Dioxide Deactivation

5.1. Introduction

In the previous chapter it was observed that CuO did not completely convert all of the CO into CO_2. The reaction of CO and O_2 has a very negative free energy, $\Delta_r G_{298}$ = -37 kcal/mol, favoring 100 % conversion of reactants into products. Complete conversion was not reached over CuO due to a deactivation of the surface. The explanation proposed was that CO_2 readsorbs onto the catalyst surface blocking the adsorption of CO. The lower activity of CuO in the presence of CO_2 was originally observed by Nobe and Blumenthal who added increased amounts of CO_2 to a CO and air mixture in a flow reactor [28]. They found that if the added CO_2 was removed, the catalyst returned to its initial activity. This phenomena was also observed in this work. The deactivation of the surface by CO_2 is reversible, but it is unknown what chemical species is present on the surface.

There are a few possible species which may form on the surface. First, CO_2 could adsorb onto the surface and dissociate. An equilibrium would be established between CO_2 and CO plus O_2. This is feasible in that a batch reactor was used for the reactions in this thesis. Second it is possible that CO_2 forms a carbonate with O present on the surface. Upon removal of gas at the end of the reaction, the lack of a partial pressure of CO_2 over the surface may result in the carbonate decomposing back into CO_2. The CO_2 would subsequently desorb. Third, CO_2 may simply molecularly adsorb onto the active site for CO adsorption. To this authors knowledge, there is no published values for the

heats of adsorption of CO or CO_2 onto CuO. The answer to the mechanism of catalyst deactivation can be obtained by adding CO_2 to the reaction and observing if a carbonate can be formed or if a change in the final gas phase equilibrium occurs.

CO oxidation did not show any obvious deactivation over Cu and Cu_2O, but this may be due to the lower partial pressures of CO_2. The reactions at high temperatures over both catalysts reached 100 % conversion but at lower temperatures the reactions were not run for sufficiently long times to see if 100% conversion would have been obtained. Addition of CO_2 to the reactions over Cu and Cu_2O would demonstrate if these surfaces also deactivate. Again, if deactivation occurs the question remains as to the cause for deactivation.. Work done by Goodman [26] suggested that CO_2 did deactivate the surface of a Cu single crystal. Post reaction TDS gave a CO_2 peak which was believed to be due to a surface carbonate that formed on the surface.

The possibility that CO_2 forms a carbonate on Cu is an extremely valuable piece of information to studies on the mechanism of methanol synthesis. The discovery that CO_2 is the carbon source of methanol [55] and that copper may be in the +1 oxidation state gives rise to the possibility that CO_2 will react with the Cu surface. UHV studies show that CO_2 does not dissociate on Cu and that it does not adsorb at temperatures greater than 130K [108,186-188]. But if CO_2 is irradiated at 77K or adsorbed onto a surface with alkali, two CO_2 species will form [188]. An activated anionic CO_2^- and an unactivated CO_2 can be seen by XPS, TDS, and surface enhanced Raman [186,188,189]. Upon annealing this surface, a CO_3^{2-} species can be observed. Calculations have shown that anionic CO_2^- is unstable alone, but in the presence of a complexing CO_2, it will be stable [190]. It has also been seen that CO_2 will be stable if formate is present on the surface and that CO_2 has favorable adsorbate-adsorbate interactions[191]. This would indicate that, at higher pressures, new chemistry will occur.

Studies of CO_2 exposed to Cu single crystals under higher pressure show that CO_2 can be dissociated on Cu [188,192-194]. There is an activation barrier for the

process which may change with different copper surface orientations [192]. The coverage of O formed on the surface is limited [194]. This can be explained by CO having a greater heat of adsorption (20 kcal/mol) than CO_2 (7 kcal/mol) and remaining on the surface. With increased temperature more CO_2 might dissociate, but the reverse reaction, CO oxidation, will also increase. The activation energy for CO_2 dissociation is 16 kcal/mol which is greater than the activation energy for CO oxidation [79].

In this chapter, experiments are performed to observe if a change in catalytic activity for CO oxidation occurs, or if adsorbed surface species exist Cu, Cu_2O, and CuO when CO_2 is present in the gas phase.

5.2. Experimental

5.2.1. Catalytic Reactions

Catalytic reactions were run over metallic copper and copper (I) oxide under 97/3 and 90/10 Torr CO/O_2, respectively, to which 25 Torr of CO_2 was added. 25 Torr of CO_2 was chosen as it was the maximum amount of CO_2 produced in any reaction without CO_2. The CO_2 was pre-mixed with the CO and O_2 prior to the reaction. Reaction were run at 275, 300, and 350°C

5.2.2. TDS and XPS Studies

TDS studies were performed only on Cu. The sample was exposed to 1 atm of CO_2 at room temperature and 300°C for 5 minutes. H_2O, CO and CO_2 were all observed in the desorption experiment. A blank of CO_2 on C was also performed. XPS studies were performed on Cu and CuO. Both samples were exposed to 25 Torr and 900 Torr of

CO_2 at room temperature and 350°C for varying amounts of time. A $CuCO_3$ powder was placed in the chamber for comparison purposes. The powder was pressed into a gold mesh on a gold foil to reduce sample charging as well as to provide a reference for the $CuCO_3$ signal.

5.3. Results/Discussion

5.3.1. Metallic Copper

Figure 5.1 shows the catalyst activity of Cu with 25 Torr CO_2 at 275, 300, and 350°C as well as the activity of a copper catalyst without CO_2 at 200, 250, and 275°C. The curves show a striking similarity between with and without CO_2. The difference being that higher temperatures, between 50 and 75°C, are needed for the reaction with CO_2 to have equivalent activity. Even the rapid rise which seemed so anomalous over metallic copper is present. The change in activity can be interpreted in a number of ways.

First CO_2 may reversible adsorb on the Cu surface. With increased temperature, less CO_2 is on the surface and the reaction proceeds by removing the surface O which is then replaced by subsurface O. The adsorbed CO_2 decreases the area on which CO lands to react with adsorbed O. The reaction mechanism is similar to what is observed without CO_2 present. This explanation is not likely as CO_2 has a low heat of adsorption and should desorb from Cu at temperatures below the reaction temperatures, but this can not be used to rule out CO_2 site blocking as the higher pressures of the reaction will force some equilibrium adsorption onto the surface at these temperatures.

Adsorbed CO_2 may affect the reaction by stabilizing the surface O. If a carbonate-like species formed, adsorbed O would be coordinated with a CO_2 as opposed to being available for reaction with CO. The higher temperatures would then be needed for the

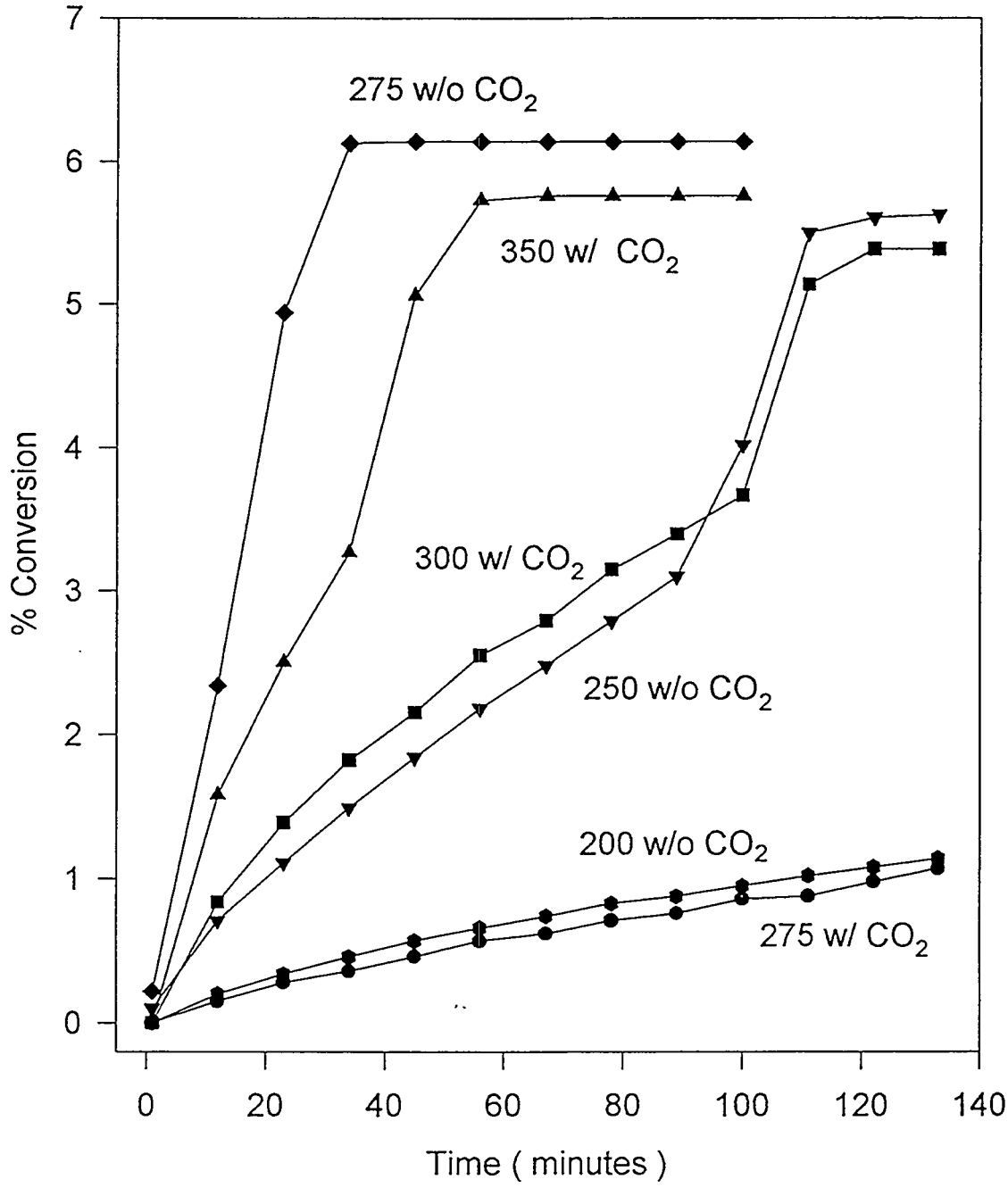

Figure 5.1. CO oxidation results for a metallic copper catalyst tested with 25 Torr of CO_2 and without CO_2 for a 97/3 Torr CO/O_2 gas mixture at different reaction temperatures.

decomposition of the CO_3 species. In that case the adsorbed CO_2 would not be reversible. A post reaction XPS would show a carbonate-like species on the surface. XPS did not show a carbonate species after the reaction in these studies. Goodman reported that CO_2 can be desorbed from the post reaction Cu surface [26]. This was not observed in the TDS that was performed after these catalytic reactions. The temperature of peak desorption in the Goodman experiment was 140°C which is below the reaction temperatures used in these experiments. If the sample in these studies was cooled in the presence of the reaction gas, CO_2 may readsorb on the surface or CO and O may remain on the surface. A TDS would then desorb CO_2 in UHV. This was purposely avoided by pumping away the gases immediately after reaction and allowing the sample to cool in UHV.

To test the possibility that CO_2 could readsorb on the surface after reaction, a repeat reaction was run. Figure 5.2 shows a fresh Cu catalyst that was tested at 300°C under 97/3/25 Torr $CO/O_2/CO_2$ and a repeat reaction over the same surface. The repeat reaction was performed after allowing the sample to cool to room temperature, pumping away the gases with a mechanical pump, adding fresh gas, and then bringing the sample to reaction temperature. The repeat reaction shows lower activity than the fresh catalyst. This was not observed if the sample was pumped to UHV and cooled in UHV. This shows that CO_2 did readsorb on the surface during the cooling of the surface. The readsorption of CO_2 still does not explain why the activity is lower.

The answer to the lower activity was discovered by considering the final explanation for how CO_2 may have affected the activity. CO_2 can dissociate on the Cu surface under reaction conditions. An XPS of the catalyst after the reaction showed oxidized Cu, similar to what was observed for the CO oxidation reactions at 200°C over metallic copper seen in chapter 4. The dissociation of CO_2 on the Cu surface was kept a higher coverage of O on the surface which inhibits CO adsorption and reaction. The

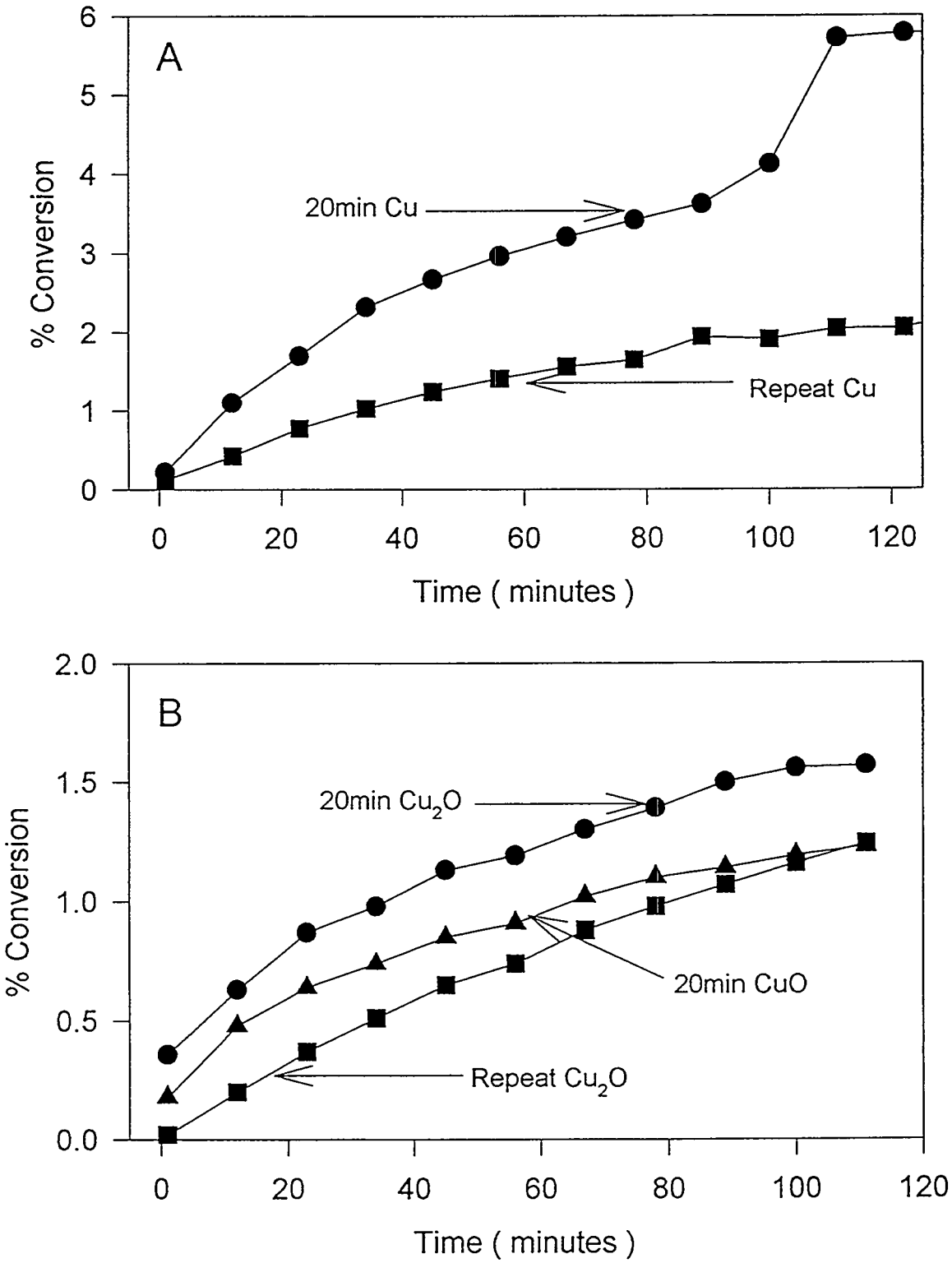

Figure 5.2. Repeated poisoning of CO oxidation runs. A) shows a fresh Cu run under a 97/3/25 Torr $CO/O_2/CO_2$ gas mixture at 300°C and the repeated reaction under the same conditions. B) shows a fresh Cu_2O and fresh CuO catalyst run under a 90/10/25 Torr $CO/O_2/CO_2$ gas mixture at 300°C and a repeated reaction over Cu_2O.

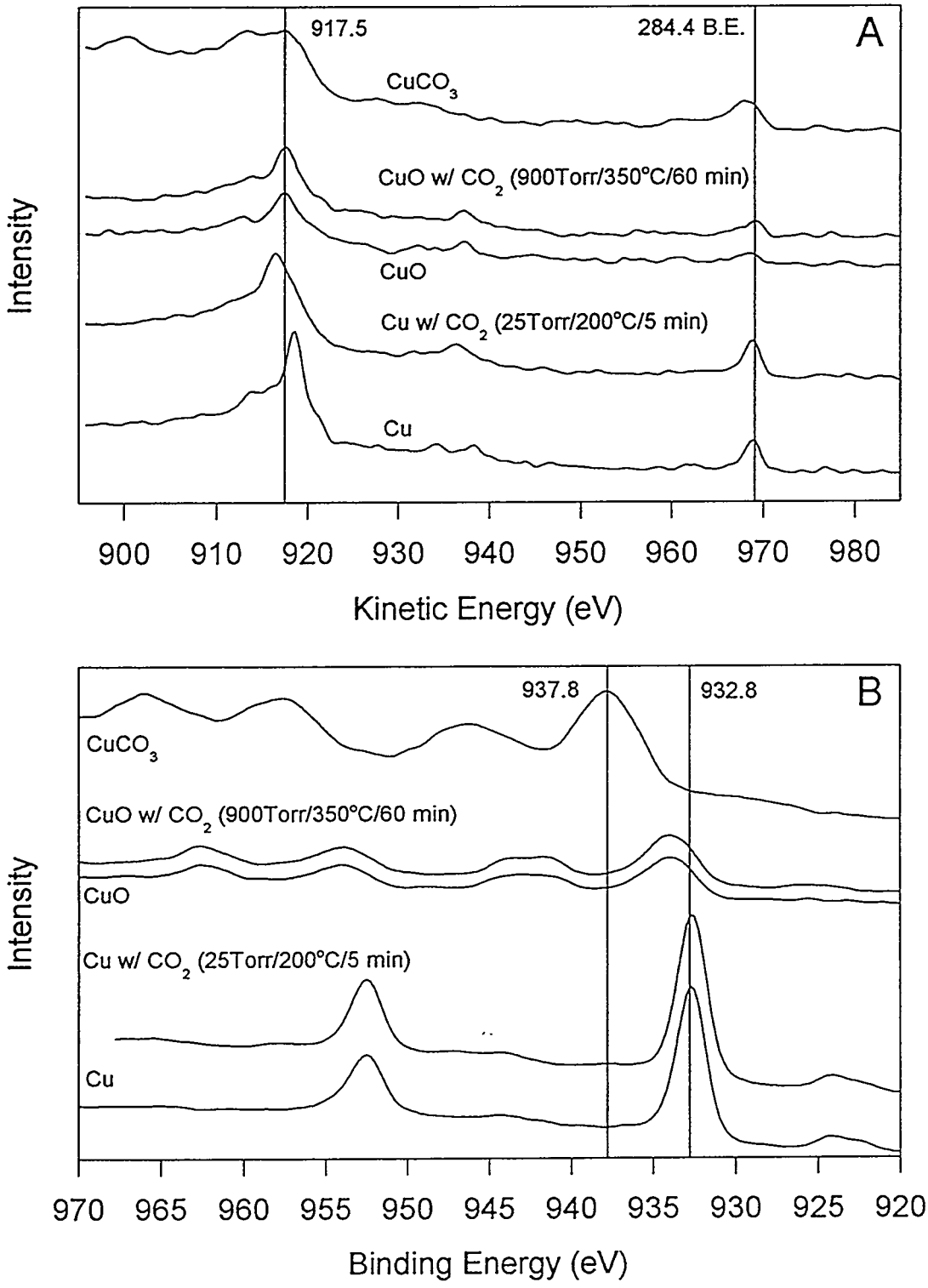

Figure 5.3. XPS of CO_2 interaction with Cu and CuO. A) shows the Cu LVV region for Cu, Cu exposed to 25 Torr CO_2 at 200°C for 5 min, CuO, CuO exposed to 900 Torr of CO_2 at 350°C for 60 minutes, and a $CuCO_3$ as reference. B) shows the Cu 2P region for the same samples in A.

increased temperature was needed for the CO oxidation reaction to overtake the dissociation reaction.

Figure 5.3 shows the XPS for a Cu surface that was exposed to 25 Torr of CO_2 at 200°C for 5 minutes. The Cu LVV region shows the distinct shift in the LVV peak which occurs when Cu oxides to the +1 oxidation state. The Cu 2P region shows that Cu does not oxidize to +2 in the presence of CO_2. Under reaction conditions Cu^{+1} does not completely form as CO does reduce the surface. The C signal at 968.3 K.E. is of graphite. No C signal from CO_2 is observed which would have appeared at lower kinetic energies by 2 to 4 eV .

To further determine whether the Cu catalyst surface would be oxidized by CO_2 when CO was present, a Cu surface was exposed to a mixture of CO and CO_2 at elevated temperatures. Figure 5.4 shows the Cu 2P region, the O 1S region, and the Cu LVV region for a Cu surface that was exposed to a 100/25 Torr mixture of CO and CO_2 at 300°C for 20 and 140 minutes. The most important result is that an O peak at 530.6 eV increases upon a 20 minute exposure. An additional 2 hours of exposure does not increase the oxygen coverage, hence the surface is at an equilibrium coverage for oxygen. The 2P and LVV regions show a decrease in intensity due to the oxygen coverage. No adsorbed CO or CO_2 can be recognized in the C region. The O coverage is very small. Annealing of the surface in UHV decreased the O signal. The O peak intensity is barely over the background and is approximately 100 times smaller than the oxygen signal for Cu_2O.

5.3.2. Copper (I) Oxide

The possibility that Cu_2O could be deactivated in a manner similar to Cu lead to running catalytic reactions over the Cu_2O in the presence of CO_2. The results are shown in figure 5.2B for a 90/10/25 Torr mixture of $CO/O_2/CO_2$ at 300°C. These results should

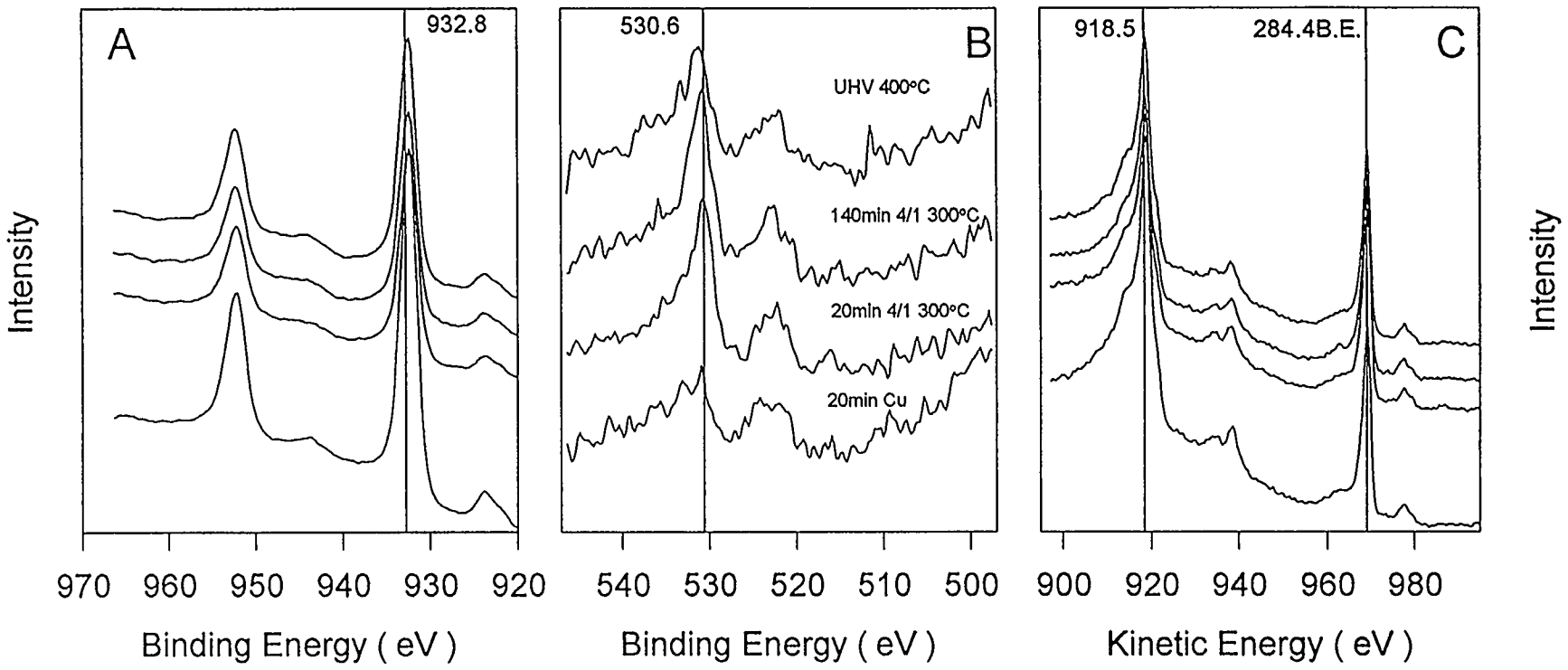

Figure 5.4. XPS of a metallic copper catalyst exposed to a 100/25 Torr CO/CO_2 gas mixture at 300°C. **A)** shows the Cu 2P region, **B)** shows the O 1S region, and **C)** shows the Cu LVV region for metallic copper, a 20 minute exposure, a 140 minute exposure, and a post experiment UHV anneal.

be compared to those obtained in chapter 4 where approximately 15% conversion was obtained in 2 hours. The CO_2 did lower the activity to 1% conversion in 2 hours. Again, the question of how does CO_2 deactivate the catalyst should have the same answers as those discussed for the deactivation of Cu. Unfortunately, there is not much known about the adsorption of CO_2 onto Cu_2O or about its ability to dissociate on Cu_2O.

The experiment which showed that CO_2 oxidized Cu also showed that it does not continue to oxidize Cu past the +1 oxidation state. This indicates that CO_2 does not dissociate on the Cu_2O surface. So, the poisoning must be due to either blocking CO adsorption sites or by stabilizing the adsorbed O. A post reaction TDS did not show any CO_2 desorption when the sample was pumped to UHV and allowed to cool in UHV. A repeat reaction was performed to see if there may be surface species which are desorbing before the sample is placed in UHV. In the repeat reaction, the Cu_2O was allowed to cool in the presence of the previous reactions gas mixture to room temperature, the gases were removed, fresh gases added, and the sample was brought back to reaction temperature. The results shown in figure 5.2B are identical to the fresh catalyst. This indicates that under reaction conditions CO_2 blocks the adsorption of CO.

5.3.3. Copper (II) Oxide and Copper Carbonate

A reaction was run over a CuO sample under Cu_2O reaction conditions, 90/10/25 Torr $CO/O_2/CO_2$, to determine whether the nature of site blocking were different between the two catalysts. The results are shown in figure 5.2B. The CuO catalyst is less active than the Cu_2O catalyst. The CuO catalyst was not observed to reduce in the 90/10/25 mixture. This was not a conclusive test. If the mechanism of CuO activity were the removal of a lattice O to form CO_2, we might have expected the catalyst to be reduced at the end of this reaction, because CO_2 will not reoxidize Cu_2O to CuO. It is not known if the adsorbed CO_2 will hinder the reoxidation of the surface by O_2. A reduced surface

would have shown activity similar to the Cu_2O surface. This would indicate that the site blocking was similar to Cu_2O. What this may show is that CO_2 does not inhibit O_2 adsorption which is why the surface remains in the +2 oxidation state in spite of the reducing gas phase.

Another explanation to the deactivation could be the formation of a copper carbonate, $CuCO_3$, from the reaction of CuO and CO_2. This may not be observed in a TDS experiment unless the sample was ramped to greater than 1000°C to decompose the carbonate. An XPS experiment was performed to see if a $CuCO_3$ species could be formed. Figure 5.3 shows the 2P and LVV regions of a CuO surface which was exposed to 900 Torr of CO_2 at 350°C for 1 hour to form the carbonate and a $CuCO_3$ reference. The CuO and the CuO exposed to CO_2 are the same. If the carbonate had formed the $2P_{3/2}$ peak would have shifted to a higher binding energy by 5 eV. The carbon peak of the carbonate would have been at 1.6 eV lower kinetic energy (this is corrected for the 0.6 eV charging which occurred for the carbonate and was determined by a Au reference standard.) The deactivation of CuO by CO_2 is due to simple site blocking.

5.4. Summary

CO_2 was found to deactivate all three oxidation states of copper for CO oxidation. The possible mechanisms for catalyst deactivation were discussed and included, surface oxidation, surface compound formation, copper carbonate formation, and competitive adsorption. XPS showed that CO_2 will oxidize metallic copper even in the presence of CO, hence the deactivation over Cu is due to surface oxygen. The surface oxygen was shown in chapter 4 to lower the reaction rate and increase the activation energy for CO oxidation. Over the copper (I) oxide surface, CO_2 was not able to oxidize the surface but did lower the activity for CO oxidation. Repeated reactions over Cu_2O did not change

the level of activity indicating that surface compounds did not form. By elimination of the other deactivation mechanisms, surface site blocking was proposed as the deactivation mechanism. The deactivation of copper (II) oxide was also investigated. Under reaction conditions favorable for Cu_2O stability, CuO did not reduce when CO_2 was present indicating that CO was unable to react with the surface. Because a $CuCO_3$ had been proposed to deactivate CuO [26], attempts were made to form a $CuCO_3$ under reaction conditions. $CuCO_3$ was not formed indicating that it is not responsible for catalyst deactivation. Surface site blocking is also proposed for the deactivation of a CuO catalyst.

Chapter 6

Copper Oxidation and Copper Oxide Reduction

6.1. Introduction

Throughout this thesis there has been evidence for the reduction and oxidation of the catalyst surface under varying atmospheres. It was shown that metallic copper would oxidized in a 66/33 Torr CO/O_2 mixture and that copper (II) oxide will be reduced upon heating in UHV. To obtain an accurate picture of the changes in the surface under varying reaction conditions, it is important to measure how any single gas or condition will affect the oxidation state of the surface. Because in CO oxidation the O_2 present can oxidize the surface and the CO present can reduce the surface, we would like to know the kinetics of both possible surface reactions. A balance between the kinetics of oxidation and reduction will determine the final oxidation state of the catalyst.

This chapter reports the initial kinetic measurements for the reactions carried out over the different catalyst surfaces. The reduction of CuO by annealing in UHV is reported first. This measurement provides information on the stability of oxygen in CuO. CO will also be used to reduce CuO. The reduction of CuO by CO was proposed as the rate determining step in CO oxidation over CuO in chapter 4. Oxidation studies will be performed using O_2 and CO_2 as oxidants. The oxidation of metallic copper is complicated by the possibility of there being subsurface oxygen, adsorbed oxygen, and oxide formation. Lastly, NO reduction by CO will be investigated as well. This reaction

is similar to CO oxidation with the exception that NO can react with itself. The NO reduction will be performed on both metallic copper and copper (II) oxide.

Obtaining the results of these studies was possible only through the use of XPS and the thin catalyst films used in this thesis. XPS allows the characterization of the oxidation state of the catalyst and is surface sensitive, between 5-20Å. If the catalyst were thicker than the films used here, the kinetics would be complicated by solid state mass transport. Experiments were performed under special conditions where changes in catalyst oxidation state could be observed and are presented in the following section.

6.2. Experimental

Reduction experiments were performed using copper (II) oxide starting material on a graphite coated stainless steel foil. A 20 minute deposition of copper was used (approximately 10 ML) and was oxidized in 100 Torr of O_2 at 300°C for 20 minutes. Prior to reduction, XPS was used to insure that the copper was in the +2 oxidation state. The CuO was reduced by heating in UHV and in CO. The UHV experiments were done at a base pressure of $1x10^{-9}$ Torr. In UHV, the sample was annealed at 300, 350, 375, 400, 425, and 450°C for varying amounts of time. At 300°C, data were taken at 5, 10, and 30 minute periods. At the higher temperatures data were taken after 1, 5, 10, and 30 minute periods. The CO reduction experiments were performed in the high pressure cell at 25 Torr of CO. The sample was heated for varying times at 50, 100, 200, and 300°C. At the conclusion of the exposure, the CO was pumped away before turning off the heating. This was done to prevent additional reduction or adsorption. The sample was transferred back into UHV within 3 minutes.

Oxidation experiments were performed using metallic copper as the starting material on a graphite coated stainless steel foil. A 20 minute deposition (approximately

10 ML) was used. The sample was oxidized by O_2 and CO_2 in the high pressure cell. Oxidation by O_2 was done under 100 Torr at 22°C and under 50 Torr at 100°C. At 22°C, the sample was exposed at 5 minute intervals and at 100°C for 2 minute intervals. For the 100°C experiments, the O_2 was removed prior to cooling of the sample to prevent readsorption. The sample was transferred into UHV within 3 minutes. At the conclusion of the O_2 experiments, the sample was flashed to 400°C to determine the extent of Cu_2O formation. Oxidation by CO_2 was performed under 25 Torr and at 200°C. Again, the gas was removed prior to sample cooling and was transferred into UHV within 3 minutes.

Exposure to a mixture of NO and CO was performed on metallic copper and copper (II) oxide, both on a graphite coated stainless steel foil. Reactions were run at 300-350°C for 2 hours to observe N_2 and CO_2 formation. Metallic copper was run under a 50/50 Torr mixture, and CuO was run under a 100/100 Torr mixture. At the end of both reactions, the sample was allowed to cool in the NO/CO mixture to 100°C where the gas was removed. At that point the sample was placed in UHV for analysis.

6.3. Results/Discussion

6.3.1. Reduction of CuO by annealing in UHV

It has been reported in the literature [77] and shown in this work that annealing CuO in UHV will reduce copper from the +2 oxidation state to the +1 oxidation state. This occurs because the ΔG^o of formation for Cu_2O from Cu is -3 kcal/mol more favorable than the formation of CuO from Cu [107]. The chemical equations are as follows :

$$Cu + \tfrac{1}{2}O_2 \Leftrightarrow CuO \qquad \Delta G^o = -31 \text{ kcal/mol}$$

$$2Cu + \tfrac{1}{2}O_2 \Leftrightarrow Cu_2O \qquad \Delta G^o = -34 \text{ kcal/mol}$$

Because UHV has a very low partial pressure of O_2, the equilibrium for both reactions will be driven to the left by Le Chatelier's principle. CuO was not observed to be reduced to Cu, but was observed to Cu_2O.

The results of annealing CuO at 350°C are shown in figures 6.1 and 6.2, a representative set of data. XPS was performed for the Cu 2P region, O 1S region, and the Cu LVV region which includes the C 1S peak and only a few curves are displayed. Figure 6.1 shows how the Cu 2P region changes with time. A gradual decrease in the shake up peaks is observed indicative of the loss of Cu^{+2} ions. The $2P_{3/2}$ and $2P_{1/2}$ peaks both show a shift to lower binding energies and a decrease in the width of the peak. After 90 minutes of annealing the shake up peaks are nearly gone and the binding energy of the Cu $2P_{3/2}$ peak is that of a Cu^{+1} ion. The area under the shake up peaks and the $2P_{3/2}$ and $2P_{1/2}$ peaks can be determined at each time interval to measure a rate of change. Figure 6.1 plots the peak areas versus annealing time. Initially, there is scatter among the data for times less than 10 minutes. Over the whole experiment it is obvious that the shake up peaks decrease and the $2P_{3/2}$ and $2P_{1/2}$ peaks increase. The changes in all peak areas were linear with time. The rate of decrease in the shake up peaks was calculated and used in an Arrhenius plot to calculate an activation energy for reduction. The observed increase in $2P_{3/2}$ and $2P_{1/2}$ peaks is due to a change in the density of the copper when oxygen is removed. Per unit volume there is more Cu in Cu_2O than CuO hence the increase is not due to increased surface area [195]. As was discussed in the catalyst characterization chapter, with increased oxidation copper wets the graphite, so reduction must have the reverse effect. It will be shown for the reduction of CuO by CO that increased 2P signals will also be observed in that case.

A change in the O 1S peak is also observed during the reduction. Figure 6.2 shows how the O 1S peak changes with time. Initially the O peak is asymmetric with a shoulder at 531.5 eV on a main peak at 529.5 eV. The shoulder decreases in intensity

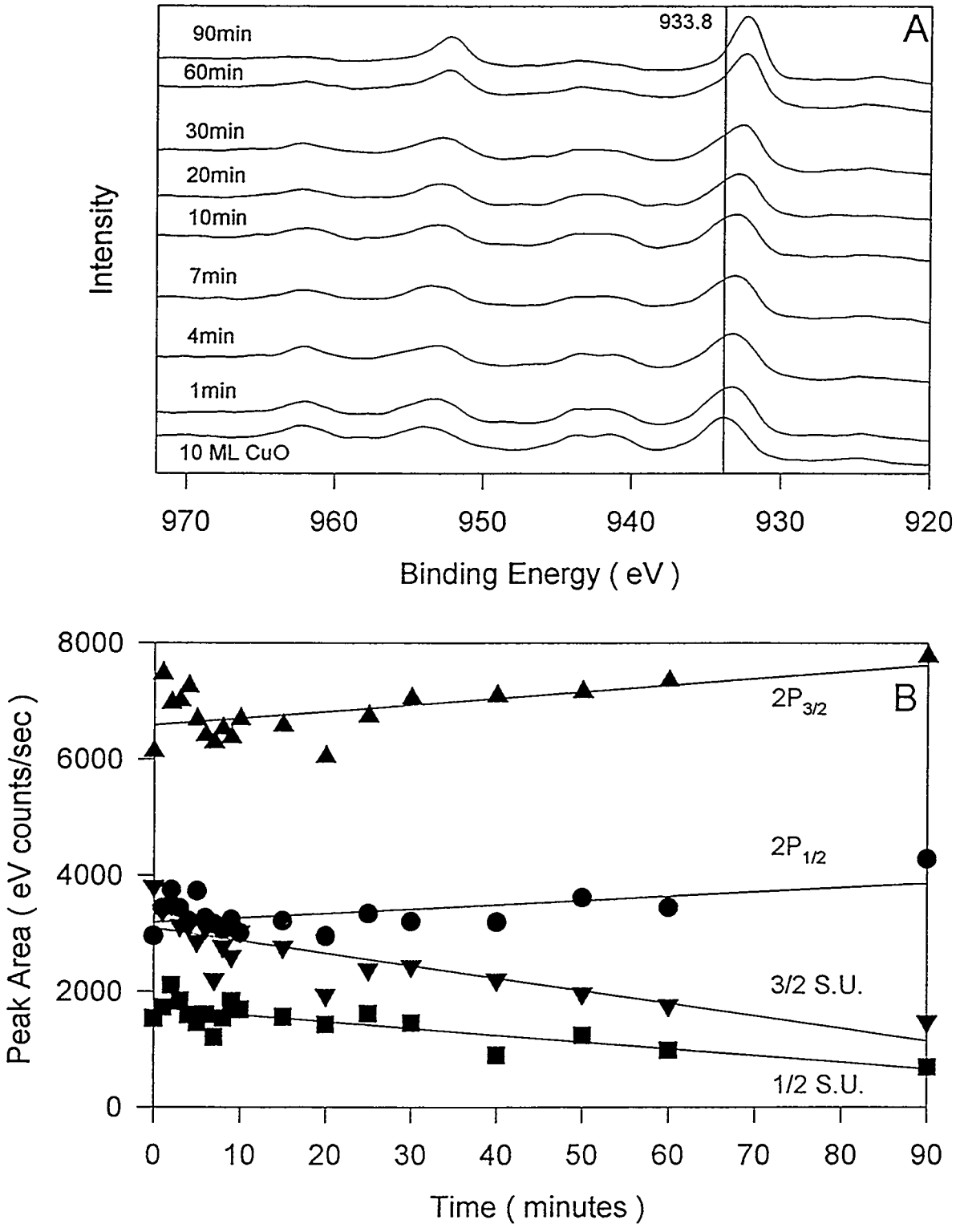

Figure 6.1. A) XPS of the Cu 2P region and B) Cu 2P XPS peak areas as a function of time for the reduction of CuO by annealing in UHV at 350°C. The lines are best fits to a first order linear regression.

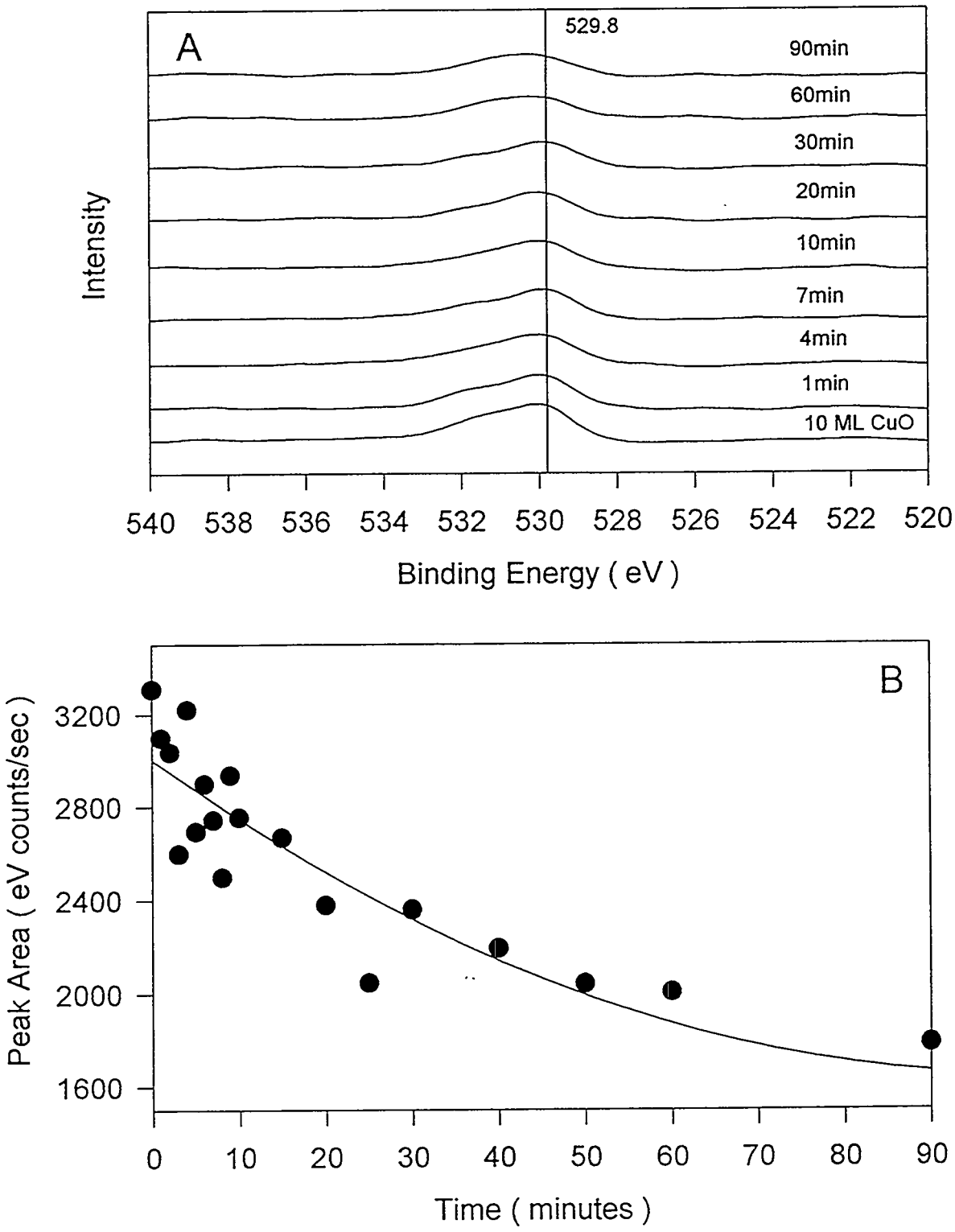

Figure 6.2 A) XPS of the O 1S region and B) O 1S XPS peak areas as a function of time for the reduction of CuO by annealing in UHV at 350°C. The line is a best fit 2nd order linear regression.

prior to loss of intensity from the main peak. After 20 minutes, The main peak shifts in binding energy to 530 eV. Because the Cu 2P binding energies, Cu LVV kinetic energy, and the AES Cu to O ratio are all in agreement with the literature values for CuO, the asymmetry of the peak is not due to different oxidation states of Cu or a lack of uniformity. Rather, the shoulder is due to O sites at the edge of CuO. The binding energies of a coordinatively unsaturated O atom would be expected to be higher and that atom would also be expected to be more reactive [10]. The change in peak area for O 1S versus annealing time is shown in figure 6.2B. The data do not have a linear dependence as was observed for the Cu 2P peaks. A second order dependence of reduction rate as a function of O might be expected if two O atoms combine in the rate determining step before desorbing into the gas phase. The total peak area has decreased by half after 90 minutes of annealing, which represents the limiting reduction at infinite reaction times. This is to be expected for a reduction of the oxide from CuO to Cu_2O. In order to calculate an activation energy for the reduction, a linear initial rate of reduction was estimated from the extent of oxidation-time data. Recall that the mechanism proposed for CO oxidation over CuO invoked a reduction of the oxide as the rate limiting step. For that case, the most reactive O atoms would be expected to react first, and it is logical to assume that these oxygens are also the first ones lost during reduction. Attempts to fit all of the data by a general kinetic model would be complicated by having to take into account the coverage effects, O_2 desorption energy, and the interfacial changes in structure and morphology of the deposited oxides which occur as the sample reduces.

An Arrhenius plot was generated by plotting the log of the rate of decrease of the Cu shake-up peaks and the O 1S peak as a function of inverse temperature and is shown in figure 6.3. A linear regression was used to fit the data. The activation energy calculated for Cu $2P_{3/2}$ and $2P_{1/2}$ are 25.0 and 26.6 kcal/mol, respectively. The similarity between the data is to be expected and is a good check of consistency sign to data fit. The activation energy calculated from the O 1S peak is 24.0 kcal/mol. These result are in

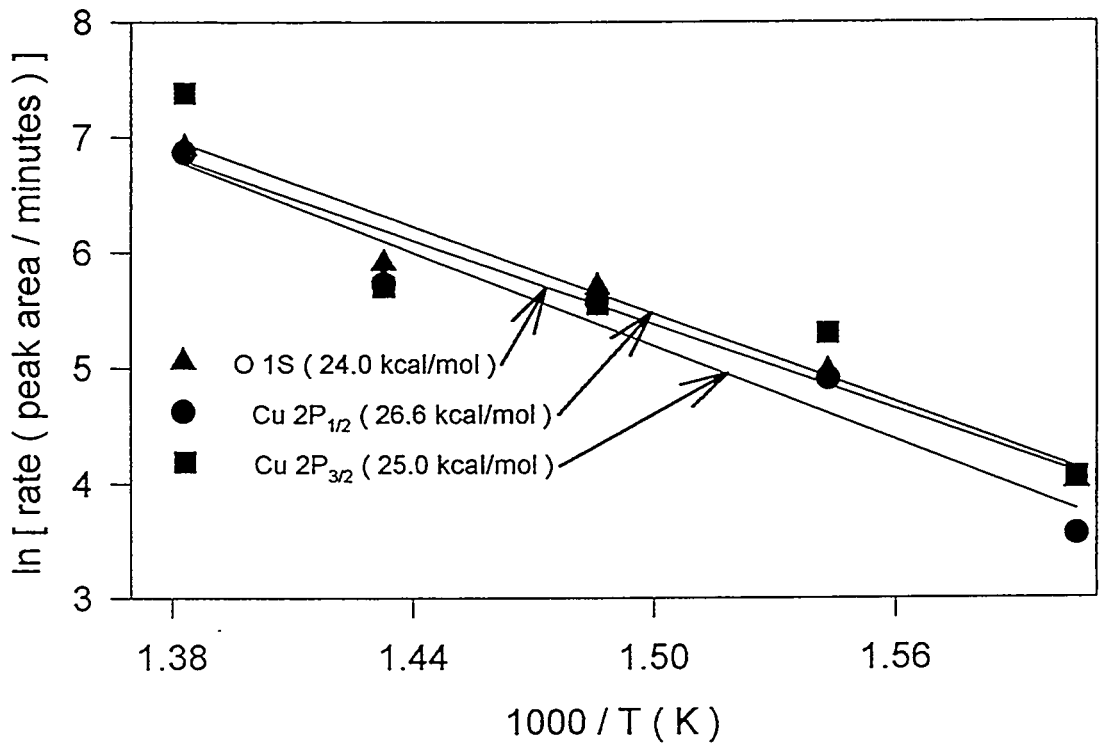

Figure 6.3. Arrenhius plots for the reduction of CuO using the initial decrease in peak intensity for the Cu $2P_{1/2}$ and Cu $2P_{3/2}$ shakeup peaks as well as O 1S peak as a function of temperature.

good agreement with a thermal desorption study of O from CuO [196] and the energy needed for O isotope exchange with the oxide [88].

6.3.2. Reduction of CuO by heating in CO

Understanding how CO reduces CuO is important to almost all catalytic studies using copper and copper oxides. Copper catalysts are usually created by precipitation of a salt onto a support and subsequent calcination (heating in air). The copper is in the +2 oxidation state after calcination. The supported catalyst is then given a pretreatment which typically includes heating in CO or H_2. Different pretreatment conditions have been observed to result in varying catalytic activity. The extent of reduction or of accompanying structural changes are not known, for example. A study of how CO

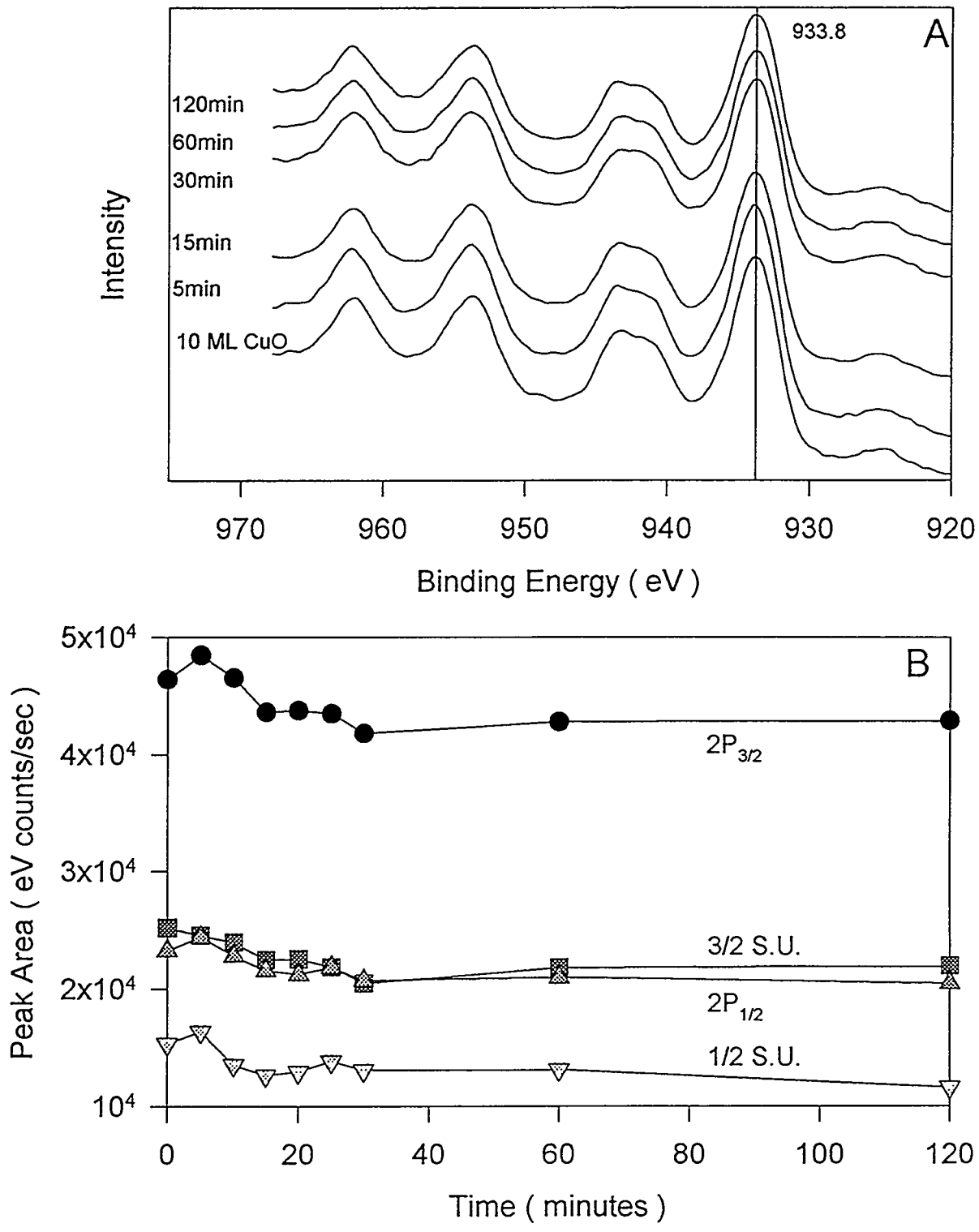

Figure 6.4. A) XPS of the Cu 2P region and B) Cu 2P XPS peak areas as a function of time for the reduction of CuO by annealing in 25 Torr CO 50°C.

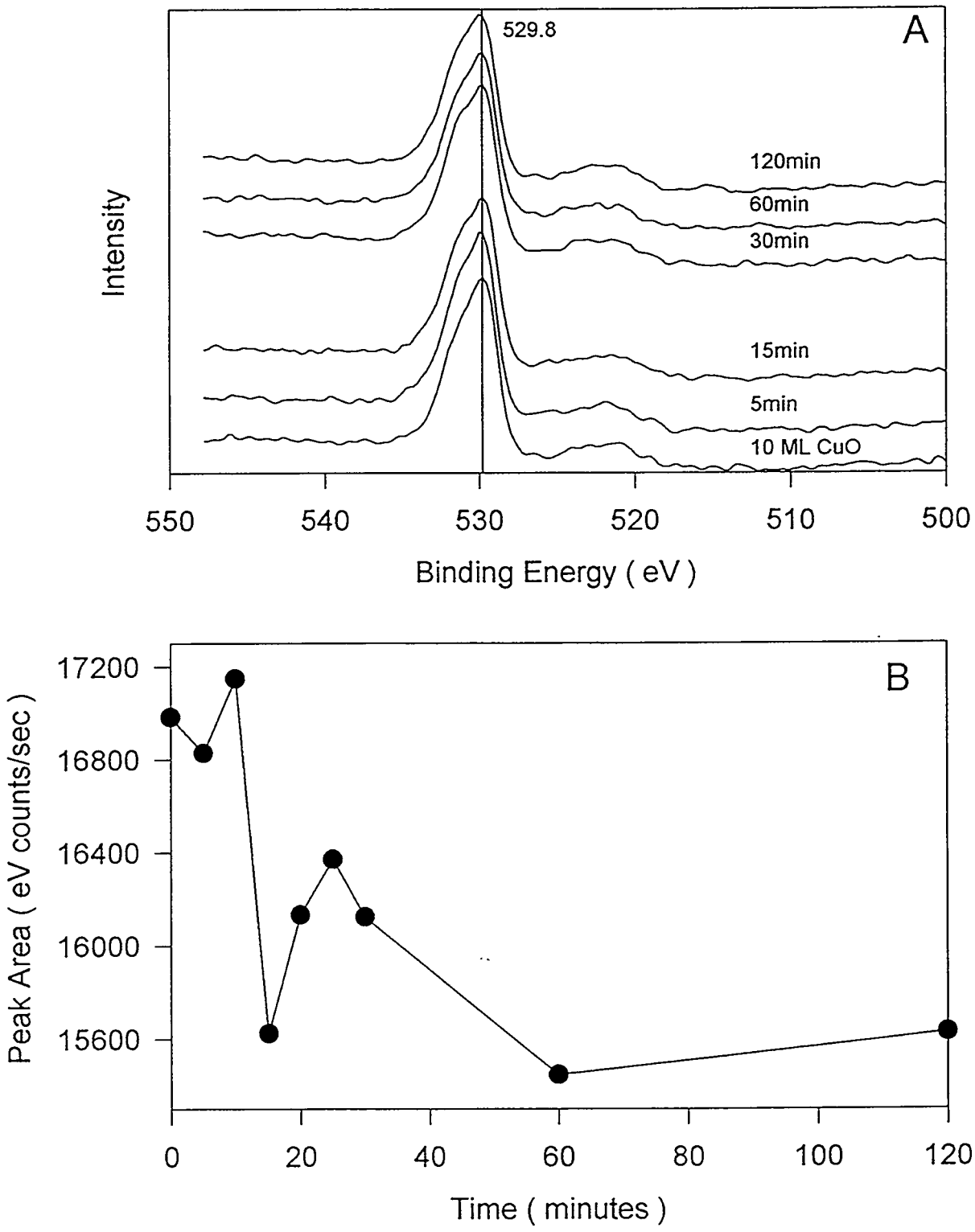

Figure 6.5. A) XPS of the O 1S region and B) O 1S XPS peak area as a function of time for the reduction of CuO by annealing in 25 Torr CO at 50°C.

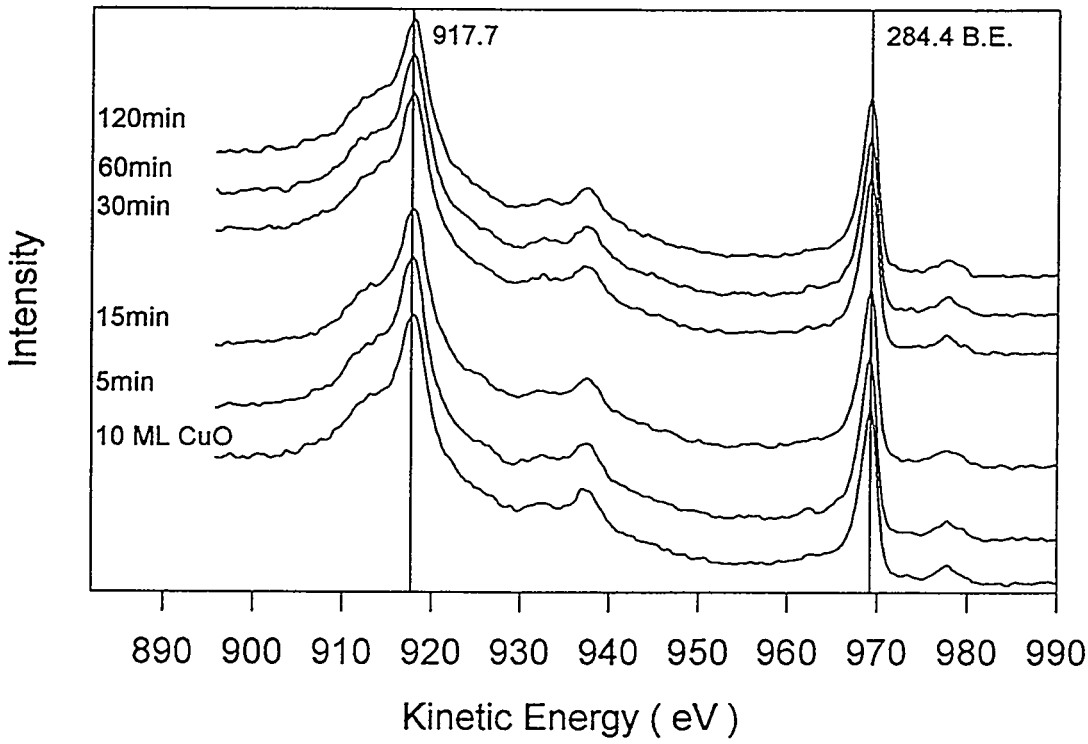

Figure 6.6. XPS of the Cu LVV and C 1S region for the reduction of CuO by annealing in 25 Torr of CO at 50°C for varying amounts of time.

reduces CuO is also needed to understand a potential basic step in the catalytic reaction of CO oxidation. Reduction of CuO by CO was studied at 4 different temperatures.

Reaction at 50°C does not result in any reduction of the CuO. Figure 6.4 shows both the spectra of the Cu 2P region and a plot of peak area versus heating time. The spectra show a possible change in binding energy for only the first 5 minute period. After 2 hours, the shake up peaks are still prominent indicating the presence of a significant amount of Cu^{+2}. The peak areas show a small decrease for the first 20 minutes but are unchanged for the remaining 100 minutes. Because the ratio of the areas of the shake up peaks to the $2P_{3/2}$ and $2P_{1/2}$ peaks does not change, there is no reduction of CuO. The change in peak areas may be due to morphology changes of the oxide film. The O 1S region and its associated peak area as a function of heating time are shown in Figure 6.5. The shoulder can be seen in every spectrum indicating even the reactive O, previously

identified in the UHV reduction, is not being removed. The peak area does decrease with time but this could be associated with the morphology changes as well. Figure 6.6 shows the Cu LVV peak and the C 1S peak. Neither peak changes during the course of the experiment. Additionally, there is no carbon peak due to either irreversible CO adsorption or carbonate formation.

Increasing the temperature to 100°C in 25 Torr CO did not result in the reduction of CuO to Cu_2O. The Cu^{+2} shake-up peaks remain after 2 hours, as can be seen in figure 6.7. Figure 6.7 also shows that the peak areas decrease over the course of the experiment as they had during the 50°C reduction, but the peak ratios changed indicating that some reduction had occurred. The O peak area, plotted in figure 6.8, also decreases by an amount similar the case of reduction at 50°C.

At 200°C, CuO begins to reduce to Cu_2O at a measurable rate. Figure 6.9 shows the Cu 2P spectra at each period and the change in peak areas during the experiment. The $2P_{3/2}$ peak gradually shifts to lower kinetic energy as the shake-up peaks decrease in intensity. The peak areas decrease in the first 40 minutes then rise for the $2P_{3/2}$ peak, remain constant for the $2P_{1/2}$ peak, and decrease for both shake up peaks. The initial change may again be associated with changes in the morphology or in structure, but the long term change is definitely "chemical" in origin. After 4 hours, the catalyst has completely reduced to Cu_2O.

The O 1S region spectra and peak areas, in figure 6.10, support this hypothesis. The O spectra shows that the reduction of CuO is different in CO than in UHV. The shoulder at 531.5 eV can be seen in all spectra, while the overall peak area is decreasing. Previously, this shoulder had been identified as being a reactive oxygen species. The total peak area has decreased to half of its initial value by the end of 4 hours. The decrease in peak area is not linear with time, as would have been expected if the reaction was a combination of atomic surface O and adsorbed CO. The nonlinearity may be explained as a consequence of the structural changes which must occur as the surface "balls up"

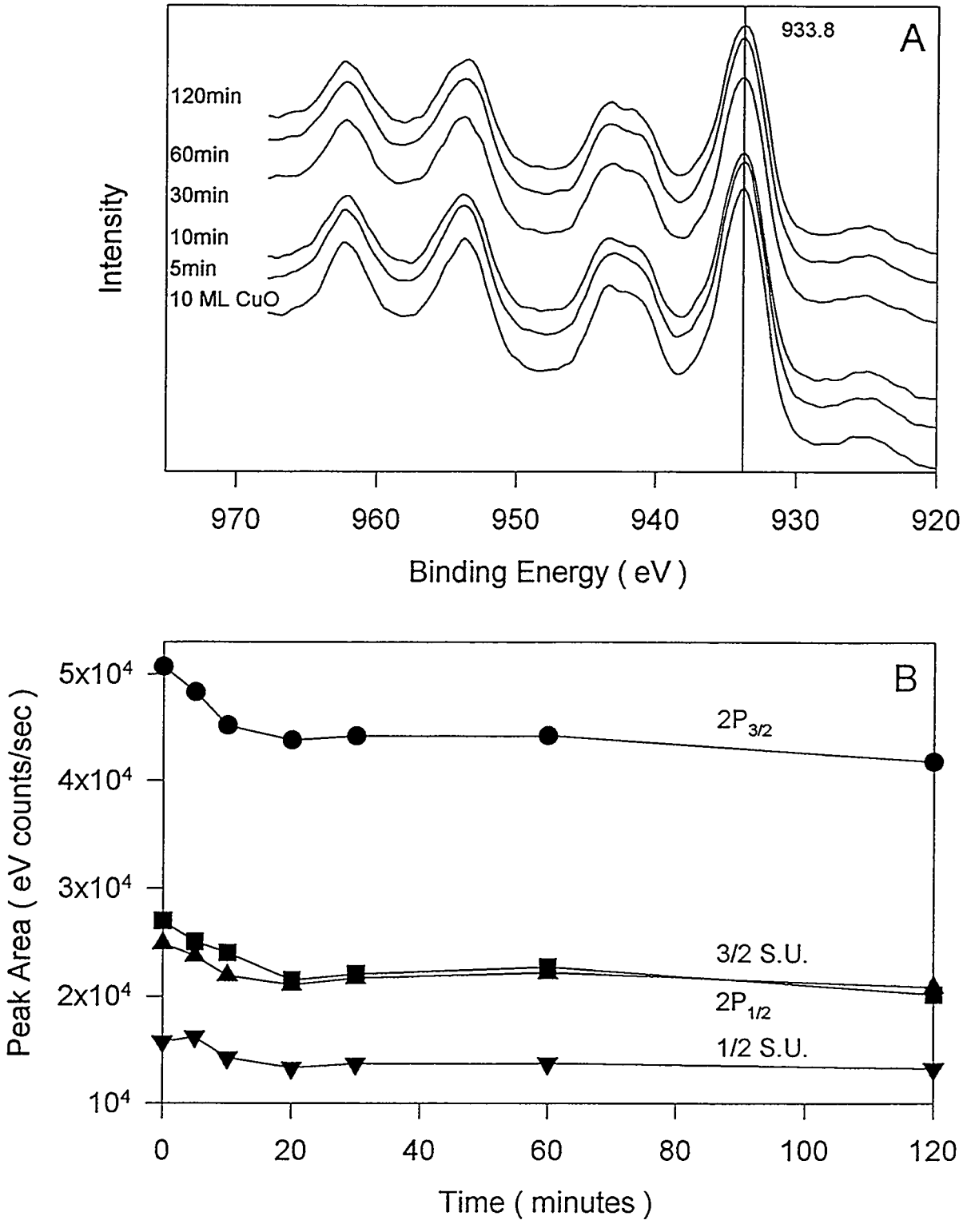

Figure 6.7. A) XPS of the Cu 2P region and B) Cu 2P XPS peak areas as a function of time for the reduction of CuO by annealing in 25 Torr CO at 100°C.

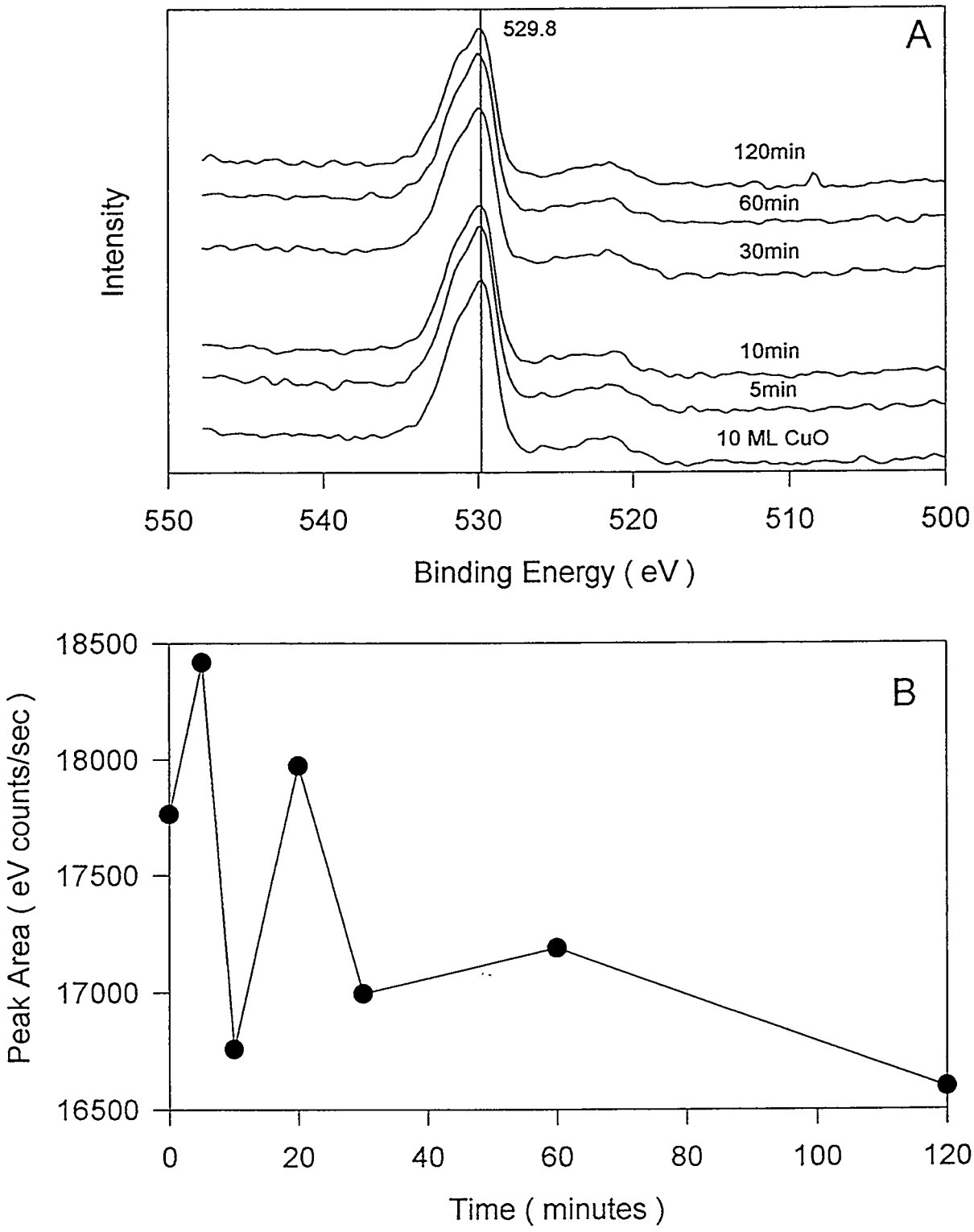

Figure 6.8. A) XPS of the O 1S region and B) O 1S XPS peak area as a function of time for the reduction of CuO by annealing in 25 Torr CO at 100°C.

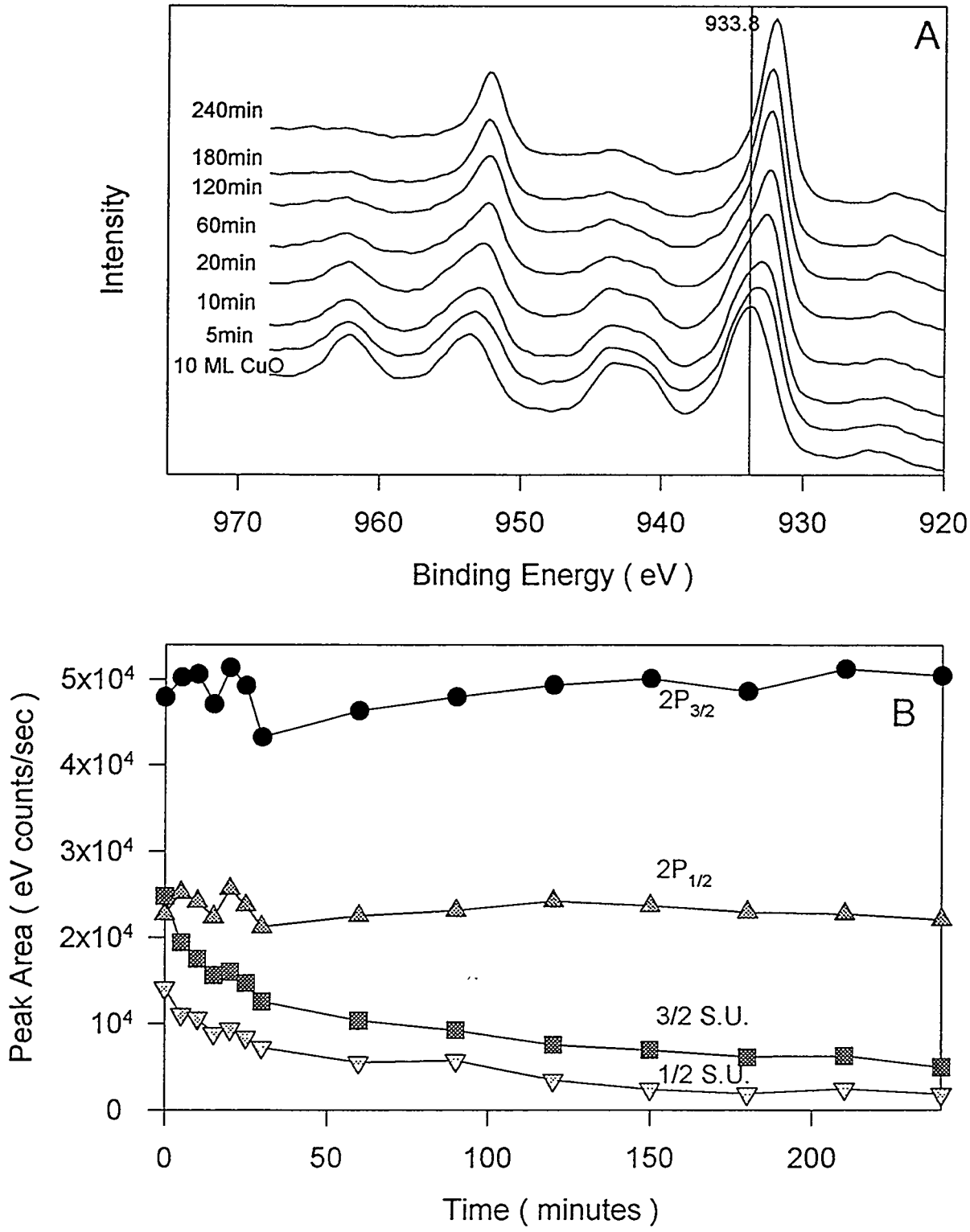

Figure 6.9. **A)** XPS of the Cu 2P region and **B)** Cu 2P XPS peak areas as a function of time for the reduction of CuO by annealing in 25 Torr CO at 200°C.

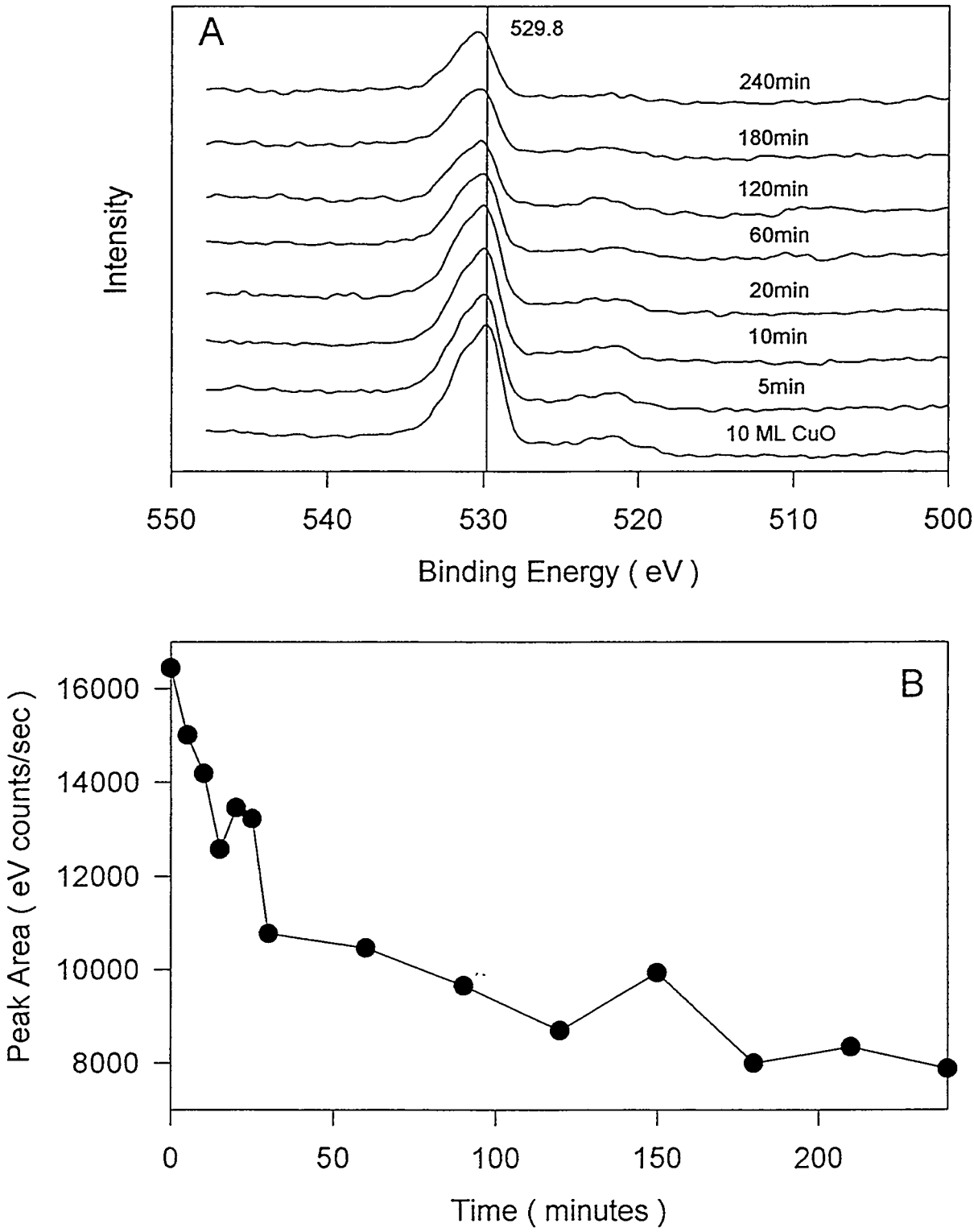

Figure 6.10. **A)** XPS of the O 1S region and **B)** O 1S XPS peak area as a function of time for the reduction of CuO by annealing in 25 Torr CO at 200°C.

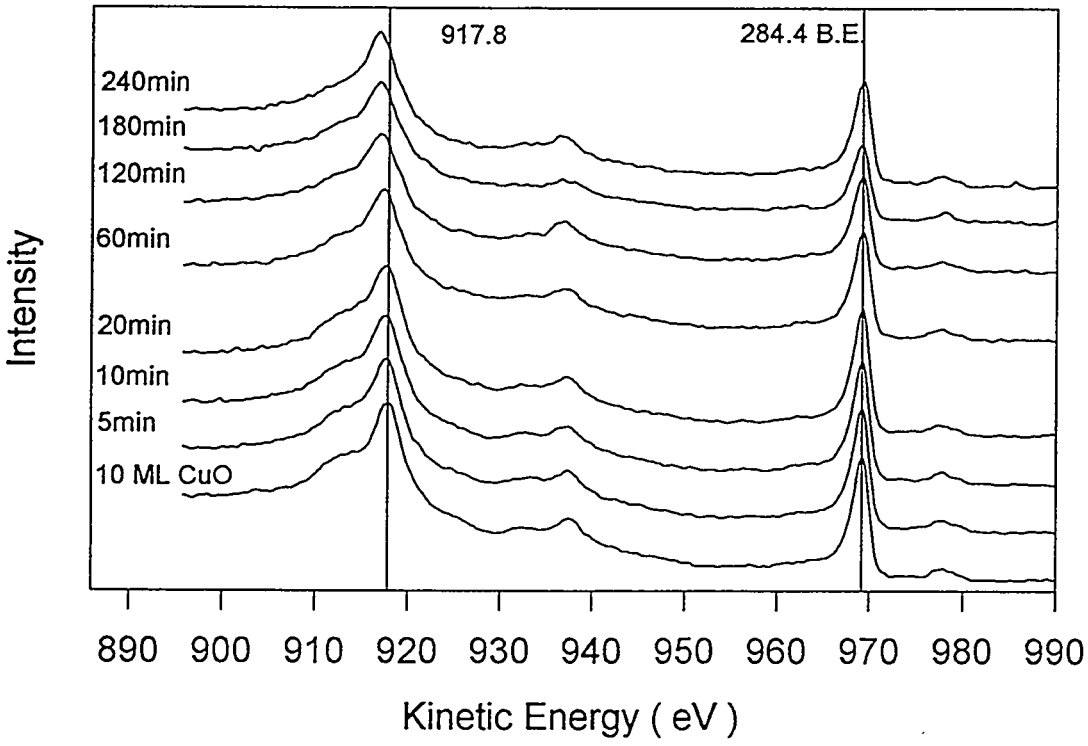

Figure 6.11. XPS of the Cu LVV and C 1S region for the reduction of CuO by annealing in 25 Torr of CO at 200°C for varying amounts of time.

on the graphite support. The change in oxidation state between CuO and Cu_2O can be better seen in the LVV region of copper, shown in figure 6.11.

The reduction reaction performed at 300°C does not help in the understanding of the possible structural changes which have occurred at lower temperatures, because CuO has been reduced to Cu_2O within 10 minutes. The Cu 2P region and peak areas are shown in figure 6.12. The Cu^{+2} shake-up peaks are gone in the second spectrum, and the $2P_{3/2}$ peak has shifted to the binding energy of Cu_2O. The $2P_{3/2}$ and $2P_{1/2}$ peak areas increased after the first reduction. The increase of peak area for Cu_2O compared to CuO was also observed during the UHV reduction described previously. The reduction did not stop at Cu_2O. The Cu peak areas decrease during the next 2 hours, and the Cu peak widths narrow as might be expected for the reduction to metallic copper.

The O 1S region shows the rapid reduction of CuO to Cu_2O and of Cu_2O to Cu. Figure 6.13 shows that after the first period, the maximum of the O 1S peak has shifted to higher binding energies and with a small shoulder also on the higher energy side. The continued reduction does not cause additional shifts in energy for the O 1S peak. The shoulder is gone within 20 minutes. The O 1S full-width-at-half-maximum does seem to increase with time but this is hard to distinguish within the error. The O 1S peak area drops to half its initial value between 5 and 10 minutes, and to one quarter after 20 minutes. The decrease after 20 minutes may follow a decline similar to the Cu 2P peak decrease. The O peak that remains at the end of the experiment is due to unreduced Cu_2O.

Figure 6.14 shows how the Cu LVV peak changes over the course of the reduction. After the 5 minute exposure the LVV peak has shifted to the value indicative of Cu_2O. With increasing exposure time, a metallic copper LVV peak grows in at 918.5 eV with a corresponding decrease in the Cu_2O peak at 916.5 eV. At the end of the experiment a shoulder due to Cu_2O is still present. Even with this thin sample, complete reduction did not occur. What is believed to have happened is the catalyst film reduced on the outside, but not on the inside. The metallic copper formed over the surface can act as a "passivating" barrier, preventing continued reduction by inhibiting mass transport. Attempts at reducing the remaining oxide at higher temperature and pressures did reduce the oxide further. This surface was exposed to 100 Torr of CO at 400°C for 2 hours and resulted in a decrease in the O intensity to 2000 counts and near-loss of the Cu_2O signal. Continued reduction under these harsh conditions would probably have resulted in complete reduction to metallic copper.

Using the initial decrease of the Cu $2P_{3/2}$, Cu $2P_{1/2}$, and O 1S peaks at 100, 200 and 300°C and by fitting the whole curve at 200°C to an exponential expression for the reduction rate as a function of the energy, an activation energy was calculated of 9 ± 1 kcal/mol. This value is below the observed activation energy for CO oxidation over CuO.

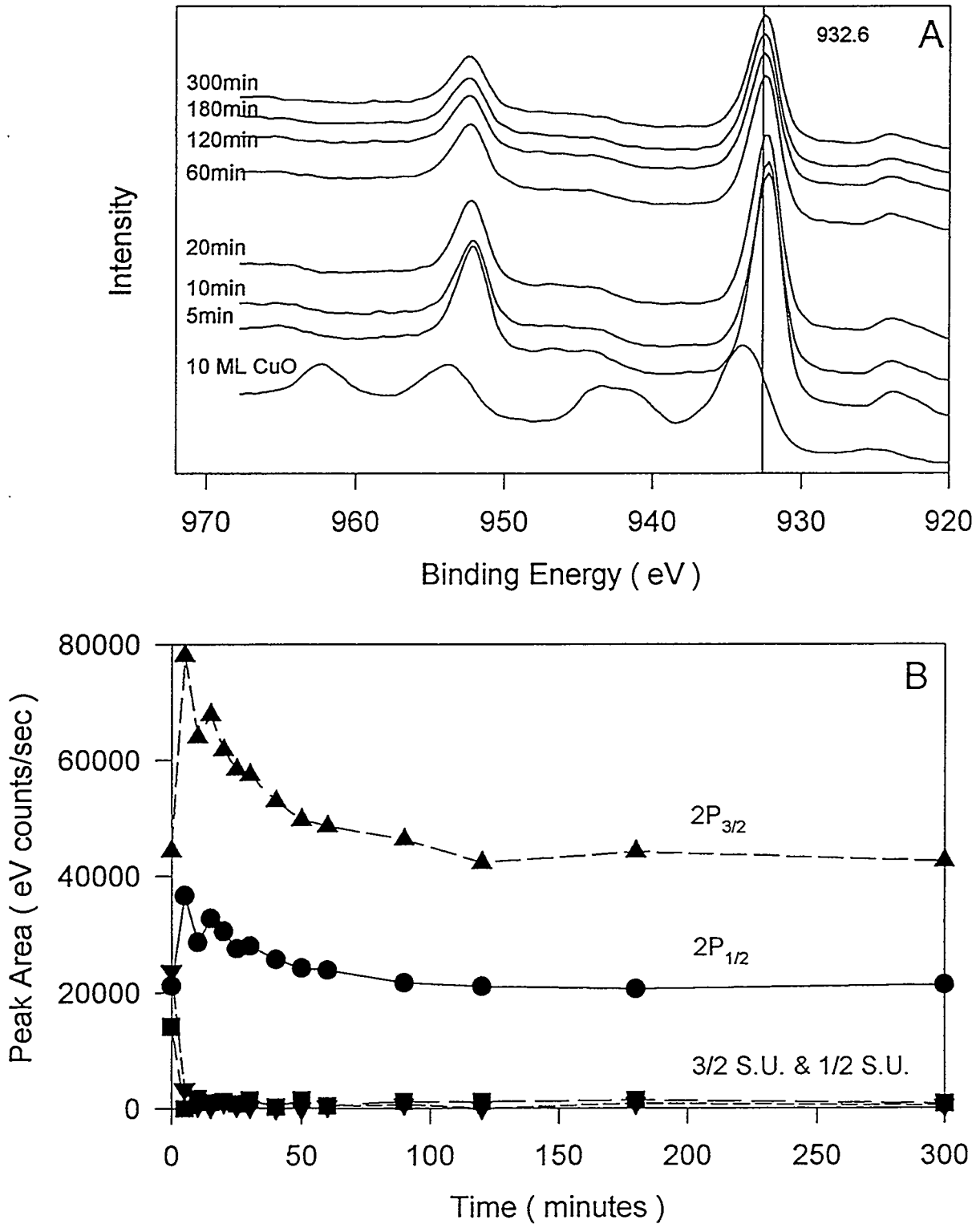

Figure 6.12. A) XPS of the Cu 2P region and B) Cu 2P peak areas as a function of time for the reduction of CuO by annealing in 25 Torr CO at 300°C.

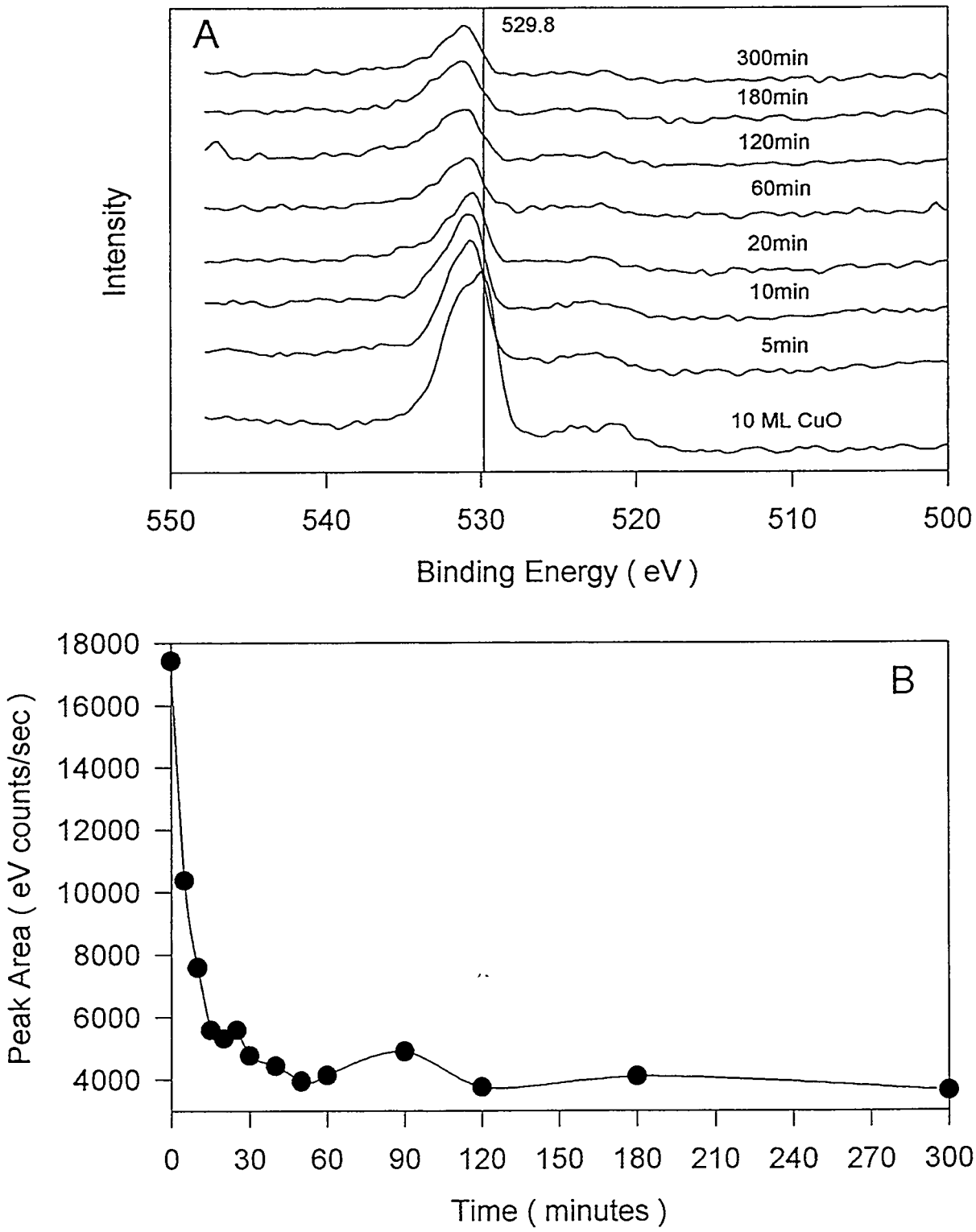

Figure 6.13. A) XPS of the O 1S region and B) O 1S peak area as a function of time for the reduction of CuO by annealing in 25 Torr CO at 300°C.

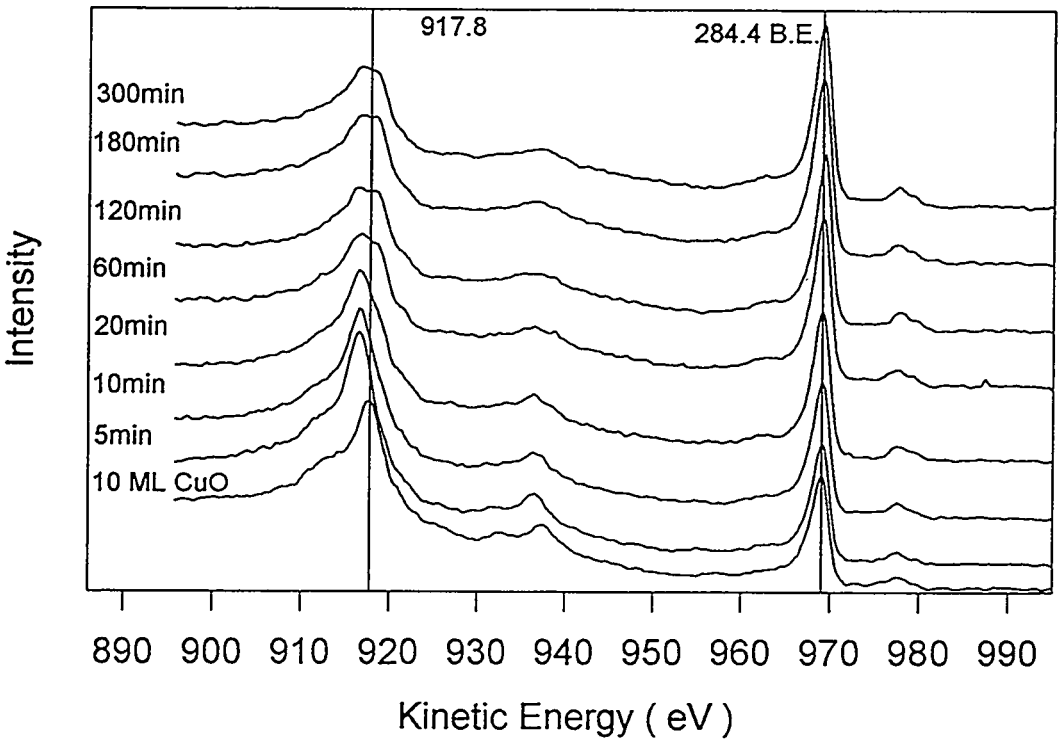

Figure 6.14. XPS of the Cu LVV and C 1S region for the reduction of CuO by annealing in 25 Torr of CO at 300°C for varying amounts of time.

Because the value of the activation energy is lower, one would have expected the CuO to have been reduced under reaction conditions, unless the oxidation of Cu_2O requires even less energy. This experiment does not clearly show why the activation energy for the reduction reaction is the value that it is.

6.3.3. Oxidation of Cu by heating in O_2

Metallurgists and material scientists have studied the oxidation of metals and the properties of metal oxides extensively, and in all cases it has been done on bulk samples [113,114,117,118,200]. Physical chemists and surface scientists have studied the physical and chemical adsorption of oxygen on metal surfaces or metal oxides [195,197-199,201,202]. This work begins to bridge the gap of surface oxidation. It is known that

metals are covered with oxide in air but the extent of oxidation is often uncertain [172]. Part of the uncertainty rests with the composition of air because it contains a partial pressure of water which may affect the extent of surface oxidation.

Copper metal is unique in that it can be prepared free of oxygen in the bulk. Oxygen free high conductivity (OFHC) copper is important in the electronics industry; its specific conductivity is decreased significantly in the presence of oxygen. The surface of copper can be etched to remove any oxidation which has occurred on the surface and will remain clean for long periods of time in a dry atmosphere. The exposure of water to copper results in the green color associated with the Statue of Liberty and other copper monuments. The mechanism of Cu oxidation by gas phase O_2 is under debate.

Exposure of copper to dry oxygen at room temperature does not lead to measurable oxidation. Figure 6.15 shows a series of 5 minute exposures of 100 Torr of dry O_2 to copper at room temperature. The Cu LVV region broadens and loses the distinct metallic copper peak after the first 5 minute exposure. Additional exposure does not affect the spectra further. The O 1S region shows that O is present on the surface after the initial exposure and that it does not increase afterwards. At the end of the experiment the copper is annealed in UHV and the clean metallic spectrum is recovered. This indicates that O_2 adsorbs at room temperature but does not dissociate. If Cu_2O had formed, it would have been stable to the UHV anneal. This is in agreement with the literature [197,198] which showed that dissociative sticking is an activated process.

Heating of a copper surface at 100°C in 50 Torr of O_2 did result in measurable surface oxidation. Figure 6.16 shows that after a 2 minute exposure the kinetic energy of the Cu LVV peak has shifted to lower energies. The peak also does not broaden as significantly as was observed at room temperature. The peak maximum continues to shift to lower energies with the 4 and 6 minute exposures. The O 1S region shows a peak which increases with exposure time. The high energy shoulder forms after the 4 minute

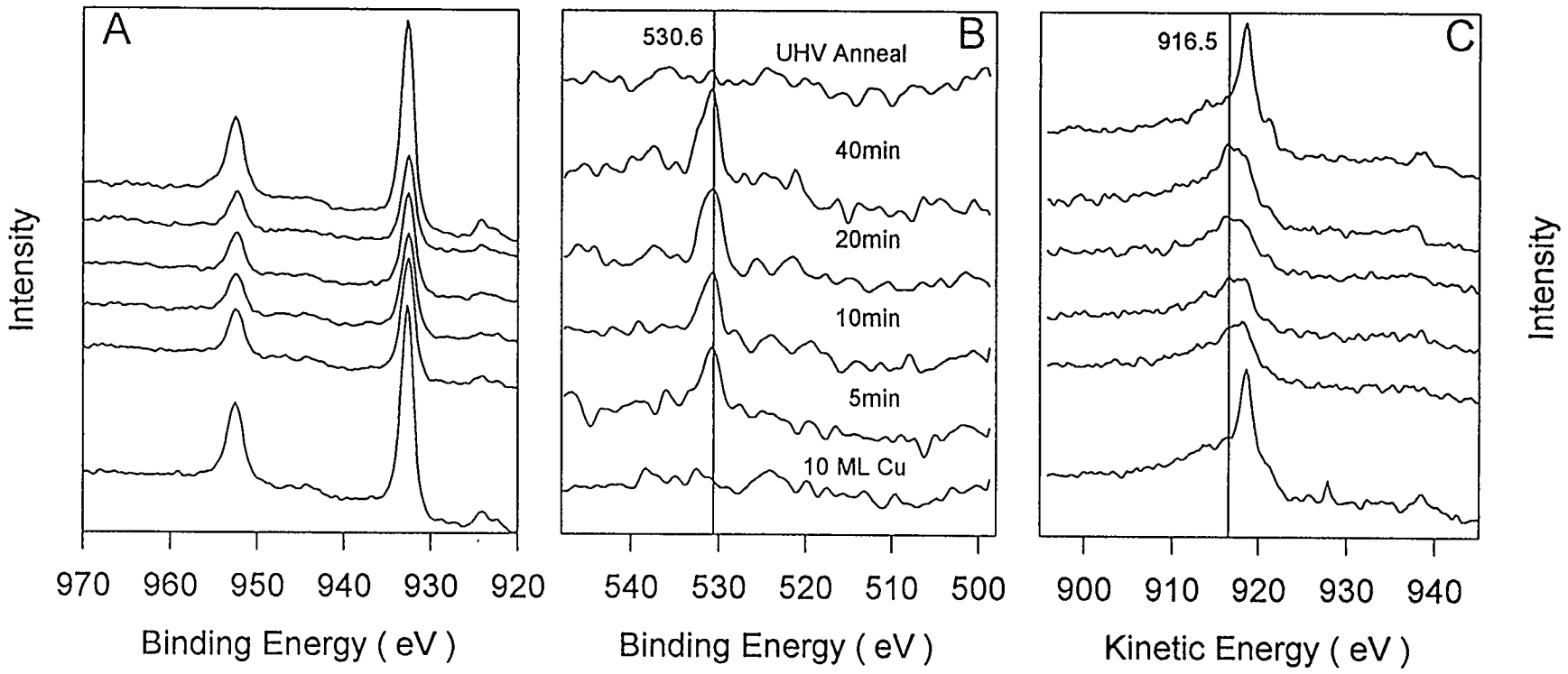

Figure 6.15. XPS spectra of A) Cu 2P region, B) O 1S region, and C) Cu LVV region of a metallic copper surface which has been exposed to 100 Torr of O_2 at 25°C for varying amounts of time and then annealed after the experiment.

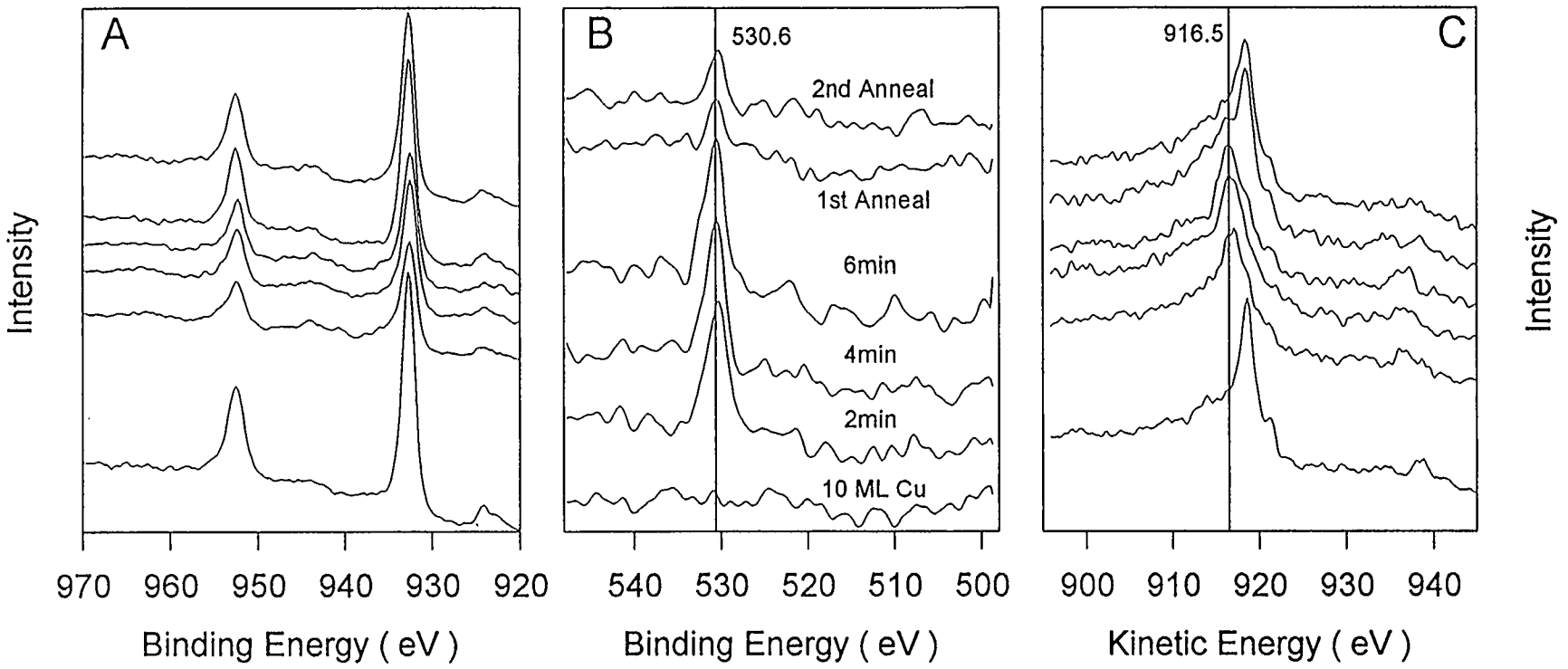

Figure 6.16. XPS of **A)** Cu 2P region, **B)** O 1S region, and **C)** Cu LVV region of a metallic copper surface which has been exposed to 50 Torr of O_2 at 100°C for varying amounts of time and then annealed after the experiment.

exposure. The nature of this oxygen remains undetermined. An anneal of the surface after the three exposures shows the extent of permanent oxidation. The LVV peak remains broader than the initial metallic peak and still shifted to lower kinetic energies. A small O 1S peak can still be observed. The binding energy of the O peak has not changed but the shoulder is absent. A second anneal was performed to test the stability of the surface oxygen. The oxygen peak remained. A more through study will be needed to obtain an activation energy for the surface oxidation of copper by oxygen. Between oxidation steps, anneals will have to be performed to distinguish the oxide oxygen from the O of adsorbed O_2.

6.3.4. Oxidation of Cu by heating in CO_2

Exposure of copper to CO_2 was demonstrated to deactivate the metallic copper catalyst towards CO oxidation by oxidizing the surface to Cu_2O. This is important for the synthesis of methanol which occurs in the presence of $CO_2/CO/H_2$ and Cu is in the +1 oxidation state during the reaction. The oxidation of the catalyst may be due to the ZnO which supports the copper or due to CO_2. CO_2 was demonstrated to be the carbon source for methanol indicating that it must lose an oxygen atom at some point during the reaction.

Oxidation of Cu to Cu_2O by CO_2 is complete after a 5 minute exposure at 25 Torr and 200°C. This is seen in figure 6.17 which shows the Cu LVV region and the O 1S region. The O peak area does not increase with additional exposures. The low temperature and exposure of CO_2 needed for oxidation of Cu shows that it may have an activation energy similar to O_2.

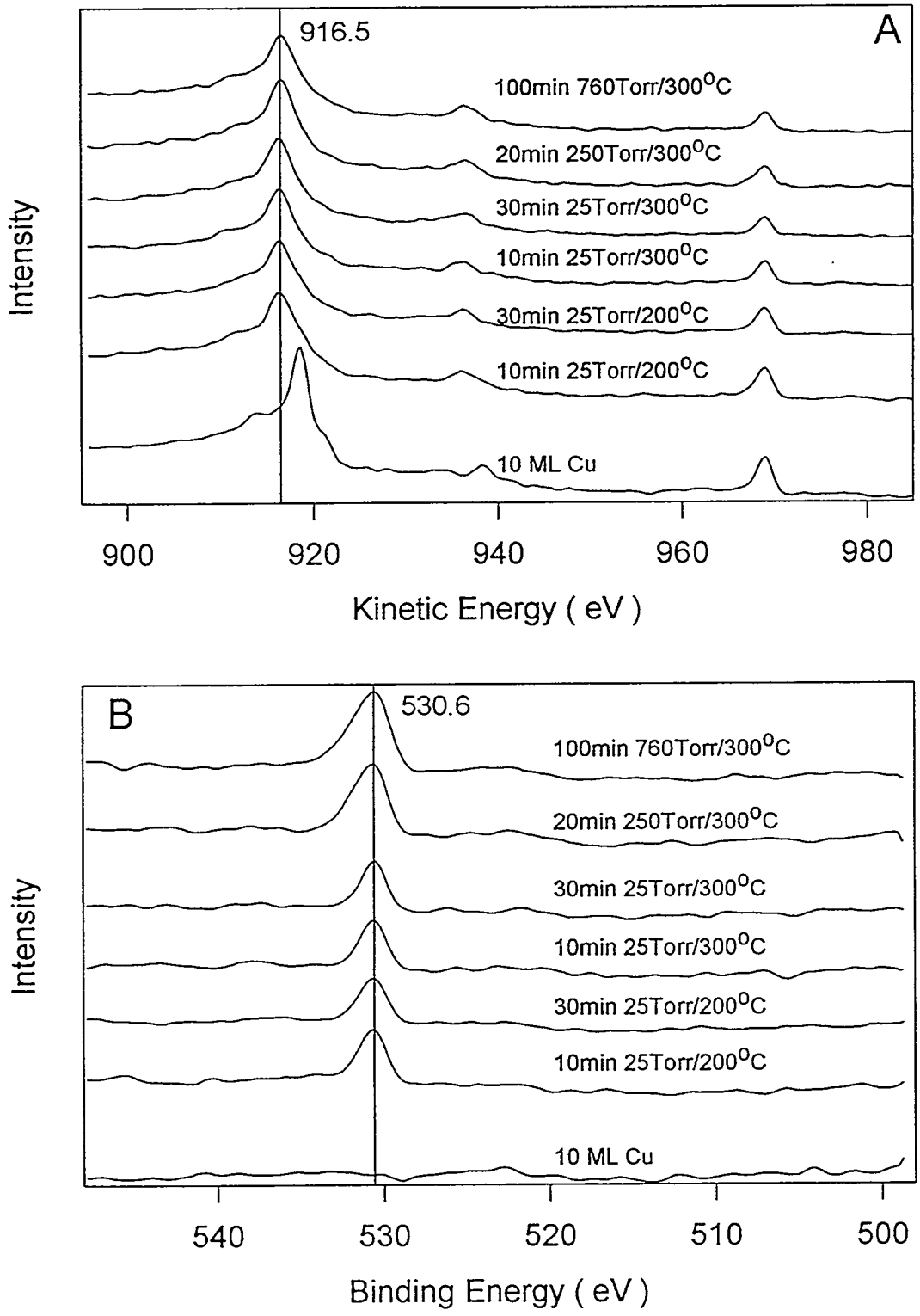

Figure 6.17. XPS of **A)** Cu 2P region and **B)** Cu LVV region for a metallic copper surface exposed to pressures of CO_2 between 25-760 Torr at 200 and 300°C for varying lengths of time.

6.3.5. Reaction of NO/CO over Cu and CuO

A mixture of NO and CO were tested over both metallic copper and CuO surfaces to observe if N_2 and CO_2 were produced. NO reduction by CO has been observed to occur over a Cu-ZSM 5 catalyst [203-206]. Electron Paramagnetic Resonance (EPR) studies have been performed *in situ* to monitor the oxidation state during the reaction [205,206]. EPR is only sensitive to atoms which are paramagnetic, i.e. Cu^0 and Cu^{+2} in this case. But if a ligand or another atom causes a transfer of charge either from Cu^0 or to Cu^{+2} to form a Cu^{+1} species, an EPR experiment would not detect that Cu^{+1} atom. The possibility that NO, with an unpaired electron, might do exactly that is not unreasonable. It is unknown which oxidation state of Cu is present. What has been observed is that during a reaction the amount of Cu EPR signal does decrease. The Cu^0 may be oxidizing during the reaction or it may be adsorbing NO. Likewise, Cu^{+2} may be reduced or it may be adsorbing NO. By attempting the reaction over Cu and CuO, we can observe if the oxidation state of Cu changes.

Figure 6.18 shows that Cu^0 is oxidized to Cu_2O and that CuO is reduced to Cu_2O. In both cases very little N_2 and CO_2 were produced at these reaction temperatures. The rate for NO oxidation of Cu^0 to Cu^{+1} must be higher than the rate for CO reduction of Cu_2O to Cu^0 because the surface did become oxidized. This is similar to what was observed for Cu^0 in a mixture of CO and O_2. In the reverse direction, the rate for reduction of CuO by CO must be faster than the rate of oxidation of Cu_2O by NO. By varying the composition of the mixture away from the stoichiometry of the reaction, measurements could be made for the activity of the reaction on the different oxidation states of copper, in a manner similar to what was performed earlier for CO oxidation.

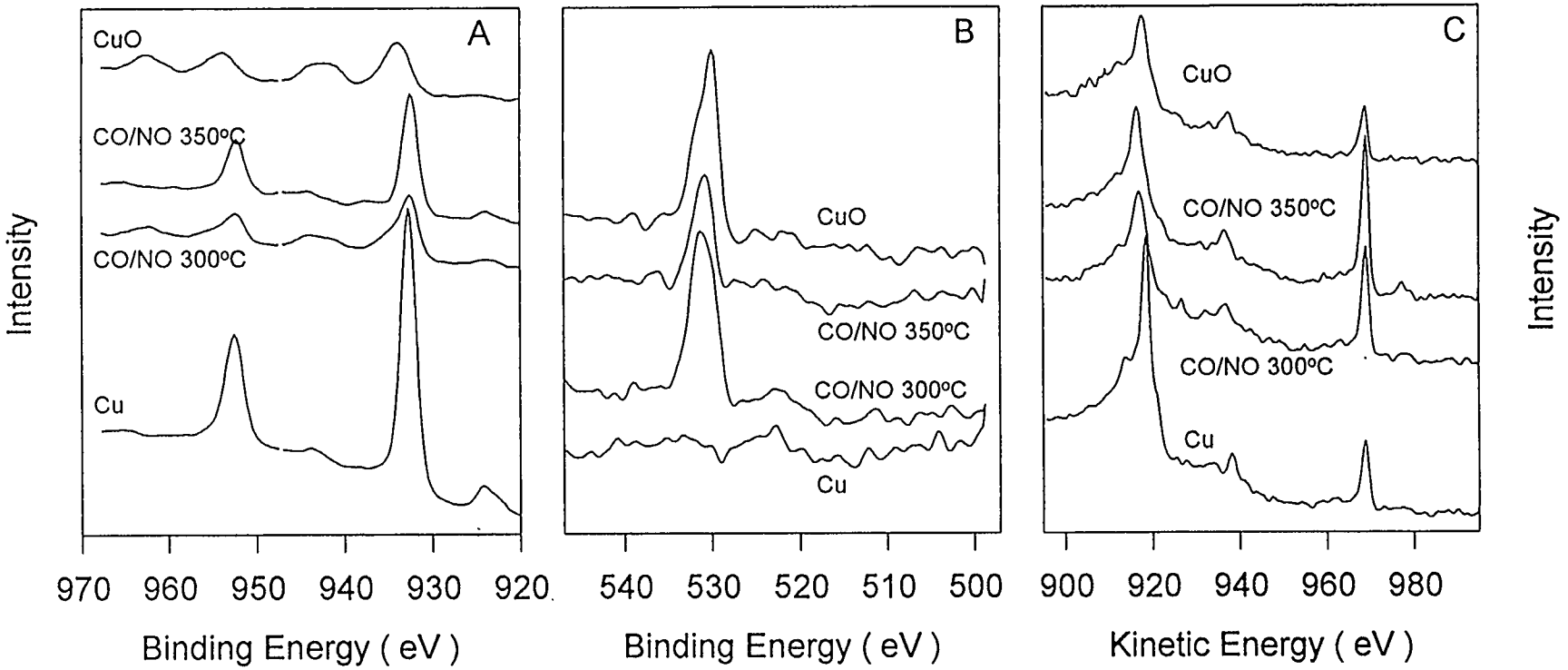

Figure 6.18. NO reduction by CO. XPS of **A)** Cu 2P region, **B)** O 1S region, and **C)** Cu LVV region for a Cu surface, a Cu surface exposed to a 50/50 Torr CO/NO mixture at 300°C for 2 hours, a CuO surface, and a CuO surface expose to a 100/100 Torr CO/NO mixture at 350°C for 2 hours.

6.4. Summary

The results of this work can be best described by a plot of the free energy for the reaction of different gases with the different oxidation states of copper. Figure 6.19 combines the results obtained in this work with literature results. The arrows indicate the direction of the reaction. The oxidation of Cu to Cu_2O by NO has no barrier. The NO molecule readily dissociates on the Cu surface. Oxidation by O_2 has a 7 kcal/mol barrier [207] and oxidation by CO_2 has a 16 kcal/mol barrier [191]. The barrier for reduction of Cu_2O to Cu is unknown for CO, but it should be lower than the UHV reduction which was reported as being 48 kcal/mol [196]. Any ratio of these oxidants and reductants between 1 and 10 will result in Cu oxidizing to Cu_2O as it is the most thermodynamically favored product, except in conditions where the composition of the mixture of gas may change, e.g. through removal of gas phase oxygen. In a sense this is what is observed when CO oxidation under a 97/3 CO/O_2 mixture over Cu is run at 200°C. The surface does become oxidized and only after the removal of gas phase oxygen does the surface become reduced. Even in the presence of CO_2 and CO the catalyst was shown to have a small oxygen coverage.

The conversion between Cu_2O and CuO is more complicated. The free energy barrier for oxidation by CO_2 is unknown but must be very large, because no oxidation was seen. O_2 has an 18 kcal/mol barrier for the oxidation of Cu_2O to CuO [207]. This work showed that UHV would reduce CuO with a 25 kcal/mol barrier and that CO would reduce CuO with a 9 kcal/mol barrier. It was unknown if NO would either reduce CuO or oxidize Cu_2O, and no measurements were made to determine barrier in either case. We would however expect the barrier for NO to lie somewhere between O_2 and CO. If the barriers are correct, then a mixture of CO and O_2 over CuO should have resulted in the reduction to Cu_2O. As this was not observed, we are missing one crucial bit of information. That is the dependence of surface oxidation or reduction on the surface

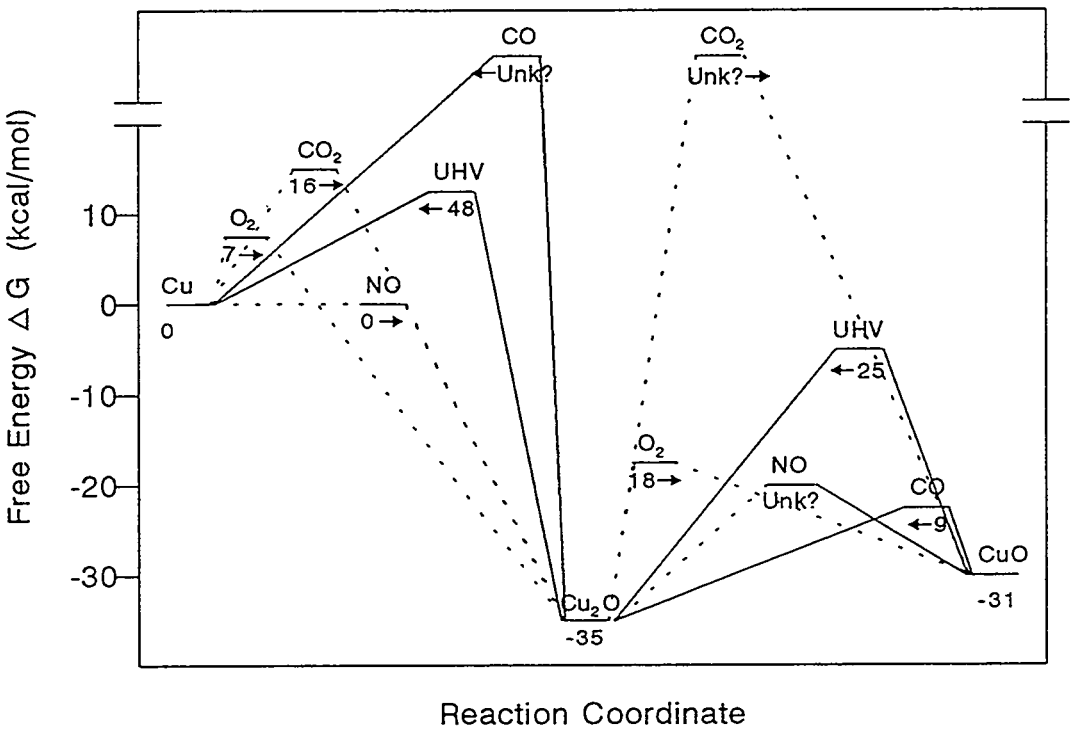

Figure 6.19. Activation energies for the reduction and oxidation of Cu, Cu_2O, and CuO by O_2, CO_2, NO, CO, and UHV.

coverage for each species during a reaction. The high coverage of O_2 on the catalyst surface must affect the ability of CO to reduce the surface. The elementary reaction steps determined here do not account for competitive adsorption on the surface. The calculated activation energies for CO oxidation over the three different oxidation states of copper can not be determined from a simple redox mechanism using the barriers for reduction or oxidation by individual gases.

Chapter 7

Conclusion

The goal of this thesis was to introduce the field of metal oxide catalysis to the techniques of surface science. There has been little fundamental study of metal oxide catalysis because of the physical and chemical complexity of the catalysts. Surface science can make great inroads into this area of catalysis through its ability to characterize the structure and composition of the catalyst surface.

In order to begin applying the methods of surface science to the study of metal oxide catalysts, a well defined model system was needed. Proper choice of a model system would minimize the experimental difficulties of studying a metal oxide without interfering with the chemistry of the metal oxide. The model metal oxide had to be well suited to the various techniques used by surface science. The model metal oxide had to be catalytically active, and the activity needed to be large enough for product formation to be detected from a sample with a small surface area. The model metal oxide needed to be compared to a real catalyst to demonstrate that the model adequately described the chemistry of the catalytic reaction. Lastly, the model metal oxide needed to be able to provide insight into the mechanisms of metal oxide catalysis. All of these requirements were combined successfully in the study of CO oxidation over the oxides of copper.

It was important to study the oxides of copper because, the oxidation reactions which are reported to occur over copper catalysts, there is always the possibility that the copper itself is oxidized. The oxidation state of copper under reaction conditions may not be known. The importance of this is proven in this work, because the catalytic activity over the three oxidation states of copper is different for CO oxidation. The following

summarizes how a model metal oxide system was developed for copper in its three oxidation states. The results of the search for a good support for the copper oxide is reviewed. After testing a wide range of supports, graphite was chosen as the support for the catalysts. The catalytic results for CO oxidation on the different oxidation states are discussed as evidence of a changing mechanism with a change in oxidation state. The effect of CO_2 deactivation of CO oxidation over the copper catalysts is different for the different oxidation states. Lastly, the interaction of individual gases with the different oxidation states of copper is discussed because of its importance to the understanding of catalytic reactions over copper oxides when the reactant gases may change the oxidation state of the surface.

7.1. Model Catalyst Development and Characterization

The development of a model metal catalyst system had to overcome the experimental difficulties of studying a bulk metal oxide catalyst. A bulk metal oxide catalyst could not be used here because it interferes with the techniques of surface science by being an electrical and thermal insulator, by having "internal" surface area not accessible to surface spectroscopies, by being non uniform in both structure and oxidation state, and by being difficult to prepare in vacuum. To circumvent these problems, it was decided to grow a thin oxide film to model the catalyst. The thin film would be grown on a support which would provide good electrical and thermal conductivity. A thin film also would not have any "internal" surfaces and could be uniformly grown in UHV.

Thin native oxides on conducting Al, Si, Mo, Ta, stainless steel, and Fe as well as conductive graphite were tried as supports for the growth of copper oxides. The growth of copper on Al_2O_3 followed a multilayer growth mode. Under CO oxidation conditions, the copper would oxidize and react with the Al_2O_3. The result was the formation of a

$CuAl_2O_4$ spinel. Attempts to measure catalytic reactions on the Cu/Al_2O_3 system showed activity until the spinel formed, at which time the activity was equal to the background. The catalyst formed the spinel within 20 minutes of limiting the CO oxidation reaction, preventing kinetic measurements from being made.

The copper on SiO_2 system was tried because silica is a common industrial support. When Cu was deposited and oxidized on SiO_2, a silicon peak in the AES was always observed. This indicated that as Cu was deposited either Si would diffuse into the Cu layer or that Cu islanding would occur. The use of SiO_2 as a support was stopped because of the difficulty associated with heating and transferring the sample.

The use of Mo and Ta as supports was attempted because it was not known how they would react under catalytic reaction conditions. Mo and Ta are commonly used as supports for surface science experiments. Both Mo and Ta were completely oxidized under reaction conditions. The oxidation of the supports prevented resistive heating of the sample and, in a few cases, resulted in the loss of the sample from the transfer piece.

A stainless steel support was tried because bulk oxidation of the foil would not occur. There were no reports as to how stainless steel might affect the chemistry of copper oxide. Two compounds were created on the surface of the stainless steel support. Fe_2O_3 could be created by oxidizing the stainless steel or $CuCr_2O_4$ could be created by annealing Cu on Fe_2O_3 above 600°C. The activity of Cu on the $CuCr_2O_4$ surface was greater than that on the Fe_2O_3 surface. The chemical complexity of the stainless steel support made it difficult to observe if changes in the catalyst were occurring during catalytic reactions.

An oxidized Fe foil was also used as a simpler alternative to the stainless steel. The support had catalytic activity for CO oxidation. Despite this, Cu and Cu_2O were tested for catalytic activity on this support. The major result obtained in this study was that the activity of Cu and Cu_2O were different. This was the first evidence that the oxidation state of copper did affect catalytic activity. Both catalysts lost activity with

time. This could have been due to S which segregated from the bulk of the Fe foil or due to compound formation with the Fe.

Graphite was tried last as a catalyst support. The graphite support was obtained by coating a stainless steel foil with a spray of micron-sized graphite particles. The graphite was free of oxygen, making possible the detection of copper oxidation by observing a change in the oxygen AES signal. The three oxidation states of copper could be prepared on graphite and well characterized by XPS, AES, and kinetic measurements of the catalytic reactions. The growth of Cu on graphite formed 3 dimensional islands. Upon oxidation, copper oxide wets the graphite surface. The graphite surface did not possess catalytic activity nor did it combust under reaction conditions. The activity of Cu on graphite showed a dependence on the amount of Cu initially deposited. This system was used to measure the catalytic ability of copper oxides for CO oxidation.

7.2. Catalytic Activity

There is a database of catalytic measurements for CO oxidation over copper. The results can be separated into two categories, low pressure UHV experiments and high pressure catalytic reaction studies. Within the low pressure work, there is agreement on the mechanism for the reaction and the observed kinetic results. The high pressure studies are not self consistent nor do they match the results of the low pressure work. The discrepancies between the low and high pressure studies has been blamed on the "pressure gap". The results varied between studies done at high pressures work and was associated with the use of different catalyst pretreatments or with different active catalysts. In this work it has been shown that the results obtained in previous low pressure UHV experiments were obtained over metallic copper catalyst while the previous high pressure results were obtained over either copper (I) oxide or copper (II) oxide catalysts.

Under certain high pressure reaction conditions, it was found that metallic copper will be oxidized to CuO. This meant that kinetic results are complicated by the fact that the catalyst changes during the reaction. Depending on when kinetic measurements were made during a high pressure reaction, a different oxidation state of copper would exist. In order to measure the kinetics over each oxidation state of copper, the CO to O_2 ratio must to be fixed at particular ratios to prevent changes in the oxidation state of the surface. Metallic copper, copper (I) oxide, and copper (II) oxide were found to be stable under a 97/3, 90/10, and 66/33 Torr ratios of CO to O_2, respectively.

There were two distinct activities associated with metallic copper, and these were found to be linked to the presence or absence of subsurface oxygen. When subsurface oxygen was present, the rate of reaction was lower than without. This had been seen previously in UHV studies in which the sample had been exposed to high oxygen pressures. The activation energy obtained for CO oxidation over the catalyst without subsurface oxygen was 8.0 kcal/mol and was in excellent agreement with the previous UHV studies. The activation energy over the catalyst with subsurface oxygen was 11 kcal/mol. The mechanism proposed for metallic copper was a Langmuir-Hinshelwood mechanism with adsorbed O reacting with adsorbed CO. Adsorbed O inhibits CO adsorption, causing the reaction over the catalyst with subsurface oxygen to be slower.

This study is the first to report the activity of copper (I) oxide for the catalytic oxidation of CO. The activation energy of the reaction was 14 kcal/mol. There was no change in oxidation state of the catalyst as the reaction proceeded towards complete use of gas phase oxygen. This was evidence that CO did not reduce the surface as part of the reaction mechanism. As the reaction proceeded, the ratio of CO to O_2 increased in the gas phase, because O_2 was the limiting reagent, making the reaction environment more reducing. If the reaction was proceeding via a redox mechanism, the catalyst would have been slowly reduced during the reaction. Because this was not observed, a Langmuir-Hinshelwood mechanism was proposed. It is known that CO adsorbs on copper (I) oxide

and that O_2 dissociates on this surface, making a Langmuir-Hinshelwood mechanism likely.

Catalytic reactions were also run on copper (II) oxide, and the results agreed well with previous high pressure reactor studies. The activation energy of the reaction was 17 kcal/mol. Copper (II) oxide was less active than both copper (I) oxide and metallic copper as a catalyst for CO oxidation.. The activity of copper (II) oxide varied with the extent of oxidation of the catalyst. This indicated that the stability of the oxide was important in the reaction mechanism. A more stable oxide was less active. Because copper (II) oxide can not dissociate gas phase oxygen, a Langmuir-Hinshelwood mechanism can be ruled out. Therefore, the mechanism over copper (II) oxide is necessarily different than the mechanism over the other oxidation states. The mechanism proposed here is a redox cycle where adsorbed CO removes a lattice O, and the O vacancy is refilled by a reaction with gas phase O_2. The rate limiting step is the removal of the lattice O, which explains why the more stable oxide is less active.

CO_2 was found to deactivate CO oxidation on copper (II) oxide, preventing complete use of the gas phase oxygen. It was unknown if CO_2 also poisoned the activity of metallic copper and copper (I) oxide, so studies were performed to see the effect of CO_2 on the reaction. When CO_2 is added to a reaction over metallic copper, the activity towards CO oxidation decreased. The cause of this was CO_2 dissociation on the metallic surface. The dissociation increased the oxygen coverage, thereby decreasing the reaction rate. The CO_2 also deactivated the copper (I) oxide catalyst. XPS showed that CO_2 could not oxidize the copper (I) oxide to copper (II) oxide, so dissociation was ruled out. TDS did not show any adsorbed CO_2 on the surface after a catalytic run. This indicated that CO_2 reversibly blocks CO adsorption sites on copper (I) oxide as the deactivation mechanism. The deactivation over the copper (II) oxide surface could have been due to the formation of a copper carbonate, but an XPS investigation showed that $CuCO_3$ could

not be formed under reaction conditions. This showed that CO_2 deactivates the CuO surface by reversibly blocking CO adsorption sites.

7.3. Redox of the Model Metal Oxide Catalysts

In order to understand the mechanism of metal oxide catalysis, investigations into how individual gases interact with the metal oxide surface were performed. If a redox mechanism occurs, data concerning the ability of the oxidant to oxidize the metal and the ability of the reductant to reduce the oxide is needed. Studies of this type are rare in that it is hard to observe the intermediate stages of oxidation or reduction. The thin film model system used here is ideal in that the uniformity of the sample makes measuring the reduction or oxidation of the catalyst possible. A bulk sample potentially has problems with solid state diffusion, which cause the formation of concentration gradients or passivating layers, hindering kinetic measurements on the change in oxidation state. In these studies, we observed the kinetics of the reduction of copper (II) oxide by exposure to UHV and CO as a function of temperature and time. We also observed the kinetics of metallic copper oxidation by O_2, CO_2, and NO.

Annealing copper (II) oxide in UHV will decompose the oxide to copper (I) oxide because the no partial pressure of oxygen in the gas phase is sufficiently low. The decrease in the Cu^{+2} 2P shake-up peaks were measured as a function of time and temperature. The decrease in the O 1S signal was also measured. The 2P shake-up peaks decreased in a first order process and the O peak decreased in a second order process. Activation energies were measured for each and found to be between 25-27 kcal/mol. This agrees well with the activation energy of gas phase O_2 isotope exchange which is a measure of O removal from the lattice.

Reduction of copper (II) oxide to copper (I) oxide by CO could be measured between 100-300°C. At 300°C and higher, the reduction of copper (I) oxide by CO to metallic copper could be observed. Unlike the UHV results, the Cu 2P peaks decreased in a non-linear manner with reduction. The O peak decreased similarly. A rate based on the initial reduction was used to calculated the activation energy. The reduction between Cu^{+2} and Cu^{+1} had an activation energy of 9 kcal/mol which is below the value obtained for the catalytic reaction results. An activation energy for the reduction of copper (I) oxide was not calculated because not enough data were acquired. Additionally, not all oxygen could be removed from the metal.

Oxygen oxidation of metallic copper is an activated process. Exposures of metallic copper to O_2 at room temperature resulted in the formation of an oxygen layer that could be removed by annealing in UHV. Exposures at higher temperatures resulted in the formation of copper (I) oxide as well as adsorbed O. Annealing in UHV removed the adsorbed O leaving some fraction of the surface oxidized.

Oxidation of metallic copper by CO_2 was reported in the CO_2 deactivation study. The activation energy for this is 16 kcal/mol. An experiment was performed to determine if a mixture of CO to CO_2 in a 4 to 1 ratio would oxidize the surface. The result showed that a small amount of oxygen was adsorbed on the surface under these conditions. This has enormous significance as to why copper has been observed in the +1 oxidation state over an industrial methanol synthesis catalyst.

It was known that NO would decompose without an activation barrier on metallic copper to form copper (I) oxide, so a mixture of NO and CO were exposed to both metallic copper and copper (II) oxide to observe what might occur. This has relevance to NO reduction over Cu-zeolites where EPR studies measures either Cu^0 or Cu^{+2}. Metallic copper expose to a 50/50 Torr mixture of CO and NO formed in a copper (I) oxide. This showed that NO was more able to oxidize Cu than CO was able to reduce copper (I) oxide. When copper (II) oxide was exposed to the same gas mixture again the copper (I)

oxide formed. In both studies N_2 and CO_2 were produced. Additional studies are needed to determine if the activation energy for reaction would be different over the different oxidation states of copper under different gas mixtures.

7.4. Future Directions

No experiments ever come to an end, only new directions are taken. The development of a model metal oxide system which is amenable to surface science studies opens a large number of research doors. Investigations of the copper system could be continued in the study of NO reduction or ammonia oxidation. Selective partial oxidation reactions, like propylene oxidation, could also be explored. Other metal oxides could be deposited in thin films, and the reactions which they catalyze may be examined. The most important aspect of the future work which can be done with this system is to observe how the oxidation state of the surface changes with the gases above it.

This model system has the benefit of working under pressures of industrial significance. Even if the metal oxide has a low catalytic turnover rate, it can be exposed to the reaction gas mixture at industrially relevant temperatures in order to observe any changes in composition. The field of industrial catalysis is filled with reports of catalyst pretreatments. These pretreatments result in an active catalyst of unknown composition. By employing similar pretreatments on this system, the final form of the catalyst could be characterized. Knowledge of the physical structure and chemical nature of the active catalysts makes possible the determination of how and why catalysts facilitate reactions. This fundamental knowledge can enable the rational design the best possible catalyst.

References

1) National Research Council, "Catalysis Looks to the Future" 1992. National Academy Press, Washingtion DC.

2) C.N. Satterfield, "Heterogeneous Catalysis in Practice" 1980. McGraw-Hill, New York.

3) *C&EN* **71** (1993) 41.

4) P.H. Emmett in: "The Physical Basis for Heterogeneous Catalysis" ed. E. Drauglis and R.I. Jaffee 1975. Plenum Press, New York.

5) M. Boudart, and G Djéga-Mariadassou, "Kinetics of Heterogeneous Catalytic Reactions" 1984. Princeton University Press, Princeton.

6) N.D. Spencer, R.L. Schoonmaker, and G.A. Somorjai, *J. Catal.* **74** (1982) 129.

7) D.R. Strongin, J. Carrazza, S.R. Bare, and G.A. Somorjai, *J. Catal.* **103** (1987) 213.

8) D.R. Strongin, and G.A. Somorjai, *J. Catal.* **109** (1988) 51.

9) G.A. Somorjai, *Surf. Sci.* **299/300** (1994) 849.

10) V.E. Henrich, and P.A. Cox, "The Surface Science of Metal Oxides" 1993. Cambridge University Press, Cambridge.

11) M.E. Levin, M. Salmeron, A.T. Bell, and G.A. Somorjai, *J. Catal.* **106** (1987) 401.

12) A.B. Boffa, A.T. Bell, and G.A. Somorjai, *J. Catal.* **139** (1992) 602.

13) W.M.H. Sachtler, *Catal. Rev.* **4** (1970) 27.

14) L.Y. Margolis, *Catal. Rev.* **8** (1973) 241.

15) G.W. Keulks, etal., *Adv. Catal.* **27** (1978) 183.

16) G.K. Boreskov, *Proc. 4th Int. Cong. Catal.* (1968) 439.

17) I. Matsura, *Proc. 6th Int. Cong. Catal.* (1976) 819.

18) D.J. Hucknall, "Selective Oxidations of Hydrocarbons" 1974. Academic Press, London.

19) J.T. Kummer, *Proc. Energy Combust. Sci.* **6** (1980) 177.

20) Y.Y. Yao, *J. Catal.* **39** (1975) 104.

21) M.E. Domagala, and C.T. Campbell, *Catal. Lett.* **9** (1991) 65.

22) O.P. van Pruissen, M.M.M. Dings, and O.L.J. Gijzeman, *Surf. Sci.* **179** (1987) 377.

23) F.H.P.M. Habraken, E.Ph. Kieffer, and G.A. Bootsma, *Surf. Sci.* **83** (1979) 45.

24) O.P. van Pruissen, O.L.J. Gijzeman, and J.W. Geus, *Vacuum* **38** (1988) 247.

25) F.H.P.M. Habraken, et al., *Surf. Sci.* **88** (1979) 285.

26) J. Szanyi, and D.W. Goodman, *Catal. Lett.* **21** (1993) 165.

27) K.I. Choi, and M.A. Vannice, *J. Catal.* **131** (1991) 22.

28) J.L. Blumenthal, and K. Nobe, *I&EC Proc. Des. Develop.* **5** (1966) 177.

29) W.E. Garner, F.S. Stone, and P.F. Tiley, *Proc. Roy. Soc. A* **221** (1952) 472.

30) I. Halasz, *React. Kinet. Catal. Lett.* **41** (1990) 115.

31) E.E. Miro, E.A. Lombardo, and J.O. Pentunchi, *J. Catal.* **104** (1987) 176.

32) R.A. Prokopowicz, P.L. Silveston, R.R. Hudgins, and D.E. Irish, *React. Kinet. Catal. Lett.* **37** (1988) 63.

33) J. Mooi, and P.W. Selwood, *J. Amer. Chem. Soc.* **74** (1952) 2461.

34) S. Sourirajan, and M.A. Accomazzo, *Can. J. Chem.* **38** (1960) 1990.

35) N.T. Thomas, L.S. Caretto, and K. Nobe, *I&EC Proc. Des. Develop.* **8** (1969) 282.

36) N.J.J. Dekker, et al., *AIChE J.* **38** (1992) 385.

37) Y. Fu, Y. Tian, and P. Lin, *J. Catal.* **132** (1991) 85.

38) T. Engel, and G. Ertl, *Adv. Catal.* **28** (1979) 2.

39) T. Huang, and T. Yu, *Appl. Catal.* **71** (1991) 275.

40) W. Dow, and T. Huang, *J. Catal.* **147** (1994) 322.

41) T. van Herwijnen, and W.A. de Jong, *J. Catal.* **63** (1980) 83.

42) C.T. Campbell, and K.A. Daube, *J. Catal.* **104** (1987) 109.

43) D.L. Roberts, and G.L. Griffin, *J. Catal.* **110** (1988) 117.

44) A. Spitzer, and H. Lüth, *Surf. Sci.* **120** (1982) 376.

45) C.V. Ovesen, P. Stoltze, J.K. Nørskov, and C.T. Campbell, *J. Catal.* **134** (1992) 445.

46) E. Colbourn, et al., *J. Catal.* **130** (1991) 514.

47) S. Fujita, M. Usui, and N. Takezawa, *J. Catal.* **134** (1992) 220.

48) J.M. Campbell, J. Nakamura, and C.T. Campbell, *J. Catal.* **136** (1992) 24.

49) E. Fiolitakis, and H. Hofman, *J. Catal.* **80** (1983) 328.

50) D.C. Grenoble, M.M. Estadt, and D.F. Ollis, *J. Catal.* **67** (1981) 90.

51) B.S. Clausen, et al., *J. Catal.* **132** (1991) 524.

52) C.T. Au, J. Breza, and M.W. Roberts, *Chem. Phys. Lett.* **66** (1979) 340.

53) C.T. Campbell, and B.E. Koel, *Surf. Sci.* **186** (1987) 393.

54) G.A. Vedage, et al., *Proc. 8th Inter. Cong. Catal.* vol. 2 p.47 (1984).

55) G.C. Chinchen, et al., *Appl. Catal.* **36** (1988) 1.

56) T.H. Fleisch, and R.L. Mieville, *J. Catal.* **90** (1984) 165.

57) J.R. Monnier, G. Apai, and M.J. Hanrahan, *J. Catal.* **88** (1984) 523.

58) M. Bowker, et al., *J. Catal.* **109** (1988) 263.

59) G.R. Sheffer, and T.S. King, *J. Catal.* **115** (1989) 376.

60) M. Muhler, et al., *Catal. Lett.* **25** (1994) 1.

61) J.F. Edwards, and G.L. Schrader, *J. Catal.* **94** (1985) 175.

62) R. Burch, R.J. Chappell, and S.E. Golunski, *J. Chem. Soc. Faraday Trans. I* **85** (1989) 3569.

63) T. Fujitani, et al., *Catal. Lett.* **25** (1994) 271.

64) J.R. Jennings, G. Owen, R.M. Nix, and R.M. Lambert, *Appl. Catal. A General* **82** (1992) 65.

65) B.S. Clausen, and H. Topsøe, *Catal. Today* **9** (1991) 189.

66) P.A. Taylor, P.B. Rasmussen, and I. Chorkendorff, *J. Phys: Condens. Matter* **3** (1991) 191.

67) P.A. Taylor, et al., *Surf. Sci.* **261** (1992) 191.

68) J. Saussey, J. Lavalley, J. Lamotte, and T. Rais, *J. Chem. Soc. Chem. Commun* (1982) 278.

69) I.E. Wachs, and R.J. Madix, *J. Catal.* **53** (1978) 208.

70) P. Hollins, and P. Pritchard, *Surf. Sci.* **89** (1979) 486.

71) C. Harendt, J. Goschnick, and W. Hirschwald, *Surf. Sci.* **152/153** (1985) 453.

72) E. Giamello, and B. Fubini, *J. Chem. Soc. Faraday Trans. I* **79** (1983) 1995.

73) D.L. Roberts, and G.L. Griffin, *Appl. Surf. Sci.* **19** (1984) 298.

74) D.F. Cox, and K.H. Schulz, *Surf. Sci.* **249**, (1991) 138.

75) K. Klier, et al., *J. Catal.* **74** (1982) 343.

76) L.E.Y. Nonneman, and V. Ponec, *Catal Lett.* 7 (1990) 213.

77) R. Burch, and R.J. Chappell, *Appl. Catal.* **44** (1988) 131.

78) R.G. Herman, et al., *Am. Chem. Soc. Div. Petr. Prepr.* **23** (1978) 595.

79) J. Nakamura, J.A. Rodriguez, and C.T. Campbell, *J. Phys.: Condens. Matter* 1 (1989) SB149.

80) C. Engdahl, and B.I. Lundqvist, *Chem. Phys. Lett.* **215** (1993) 103.

81) H-S. Choi, J-T. Lin, and R.L. Kuczkowski, *J. Catal.* **99** (1986) 72.

82) R.K. Grasselli, and J.D. Burrington, *Adv. Catal.* **30** (1981) 133.

83) B.J. Wood, H. Wise, and R.S. Yolles, *J. Catal.* **15** (1969) 355.

84) K.H. Schulz, and D.F. Cox, *J. Catal.* **143** (1993) 464.

85) K.H. Schulz, and D.F. Cox, *J. Phys. Chem.* **97** (1993) 647.

86) K.H. Schulz, and D.F. Cox, *J. Phys. Chem.* **97** (1993) 3555.

87) K.H. Schulz, and D.F. Cox, *Surf. Sci.* **262** (1992) 318.

88) G.K. Boreskov, *Adv. Catal.* **15** (1965) 285.

89) C.R. Adams, and T.J. Jennings, *J. Catal.* **3** (1964) 549.

90) H.H. Voge, C.D. Wagner, and D.P. Stevenson, *J. Catal.* **2** (1963) 58.

91) R.K. Grasselli, and J.D. *Adv. Catal.* **30** (1981) 133.

92) G.W. Keulks, L.D. Krenzke, and T.M. Noterman, *Adv. Catal.* **27** (1978) 183.

93) M. Bowker, and R.J. Madix, *Surf. Sci.* **95** (1980) 190.

94) N.W. Cant, et al., *J. Catal.* **91** (1985) 197.

95) J.N. Russell, S.M. Gates, and J.T. Yates, *Surf. Sci.* **163** (1985) 516.

96) R.P.H. Gasser, "An Introduction to Chemisorption and Catalysis by Metals" 1985. Oxford University Press, Oxford U.K.

97) K.B. Lewis, Ph.D. Thesis, Department of Chemistry, University of California, Berkelely, 1988.

98) G. Ertl, and J. Küppers, "Low Energy Electrons and Surface Chemistry" 1974. Verlag Chemie, Weinheim.

99) P.W. Palmberg, G.E. Riach, R.E. Weber, and N.C. MacDonald, "Handbook of Auger Electron Spectroscopy" 1972. Physical Electronics Industries, Eden Prairie MN.

100) P.W. Palmberg, G.K.Bohn, and J.C. Tracy, *App. Phys. Lett.* **15** (1969) 254.

101) J.C. Rivière in "Practical Surface Analysis by Auger and X-ray Photoelectron Spectroscopy" ed. D. Briggs and M.P. Seah, 1983. John Wiley and Son.

102) Muilenberg, G. E., ed., "Handbook of X-ray Photoelectron Spectroscopy," 1979. Perkin Elmer Corp., Eden Praire MN.

103) L. Fiermans, R. Hoogewijs, and J. Vennik, *Surf. Sci.* **47** (1975) 1.

104) M.P. Seah, and W.A. Dench, *Surf. Interface. Anal.* **1** (1979) 2.

105) E. Bauer, *Appl. Surf. Sci.* **11/12** (1982) 479.

106) G.H. Vurens, Ph.D. Thesis, Department of Chemistry, University of Lieden, Lieden, 1989.

107) "Handbook of Chemistry and Physics" ed. R.C. Weast 1984. CRC Press, Boca Raton Florida.

108) J.A. Rodriguez, and D.W. Goodman, *Surf. Sci. Reports* **14** (1991) 1.

109) M.A. Barteau, *J. Vac. Sci. Technol. A* **11** (1993) 2162.

110) V.E. Henrich, and P.A. Cox, *Appl. Surf. Sci.* **72** (1993) 277.

111) Q.L. Guo, and P.J. Møller, *Surf. Sci.* **244** (1991) 288.

112) R. Weissman, and K. Müller, *Surf. Sci. Reports* **105** (1981) 251.

113) J. Xue, and R. Dieckman, *J. Phys. Chem. Solids* **51** (1990) 1263.

114) R.A. Rapp, *Pure & Appl. Chem.* **56** (1984) 1715.

115) C. Kaito, et al., *J. Cryst. Growth* **74** (1986) 469.

116) R. Guan, H. Hashimoto, K.H. Kuo, and T. Yoshida, *Acta. Cryst.* **B43** (1987) 343.

117) J.H. Park, and K. Nateson, *Oxidation of Metals* **39** (1993) 411.

118) W.J. Moore, and B. Selikson, *J. Chem. Phys.* **19** (1951) 1539.

119) M. Shelef, et al., *J. Catal.* **137** (1992) 114.

120) H.Kung, *J. Catal.* **134** (1992) 691.

121) J. Laine, F. Severino, A. López-Agudo, and J.L.G. Fierro, *J.Catal.* **129** (1991) 297.

122) V. Di Castro, et al., *J. Electron Spectrosc. Relat. Phenom.* **52** (1990) 415.

123) T.V. Mulina, A.V. Filipov, and V.A. Chumachenko, *React. Kinet. Catal. Lett.* **37** (1988) 95.

124) T. Huang, T.Yu, and S. Chang, *Appl. Catal.* **52** (1989) 157.

125) M. Lo Jacono, A. Cimino, and M. Inversi, *J. Catal.* **76** (1982) 320.

126) A. Barrie, *Chem. Phys. Lett.* **19** (1973) 109.

127) G.A. El-Shobaky, T. El-Nabarawy, and G.A. Fagal, *Appl. Catal.* **52** (1989) 33.

128) R.M. Friedman, J.J. Freeman, and F.W. Lytle, *J. Catal.* **55** (1978) 10.

129) R. Hierl, H. Knözinger, and H. Urbach, *J. Catal.* **69** (1981) 475.

130) E.D. Pierron, J.A. Rashkin, and J.F. Roth, *J. Catal.* **9** (1967) 38.

131) R.M. Jaeger, et al., *Surf. Sci.* **259** (1991) 235.

132) Q.L. Guo, and P.J. Møller, *Vacuum* **41** (1990) 1114.

133) S.F. Tikhov, et al. *J. Catal.* **134** (1992) 506.

134) J.G. Chen, M.L. Colaianni, W.H. Weinberg, and J.T. Yates, *Surf. Sci.* **279** (1992) 223.

135) G. Ertl, et al., *Appl. Surf. Sci.* **5** (1980) 49.

136) K.T. Jacob, and C.B. Alcock, *J. Amer. Ceramic Soc.* **58** (1975) 192.

137) R.V. Kasowski, F.S. Ohuchi, and R.H. French, *Physica B* **150** (1988) 44.

138) F.S. Ohuchi, R.H. French, and R.V. Kasowski, *J. Vac. Sci. Technol. A* **5** (1987) 1175.

139) S.V. Pepper, *J. Appl. Phys.* **47** (1976) 801.

140) X. Xu, J. He, and D.W. Goodman, *Surf. Sci.* **284** (1993) 103.

141) X. Xu, S.M. Vesecky, and D.W. Goodman, *Science* **258** (1992) 788.

142) D.B. Clark, I. Suzuki, and A.T. Bell, *J. Catal.* **142** (1993) 27.

143) A.R. Balkenende, C.J.G. van der Grift, E.A.Meulenkamp, and J.W. Geus, *Appl. Surf. Sci.* **68** (1993) 161.

144) X.Xu, and D.W. Goodman, *J. Phys. Chem.* **97** (1993) 683.

145) E.G.M. Kuijpers, et al., *Appl. Catal.* **25** (1986) 139.

146) G.A. Somorjai, "Principles of Surface Chemistry" 1972. Prentice-Hall, Englewood Cliffs, New Jersey.

147) B. Marchon, et al., *J. Phys. Chem.* **92** (1988) 5744.

148) M.E. Bussel, and G.A. Somorjai, *Catal. Lett.* **3** (1988) 1.

149) M.R. Smith, and U.S. Ozkan, *J. Catal.* **141** (1993) 124.

150) A.A. Davydov, et al., *J. Catal.* **55** (1978) 299.

151) J.M. Peacock, et al., *J. Catal.* **15** (1969) 373.

152) P.N. Tiwari, T.G. Alkhazov, K.U. Adzamov, and A.K. Khanmamedova, *J. Catal.* **120** (1989) 278.

153) A. Boschi, C. Ferro, G. Luzzi, and L. Papagno, *J. Vac. Sci. Technol.* **16** (1979) 1037.

154) Y. Mizokawa, et al., *Surf. Sci.* **182** (1987) 431.

155) J.R. Lince, et al. *Surf. Sci.* **277** (1992) 43.

156) Th. Detzel, N. Nemmel, and Th. Fauster, *Surf. Sci.* **293** (1993) 227.

157) D.L. Williamson, and F.R. Yeatts, *J. Appl. Phys.* **51** (1980) 388.

158) K. Hono, H.W. Pickering, and T. Sakurai, *Appl. Surf. Sci.* **35** (1988-89) 327.

159) O.P. van Pruissen, E. Boellaard, O.L.J. Gijzeman, and J.W. Geus, *Appl. Surf. Sci.* **27** (1986) 1.

160) O.P. van Pruissen, et al., *Appl. Surf. Sci.* **27** (1986) 24.

161) O.P. van Pruissen, and O.L.J. Gijzeman, *Appl. Surf. Sci.* **27** (1986) 52.

162) O.P. van Pruissen, O.L.J. Gijzeman, and J.W. Geus, *Appl. Surf. Sci.* **29** (1987) 317.

163) K. Kishi, and J. Nishioka, *Surf. Sci.* **227** (1990) 97.

164) M. Langell, and G.A. Somorjai, *J. Vac. Sci. Technol.* **21** (1982) 858.

165) A.N. Buckley, and R. Woods, *Aust. J. Chem.* **37** (1984) 2403.

166) I. Jirka, *Surf. Sci.* **232** (1990) 307.

167) I. Jirka, and J. Dubský, *Appl. Surf. Sci.* **40** (1989) 135.

168) G. Moretti, and P. Porta, *Surf. Sci.* **287/288** (1993) 1076.

169) S. DiNardo, et al., *Surf Sci.* **287/288** (1993) 1087.

170) B. Marchon, J. Carrazza, H. Heinemann, and G.A. Somorjai, *Carbon* **26** (1988) 507.

171) G. Panzer, B. Egert, and H.P. Schmidt, *Surf. Sci.* **151** (1985) 400.

172) T.L. Barr, *J. Phys. Chem.* **82** (1978) 1801.

173) C.R. Brundle, *Faraday Discuss. Chem. Soc.* **60** (1975) 159.

174) M.Bowker, H. Houghton, and K.C. Waugh, *J. Chem. Soc. Faraday Trans. I.* 77 (1981) 3023.

175) G.C. Chinchen, et al., *Appl. Catal.* **30** (1987) 333.

176) J. Valyon, and W.K. Hall, *J. Phys. Chem.* **97** (1993) 1204.

177) G. Ertl, et al., *Appl. Surf. Sci.* **5** (1980) 49.

178) J.A. Labinger, and K.C. Ott, *Catal. Lett.* **4** (1990) 245.

179) J. Bloch, D.J. Bottomley, S. Janz, and H.M. van Driel, *Surf. Sci.* **257** (1991) 328.

180) T.M. Hupkens, J.M. Fluit, and A. Niehaus, *Surf. Sci.* **165** (1986) 327.

181) J. Oudar, "Physics and Chemistry of Surfaces," 1975. Blackie & Son, Ltd., Glasgow.

182) R.C. Yeates, J.E. Turner, A.J. Gellman, and G.A. Somorjai, *Surf. Sci.* **149** (1985) 175.

183) B.C Sales, J.E. Turner, and M.B. Maple, *Surf. Sci.* **114** (1982) 381.

184) P.T. Lynch, G. Emig, and S.E. Wanke, *J. Catal.* **97** (1986) 456.

185) P.J. Berlowitz, C.H.F. Peden, and D.W. Goodman, *J. Phys. Chem.* **92** (1988) 5213.

186) R.G. Copperthwaite, et al., *Catal. Lett.* **1** (1988) 11.

187) W. Akemann, and A. Otto, *Surf. Sci.* **287/288** (1993) 104.

188) V.M. Browne, et al., *Appl. Surf. Sci.* **47** (1991) 375.

189) T. Haas, and J. Pritchard, *J. Chem. Soc. Faraday Trans.* **86** (1990) 1889.

190) H. Freund, and R.P. Messmer, *Surf. Sci.* **172** (1986) 1.

191) I. Chorkendorff, P.B. Rasmussen, H. Christoffersen, and P.A. Taylor, *Surf. Sci.* **287/288** (1993) 208.

192) P.B. Rasmussen, P.A. Taylor, and I. Chorkendorff, *Surf. Sci.* **269/270** (1992) 352.

193) V.V. Grigo'ev, *Kinet. Katal.* **32** (1991) 230.

194) D.B. Clarke, I. Suzuki, and A.T. Bell, *J. Catal.* **142** (1993) 27.

195) A.P. Baddorf, and J.F. Wendelken, *Surf. Sci.* **256** (1991) 264.

196) B. Halpern, and J.E. Germain, *J. Catal.* **37** (1975) 44.

197) J. Hall, O. Saksager, and I. Chorkendorff, *Chem. Phys. Lett.* **216** (1993) 413.

198) A. Hodgson, A.K. Lewin, and A. Nesbitt, *Surf. Sci.* **293** (1993) 211.

199) L.H. Dubois, *Surf. Sci.* **119** (1982) 399.

200) G.R. Wallwork, and W.W. Smeltzer, *Corr. Sci.* **9** (1969) 561.

201) H. Tillborg, A. Nilsson, B. Hernnäs, and N Mårtensson, *Surf. Sci.* **269/270** (1992) 300.

202) F. Jensen, F. Besenbacher, and I. Stensgard, *Surf. Sci.* **269/270** (1992) 400.

203) Y. Teraoka, et al., *Catal. Lett.* **12** (1992) 361.

204) M. Iwamoto, et al., *J. Phys. Chem.* **96** (1992) 9360.

205) J. Valyon, and W.K. Hall, *J. Phys. Chem.* **97** (1993) 1204.

206) Y. Li, and W.K. Hall, *J. Catal.* **129** (1991) 202.

207) A. Yanase, and H. Komiyama, *Surf. Sci.* **248** (1991) 11.